RESEARCH

Keeping Utah Moving

Utah Department of Transportation - Research Division
4501 South 2700 West - P.O. Box 148410 - SLC,UT 84114-8410

Report No. UT-18.13

LATERAL RESISTANCE OF PIPE PILES ADJACENT TO A 20-FT HIGH MSE WALL

Prepared For:

Utah Department of Transportation
Research Division

Submitted By:

Brigham Young University
Department of Civil and Environmental Engineering

Authored By:

Kyle M. Rollins
Jason J. Besendorfer
Ryan T. Budd

Final Report
August 2018

DISCLAIMER

The authors alone are responsible for the preparation and accuracy of the information, data, analysis, discussions, recommendations, and conclusions presented herein. The contents do not necessarily reflect the views, opinions, endorsements, or policies of the Utah Department of Transportation, the US Department of Transportation, or other agencies that provided funding for the project. The Utah Department of Transportation makes no representation or warranty of any kind, and assumes no liability therefore.

ACKNOWLEDGMENTS

Funding for this study was provided by FHWA pooled fund study TPF-5(272) "Evaluation of Lateral Pile Resistance Near MSE Walls at a Dedicated Wall Site," supported by Departments of Transportation from the states of Florida, Iowa, Kansas, Massachusetts, Minnesota, Montana, New York, Oregon, Texas, Utah, and Wisconsin. Utah DOT served as the lead agency with Jason Richins and David Stevens as the research project managers and Jon Bischoff as the geotechnical champion. This support is gratefully acknowledged; however, the opinions, conclusions and recommendations in this report do not necessarily represent those of the sponsoring organizations.

In addition, significant in-kind contributions from a number of entities made it possible for this project to be undertaken with a scope sufficient to accomplish the project objectives. We gratefully acknowledge the assistance of Chris Ragan at Atlas Tube in donating the circular and square steel piles along with Price Bethel at Spartan Steel in donating the H piles used in this study. Eric Hendricksen at Desert Deep Foundations, Inc. provided pile driving services at cost and Carl Clyde at Geneva Rock, Inc. donated site grading services and the use of their land for the MSE abutment test site. Lastly, the Reinforced Earth Company and SSL, Inc. donated wall panels and reinforcing elements necessary to construct the abutment wall.

TECHNICAL REPORT ABSTRACT

1. Report No. UT-18.13	2. Government Accession No. N/A	3. Recipient's Catalog No. N/A
4. Title and Subtitle LATERAL RESISTANCE OF PIPE PILES ADJACENT TO A 20-FT HIGH MSE WALL		5. Report Date August 2018 6. Performing Organization Code N/A
7. Author(s) Kyle M. Rollins, Jason J. Besendorfer, Ryan T. Budd		8. Performing Organization Report No. N/A
9. Performing Organization Name and Address Brigham Young University Department of Civil and Environmental Engineering 368 CB Provo, UT 84602		10. Work Unit No. 4205315D 11. Contract or Grant No. 14-8434
12. Sponsoring Agency Name and Address Utah Department of Transportation 4501 South 2700 West P.O. Box 148410 Salt Lake City, UT 84114-8410		13. Type of Report & Period Covered Final Report May 2014 – Aug. 2018 14. Sponsoring Agency Code PIC No. UT11.404

15. Supplementary Notes

Prepared in cooperation with the Utah Department of Transportation, the U.S. Department of Transportation, Federal Highway Administration, and other state DOTs on pooled fund study TPF-5(272)

16. Abstract

A 20-foot tall Mechanically Stabilized Earth (MSE) retaining wall was constructed, and piles were driven at various distances behind the wall. Lateral pile load tests were conducted in the direction of the wall, and the performance of the pile, wall, and reinforcement were measured. The piles were 12.75-inch diameter pipe piles. One half of the wall was reinforced with welded wire grid reinforcement while the other half had ribbed strip reinforcements. For each reinforcement type, tests were performed on four piles located at nominal distances of 5, 4, 3 and 2 pile diameters from the back of the wall to the center of the pile. The objective of the testing was to characterize the relationship between the lateral pile resistance and the distance of the pile behind the back face of the MSE wall.

Based on the measured load-displacement curves from the tests, the lateral resistance of the piles decreased as the spacing behind the wall decreased. P-multipliers were developed to account for reduced lateral resistance for each pile. A best-fit line was developed showing the variation of p-multiplier with normalized pile spacing behind the wall including data from previous studies. The best-fit curve suggests that a p-multiplier of 1 (no reduction in lateral resistance) can be used when the normalized distance from the back face of the wall to the center of the pile is at least 4 pile diameters, and the p-multiplier decreases relatively linearly for smaller spacings. Multilinear regression equations were developed to compute the maximum tensile force on the reinforcement as a function of pile head load and other factors.

17. Key Words		18. Distribution Statement		23. Registrant's Seal
Laterally loaded piles, MSE wall, p-multiplier, welded wire reinforcement, ribbed strip reinforcement, p-y curve, tensile force, reinforcement load, bridge abutments		Not restricted. Available through: UDOT Research Division 4501 South 2700 West P.O. Box 148410 Salt Lake City, UT 84114-8410 www.udot.utah.gov/go/research		N/A
19. Security Classification (of this report) Unclassified	20. Security Classification (of this page) Unclassified	21. No. of Pages 270	22. Price N/A	

TABLE OF CONTENTS

LIST OF TABLES

LIST OF FIGURES

EXECUTIVE SUMMARY

Pile foundations for bridges must often resist lateral loads produced by earthquakes and thermal expansion and contraction of the superstructure. Right-of-way constraints near bridge abutments are leading to an increased use of mechanically stabilized earth (MSE) walls below the abutment. Previous research has shown that lateral pile resistance can be greatly reduced when piles are placed close to MSE walls, but design codes do not address this issue. A 20-ft tall MSE wall was constructed, and eight lateral pile load tests were conducted on 12.75-inch diameter pipe piles spaced at nominal distances of 2, 3, 4 and 5 pile diameters from the back face of the wall to the center of the pile. The MSE wall was constructed using welded-wire grid on one side and ribbed strip reinforcements on the other side. Results showed that measured lateral resistance decreases significantly when pipe piles are located closer than about four pile diameters from the wall. LPILE software was used to back-calculate P-multipliers that account for the reduced lateral resistance of the pile as a function of normalized spacing from the wall. Based on results from this study and previous data, lateral pile resistance is relatively unaffected (p-multiplier = 1.0) for piles spaced more than approximately 3.9 pile diameters (3.9D) from the MSE wall. For piles spaced closer than 3.9D, the p-multiplier decreased linearly as distance to the wall decreased. P-multipliers were not affected by differences in reinforcement length to height (L/H) ratio or reinforcing type.

Lateral pile loads induced tensile forces in the soil reinforcement such that as pile load increased, the maximum induced tensile force increased. Results also indicate that maximum tensile forces typically occurred in the soil reinforcement near the pile location. Past research results were combined with data from this study, and a statistical regression analysis was performed using all reinforcement strain data. Regression equations were developed to predict the peak induced tensile force in welded-wire grids and ribbed strips based on independent variables including lateral pile load, normalized pile distance (S/D), transverse distance (T/D), L/H ratio, and vertical stress. The equations had an R^2 value of 0.75 to 0.79 indicating that they account for approximately 75 to 79% of the observed variation for all tests to date.

1 INTRODUCTION

Increasing right-of-way constraints have led to the increased popularity of Mechanically Stabilized Earth (MSE) walls near bridge abutments. Piles located within the reinforced zone of MSE walls that are used to support bridge abutments must resist both vertical loads from the bridge superstructure as well as lateral loads produced by earthquakes and thermal expansion and contraction. Currently, there is little guidance to design for the lateral resistance of piles behind MSE walls. Common methods employed at this time are spacing the piles far enough behind the wall (often 6 to 8 pile diameters) to negate the walls influence; assuming there is no lateral resistance from the wall; or placing the pile close to the wall and assuming a lateral resistance reduction factor based on engineering judgment. These methods are inefficient for the following reasons: (1) increasing the distance between the wall and the pile increases cost by increasing the bridge span; (2) assuming no lateral resistance increases foundation costs because the pile size and/or the number of piles required will increase; and (3) using engineering judgment gives no standard of design for reduction factors.

Research performed by Pierson et al (2008) on concrete shafts behind an MSE wall reinforced by geosynthetic reinforcement indicates that lateral resistance decreases as pile spacing from the wall decreases with significant wall distortion in the masonry block wall. Further research conducted by Rollins et al (2013) on steel piles with metallic reinforcement confirms the research by Pierson et al (2008) and also found that p-multipliers based on pile spacing behind an MSE wall may be used to account for the decreased lateral soil resistance near an MSE wall. Rollins et al (2013) concluded that induced tensile forces in reinforcements from pile loading could be estimated using variables such as pile load, pile spacing behind the wall, and transverse distance of the pile from the reinforcement.

Although the research conducted to date is valuable, results are limited to a handful of tests with a significant number of variables with respect to soil density, reinforcement type, and reinforcement length to height ratios. Trends appear to be emerging but there is not enough information for developing design recommendations. Because of the limited data and the large number of variables, further testing is needed to provide better understanding of the MSE wall-pile interactions and to develop design recommendations.

1.1 Objectives

The main objectives of this research investigation are:

1. Measure reduced lateral pile resistance vs. displacement curves for pipe piles at different distances behind an MSE wall with welded-wire reinforcement
2. Measure the increase and distribution of tensile force in the welded-wire reinforcement induced by lateral pile loading.
3. Develop design rules (e.g. p-multipliers) to account for reduced pile resistance as a function of spacing behind the MSE wall
4. Develop a design approach to predict maximum reinforcement force induced by pile loading.

1.2 Scope of Work

To accomplish the research objectives, a full-scale MSE wall was constructed to conduct research on laterally loaded steel piles. The wall was constructed in two phases using welded-wire grid and steel strip reinforcements so that the performance of the two reinforcement systems could be evaluated separately but with comparable backfill conditions. Because each reinforcement system develops resistance in different ways, this allows separate design approaches to be developed if necessary. During Phase I lateral pile load tests were performed at a wall height of 15 feet with a reinforcement length to height (L/H) ratio of about 0.9, which might be common for seismic design. During Phase II, tests were conducted at a wall height of 20 feet with an L/H ratio of about 0.7, which is more typical for static loading. The difference in reinforcement L/H ratios makes it possible to determine if reinforcement length has any effect on lateral pile resistance or induced force in the reinforcements.

Pile types consisted of pipe, square and H piles and were located behind the wall in the reinforced zone at distances of approximately 2, 3, 4 and 5 pile diameters from the back face of the wall. The variation in pile type makes it possible to determine if the p-multipliers or induced tensile force are affected by the shape of the piles.

This systematic examination of the interaction between piles and MSE walls has been the focus of research from Hatch (2014), Han (2014), Besendorfer (2015), Budd (2016), and Luna (2016). This report focuses on the behavior of the pipe piles located in both the welded-wire grid reinforcement and ribbed strip reinforcement zone at a wall height of 20 feet with an L/H of about 0.7 (Besendorfer, 2015 and Budd, 2016). The test procedures, results, and analysis are described herein.

2 LITERATURE REVIEW

Currently, little guidance is given for designing the lateral resistance of loaded piles behind mechanically stabilized earth (MSE) walls. A review of MSE walls, soil reinforcement resistance to pullout, laterally loaded analysis of piles, and case histories of full-scale lateral load testing of piles is presented in this chapter.

2.1 MSE Walls

MSE walls are cost effective retaining structures that use reinforcing in the soil behind the wall to add strength and stability to the structure. Layers of reinforcing holds the facing system in place, which allows for construction of high vertical walls and prevents soil raveling from occurring. MSE walls were first built commercially in the early 1970's and are now widely used in practice. MSE walls are typically used on projects that have bridge abutments, wing walls or in areas where right-of-way is restricted. Advantages of MSE walls over conventional walls include: (Berg et al 2009)

- Simple and rapid construction procedures;
- Do not require large construction equipment or skilled laborers;
- Require less site preparation than alternative systems;
- Require less space in front of the structure for construction;

- Reduce right-of-way acquisition;
- Are technically feasible to heights greater than 100 feet; and
- Are more tolerant to deformations than alternative systems.

There are two general categories of reinforcing used in MSE walls: extensible and inextensible reinforcing. Extensible reinforcing is defined as a material that deforms with the surrounding soil and consists of any type of geosynthetic, such as geotextiles or geogrid, and is usually made of polyethylene or polyester. Inextensible reinforcing is defined as material that deforms considerably less than the surrounding soil and consists of steel or galvanized steel strips and welded-wire grids or mats (Berg et al 2009).

Typically, MSE walls have been designed using the Allowable Stress Design (ASD) method or the Load Resistance Factor Design (LRFD) method. Both methods evaluate the external and internal stability of the stabilized mass. The difference between the ASD and LRFD methods is how they design for uncertainty. ASD combines all load and material stress uncertainties into one factor of safety, regardless of the method used to estimate resistance. LRFD accounts for uncertainty in both material resistance and load and can provide more consistent levels of safety in the overall design by using resistance factors and load factors.

External and internal stability analyses are evaluated during the design process of MSE walls. External stability analysis of MSE walls assumes that the reinforced soil and wall act as one consistent mass. External failures include sliding, overturning, and bearing as shown in Figure 2-1.

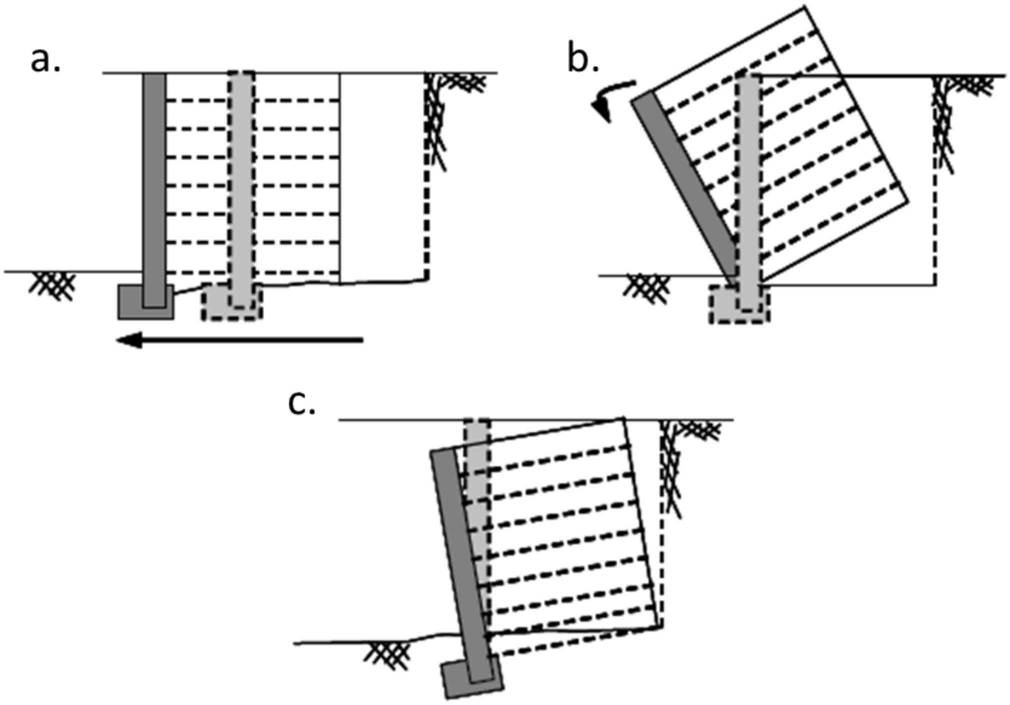

Figure 2-1: External stability failure cases: (a) sliding, (b) overturning, and (c) bearing.

Internal failure for an MSE wall can occur in two different ways: elongation and pullout of the reinforcement. Elongation occurs when tensile forces acting on the reinforcement are larger than yield strength of the reinforcing material and results in stretching or breaking of the reinforcement. Pullout occurs when tensile forces acting on the reinforcement are larger than the pullout resistance of the surrounding soil. In both cases, failure leads to large movement and possible collapse of the structure. The relevant steps for analyzing internal stability are as follows: (Berg et al 2009)

- Select the type of soil reinforcement;
- Define the critical failure surface (for selected reinforcement type);
- Define unfactored loads;

- Establish the vertical layout of soil reinforcements;
- Calculate factored horizontal stress and maximum tension for each reinforcement layer; and
- Calculate nominal and factored pullout resistance of soil reinforcements and check established layout.

Internal stability calculations vary depending on whether the reinforcing is extensible or inextensible.

The critical failure surface for inextensible reinforcing, as shown in Figure 2-2, is assumed to be bilinear, located at the zone of maximum tensile force in the reinforcement and passes through the toe of the wall. Maximum tensile forces for each reinforcement layer can be calculated using Equation 2-1 and are directly related to the type of reinforcement used (Berg et al 2009).

Figure 2-3 shows the relationship between reinforcing material used and the overburden stress. The coefficient of lateral stress, K_r, obtained from Figure 2-3 is used to calculate the horizontal stress as shown in Equation 2-2. Vertical spacing, S_v, of inextensible reinforcement with pre-cast concrete facings is generally constant. In order to increase resistance, the size of reinforcement or number of reinforcement members can be increased. In the case of welded wire grids, the diameter is increased and/or the number of longitudinal bars is increased.

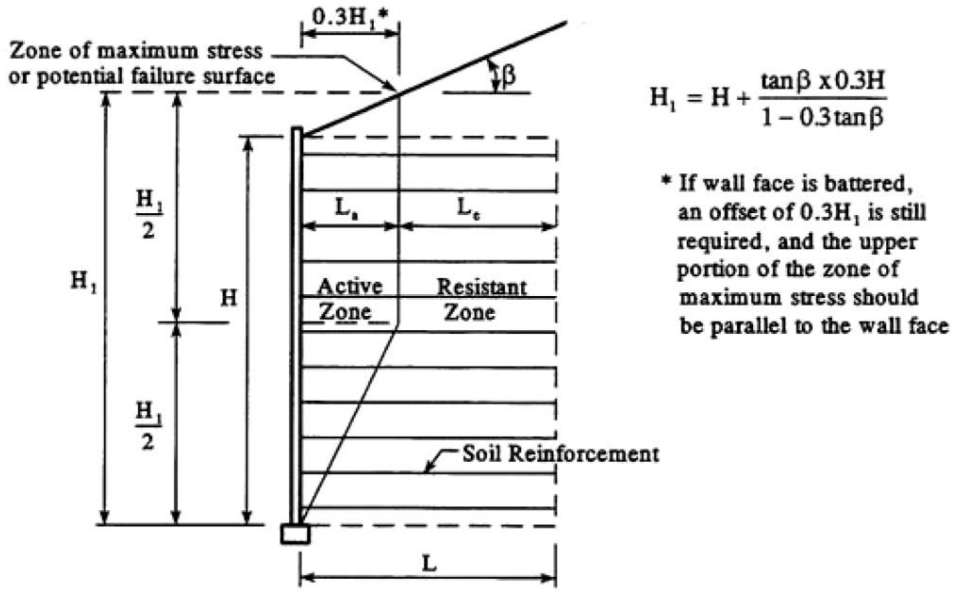

Figure 2-2: Potential failure surface location for MSE walls with inextensible reinforcement (Berg et al 2009).

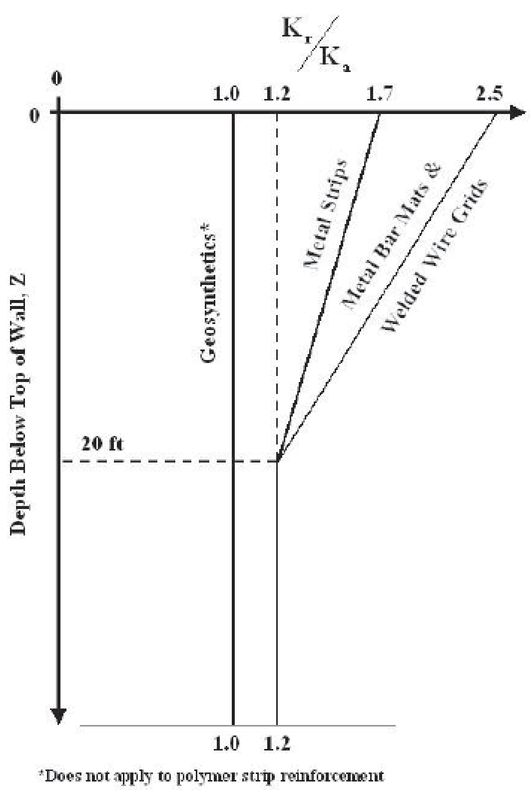

Figure 2-3: Variation of the coefficient of lateral stress ratio with depth in an MSE wall (Berg et al 2009).

$$T_{max} = \sigma_H S_v \tag{2-1}$$

where

T_{max} is the maximum tensile force in a reinforcement layer,

σ_H is the horizontal stress along the failure surface (see Equation 2-2), and

S_v is the vertical spacing between reinforcement layers.

$$\sigma_H = K_r \sigma_v + \Delta\sigma_h \tag{2-2}$$

where

K_r is the coefficient of lateral stress (see Figure 2-3),

σ_v is the vertical stress (see Equation 2-3), and

$\Delta\sigma_h$ is horizontal stress due to external surcharges.

$$\sigma_v = \gamma_r Z + q + \Delta\sigma_v \tag{2-3}$$

where

γ_r is the moist unit weight of the reinforced soil,

Z is the depth to the reinforced layer from the top of wall,

q is a uniform surcharge load, and

$\Delta\sigma_v$ is a concentrated vertical surcharge load.

The pullout capacity, P_r, for each reinforcement is the force required to generate sliding of the reinforcement. Pullout capacity is dependent on the length, cross-sectional area and material type of the reinforcements as well as surcharge loads and soil properties. Equation 2-4 shows how to calculate pullout capacity, P for a unit of reinforcement.

$$\boldsymbol{P_r = F^* \alpha \sigma'_v L_e C b} \tag{2-4}$$

where

P_r is the pullout capacity of the reinforcement per unit width,

F* is the pullout resistance factor (see Equation 2-5a for welded wire, and Equation 2-5b for ribbed strip, where interpolation is used for depths between 0 and 20 feet below the wall),

α is a scale effect correction factor equal to 1 for metallic reinforcements,

σ'_v is the vertical effective stress at the reinforcement layer,

L_e is the length of embedded reinforcement resisting the soil at a given point,

C is the reinforcement effective unit perimeter equal to 2 grids and strips, and

b is the gross width of the welded-wire grid or ribbed strip reinforcement.

$$\boldsymbol{F^* = \begin{cases} 20(t/S_t), Z = 0 \\ 10(t/S_t), Z \geq 20\ ft \end{cases}} \tag{2-5a}$$

$$\boldsymbol{F^* = \begin{cases} 1.2 + log(C_u) \leq 2, Z = 0 \\ \quad tan\phi \geq 20\ ft \end{cases}} \tag{2-5b}$$

where

t is the transverse bar thickness of the reinforcement,

S_t is the spacing between transverse bars,

Z is the depth to the reinforcement layer below the top of the wall

C_u is the uniformity coefficient of the backfill, and

ϕ is the friction angle.

$$\boldsymbol{R_c = \frac{b}{S_h}} \tag{2-6}$$

where

b is the width of the reinforcement, and

S_h is the horizontal center to center spacing of reinforcement on the same layer.

The horizontal spacing between reinforcement, S_h, calculated in Equation 2-6 factors in the section of wall that is affected by the reinforcement. For this study, S_h was not used in the calculations because strain gauges measured the induced pile load directly, and the reinforcement was the prime focus of induced load, not the wall. Therefore, b is used for this study.

2.2 Tests for Pullout Resistance Factors

A total of 402 full-scale pullout tests were performed on inextensible reinforcements at Texas Tech University. The primary purpose of the testing program was to evaluate pullout resistance factors (F*) for ribbed steel strips and welded wire grid reinforcements in sandy backfill (Lawson 2013). The backfill material was classified as a poorly graded sand with silt (SP-SM) with a maximum dry unit weight of 124.5 pcf, an optimum moisture content of 7.8 percent and an average relative compaction of 95.7 percent. A portion of the ribbed steel strips were tested in under-compacted soil with a relative compaction of approximately 91 percent. A comparison of the change in compaction to the change in F* values is found in Table 2-1 and provides valuable insight on how small changes in relative compaction can greatly affect the soil resistance on the reinforcement. In general, a change in relative compaction of 4 % affected the pullout resistance factor by 34% (Lawson 2013).

After creating a database, statistical analyses were performed on the data. The objective of the analyses was to identify key variables that affect the measured F* value and to develop F* prediction models and intervals based on the new data set (Lawson 2013). Results of the statistical analyses agree with AASHTO that depth of fill, transverse bar diameter and transverse bar spacing influence F* in welded-wire grids. Embedment length, longitudinal bar diameter and spacing were significant variables affecting F* that the AASHTO equation does not take into account. This study shows that as longitudinal and transverse bar spacing decreases or the transverse bar diameter increases, F* increases.

Table 2-1: Influence of relative compaction on pullout resistance factor, F* (Lawson 2013).

Degree of Compaction	Mean F*	Lower Confidence Interval	Upper Confidence Interval
Under-compacted backfill	1.77	1.50	2.09
Properly compacted	2.69	2.26	3.20

A nonlinear regression was used to define the relationship between F* and the depth of fill, opposed to a bilinear regression line used by AASHTO (Lawson 2013). Figure 2-4 and Figure 2-5 show the measured F* values versus the depth of fill for the welded-wire grid and ribbed strip reinforcements, respectively, and includes the AASHTO bilinear equation as a solid black line for comparison. At depths shallower than ten feet, the data from this study produced F* values up to 2.5 times (near the surface) greater than those used by AASHTO. It is important to note that the scatter in the measured F* values is significant even in these tests where compaction was closely controlled. The scatter is greatest at the top of the wall presumably owing to differences in the potential for dilation associated with small changes in relative compaction. Therefore, scatter in the tensile force induced by lateral pile loading which occurs near the top of the wall should be expected to be significant.

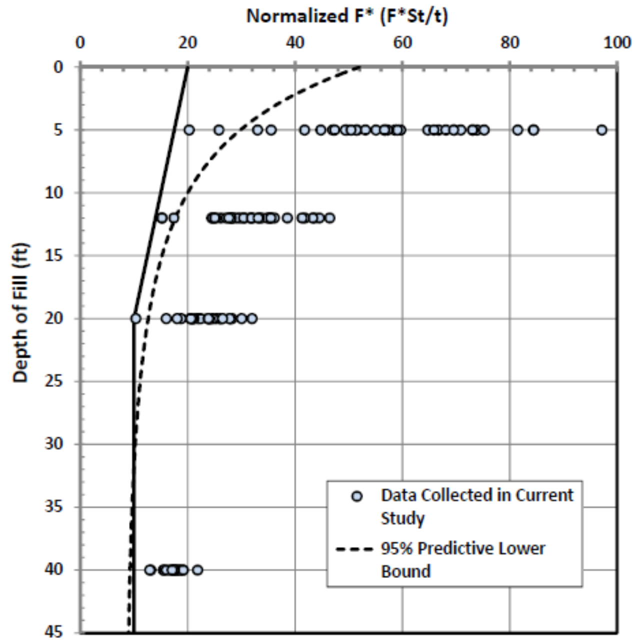

Figure 2-4: Normalized pullout resistance factor, F*, vs. depth of fill for welded-wire grid reinforcements in sandy backfill (Lawson 2013).

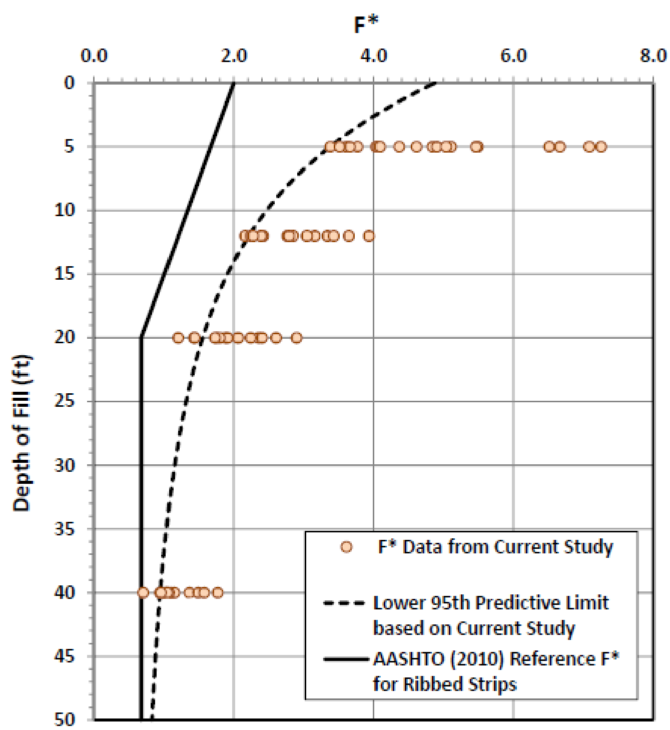

Figure 2-5: Normalized pullout resistance factor, F*, vs. depth of fill for ribbed steel strip reinforcements in sandy backfill (Lawson 2013).

2.3 Laterally Loaded Analysis of Piles

A common way to analyze laterally loaded piles is by using the p-y method. The p-y method is based on modeling the soil-pile interaction as a nonlinear beam on an elastic foundation (BEF) where a series of springs are used to model soil behavior, as shown in Figure 2-6. Analysis of laterally loaded piles with the p-y method is generally performed by finite difference and finite element software including COM624, LPILE, FB-Pier, etc. LPILE is perhaps the most widely used program in the United States and was the software used for analysis on this project.

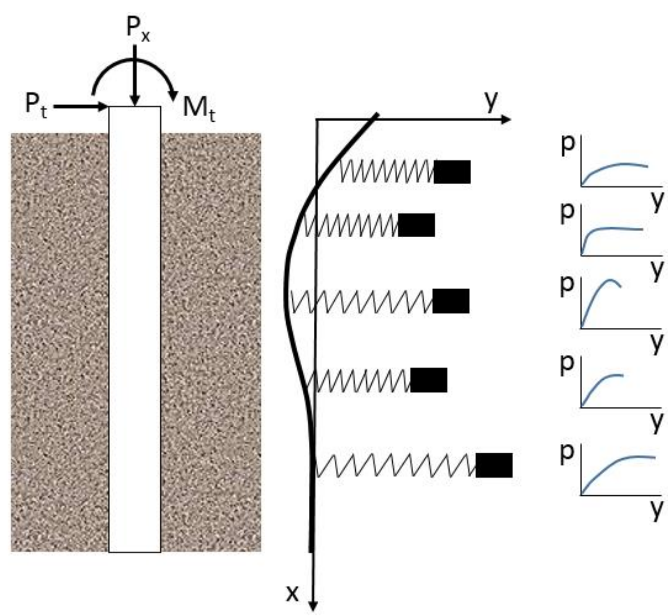

Figure 2-6: Conceptual model of the p-y method (Isenhower et al. 2015).

LPILE is a finite difference program that analyzes the lateral loading of driven piles and drilled shafts. LPILE is the commercial version of the computer program COM624 which was originally developed by Reese and Matlock at the University of Texas in the 1970s and is one of the most widely used programs for lateral pile load analysis. The program is capable of producing deflection, shear, bending moment and soil response of the pile to the maximum depth the pile is driven. LPILE also automatically generates p-y curves based on soils from full-scale load tests previously studied. Soil types programmed into LPILE include clay, sand, weak rock, and a number of specialty soils. The program also allows manual entry of soil parameters.

API sand and Reese sand are two of the sand types in LPILE with similar criteria and differ primarily in the initial modulus of subgrade reaction and the shape function of the curves. The API sand criteria uses a more convenient equation for computation and will be the soil criteria used for analysis on this project. The API procedure for computing p-y curves is as follows: obtain values for the angle of internal friction, soil unit weight, and pile diameter; compute the ultimate soil resistance; and develop the load-deflection curve based on the smallest calculated ultimate bearing capacity value. Values for soil properties are either obtained through field testing, correlation, or empirical means and are used in LPILE as input parameters.

Two models are used for computing the ultimate bearing capacity, p_u, for piles in sand. The first model is a passive wedge-type failure for soil resistance near the ground surface and can be calculated using Equation 2-8. An example of wedge failure is demonstrated in Figure 2-7. The second model is for failure at deeper depths caused by lateral flow of soil around the pile and is calculated using Equation 2-9. At a given depth, x, the model giving the smallest value of P_u should be used as the ultimate bearing resistance when developing the p-y curve. The p-y relationships for sand are non-linear but may be approximated by using Equation 2-10.

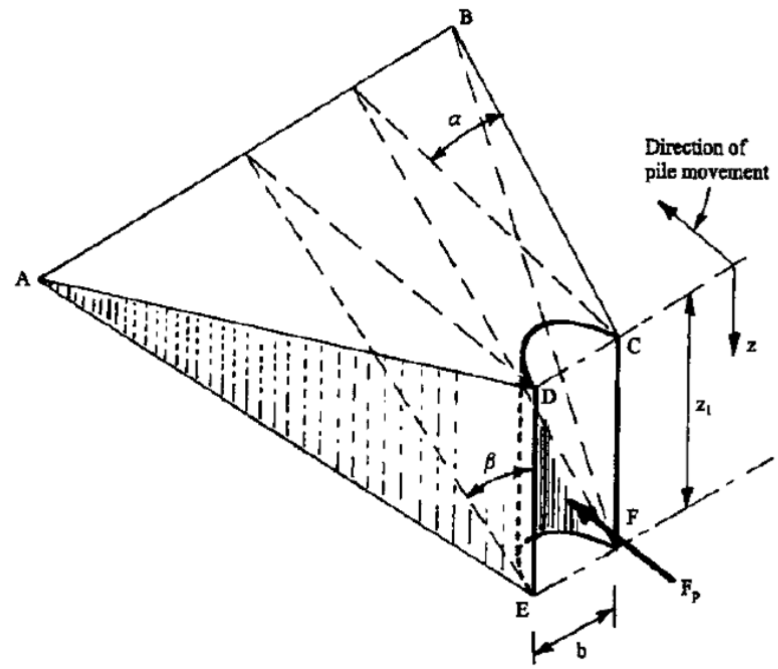

Figure 2-7: Passive wedge failure of laterally loaded piles in sand at shallow depths (Isenhower et al. 2015).

$$\boldsymbol{P_{us} = (C_1 x + C_2 b)\gamma' x} \quad \textbf{(2-7)}$$

$$\boldsymbol{P_{ud} = C_3 b\gamma' x} \quad \textbf{(2-8)}$$

where

P_u is the ultimate resistance in force per unit length (s = shallow, d = deep),

γ' is the effective unit weight of soil,

x is depth from ground surface,

ϕ' is the angle of internal friction of sand in degrees,

C_1, C_2, and C_3 are coefficients determined from Figure 2-8 as a function of ϕ', and

b is the average pile diameter from the ground surface to depth x.

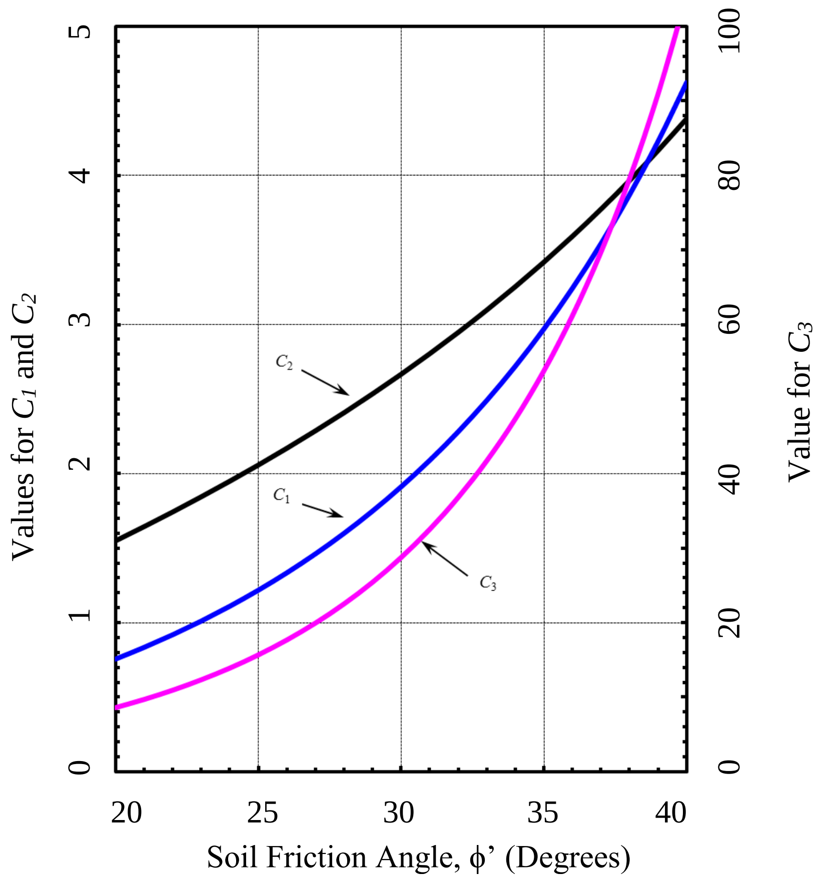

Figure 2-8: Ultimate bearing coefficients as a function of the internal angle of friction (API, 1982).

$$\boldsymbol{p = Ap_u \tanh\left(\frac{kx}{Ap_u}y\right)} \qquad \textbf{(2-9)}$$

where

p is resistance on the p-y curve,

A is $\left(3.0 - 0.8\frac{x}{b}\right) \geq 0.9$ for static loading, 0.9 for cyclic loading,

p_u is computed from Equations 2-8 and 2-9, and is the smaller of the two values,

k is the initial modulus of subgrade reaction as determined from Figure 2-9,

x is depth from ground surface, and

y is deflection on the p-y curve.

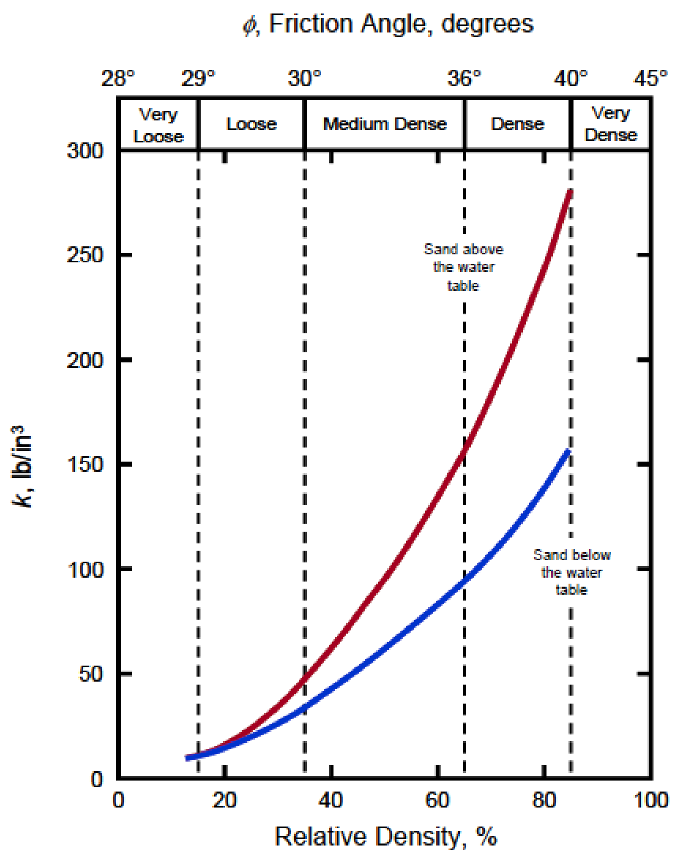

Figure 2-9: Soil modulus reaction based on friction angle or relative density of soil (API, 1982).

2.4 Full-Scale Load Tests

Several full-scale load tests have been performed on laterally loaded piles or shafts behind MSE walls over the last decade including work from Pierson (2009), Rollins et al (2013), Hatch (2014), Han (2014) and Besendorfer (2015). The following sections will discuss the full-scale load tests performed to date including the conclusions and limitations drawn from each test.

2.4.1 Laterally Loaded Shafts Behind an MSE Block Wall

The first full-scale lateral load test behind an MSE wall was performed by Pierson and Parsons in 2007. The project was located in Kansas DOT right-of-way near Kansas City, Kansas.

The research consisted of laterally loading eight 36-inch diameter cast-in-place reinforced concrete shafts behind a 20 foot high masonry block retaining wall with Tensar UX1400 and UX1500 extensible geogrid reinforcements. The shafts were generally 20 feet long, and spaced a normalized distance of one shaft diameter (1D) to four shaft diameters (4D) behind the back face of the wall. Backfill consisted of crushed limestone gravel with an angle of friction of 51 degrees (Pierson et al 2009).

Instrumentation was used to monitor lateral load and displacement of shafts, wall displacements, pressures behind the wall facing, strain within the reinforcing and movement within the wall (Parsons et al 2009). Shaft data was obtained by monitoring hydraulic pressure, load cells and linear variable differential transformers (LVDTs). Inline load cells were used on all of the single pile tests. Each test shaft and reaction shaft were fitted with two LVDTs at different elevations to determine the change in elevation. The reaction and reference beams were also fitted with LVDTs to monitor movement. Inclinometers were placed inside the shafts to monitor shaft deflection and measurements were taken at different load steps. A pile head load vs. deflection plot presented in Figure 2-10 for four single shaft tests located at different distances behind the wall indicates that lateral soil resistance decreases as the normalized distance decreases. However, it should be noted that the reduction does not appear to decrease uniformly with distance. For example, the lateral resistance of the pile at 3D decreases by about 30% on average relative to the pile at 4D; however, the lateral resistance for the pile at 2D is about the same as that for the 3D pile. This could be a result of non-uniform compaction between the pile and the wall face.

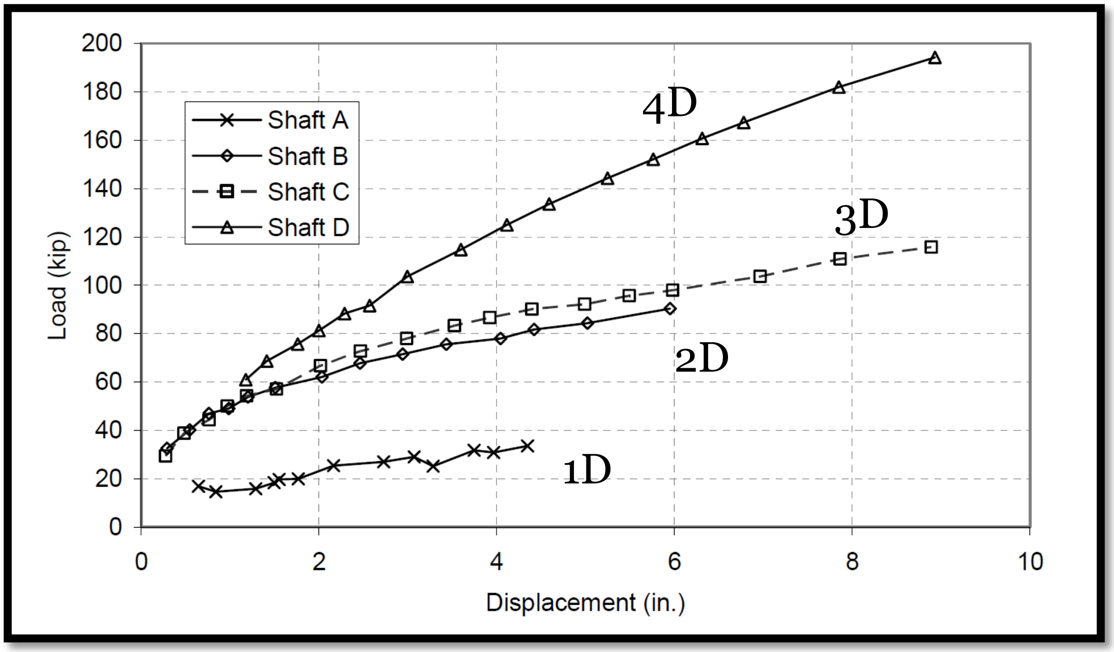

Figure 2-10: Load at 2.5 minutes vs. deflection of laterally loaded single shafts (Pierson et al 2009).

Geogrid was instrumented with strain gauges, located on the top and bottom of the reinforcement for redundancy. Data from the strain gauges was used to measure load transferred to the reinforcements. They found that as geogrid stiffness (strength) increased the wall deflection decreased and the area of wall displacement increased. (Pierson et al 2011). Post-test tension cracks were observed at the edge of the reinforced soil block indicating that failure of the wall was external and that reinforcement length was critical on this project. In general, strain was highest near the pile and decreased as distance from the pile increased.

Pressure cells were placed behind the wall face and were used to measure pressure at multiple elevations directly in front of the loaded shafts. Wall deflection was measured by placing targets on the wall face and measuring target movements between each load with a digital camera on a fixed tripod. Movement measured from the targets and LVDTs were consistent with each other. Because the wall and shafts were built for research, wall deflections of over 6 inches were measured on some of the tests. Figure 2-11 shows that 9 inches of shaft movement deflects the wall 6 inches, indicating that the wall is not resisting the pile load very effectively. Further evidence of poor lateral resistance is that wall movement is reduced by approximately 60 percent when spaced two pile diameters from the deflection in line with the shaft.

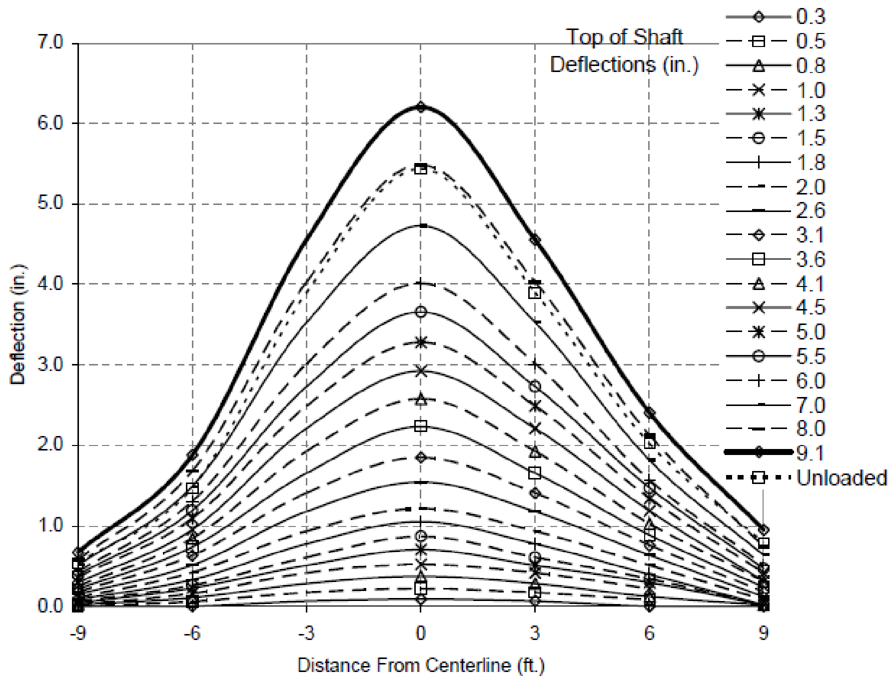

Figure 2-11: Wall deflection based on distance from centerline of Shaft C located 3D behind the wall face near the top of wall (Pierson et al 2009).

2.4.2 Full-Scale Load Testing Near UDOT Bridge Abutment Walls

Lateral load tests behind MSE walls were performed in Utah County, Utah at the following sites: Pioneer Crossing, U.S. Highway 89 and Provo Center Street (Price 2012, Nelson 2013, Rollins et al, 2013). Each site was located in Utah Department of Transportation (UDOT) right-of-way and where bridges were under construction. Testing was performed on a total of eight steel piles with diameters from 12.75 to 16 inches and at distances of 1.7D to 7.5D from the wall face.

Reinforcement was all inextensible, but both welded-wire grid and ribbed strip reinforcements were employed along with one-stage and two stage walls. Wall heights ranged from about 20 to 40 ft. Four of the piles tested were production piles used to support the bridges and had set locations. The remaining four piles were installed specifically for testing purposes. The variables for each laterally loaded pile are shown in Table 2-2.

Test results from Rollins et al (2013) confirmed Pierson's conclusion that lateral resistance decreases as the normalized distance from the wall decreases. To account for the reduced lateral resistance due to proximity to the wall, Rollins et al (2013) computed p-multipliers for each test pile using the computer program LPILE. The p-multipliers were then plotted versus distance from the wall face and best-fit curves were developed as shown in Figure 2-12. According to Figure 2-12, the length to height (L/H) ratio and normalized distance behind the wall both play a role in determining p-multiplier values. The data suggest that with L/H ratios of 1.1 and 1.6, a p-multiplier of 1 can be used when the normalized distance from the back face of the wall is 5.2 and 3.8 pile diameters, respectively. It should be noted that the friction angle (ϕ) and/or the lateral stiffness factor (k) used to analyze many of the Price (2012) and Nelson (2013) tests were either much higher or lower than would be expected for the type of soil they were tested in. This is, in part, caused by not accounting for the surcharge loads when calculating p-multipliers. Surcharge loads were later considered to increase the effective wall height changing the L/H ratios to be approximately 1.0 to 1.4. Figure 2-13 shows an alternative interpretation of the results which indicate that the p-multipliers are only affected by spacing less than approximately 3.8D.

Table 2-2: Test data and information from UDOT bridge tests (Price 2012, Nelson 2013).

	US Highway 89		**Pioneer Crossing**			**Provo Center Street**		
Test Pile	TP1	TP2	TP3	TP4	TP5	TP6	TP7	TP8
Outside Pile Diameter [in]	12.75	12.75	16	16	16	12.75	12.75	12.75
Pile Wall Thickness [in]	0.375	0.375	0.375	0.375	0.375	0.375	0.375	0.375
Wrapped with HDPE? If Yes, Thickness [mm]	No	No	Yes, 10	Yes, 10	Yes, 10	No	No	No
Distance from Back Wall Face to Center of Pile [ft]	7.7	4.0	3.8	6.9	2.2	1.3	2.8	6.7
Normalized Pile Spacing [pile diameters]	7.2D	3.8D	2.9D	5.2D	1.6D	1.3D	2.7D	6.3D
Wall Height at Time of Testing [ft]	20.5	20.5	29.8	37.7	34.7	23.25	23.25	23.25
Reinforcement Length [ft]	33	33	50	42	39	28	28	28
Reinforcement Length-to-Full Height of Wall (Surcharge included)	1.29	1.42	1.27	0.98	0.97	1.03	1.20	1.03
Wall Facing Type	Concrete Panel		Concrete Panel			Welded Wire		
Inextensible Reinforcement Type	Grids		Grids			Strips		
Vertical Spacing of Reinforcement [ft]	2.5		2.5			2		
Surcharge Load [psf]	708	383	1363	735	808	657	135	657
Wall Panel Dimensions [ft]	5x12		5x10			4.8x9.75		
Backfill Material	Sandy Gravel		Sandy Gravel			Sandy Gravel		
Moist Unit Weight of Soil [pcf]	141.8		142.0			134.9		

Price (2012) and Nelson (2013) also analyzed the normalized load in the reinforcement as a function of normalized distance from the pile for both types of reinforcement. The maximum tensile force is normalized by the maximum pile load and plotted against the transverse distance between the pile and reinforcement normalized by the longitudinal distance between the pile and the wall, as shown in Figure 2-14 and Figure 2-15. They determined that the normalized force decreases exponentially as the normalized distance increases. They developed an envelope between the best fit curve of the data and conservative test data values, as shown in Figure 2-14 and Figure 2-15.

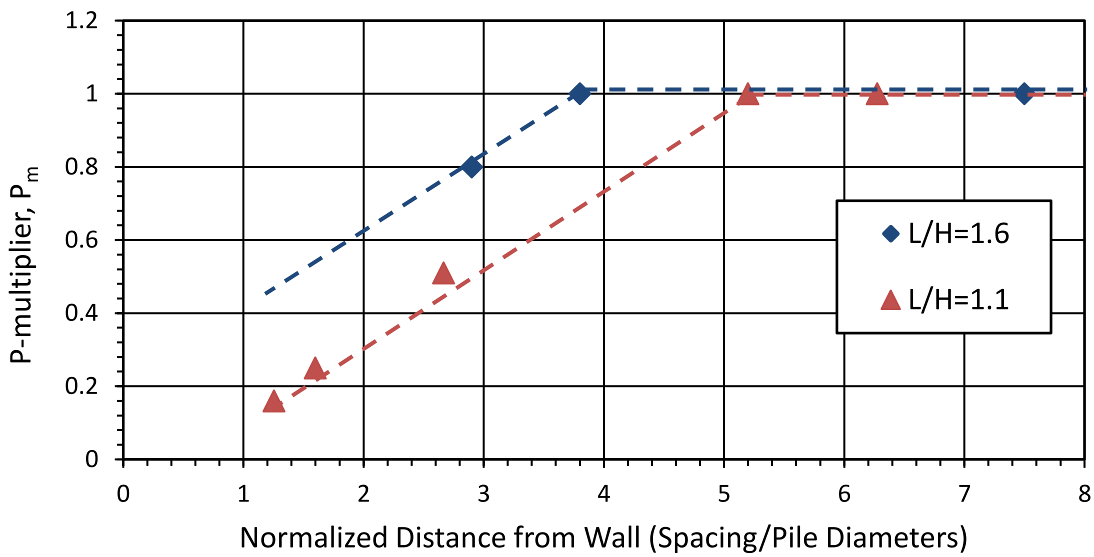

Figure 2-12: Tentative p-multiplier curves as a function of normalized distances for two reinforcement ratios (Rollins et al 2013).

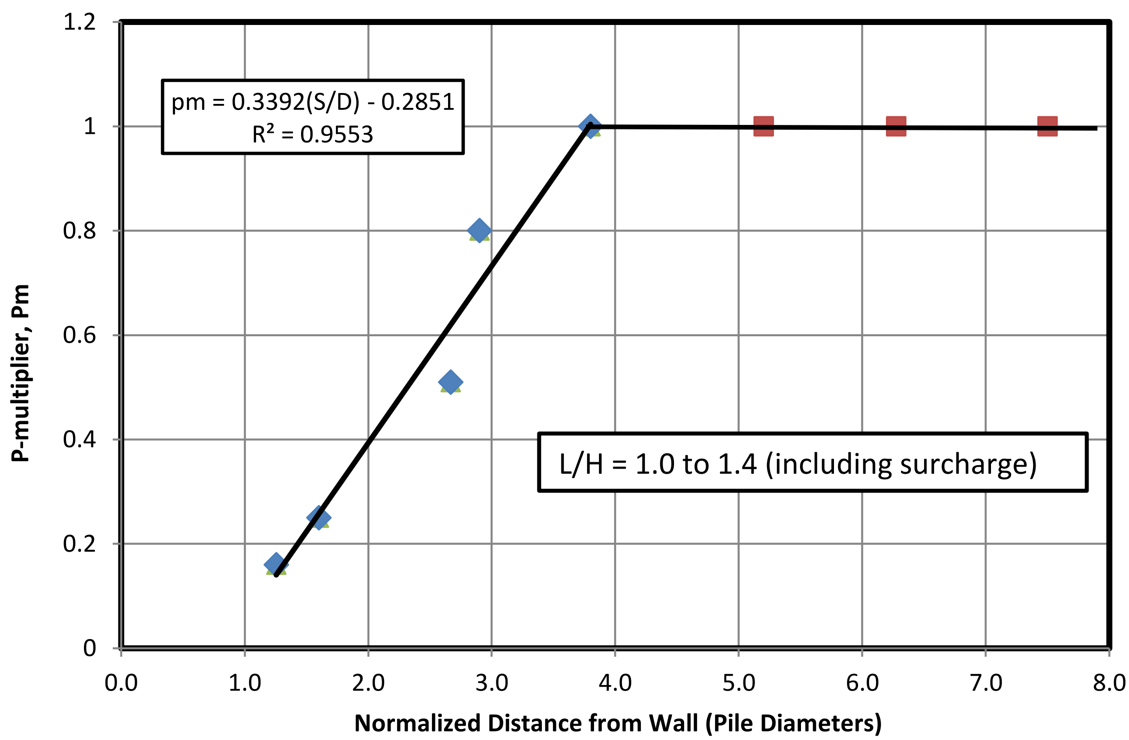

Figure 2-13: P-multiplier curves as a function of normalized distance with reinforcement ratios corrected for surcharge (Rollins et al 2013).

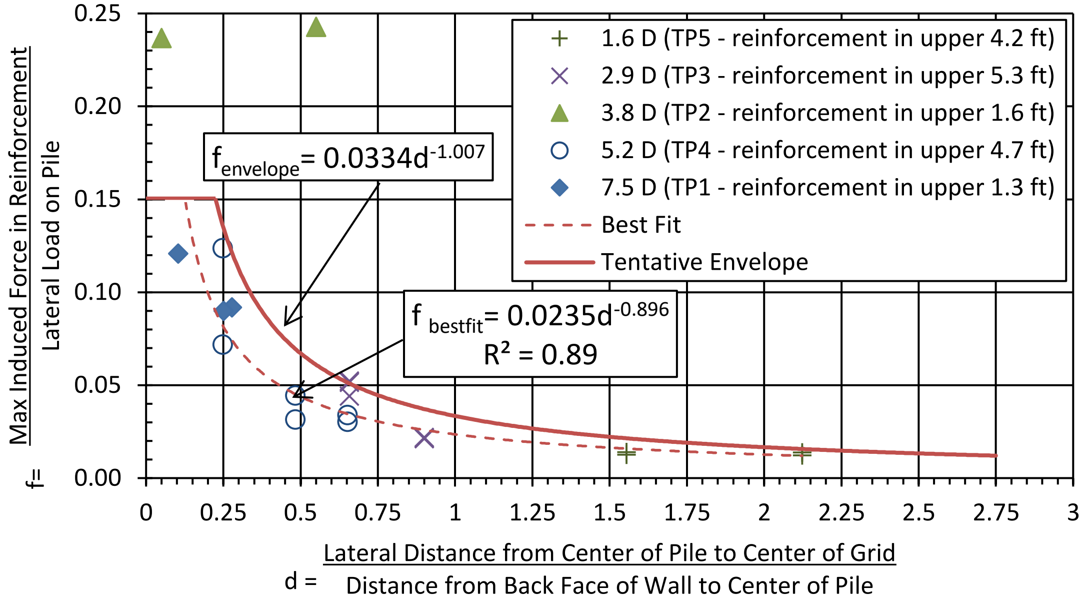

Figure 2-14: Plot of normalized induced force in wire grid reinforcement vs. normalized distance from pile (Rollins et al 2013).

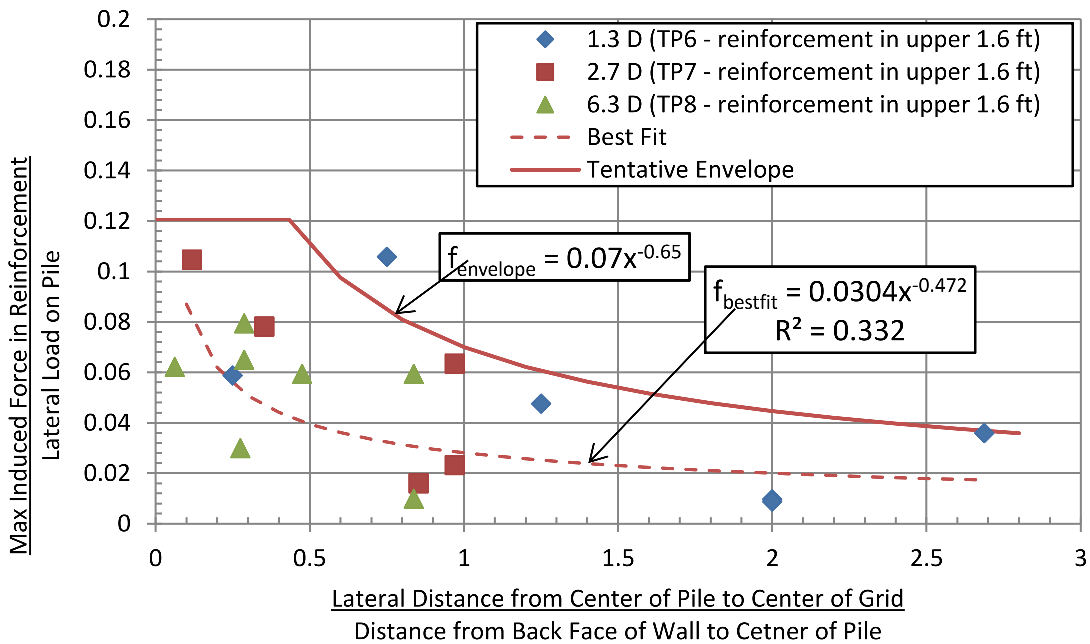

Figure 2-15: Plot of normalized induced force in strip reinforcement vs. normalized distance from pile (Rollins et al 2013).

2.4.3 Full-Scale Lateral Load Testing Behind an MSE Wall

Additional research has been completed on laterally loaded piles behind an MSE wall of which this report is a part. Tests were performed at wall heights of 15 feet and 20 feet with a constant reinforcement length to examine the influence of the reinforcement length to height (L/H) ratio on pile performance. Inextensible welded-wire grids and ribbed strips were each used on one half of the wall for soil reinforcement. Pipe, square and H-piles were used as test piles to determine if the pile shape is a factor affecting the soil resistance. Further test layout and the instrumentation of piles, reinforcing, MSE wall, etc. will be discussed later in this report.

Reports for the 15-foot phase of the wall for both the ribbed strip and welded-wire grid sections of the wall using steel pipe piles were completed by Han (2014) and Hatch (2014), respectively. Data from these studies confirm that lateral pile resistance decreases as normalized distance between the pile and wall decreases. Their data also show that the L/H ratio does not influence the p-multiplier as previously suspected based on the limited set of test results available to Price (2012) and Nelson (2013). Figure 2-16 shows a best fit line representing previous test data from Price (2012), Nelson (2013), Hatch (2014) and Han (2014), and omits the lines based on the L/H ratio. Data to this point indicates that if a pile is spaced 3.8 pile diameters or greater behind an MSE wall, it will not have reduced soil resistance due to its proximity to the wall and have a p-multiplier of 1. Furthermore, if a pile is closer than 3.8 pile diameters to the MSE wall, the p-multiplier will be reduced linearly as shown in Figure 2-16. Results from these tests also indicate that induced reinforcement load increases as pile load increases, and as pile spacing and transverse distance from reinforcement to the pile decreases. Maximum wall deflections of less than 0.5 inches were measured for pile head loads of more than 50 kips and pile head deflections of 3 inches or more. This indicates that inextensible reinforcement is ideal to resist laterally loaded piles.

2.5 Limitations of Existing Research and Need for Additional Research

As indicated previously, this report addresses lateral loading of steel pipe piles at the 20-ft phase of the MSE wall. Additionally, lateral pile load tests have never before been performed near an MSE wall with an L/H ratio of about 0.7, which is typical of static loading conditions. This research will investigate the effects that an L/H ratio of 0.7 has on lateral resistance and p-multipliers.

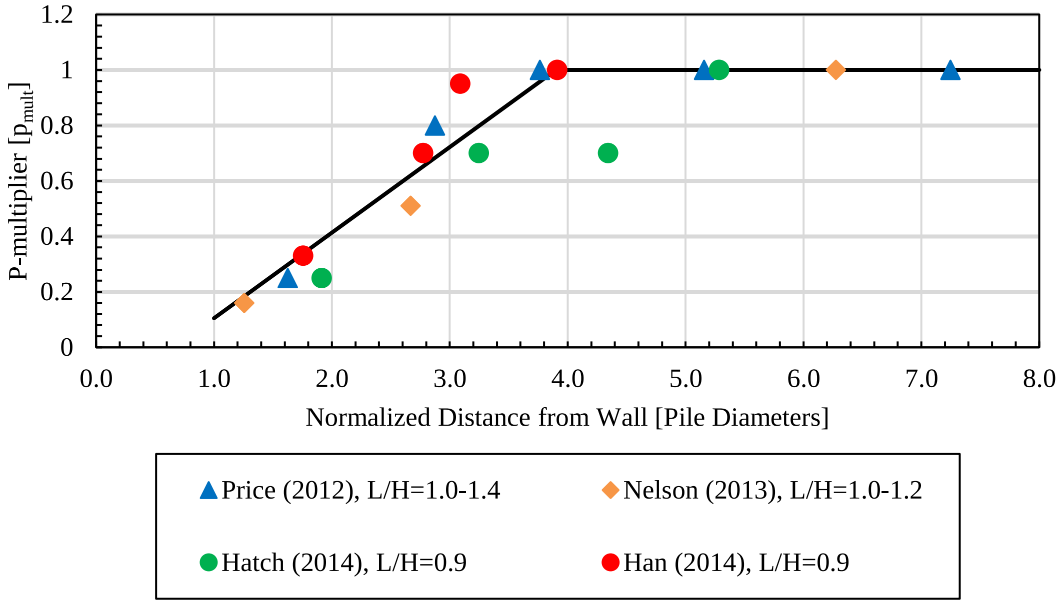

Figure 2-16: P-multiplier chart for steel pipe piles accounting for surcharge load.

3 TEST LAYOUT

Testing for this project was conducted on Geneva Rock property located on the south side of Point of the Mountain in Utah County, near Lehi, Utah. Coordinates for the site are 40.453194, -111.899304. The general site location and a close-up view of the site are shown in Figure 3-1.

Figure 3-1: Location of the project site (Google earth, 2015).

3.1 Site Preparation

Prior to site grading and wall construction, the test location consisted of an existing slope ranging between 3:1 (horizontal to vertical) and 5:1 in steepness. Grading of the site was completed using a CAT D9T bulldozer with built-in automatic leveling and elevation instrumentation. After initial grading of the staging area and project site was completed, a 2-foot-deep cut was excavated along the length of the wall face location to provide minimum embedment for the leveling pad and MSE wall. The cut was extended 25 feet back from the wall location with approximate cuts of 5 to 7 feet deep into the hillside near the reaction pile locations. Excess fill from the cuts was stored east of the site for later use. Site grading and cuts are shown in Figure 3-2.

Figure 3-2: Project site after completion of site grading.

3.2 Piles

Test piles for this site consisted of round A252-Grade 3 12.75x0.375 pipe piles, HSS 12x¼ square piles and HP 12x74 H-piles. All piles had a yield strength of approximately 57,000 psi. Round and square piles were donated by Atlas Steel and H-piles were donated by Skyline Steel and Spartan Steel.

A total of twenty-five 40-foot long steel piles were driven to a depth of 18 feet below grade prior to wall construction. A summary of the blow counts for the piles used in this study are located in Table 3-1 (see Appendix G for pile driving blowcounts for pipes with ribbed strip reinforcement). The piles were driven by Desert Deep Foundations using an ICE I-30V2 diesel hammer. The hammer was installed on tracks inside of a steel cage tower, aligned with the pile and held in place by a crane. Figure 3-3 shows the pile driving set up. All pipe and square piles were driven open ended and were plugged with soil during installation. Plugs ranged between 10.3 and 10.9 feet above the pile toe for the pipe piles used in this study. For the purposes of this research, the test piles were considered hollow.

Pile locations were designed and laid out to nominal distances of 2D, 3D, 4D and 5D from the back of the wall panel to the center of the pile where D is the outside diameter of the pile. Piles were spaced at 5 feet parallel to the wall. The actual normalized distances for piles 2D, 3D, 4D and 5D for the welded wire side are 1.8D, 3.4D, 4.3D and 5.2D, respectively. The actual horizontal spacing for the welded wire side between piles 2D, 3D, 4D and 5D are 5’5”, 4’7” and 4’7”, respectively. The actual normalized distances for piles 2D, 3D, 4D and 5D for the ribbed strip side are 1.7D, 2.8D, 2.9D and 3.9D, respectively. The actual horizontal spacing for the ribbed strip side between piles 2D, 3D, 4D and 5D are 5’2”, 4’11” and 5’0”, respectively. Normalized spacing varied from design values owing to construction tolerances when driving piles.

Additional test piles were driven behind the designed reinforced soil mass and used as control tests since they were not influenced by the proximity of the retaining wall. The control piles were also used to support the reaction beam during testing. Pile locations are shown in Figure 3-4.

Table 3-1: Blow counts (N) of driven pipe piles behind the SSL portion of the wall.

Depth (ft)	N (blow counts)			
	1.8D	3.4D	4.3D	5.2D
1				
2	1	1		
3	1	1		
4	1		2	1
5	1	1		
6	1	1		
7	3	1	2	2
8	3			
9	3			2
10	5		7	2
11	5		6	6
12	5		7	6
13	3		5	5
14	3	25	4	3
15	3	3		2
16	3		3	2
17	3		4	3
18	3	5	3	4
Total	47	38	43	38

Figure 3-3: Installation of piles using a diesel hammer.

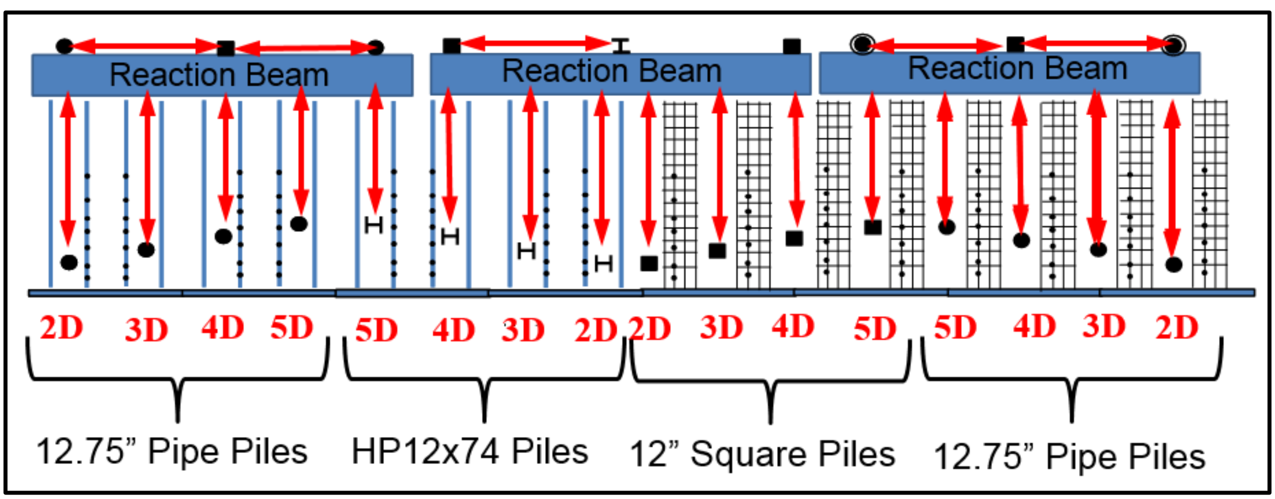

Figure 3-4: Plan view of pile locations.

3.3 MSE Wall

The MSE wall was designed according to the AASHTO 2012 LRFD code and completed in two phases. Phase 1 consisted of constructing the MSE wall to a height of 15 feet and testing select piles. At the completion of testing, Phase 2 began by resuming the wall construction to a final height of 20 feet and running similar testing as that in phase one. The elevation view for both phases is shown in Figure 3-5.

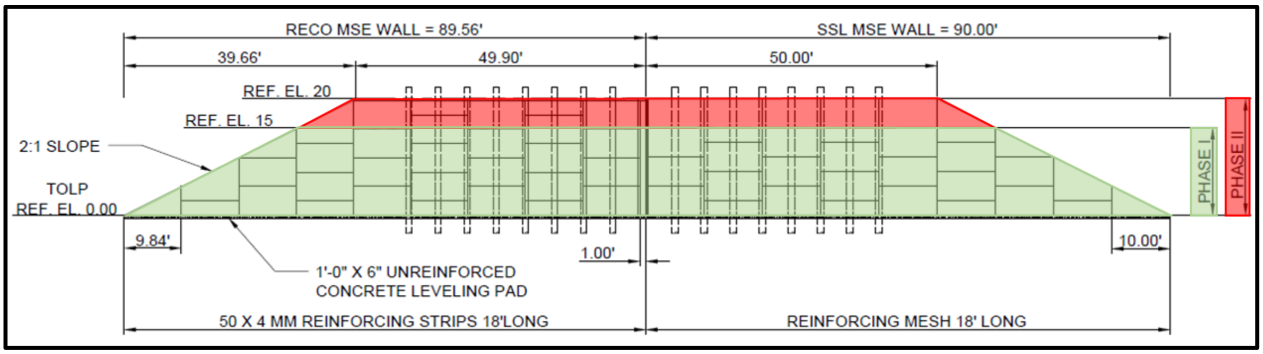

Figure 3-5: Elevation view of the MSE wall highlighting different phases of construction.

The MSE wall was constructed by Hadco, Inc. using two different wall systems. The eastern half of the wall consists of 50 feet of main wall and 40 feet of wing wall and was built using the SSL wall system. The SSL wall system consists of 5’x10’ reinforced concrete panels with textured facings (see Figure 3-7) and 18-foot long soil reinforcements. Reinforcements are attached to 0.75-inch loops in the wall by two W30 connector pins as shown in Figure 3-6. Welded wire reinforcements are spaced every 30 inches vertically and approximately every 60 inches horizontally. The number of longitudinal wires and transverse spacing in the reinforcement changes based on the reinforcement layer as shown in Table 3-2.

Table 3-2: Design details for the welded-wire grid reinforcement based on location from top of wall.

Grid Layer (From Top of Wall)	Depth From Top of Wall (in)	Longitudinal Wire			Transverse Wire	
		Number	Size	Spacing (in)	Size	Spacing (in)
1	15	6	W11	8	W11	6
2	45	5	W11	8	W11	12
3	75	5	W11	8	W11	12
4	105	5	W11	8	W11	12
5	135	5	W11	8	W11	12
6	165	6	W11	8	W11	12
7	195	6	W11	8	W11	12
8	225	6	W11	8	W11	12

*W11 wire has a diameter of 0.374 in.

Figure 3-6: Welded-wire grid reinforcement connected to wall loops by W30 pin connectors.

The western half of the wall entails 50 feet of main wall and 40 feet of wing wall and was built using the Reinforced Earth Company (RECO) wall system. The RECO wall system is comprised of 5'x10' reinforced concrete panels with smooth facings (see Figure 3-7) and 18-foot galvanized steel ribbed strip soil reinforcements connected to the wall panel with bolts, as shown in Figure 3-9. The strips were 0.16 inches thick and 1.97 inches wide (4 mm x 50 mm). Ribbed strip reinforcements are spaced 30 inches vertically and horizontally. Plan views for both wall systems are shown in Figure 3-10. A complete set of the SSL wall plans are included in Appendix B for reference.

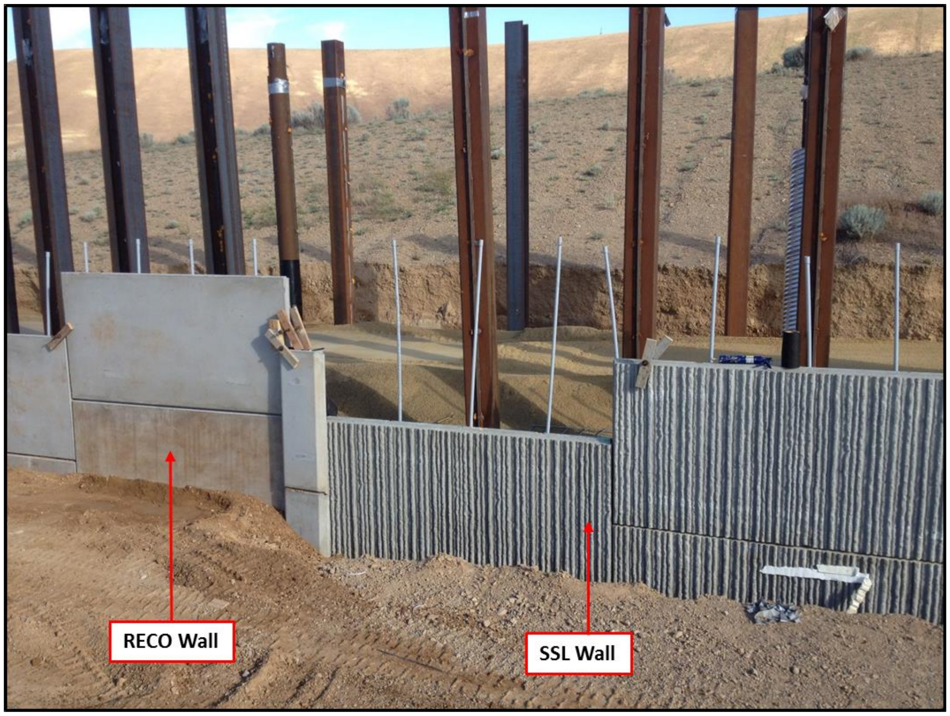

Figure 3-7: Different wall systems used for this project.

Figure 3-8: SSL galvanized steel welded-wire grid soil reinforcing layout with test piles.

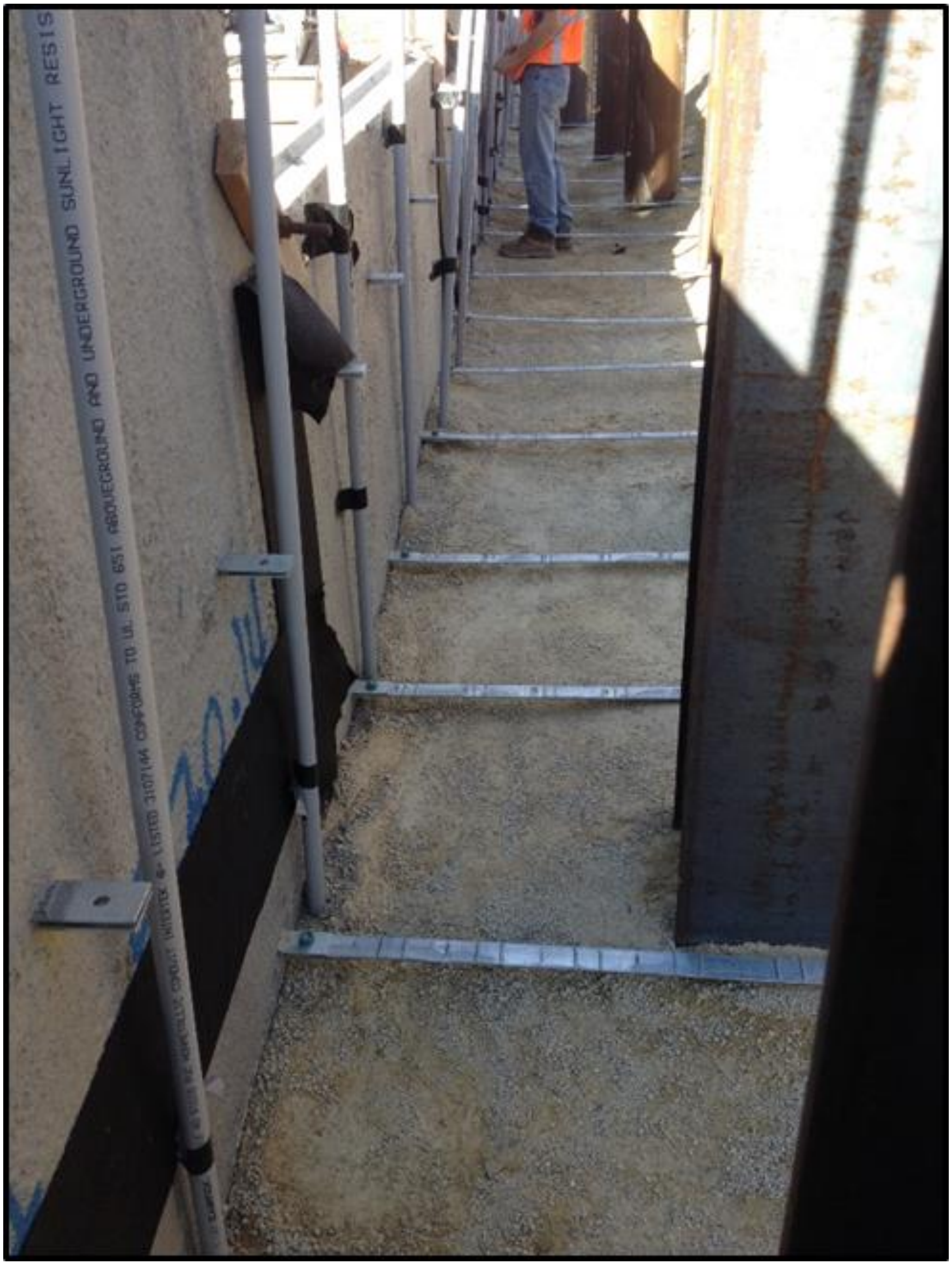

Figure 3-9: RECO steel ribbed strip soil reinforcing set up.

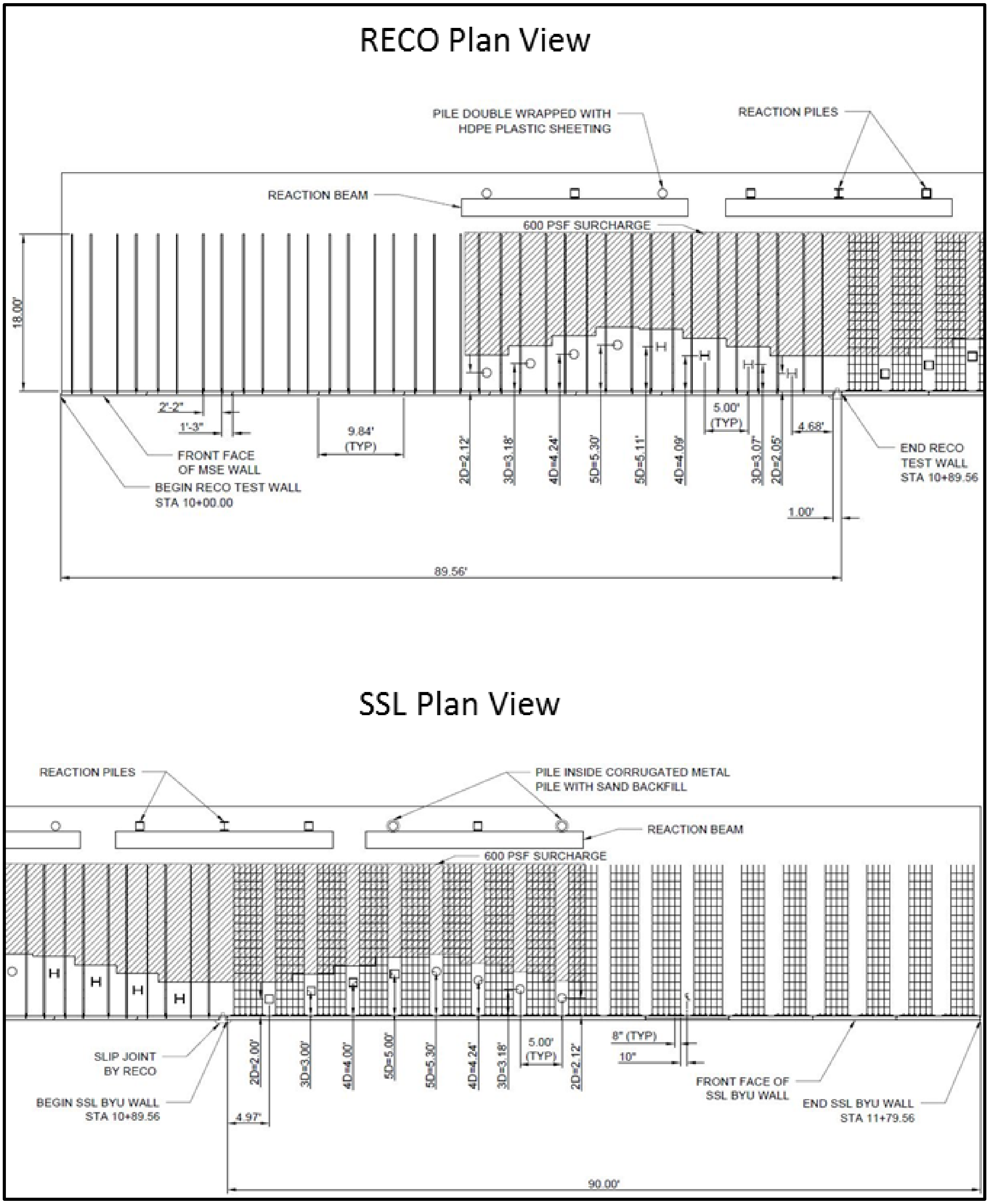

Figure 3-10: Plan view of the project.

3.3.1 Backfill

After the initial row of wall panels were leveled and installed, backfill was placed in 12-inch lifts behind the test piles as shown in Figure 3-11, and in 6-inch lifts between the test piles and the back of the wall. Prior to compaction, the backfill was moisture conditioned (see Figure 3-11) within 2 percent of optimum as determined by the Standard Proctor test.

Figure 3-11: (a) Backfill lifts behind test piles; (b) moisture conditioning of backfill.

Each lift was compacted using a vibratory roller compactor behind the test piles (see Figure 3-12), a vibratory plate compactor between the test piles and the back of wall, and a jumping jack compactor directly around test piles behind the reinforced zone as shown in Figure 3-13. After compaction of each lift, a nuclear density gauge, as shown in Figure 3-14, was used to obtain unit weights and moisture contents of the backfill to ensure consistent compaction.

Figure 3-12: Compaction of backfill behind the test piles using a vibratory roller compactor.

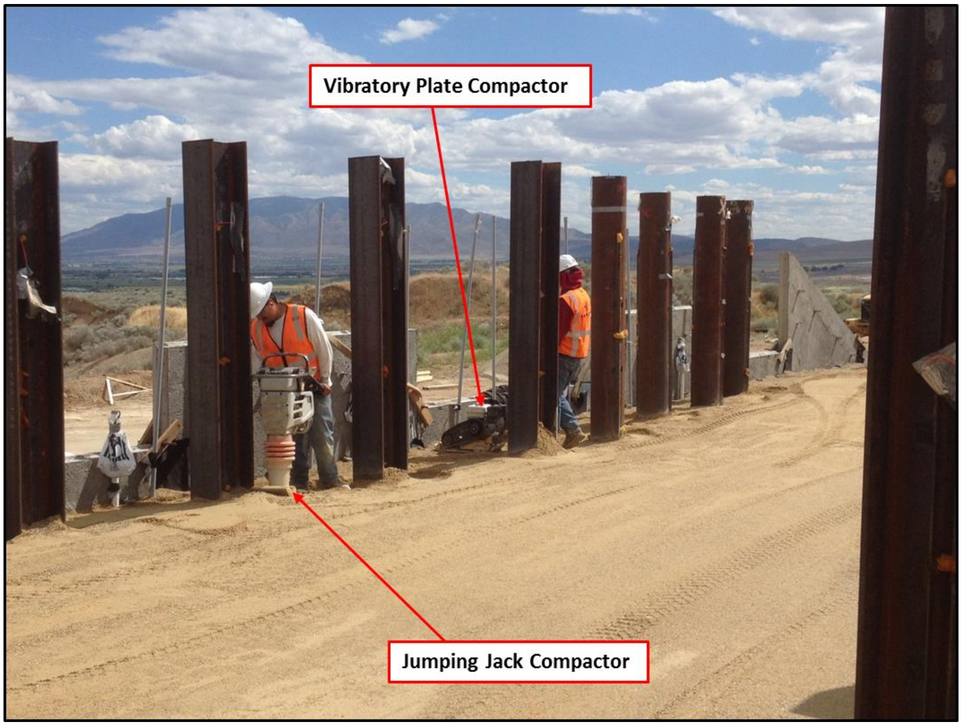

Figure 3-13: Compaction of backfill between the test piles and the back of wall using jumping jack and vibratory plate compactors.

Figure 3-14: Density and moisture testing of backfill using a nuclear density gauge.

Geneva Rock provided the backfill, which was classified as AASHTO A-1-a material and as a silty sand with gravel (SP-SM) according to the Unified Soil Classification System (USCS). The backfill for Phase 1 had a standard proctor density of 128.0 pcf and an optimum moisture content of 7.8%. The backfill for Phase 2 had a standard proctor density of 126.7 pcf and a calculated optimum moisture content of 9.7%. Test results of the backfill properties are included in Appendix C. The target density for the compacted backfill was 95% of standard proctor. Actual average moisture contents were 6.0% behind the test piles and 5.2% between the test piles and the back of wall, as shown in Figure 3-15. The actual average relative compaction of the backfill was approximately 96% in the fill behind the test piles and approximately 92% between the test piles and back of wall, as shown in Figure 3-16. Lower compaction between the wall and piles is typical in normal MSE wall construction because it is difficult to get compaction in small or confined areas and heavy compaction is likely to displace the wall panels laterally. Compacted backfill properties are shown in Table 3-3 and Table 3-4 and also include the standard deviation and coefficient of variation for each data set.

Table 3-3: Backfill properties between test piles and back of MSE wall.

	Moisture Content [%]	Dry Unit Weight [pcf]	Moist Unit Weight [pcf]	Relative Compaction [%]
Average	5.2	116.7	122.8	91.8
Standard Deviation	1.58	3.22	3.76	2.78
Coefficient of Variation	0.303	0.028	0.031	0.030

Table 3-4: Backfill properties behind the test piles.

	Moisture Content [%]	Dry Unit Weight [pcf]	Moist Unit Weight [pcf]	Relative Compaction [%]
Average	6.0	122.8	130.1	96.4
Standard Deviation	1.66	2.64	3.14	2.32
Coefficient of Variation	0.276	0.021	0.024	0.024

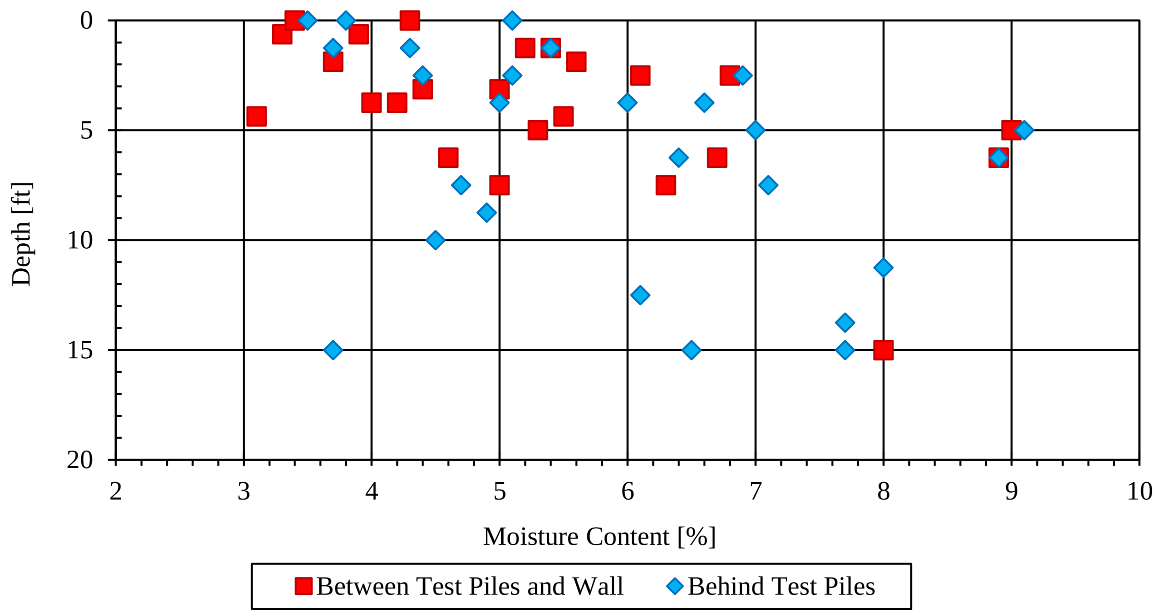

Figure 3-15: Measured moisture content of backfill.

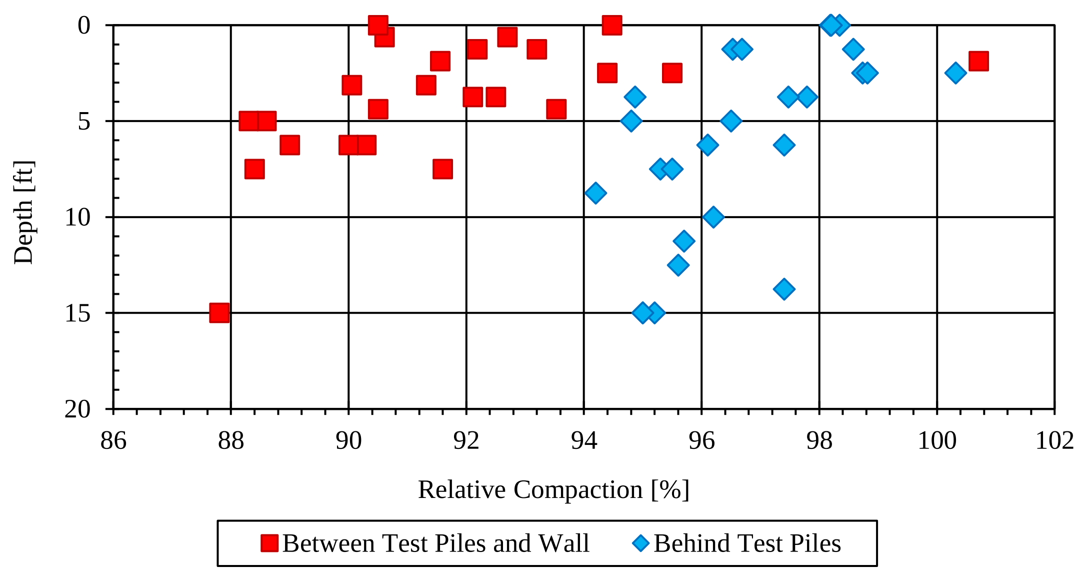

Figure 3-16: Measured relative compaction of backfill.

3.3.2 Surcharge

Prior to pile load testing, concrete blocks with dimensions of 2’x2’x6’ were placed on either side of the test pile and load apparatus to induce a surcharge load representative of the weight of the abutment and approach fill at a typical bridge abutment. The concrete blocks were typically placed 3 blocks wide, 2 blocks high and 2 blocks deep as shown in Figure 3-17. The area of surcharge covered approximately 12 feet directly behind the pile and approximately 6 feet to either side perpendicular to the load apparatus with a gap approximately one foot wide to accommodate the loading strut. The surcharge created by the concrete blocks simulates a portion of the abutment wall and backfill about 5 ft high with an overall unit weight of 120 pcf.

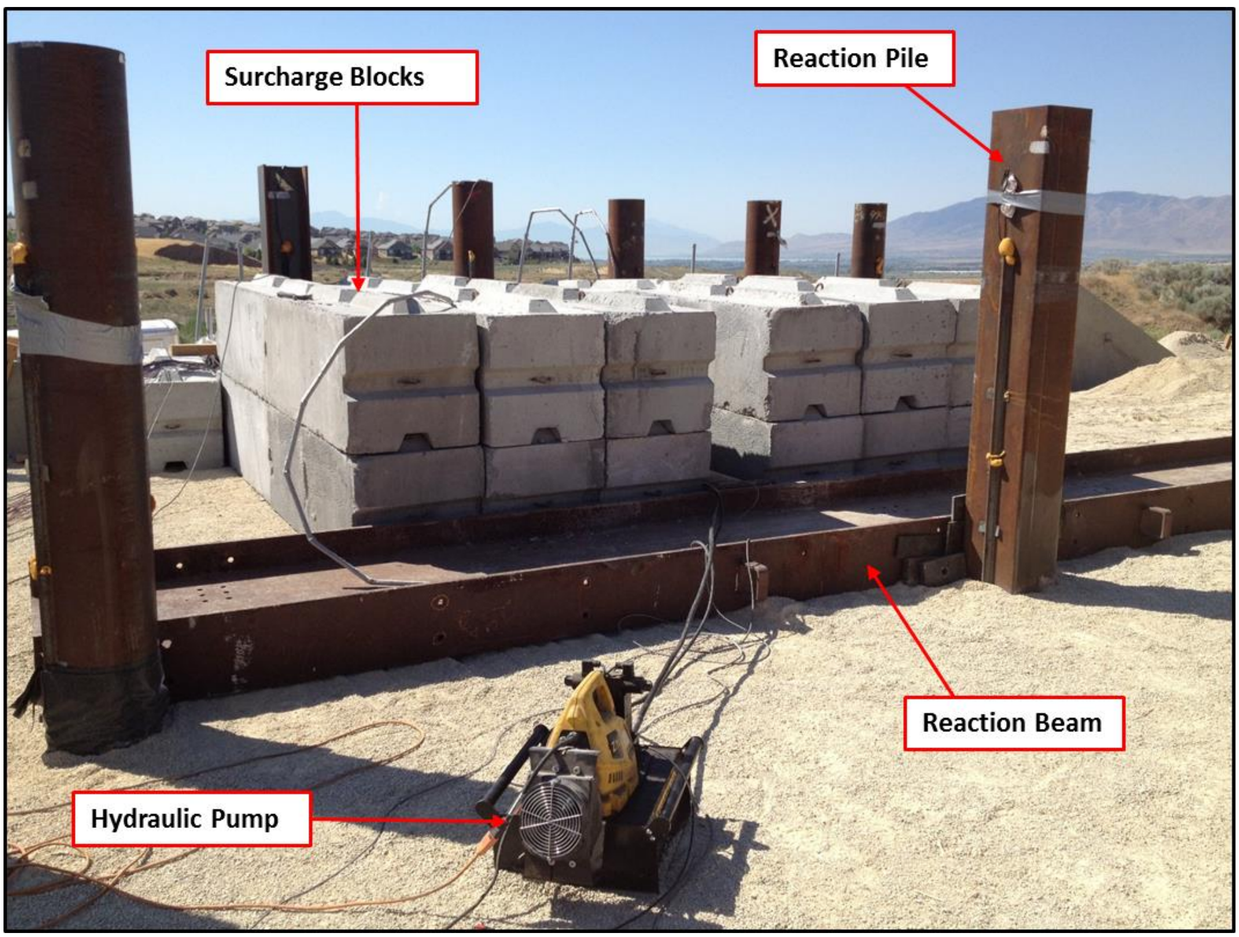

Figure 3-17: Typical set up for pile load testing.

3.4 Loading System

As mentioned in section 3.2, piles were installed behind the reinforced earth mass to support the reaction beam during load testing of the piles as shown in Figure 3-17. Therefore, the load applied to the test pile did not influence the load in the reinforcements. A load apparatus was then set in place to connect the test pile with the reaction beam. The apparatus, beginning closest to the test pile, consisted of an inline load cell, a hydraulic jack and steel strut as shown in Figure 3-18.

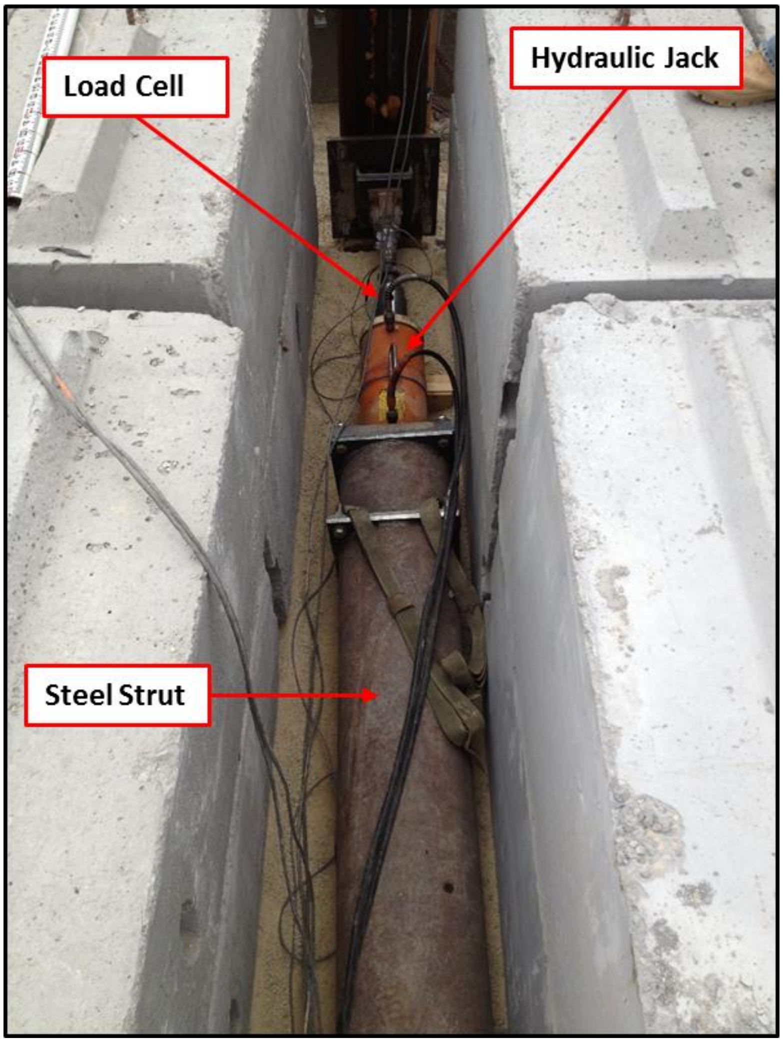

Figure 3-18: Load apparatus configuration.

Each test pile had a steel C-channel welded to the pile at approximately one foot above the ground surface which allowed for a flat surface to apply the load. The C-channel was connected with an inline load cell, which was attached to the hydraulic jack. A hydraulic pump, as seen in Figure 3-17, was also attached to the hydraulic jack via hydraulic hoses to regulate load pressures. Both a pressure transducer on the hydraulic pump and inline load cell were used to measure loading throughout the testing of the pile. Any remaining space between the hydraulic jack and the reaction beam was filled with steel struts and steel plates.

4 INSTRUMENTATION

A variety of instruments were used at each test pile to measure the applied load, deflection, strain and rotation on the pile as well as wall deflection, ground displacement and strain in the soil reinforcements. This chapter discusses the layout and instruments used to obtain data on this project.

4.1 Load Cell and Pressure Transducers

An in-inline load cell and pressure transducer were used to measure the applied load on the pile. The load cell was located between the pile and the hydraulic jack. The pressure transducer was attached to the hydraulic pump. Readings for the pressure transducer and load cell were collected at a rate of 2 readings per second by an Optima Electronics Corp. MEGADAC 5414AC (MEGADAC) data collector. Although loads from both instruments were recorded, they did not correlate with one another. Lab testing verified that the load cell was giving erroneous readings, most likely due to eccentric loading. As a result, the data collected from the pressure transducer was used for the data analyses for each pile discussed in this report.

4.2 String Potentiometers

String potentiometers were used to measure pile head displacement and rotation, wall displacement and horizontal ground displacement. Data from the string potentiometers was collected at a rate of 2 readings per second and stored in the MEGADAC data collector.

As shown in Figure 4-1, string potentiometers were attached to a 2x4 that was clamped to a wooden 4x4 independent reference beam. The reference beam was strapped on each end to stationary concrete blocks that were located outside of the testing area of influence (typically > 6 feet from the test pile). Pile head deflection was measured by connecting a string potentiometer to an eyebolt that was magnetically attached to the side of the pile at the same elevation as the applied load. Another string potentiometer was connected to an eyebolt 3 feet above the first by clamping a 2x4 to the side of the pile. Pile head rotation was calculated by taking the difference of the pile head deflections at the load point and 3 feet above the load point and using trigonometry to find the angle at which the pile head was rotated.

Horizontal ground displacement was measured by connecting string potentiometers to steel stakes that were driven into the ground as shown in Figure 4-2. Stakes were typically spaced at 1-foot intervals from the front face of the pile. Horizontal displacement was measured by taking the difference of the initial and measured values recorded from the string potentiometers. Wall displacement was measured by installing an eyehook into the top of the concrete wall panel directly in front of the pile and connecting a string potentiometer to the eyehook. The difference of the initial and measured values were taken to find the wall displacement at any given load.

Vertical ground displacement was measured using a survey level and rod. Elevation measurements of the ground surface were taken before and after the pile load tests at 1-foot intervals from the pile face.

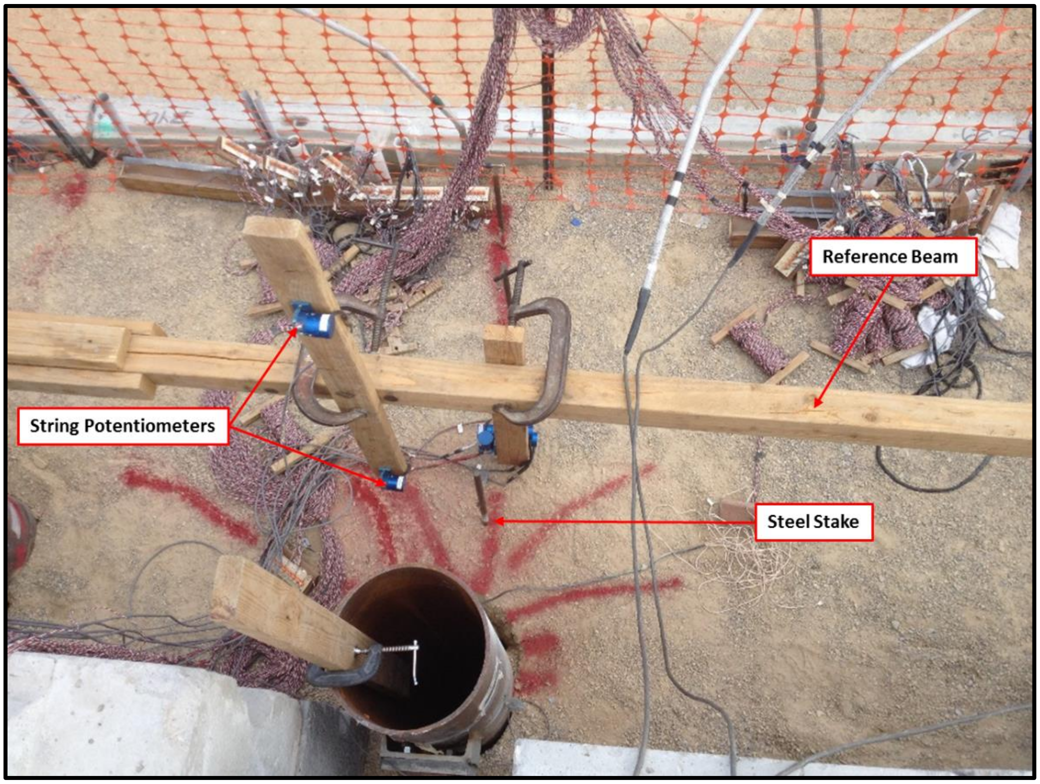

Figure 4-1: Instrumentation setup of a typical pile load test.

Figure 4-2: Horizontal ground displacement setup.

4.3 Strain Gauges

Strain gauges were installed on the soil reinforcing and test piles to determine tensile force and bending moment, respectively. The following two sections discuss the installation and configuration of the strain gauges to the soil reinforcement and piles, respectively.

4.3.1 Soil Reinforcement Strain Gauges

Electrical resistance strain gauges were installed on the reinforcement at BYU facilities prior to shipping them to the project site. For the welded wire reinforcement, strain gauges were placed on the second longitudinal wire from the right, as shown in Figure 4-3, at increments of 0.5, 2, 3, 5, 8, 11, and 14 feet from the back of the wall face. The ribbed strips also had strain gauges installed at increments of 0.5, 2, 3, 5, 8, 11, and 14 feet from the back of the wall face. To minimize bending effects, a strain gauge was placed on the top and bottom of the reinforcement at each distance interval. The strain gauges were attached with epoxy and protected by wrapping the lead wires in electrical tape and securing them to the sides of the reinforcement as shown in Figure 4-3 for welded wire grids. To minimize damage, the lead wires were run through a PVC conduit attached vertically to the back face of the wall panel and connected to terminal strips at the ground surface, as shown in Figure 4-4. The terminal strips were directly connected to the MEGADAC data collector during pile testing.

The top 4 layers of soil reinforcing were instrumented with strain gauges. Each layer had one grid on each side of the test pile that was connected to the data collector during pile load testing. Table 4-1 shows the soil reinforcement configuration for each test pile for the welded wire grids. For the ribbed strip reinforcement, each layer had two strips instrumented on the same side for each pile tested (between piles 1.7D and 2.8D and between piles 2.9D and 3.9D). Table 4-2 shows the soil reinforcement configuration for each test pile for the ribbed strips.

Figure 4-3: Typical strain gauge setup for a welded-wire grid layer.

Figure 4-4: Strain gauge connections to terminal strips.

Table 4-1: Transverse distance from pile center to instrumented longitudinal bar on the reinforcing (looking in the direction of loading (South).

	Layer Depth (in)							
	15		**45**		**75**		**105**	
Test	Left	Right	Left	Right	Left	Right	Left	Right
1.8D	17.5	42	-	43	22	43	17	35
3.4D	24.5	43	23	37.5	23	38	31	38
4.3D	17.5	40.5	18.5	33.5	17.5	34.5	19	34
5.2D	15	46.5	22.5	38.5	21.5	46	23	39

* The grid left of the 1.81D pile in Layer 2 was not instrumented.

Table 4-2: Reinforcement number and horizontal distance from pile center to reinforcement center for all instrumented soil reinforcements

	Layer Depth							
Test	**15 in**		**45 in**		**75 in**		**105 in**	
1.7D	21 - 9.5in	22-35.0in	20-11.0in	19-37.5in	1 - 9.0in	2-36.0in	10 - 9.0in	9 - 35.0in
2.8D	22-24.5in	21-50.0in	19-20.5in	20-47.0in	2-22.5in	1-49.5in	9 - 23.5in	10-50.0in
2.9D	23-10.0in	24-35.5in	18-12.0in	17-38.0in	5-11.5in	6-37.0in	13-10.5in	12-38.0in
3.9D	24-26.0in	23-51.0in	17-22.5in	18-49.0in	6-24.5in	5-50.0in	12-24.5in	13-51.5in

4.3.2 Pile Strain Gauges

Waterproof electrical resistance strain gauges were installed on the test piles prior to shipping them to the project site. Strain gauges were placed on each side of the pile for redundancy at depths of 4, 6, 8, 11, 14, 17 and 20 feet below the top of the pile, or 2, 4, 6, 9, 12, 15 and 18 feet below the load point. The strain gauges were attached with epoxy and further protected from the elements by spraying foam insulation around the gauges and wires, then covering them with angle iron. The angle iron was tack welded onto the pile between strain gauge locations and acted as protection during pile driving (see Figure 4-5). Lead wires were bundled in bags and taped near the top of the pile for transportation and pile driving. Wires that were sheared or damaged prior to testing were repaired to the extent possible. However, some strain gauges were inevitably bad or malfunctioning and were removed from calculations during the data analyses. The pile strain gauges were connected to terminal strips, as shown in Figure 4-5, which directly connected to the MEGADAC data collector during testing of the piles.

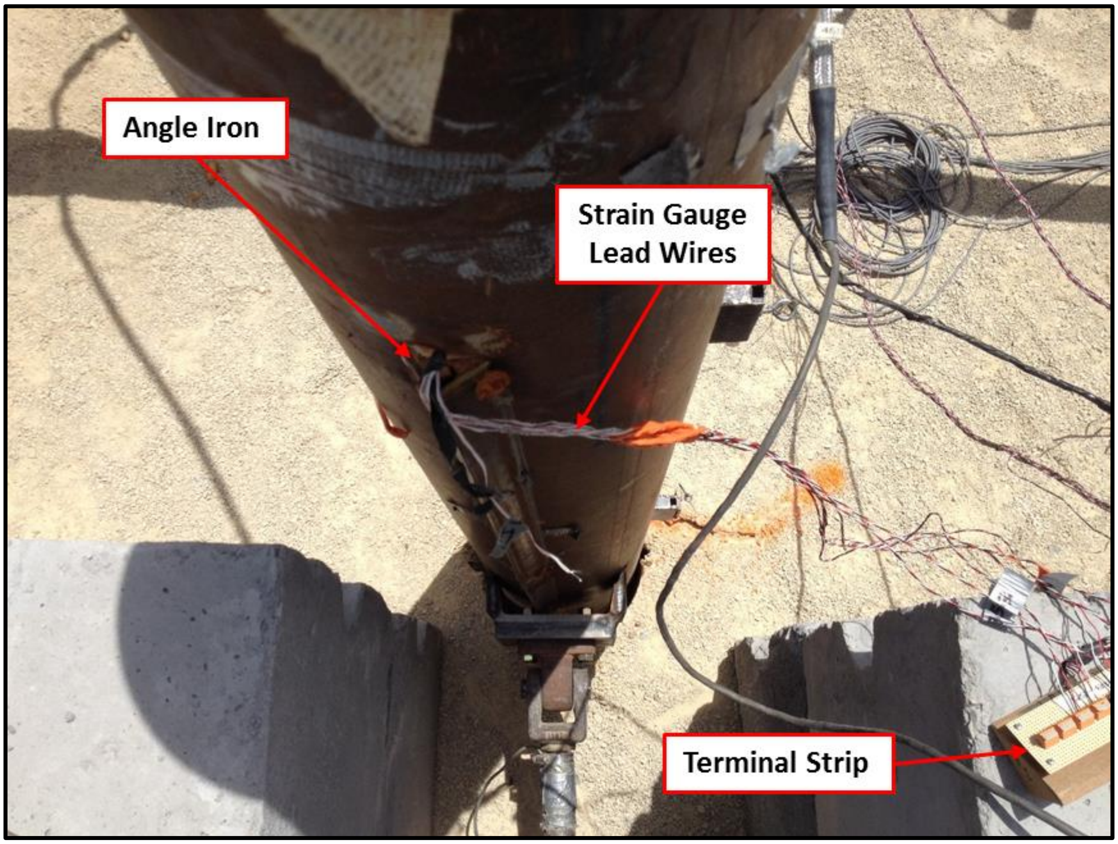

Figure 4-5: Typical pile instrumentation setup.

4.4 Shape Arrays

Four high-bandwidth Measurand® Shape Accel Arrays (Shape Arrays) were used on this project to measure horizontal wall deflection. Shape Arrays are similar to inclinometers but can measure much larger deformations and have the ability to be placed horizontally to measure vertical deformation. They are designed to collect high frequency data from all sensors continuously. The outer shell of a Shape Array consists of two layers of braided stainless steel which provide twist resistance and pull strength.

Prior to testing, the Shape Arrays were calibrated at BYU and transported to the test site. The Shape Arrays were placed inside 1.05-inch inside-diameter PVC conduit which had previously been installed vertically on the back of the wall panels. Generally, four vertical arrays were installed for each test. One array was installed approximately in front of the test pile while the others were spaced at varying distances to the side, as shown in Table 4-3. Each Shape Array consists of 24 segments that are each 1-foot long. Each foot-long segment is connected by joints and contains 3 MEMS accelerometers which measure tilt along the x, y and z axes. During testing, the accelerometers continuously send signals to the computer running Measurand SAA Recorder software. Typically, two sets of data were collected at each load deflection interval.

Table 4-3: Transverse distance (in inches) from the center of pile to the Shape Array.

	Array Number			
Test	**45104**	**45112**	**45115**	**45134**
1.8D	32.5	5	38	56.5
3.4D	34	72	105	10
4.3D	51	26	11	7
5.2D	92	6	34	62

4.5 Digital Imagery Correlation

Digital Image Correlation (DIC) is a 3D, full-field optical system that can measure deformation and strain on most materials. DIC was proposed in the early 1980s for solid mechanics applications and many of the procedures used today are direct results of early development in fluid mechanics (Hild). Tests can be applied to large or small areas and can be compared with other testing methods for accuracy (Measurement Principles of DIC). Hundreds to thousands of visible points are placed on an object and allow cameras to identify specific locations throughout the test period. During image evaluation, the images are divided into small local facets as shown in Figure 4-6. The position of the cameras in relation to one another is calculated when the system is calibrated and pixels within each facet are tracked. This information allows a correlation algorithm to be used to calculate the three dimensional position of each point from which contours of displacement, deformation, and strain on the wall can be determined. The system is sensitive to measurements down to 1/100,000 of the field of view (Measurement Principles of DIC).

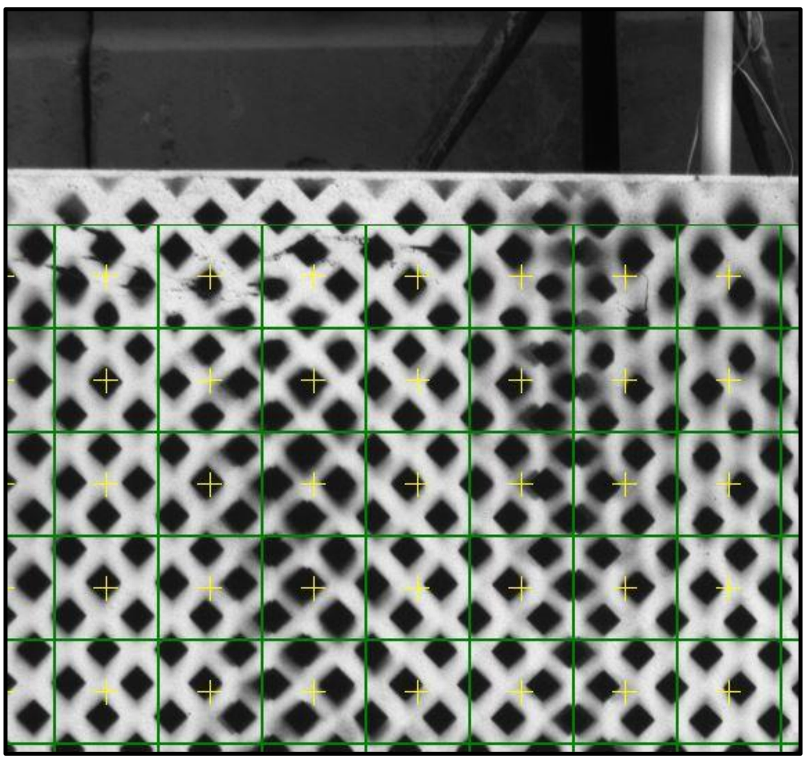

Figure 4-6: Example of facets in the DIC evaluation process.

The system setup for this project was the Q-400 DIC Standard 3D manufactured by Dantec Dynamics and included two cameras on a tripod connected to a computer running ISTRA-4D software, version 4.4.1, as shown in Figure 4-7. A black and white grid pattern was painted onto the wall surface to increase contrast and to make up the visible points required by the DIC system. Prior to load testing, the system was calibrated using a black and white checkered board. This required taking multiple images of the board at different angles at a distance similar to that during testing. Camera angle, shutter speed and focus were all adjusted during the calibration process. Cameras were spaced approximately 25 feet from the wall face and centered on the test pile. Video images were typically focused on a 10-ft-high by 12-ft-wide area near the top of the wall.

During pile load testing, images were captured directly after and 5 minutes after each pile load increment. A total of 25 to 30 images were taken for each pile load test. Images were later evaluated using the ISTRA-4D software to determine wall deflection and provide contours of deflection.

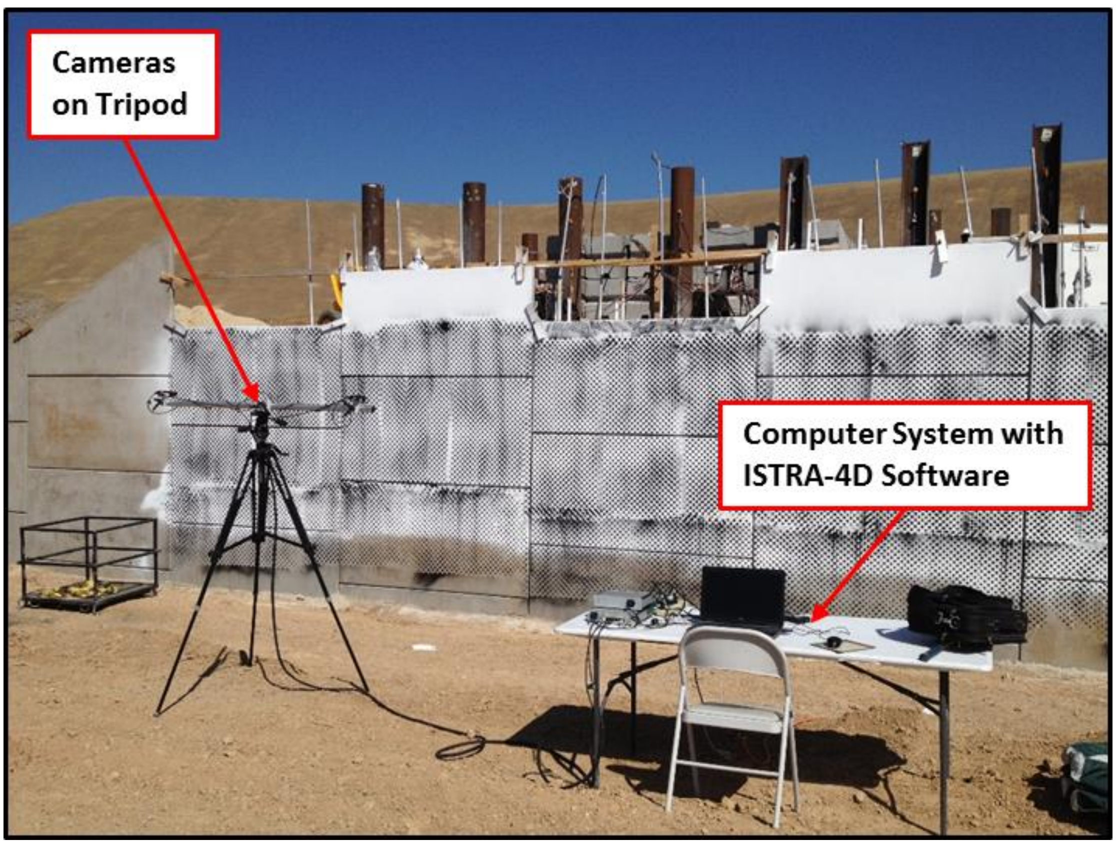

Figure 4-7: Typical DIC test setup.

5 LATERAL LOAD TESTING FOR WELDED WIRE REINFORCEMENT

Lateral load testing of the round piles adjacent to the 20-foot tall MSE wall with welded-wire reinforcement took place between August 7 and August 11, 2014. Prior to loading the four test piles, a reaction pile located outside of the reinforced mass but still within the compacted backfill was tested parallel to the MSE wall and used as a reference for the 5D pile. Testing was performed on all piles using a displacement control method in which load was applied to induce pile head deflection in 0.25-inch increments. Load was applied at a height of one foot above the ground surface and each pile was loaded up to a maximum of 3 inches of displacement. At each displacement increment fluid flow into the jack was locked off for 5 minutes while the pile load and deflection came to equilibrium. Readings were taken at the peak load, the 1-minute hold and the 5-minute hold. Typically, pile head load decreased rapidly from the peak load to the 1-minute hold then decreased very slowly to the 5-minute hold while deflection remained relatively constant. The peak load is most likely to simulate rapid loading such as that produced by earthquakes while the 1-minute and 5-minute holds are more demonstrative of static loading conditions.

5.1 Load Displacement Curves

Load displacement curves for the four test piles near the MSE wall and the companion test pile or “reaction pile” away from the wall are shown in Figure 5-1 through Figure 5-3 for the peak load, the 1-minute hold and the 5-minute hold, respectively. Loads were measured using a pressure gauge on the hydraulic pump. Deflections were measured using the string potentiometer attached to the pile at the load elevation and connected to an independent reference frame. The measured load-deflection curve for the 1-minute and 5-minute holds were obtained by averaging the 30 seconds of load right after the hold interval. Load-deflection curves for individual test piles of the average peak, 1-minute hold and 5-minute hold are located in Appendix D for reference.

The load-deflection curves shown in these figures indicate that the lateral resistance generally decreases as the distance between the pile and wall decreases. The reaction pile and the 5.2D pile should in theory have similar load-deflection curves. However, the 5.2D pile has approximately 73% of the resistance of the reaction pile. This is most likely due to the compaction differences between the two piles. The backfill around the reaction pile was compacted with a roller compacter and had an average relative compaction of 96.4%, whereas the backfill between the 5.2D pile and the wall was compacted with a vibratory plate compacter and had an average relative compaction of 91.8% (see Table 3-3 and Table 3-4). Lower pile loads on the 4.3D test were likely caused because the hydraulic pump was malfunctioning for the first half of the test. Once the pump was fixed, the pile was reloaded to 1.5 inches of deflection because it is difficult to reapply load and get virgin load-deflection responses. Loads from 0 to 1.5 inches of deflection were recorded much lower than what was actually produced. Therefore, load points between 1.0 to 1.5 inches of deflection were interpolated and manually adjusted, but all points between 0 and 1.5 inches of deflection are likely still lower than actual loads induced on the pile. Corrections to 4.3D are addressed further in Chapter 6.

Generally, the 5.2D and 4.3D piles develop very similar lateral resistance for a given deflection suggesting that neither pile is significantly affected by the presence of the wall or that the reinforcements are retaining the soil sufficiently so that lateral resistance is not reduced at these larger pile spacings. However, for the piles spaced at 3.4D and 1.8D the lateral resistance typically decreases by 21% and 51%, respectively, relative to the pile at 5.2D spacing. In general, the average decrease in lateral resistance at 3 inches of deflection from peak load to 1-minute and 5-minute holds is 7% and 10%, respectively.

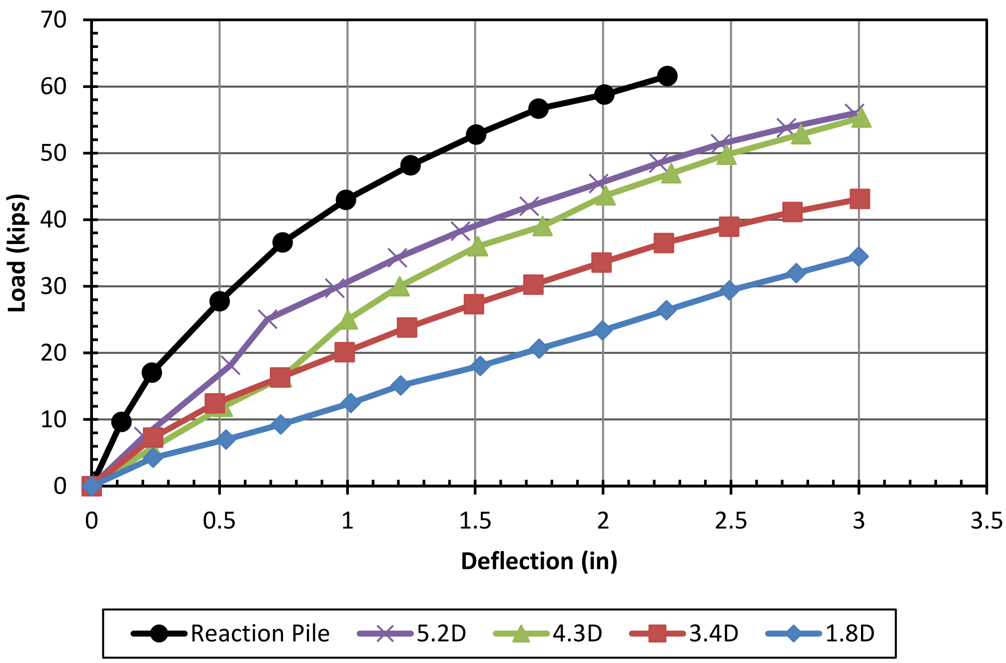

Figure 5-1: Pile head load versus pile head deflection for the average peak load.

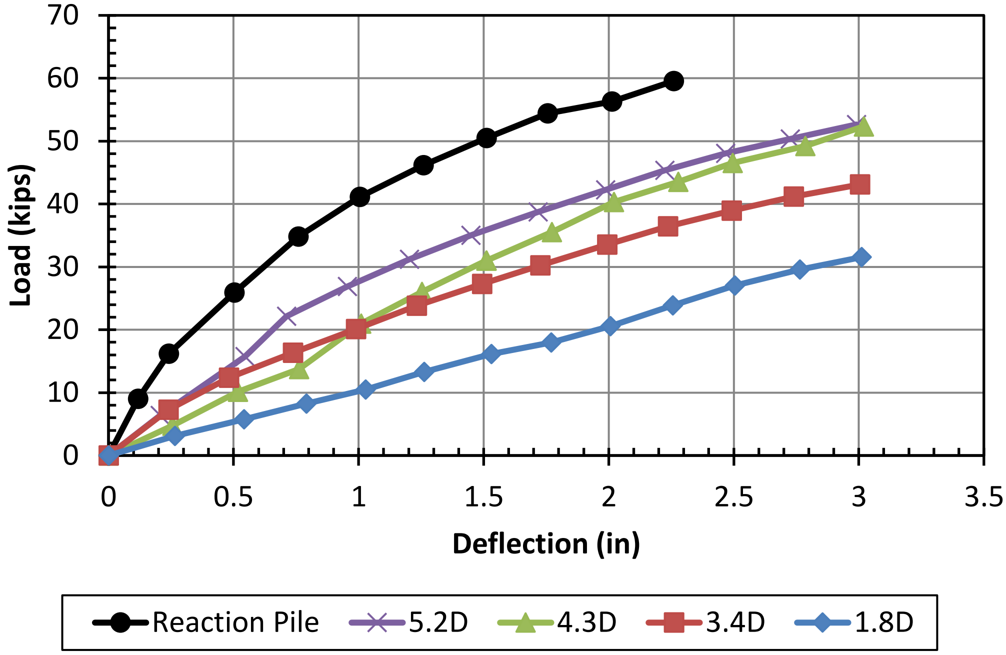

Figure 5-2: Pile head load versus pile head deflection for the 1-minute hold.

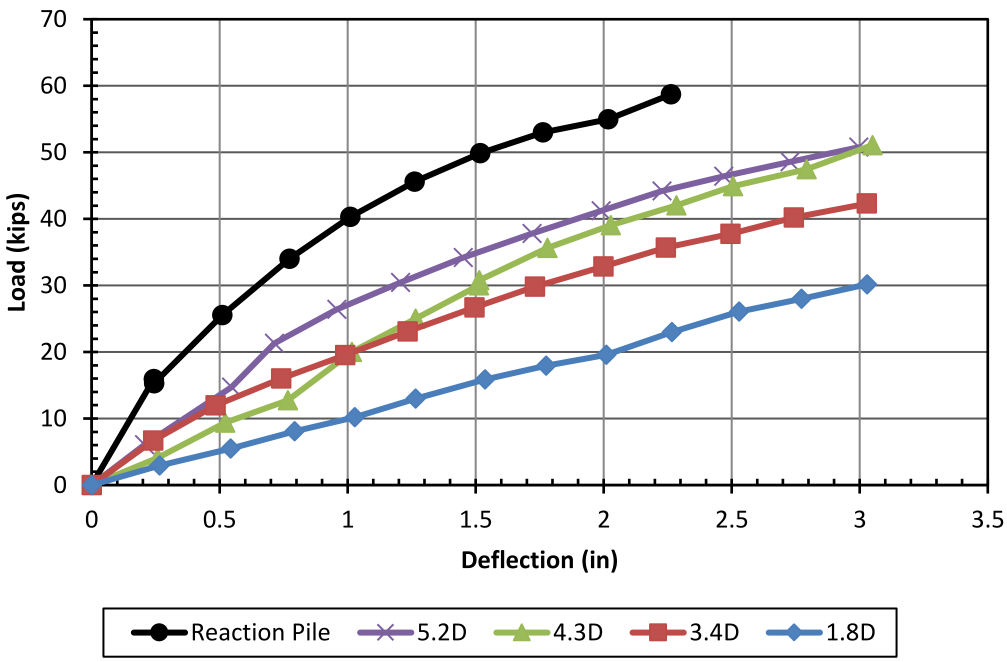

Figure 5-3: Pile head load versus pile head deflection for the 5-minute hold.

5.2 Pile Head Rotation

Pile head load versus pile head rotation for each test pile is shown in Figure 5-4. Pile head rotation, θ, in degrees was calculated using the equation:

$$\boldsymbol{\theta = sin^{-1}\left(\frac{d_{3ft} - d_{lp}}{36\ in}\right)} \quad \textbf{(5-5)}$$

where

θ is the pile head rotation,

d_{3ft} is the pile displacement 3 feet above the load point, and

d_{lp} is the pile displacement at the load point.

String potentiometer measurements and pile head loads were taken at the one-minute hold reading for each pile. As would be expected, the pile head rotation increases as the pile head load increases for each test pile. Typically, for a given load, the pile head rotation increases as the pile spacing decreases. This is most likely because the soil resistance decreases as the pile spacing decreases allowing the pile greater resistance to bending. As discussed previously, the 4.3D pile test experienced a loss of power to the hydraulic jack during testing and certain data points read very low and were adjusted based on other data points for that test and the typical curve from other test piles. At larger deflections, the load-rotation curves for the 4.3D pile is similar to that for the 5.2D pile as was the case for the load-deflection curves discussed previously. This result again suggests that there is little variation in lateral soil resistance for these two piles.

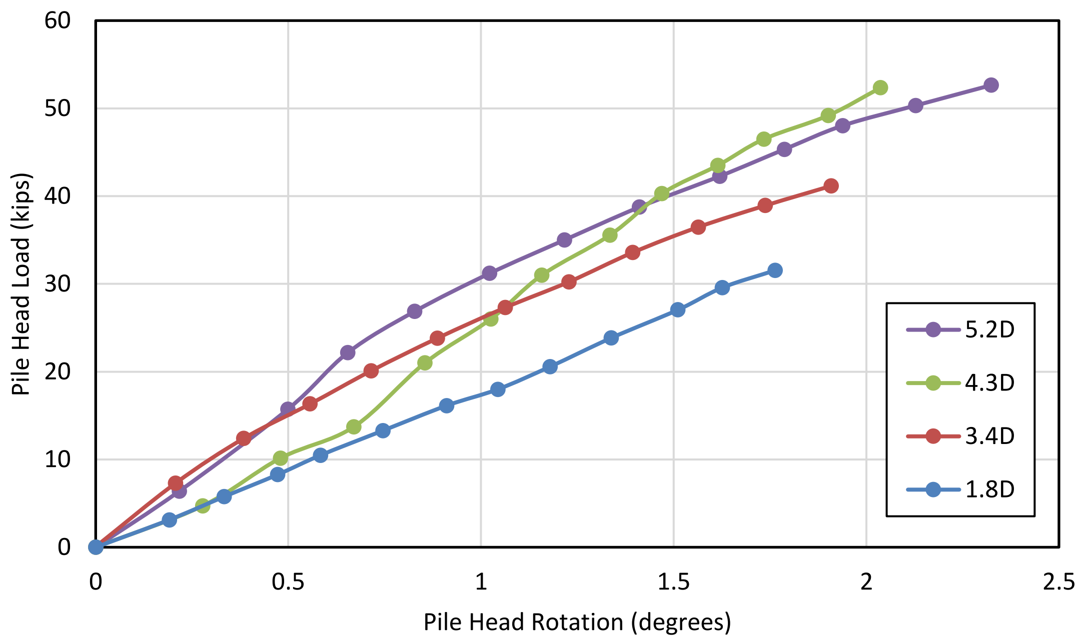

Figure 5-4: Pile head load versus pile head rotation for each test pile.

5.3 Soil Reinforcement Performance

As described previously, strain gauges were attached to the top and bottom of the welded-wire grid reinforcements and placed at intervals of 0.5, 2, 3, 5, 8, 11 and 14 feet from the back face of the wall (see section 4.3.1). The data collected from the strain gauges at each interval were averaged and used to calculate the load induced in the reinforcement. At certain intervals, one or sometimes both strain gauges were damaged or not working properly. For instances where only one gauge was working, that strain value was generally used in the calculations. When both strain gauges were damaged, the interval was omitted. Equation 5-1 was used to calculate the induced reinforcement load as follows:

$$T_i = EA(\mu\varepsilon_i - \mu\varepsilon_0)(10^{-6})B \tag{5-1}$$

where

T_i is the induced tension in kips for the entire welded-wire grid at the i^{th} data point,

E is the modulus of elasticity of the steel (29,000 ksi),

A is the cross-sectional area (in.^{2}) of the instrumented wire,

$\mu\varepsilon_i$ is the average micro strain for the i^{th} data point,

$\mu\varepsilon_0$ is the average initial micro strain, and

B = n-1 where n is the number of longitudinal bars on the reinforcement grid.

An example of the load distribution induced in the soil reinforcement behind the back of the MSE wall is shown in Figure 5-5 through Figure 5-8. Figure 5-5 and Figure 5-6 show tensile force distributions in layer L4 (approximately 105 inches below ground surface) during the lateral load test on the pile at 3.4D. These figures illustrate the similarities in the induced reinforcement loads when the transverse spacings (38 and 31 inches) are similar. Figure 5-7 and Figure 5-8 are of the 5.2D pile at layer L3 (approximately 75 inches below ground surface) measuring strain from a near and far transverse distance and illustrate the differences in the induced reinforcement loads when the transverse spacings (46 and 21.5 inches) vary. Typically, peak reinforcement loads increase as transverse spacings decrease. Figure 5-7 and Figure 5-8 also show that peak loads occur nearer to the pile face as transverse distance to the pile decreases, and farther in front of the pile face as the transverse distance increases. Because shear forces act to the side and front of the pile during loading, it makes sense that peak loads occur farther in front of the pile with increased transverse spacing of the reinforcement.

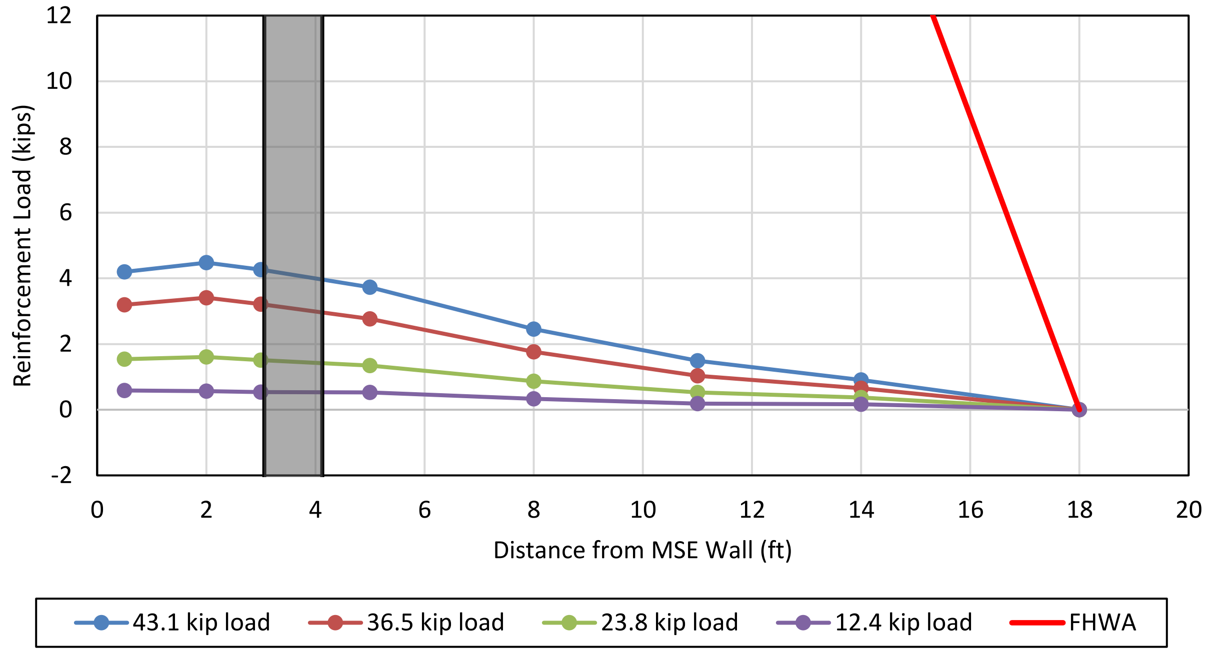

Figure 5-5: Induced loads in the soil reinforcement at different pile head loads relative to distance from the back of the MSE wall (3.4D pile, layer L4, 38 in. transverse spacing).

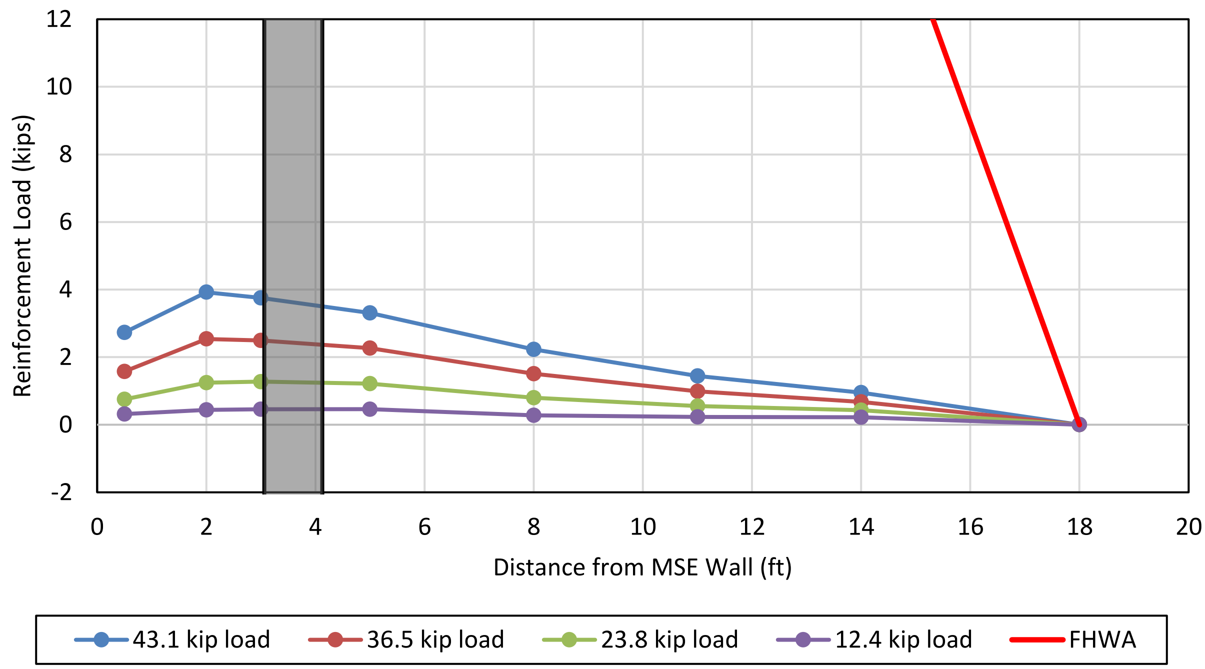

Figure 5-6: Induced loads in the soil reinforcement at different pile head loads relative to distance from the back of the MSE wall (3.4D pile, layer L4, 31 in. transverse spacing).

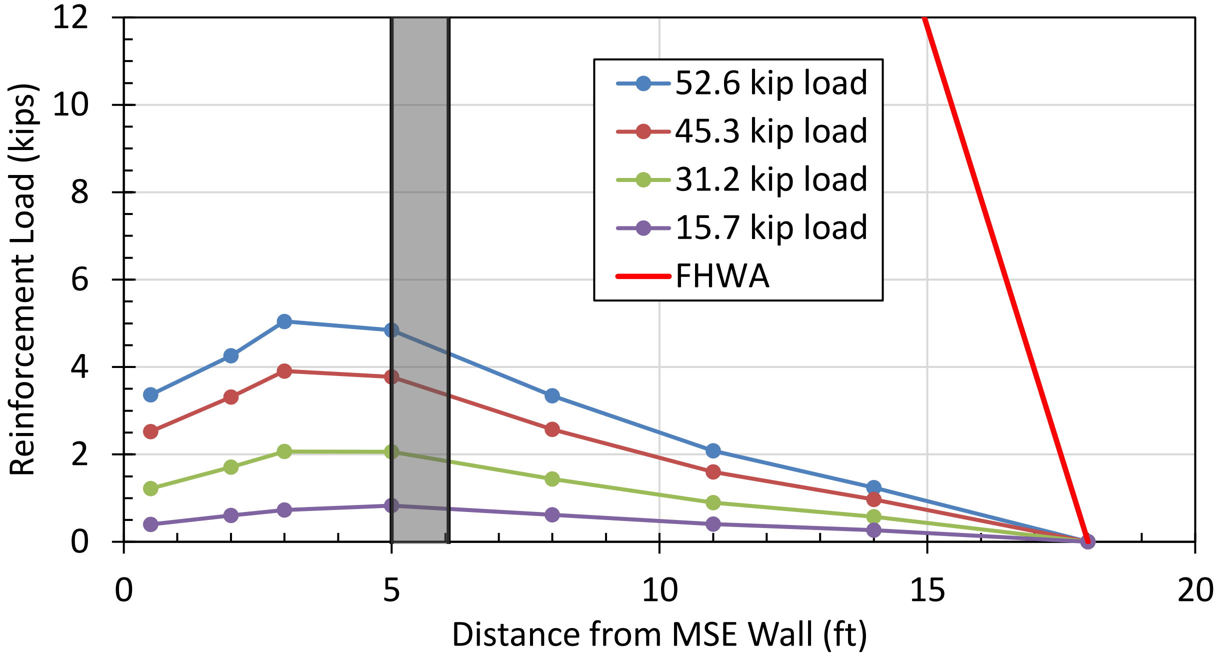

Figure 5-7: Induced loads in the soil reinforcement at different pile head loads relative to distance from the back of the MSE wall (5.2D pile, layer L3, 46 in. transverse spacing).

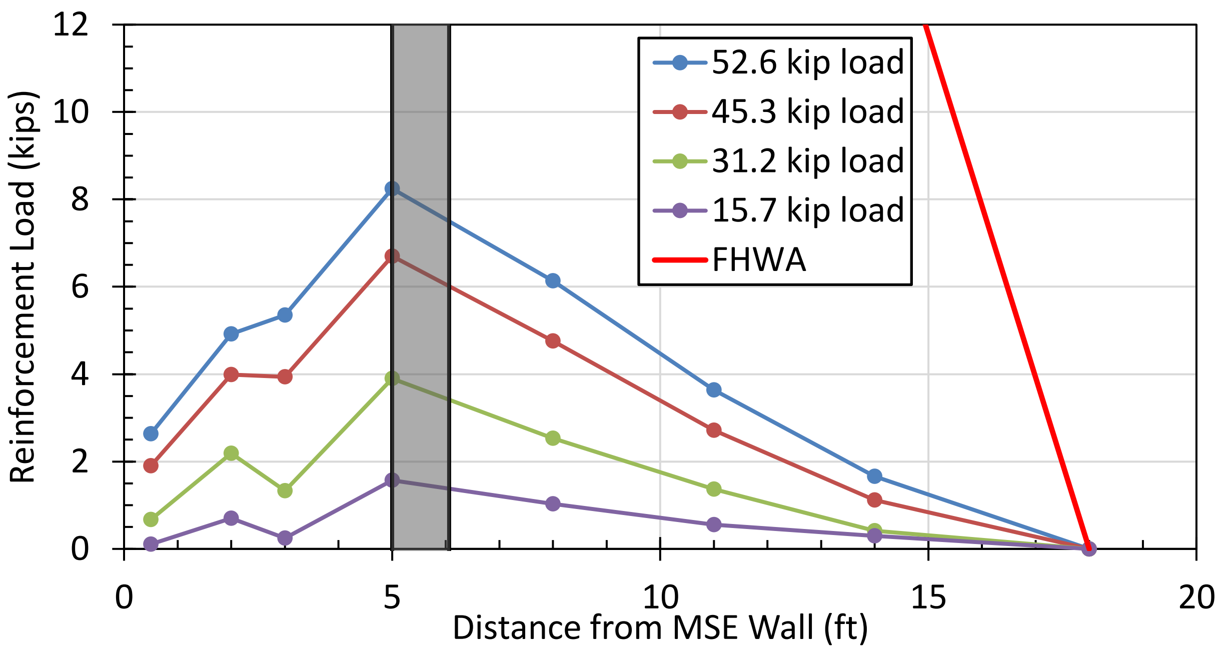

Figure 5-8: Induced loads in the soil reinforcement at different pile head loads relative to distance from the back of the MSE wall (5.2D pile, layer L3, 21.5 in. transverse spacing).

Each figure contains a red line defining the ultimate pull-out resistance from the FHWA equation (see section 2.1, Equation 2-4). It should also be noted that the pullout capacity of the welded-wire grids were designed for live surcharge loads, which increases the load factor on the demand, while no additional resistance is included from vertical stress. Calculating in this way increases the pullout resistance of the measured values. The calculated FHWA pullout resistance is much higher than the measured resistance, as shown in Figure 5-5 through Figure 5-8, which indicates that the pullout resistance of the reinforcement was nowhere near capacity. Induced reinforcement load plots for layers L1 through L4 for each test are located in Appendix F for reference.

Figure 5-9 depicts an idealized model of what is most likely occurring in the reinforcement. The model indicates that as the pile is loaded, the soil in front of the pile is being pushed toward the wall relative to the grid reinforcement causing skin friction on the reinforcement. The soil movement increases tension on the grid as the load is transferred from the soil to the reinforcement by skin friction. As the pile is loaded, the reinforcement behind the pile acts as an anchor as the grid moves toward the wall relative to the soil. Skin friction develops in the opposite direction leading to a decrease in tension in the reinforcement behind the pile as load is transferred to the surrounding soil by skin friction. This would cause the maximum tensile force to develop at or near the pile as observed in the measured distributions. However, at greater transverse distances away from the pile, the shear zone would move closer to the wall so the maximum tensile force would occur closer to the wall. Positive tensile force in the reinforcement at the wall face is likely caused from active earth pressure resulting from the pile head load. Negative tension (compression) near the wall face during testing is likely a result of the reinforcement bending due to uneven soil movement.

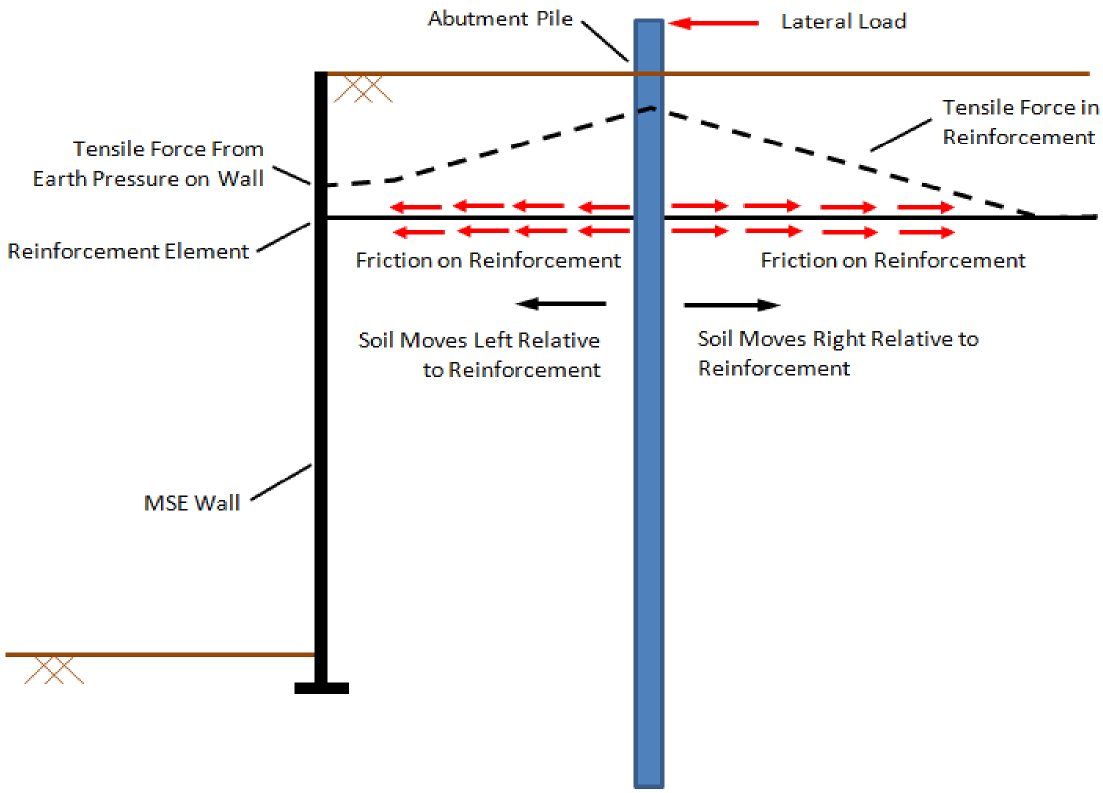

Figure 5-9: Interaction of soil and wall reinforcement for a laterally loaded pile behind an MSE wall (Hatch 2014).

The maximum induced load in the reinforcement at each pile head load increment is shown in Figure 5-10 through Figure 5-17 for each reinforcement layer during load tests on the 1.8D, 3.4D, 4.3D and 5.2D test piles. Each test pile consists of a near and far reinforcement based on the transverse distance of the pile center and the longitudinal bar of the reinforcement where the strain gauge is located. Exact distances of the strain gauges to the center of pile can be found in Table 4-1 with the smaller and larger distances representing the near and far locations, respectively. Because of previous testing at the 15-foot level, some reinforcements occasionally had residual strain in the readings, which were zeroed out at applied loads of zero. The figures show that as pile load increases, maximum induced tensile force in the reinforcement for each layer increases.

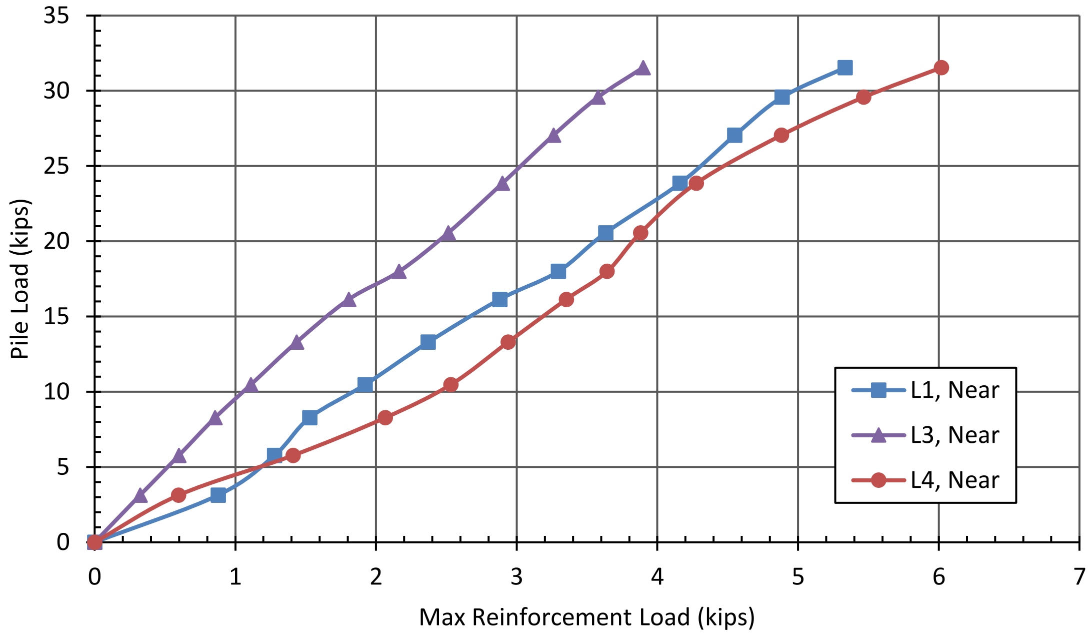

Figure 5-10: Relationship between the pile head load and the maximum reinforcement tensile force nearest to the 1.8D pile.

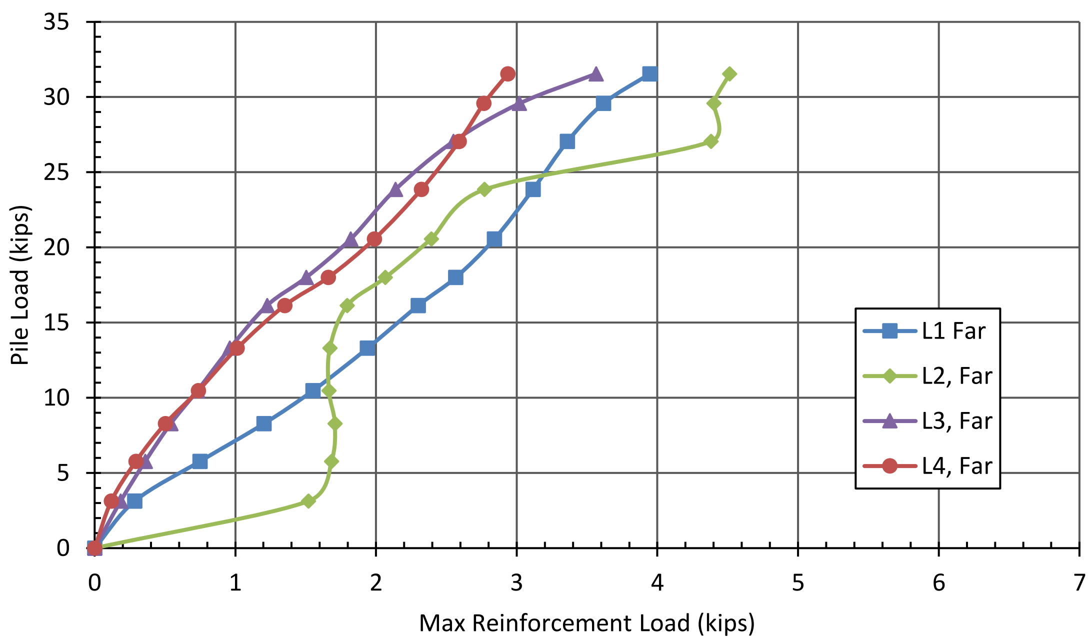

Figure 5-11: Relationship between the pile head load and the maximum reinforcement tensile force farthest from the 1.8D pile.

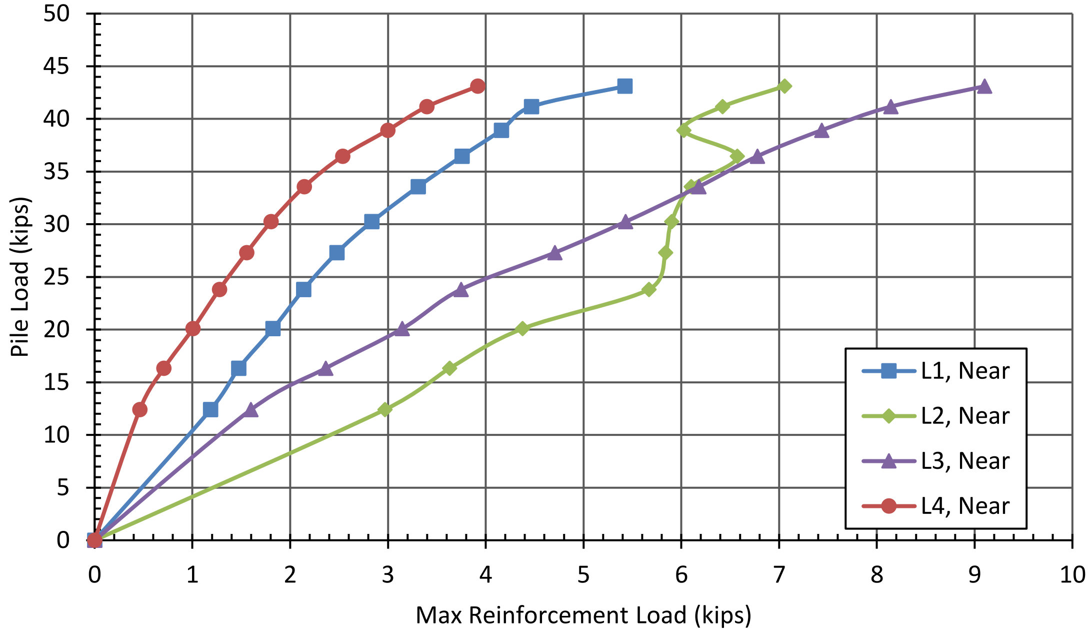

Figure 5-12: Relationship between the pile head load and the maximum reinforcement tensile force nearest to the 3.4D pile.

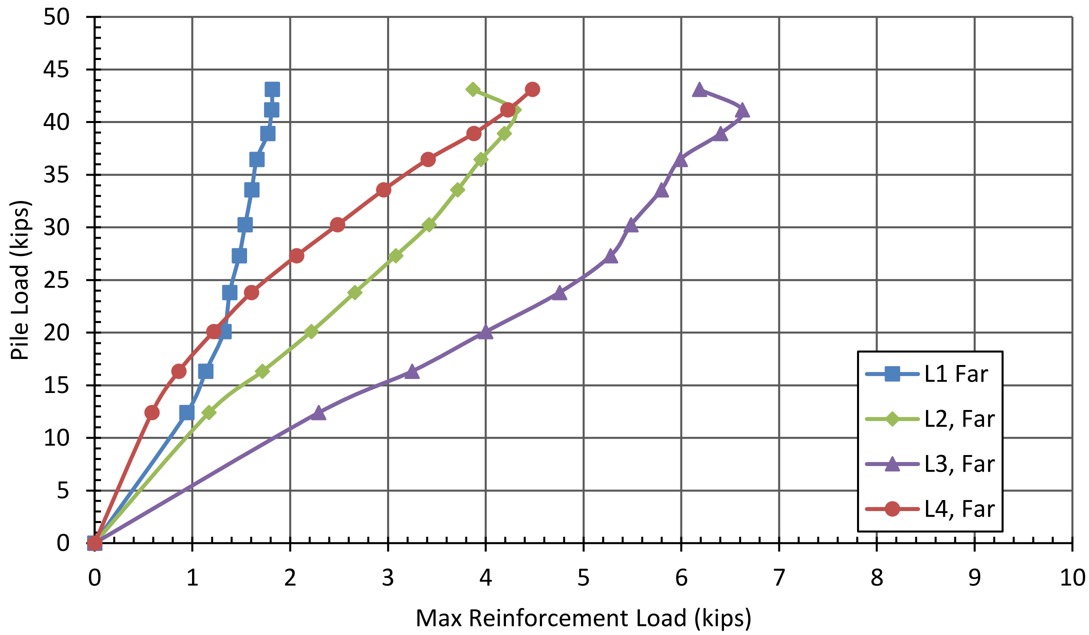

Figure 5-13: Relationship between the pile head load and the maximum reinforcement tensile force farthest from the 3.4D pile.

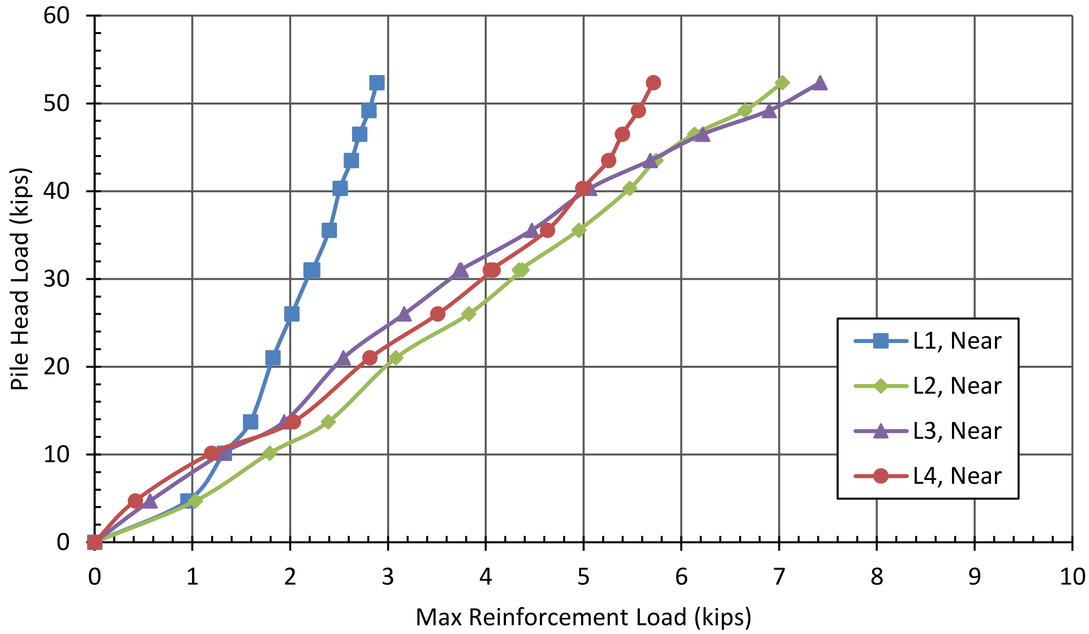

Figure 5-14: Relationship between the pile head load and the maximum reinforcement tensile force nearest to the 4.3D pile.

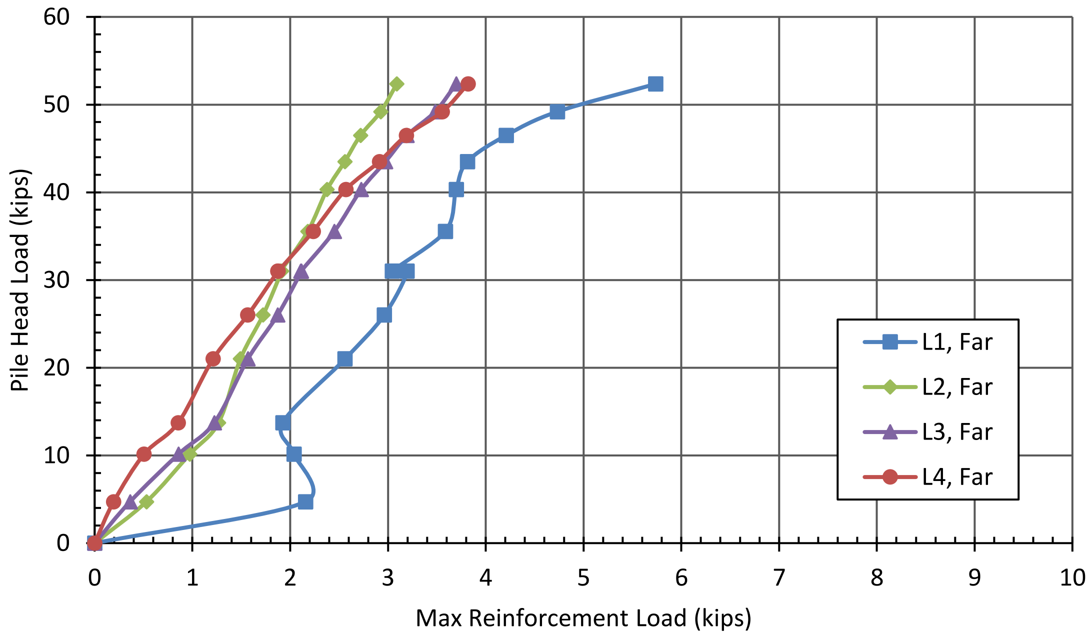

Figure 5-15: Relationship between the pile head load and the maximum reinforcement tensile force farthest from the 4.3D pile.

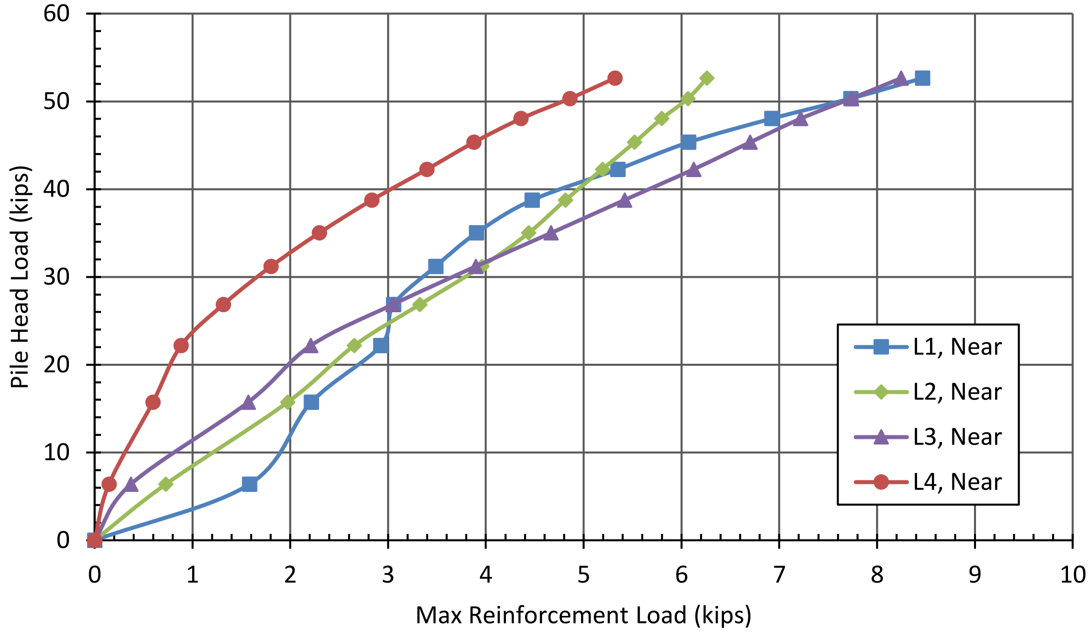

Figure 5-16: Relationship between the pile head load and the maximum reinforcement tensile force nearest to the 5.2D pile.

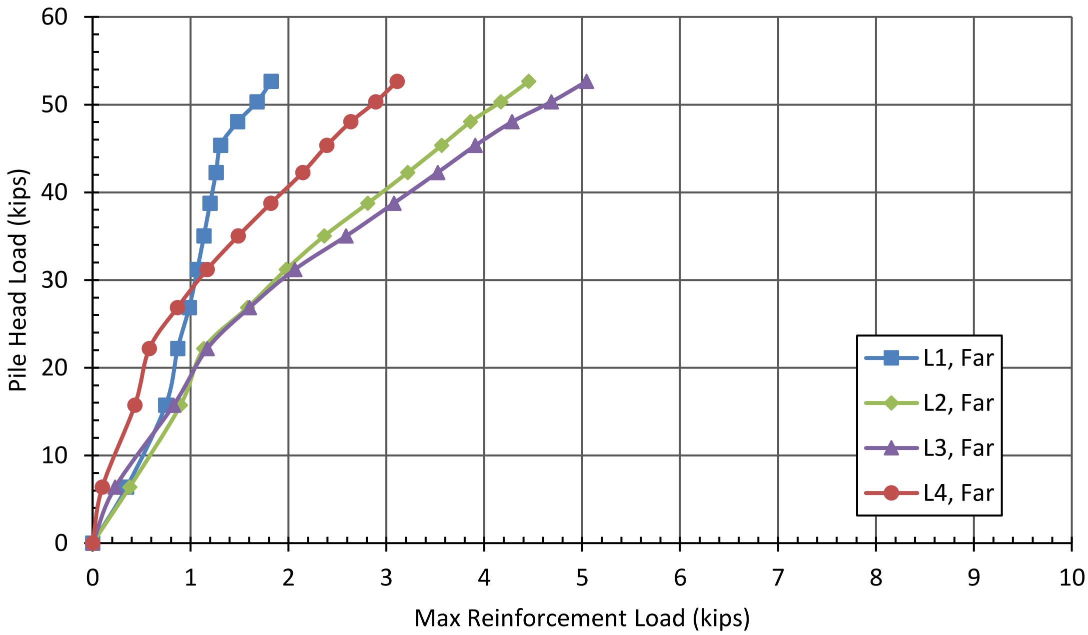

Figure 5-17: Relationship between the pile head load and the maximum reinforcement tensile force farthest from the 5.2D pile.

Maximum tensile forces for the 1.8D test were measured in Layers 1, 2 and 4 as shown in Figure 5-10 and Figure 5-11. The near reinforcement for Layer 2 of the 1.8D pile was not instrumented with strain gauges and, therefore, did not have any data as shown in Figure 5-10. It is likely that Layer 2 for the near reinforcement would have had a tensile force similar to that of Layer 1 had it been recorded. Figure 5-12 and Figure 5-13 indicate that Layers 2 and 3 have the highest maximum induced tensile forces in the reinforcement for the 3.4D test. The 4.3D test shows that Layers 2, 3 and 4 all have similar induced forces while Layer 1 is highest in one reinforcement (Figure 5-15) and lowest in the other (Figure 5-14). Layers 2 and 3 have the highest induced tensile force for the 5.2D test with the exception of Layer 1 on the near layer. Typically, the maximum induced tensile force in the layers increases with depth as pile spacing from the wall increases.

In general, the reinforcement data agree with Hatch (2014), Han (2014) and Besendorfer (2015) in the following ways: the peak induced load in the reinforcement is located at the pile or between the wall and the pile; as transverse distance from the pile increases, the induced reinforcement load decreases; as pile head load increases the induced reinforcement load increases; and as the pile spacing increases, the depth of the maximum induced load on the reinforcement typically increases.

5.4 Statistical Analysis of Load in Reinforcement

The development of tensile force owing to lateral pile loading adjacent to an MSE wall is a relatively complicated soil structure interaction problem. The pile is interacting with the soil, soil is interacting with the reinforcements, and the reinforcements are interacting with the wall. As a result, it was not possible to develop any meaningful simple models to describe the observed behavior. With the help of Dr. Dennis Eggett (BYU Statistics Department), a multiple regression statistical analysis was performed using data from Phase II (Budd 2016), Phase I (Hatch 2014), and data previously collected from UDOT bridge construction (Price 2012). The Statistical Analysis System (SAS) software program was used to run the regression analysis using the general linear modeling (GLM) procedure. SAS was used to determine the statistically significant parameters in the model, after which the Data Analysis pack for Microsoft® Excel was used to fine tune the model by eliminating parameters and thereby simplifying the model without decreasing the R^2 value significant.

The regression analysis was performed by assigning the maximum tensile stress on the soil reinforcement as the dependent variable. Data was obtained for each load increment for each pile load test. The independent variables tested in this analysis were pile head load, normalized transverse distance from the pile center (T/D) where D is the pile diameter, vertical stress (σ_v) in lbs/ft^2, normalized spacing of the pile behind the MSE wall (S/D), and the reinforcement length to height ratio (L/H). In computing the vertical stress, the weight of the surcharge was considered and the surcharge height was also considered to increase the effective wall height H in accordance with AASHTO code requirements.

After the SAS analysis was completed, the relevant parameters were all of the independent variables and the following two-way interactions: vertical stress by L/H ratio, load by load, vertical stress by transverse distance, and load by transverse distance. Table 5-1 presents the R^2 value after the SAS analysis, and subsequent R^2 values after removing the next least significant term. Terms were removed from top to bottom in order of least significance to most significance, where the final R^2 value is the result of load as the final parameter. As seen in Table 5-2, two terms could be eliminated without markedly decreasing the R^2 value; however, removing additional terms would reduce the R^2 value by 3 to 5% for each term eliminated. Therefore, a somewhat more complicated equation was accepted to maintain a higher R^2 value.

Table 5-1: Effect of term elimination on R^2 values.

Term Removed	Resulting R^2 value	Decrease in R^2 value
None	79.7%	-
σ*(T/D)+	79.4%	0.3%
P*(T/D)+	78.9%	0.5%
P^2	75.5%	3.4%
σ*(L/H)	70.6%	4.9%
L/H	67.3%	3.3%
S/D	63.7%	3.6%
σ	56.6%	7.1%
T/D	47.9%	8.7%

+Terms removed before computing the prediction equation.

Table 5-2: Final results of the statistical analysis with tensile force as the dependent variable.

Parameter	Coefficient	Standard Error	t-stat	P-value	Lower 95%	Upper 95%
Intercept	0.071797	0.0621477	1.155	2.48E-01	-0.050195	0.193789
P	0.025643	0.0010456	24.525	1.96E-99	0.023591	0.027696
T	-0.075961	0.0041800	-18.172	5.10E-62	-0.084166	-0.067756
σ	0.000372	0.0000452	8.230	7.61E-16	0.000283	0.000460
S/D	-0.045289	0.0035865	-12.628	1.86E-33	-0.052329	-0.038249
P^2	-0.000226	0.0000197	-11.454	3.15E-28	-0.000265	-0.000187
L/H	0.526285	0.0622950	8.448	1.39E-16	0.404004	0.648566
σ*(L/H)	-0.000575	0.0000452	-12.724	6.71E-34	-0.000663	-0.000486

Data for the measured maximum tensile force and computed maximum tensile force were not normally distributed but were log normally distributed. Therefore, a base 10 log transformation was applied to the tensile force before running the analysis to account better for scatter in the data. A total of 806 data observations were used in the regression analysis resulting in an R^2 value of 0.789. An R^2 of 0.79 indicates that the equation accounts for approximately 79 percent of the observed variation in the tensile force for the welded-wire grid reinforcements. P values are used to understand the statistical significance of a variable, with lower values being more significant. P values for this regression analysis were all less than 0.001 as shown in Table 5-2 indicating that all of the terms in the final equation are statistically significant. The final results of the log form regression analysis are presented in Table 5-2.

Based on the regression analysis, the maximum tensile force, F, in kips is given by the equation:

$$\boldsymbol{F=10^\wedge\left(0.072+0.026P-0.076\left(\frac{T}{D}\right)+3.7x10^{-4}\sigma_v-0.045\left(\frac{S}{D}\right)+0.53\left(\frac{L}{H}\right)-5.7x10^{-4}\sigma_v\left(\frac{L}{H}\right)-2.3x10^{-4}P^2\right)-1} \qquad \textbf{(5-2)}$$

where

P is the pile head load (kips),

T is the transverse distance from the reinforcement to the pile center (in.),

D is the outside pile diameter (in.),

σ_v is the vertical stress (psf),

S is the spacing from the pile center to the back face of the wall (in.),

L is the length of the reinforcement (ft.), and

H is the combined height of the wall and equivalent height of surcharge (ft.).

Parameter coefficients from Table 5-2 were limited to two significant figures in Equation 5-2. Note that reducing the coefficients to two significant figures simplifies the statistical regression equation without any significant loss in accuracy or change in R^2.

Predicted maximum tensile forces were then computed by taking the field data for the above parameters and plugging them into Equation 5-2. A comparison of the predicted and measured maximum tensile forces in log form is shown in Figure 5-18. Data on the red 1:1 line indicates that the measured and predicted values are equal. The red dashed lines are associated with plus or minus one standard deviation which encloses approximately 68% of the data points. The black dashed lines indicate plus or minus two standard deviations which enclose approximately 95% of the data points. For convenience in showing measured and computed tensile forces directly, the data was transformed out of log form and is shown in Figure 5-19.

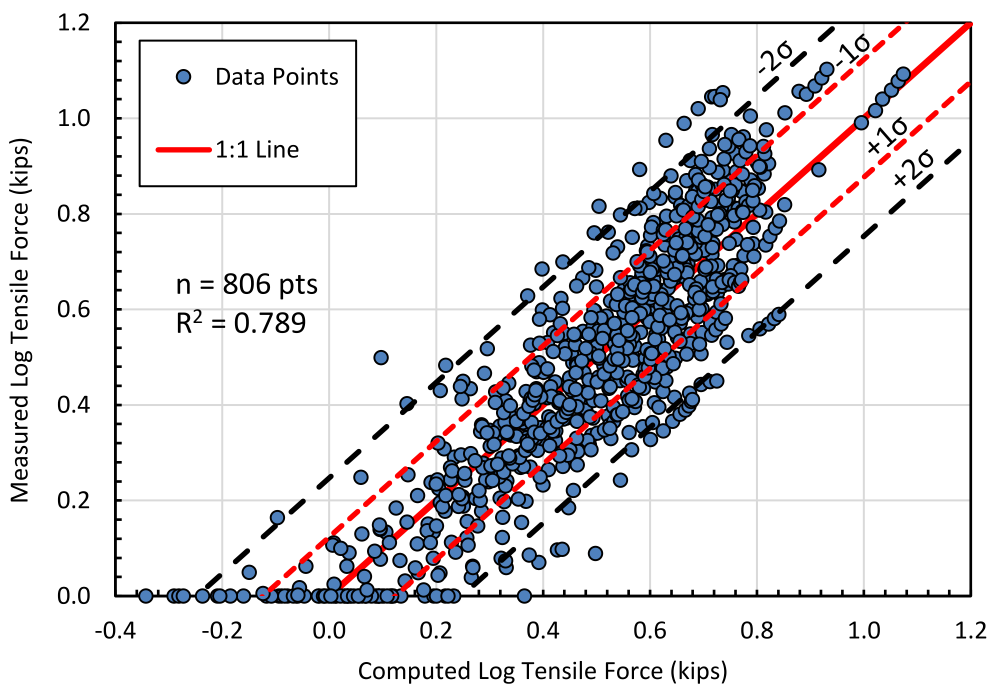

Figure 5-18: Measured versus computed logarithmic tensile force results.

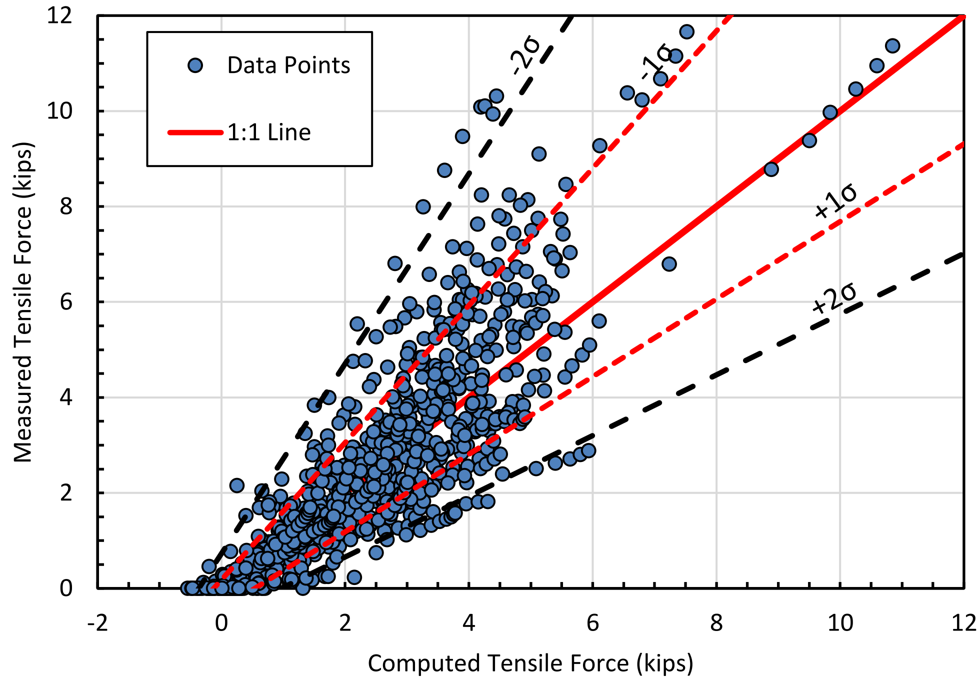

Figure 5-19: Measured versus computed tensile force results.

Data that is not located on the 1:1 red line in Figure 5-18 and Figure 5-19 demonstrates the difference (or residual) of the predicted data from the measured data. The residual for the data was calculated by using the following equation:

$$\boldsymbol{R = log(F_{measured} + 1) - log(F_{predicted} + 1)} \qquad \textbf{(5-3)}$$

where

R is the residual,

$F_{measured}$ is the measured maximum tensile force, and

$F_{predicted}$ is the predicted maximum tensile force.

The log residual is plotted against each independent variable in Figure 5-20 through Figure 5-24. If the regression equation is adequately capturing the influence of a variable, then the residuals will be uniformly distributed about zero with respect to the independent value. However, if the residuals trend upwards or downwards as the independent value increases, then the regression equation may need to be revised over some data range. In general, the residuals fall within the range of -0.3 to 0.4 and appear to be uniformly scattered with respect to zero for all the independent variables. Generally, these results indicate that the regression equation is adequately accounting for the influence of the variables in the equation. However, there is a slightly upward trend towards positive residuals at greater stress levels in Figure 5-24. To further illustrate the uniformity of the scatter about zero and the validity of the equation, residuals were plotted as a function of computed log force as shown in Figure 5-25. The linear regression line from Figure 5-25 is centered on zero along the x-axis, demonstrating there is no bias in the regression equation based on residuals.

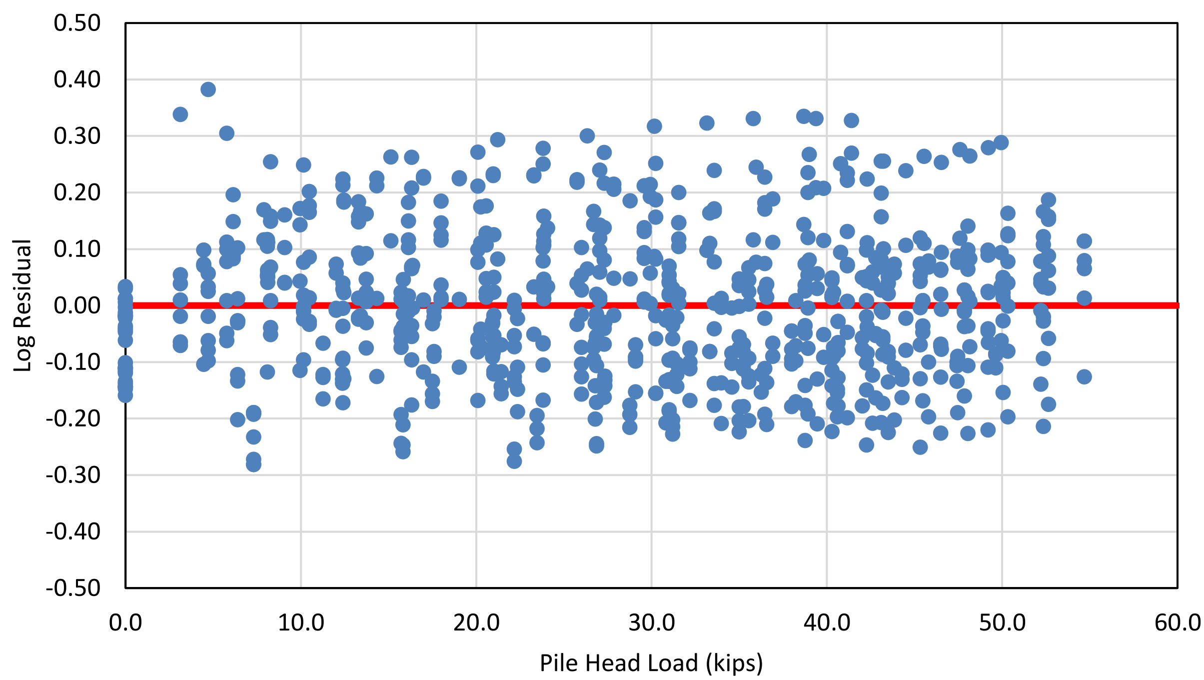

Figure 5-20: Log residual of the pile head load variable for the multiple regression analysis.

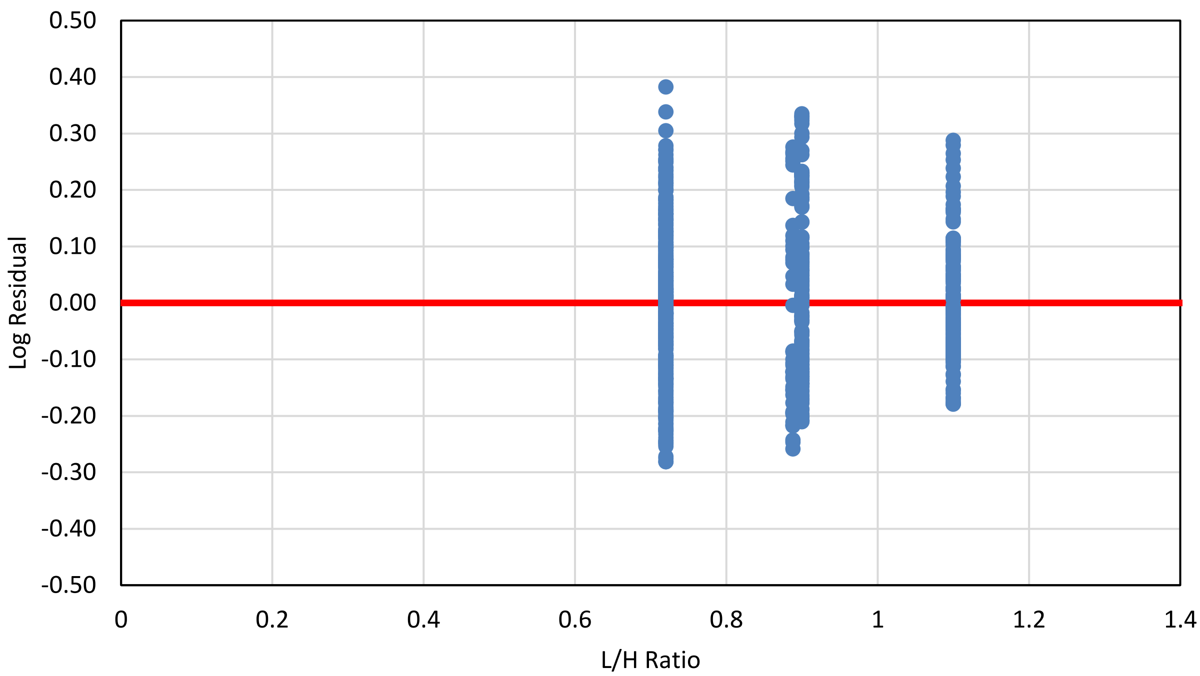

Figure 5-21: Log residual of the L/H ratio variable for the multiple regression analysis.

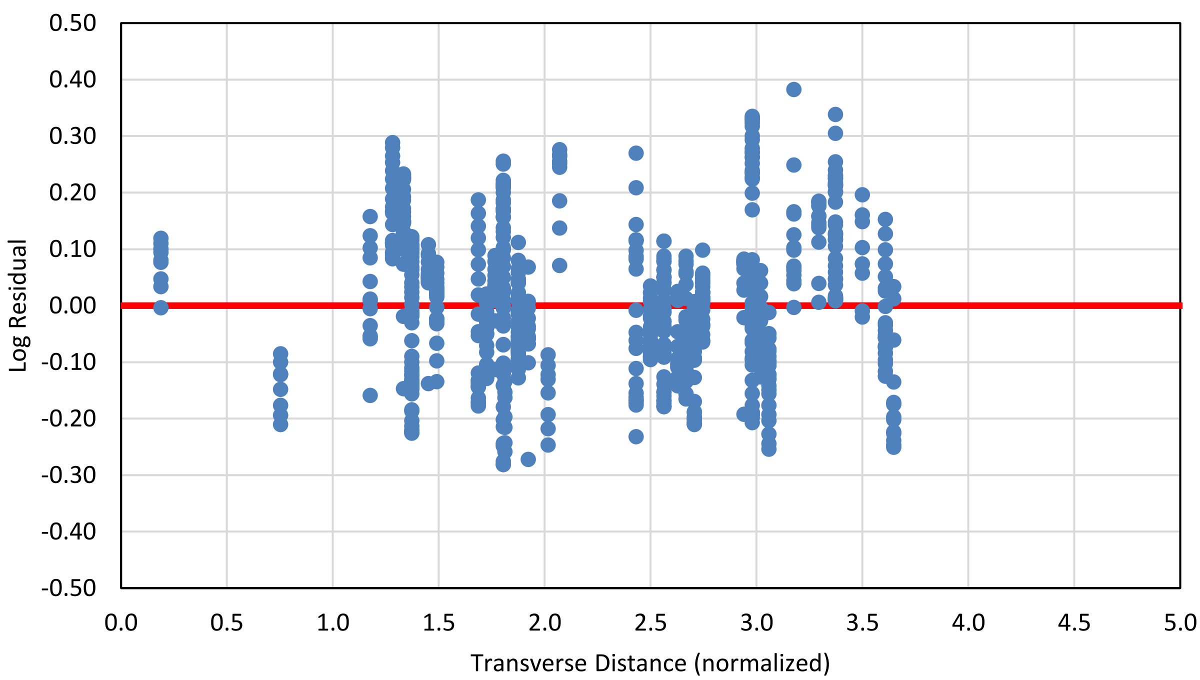

Figure 5-22: Log residual of the normalized transverse distance variable for the multiple regression analysis.

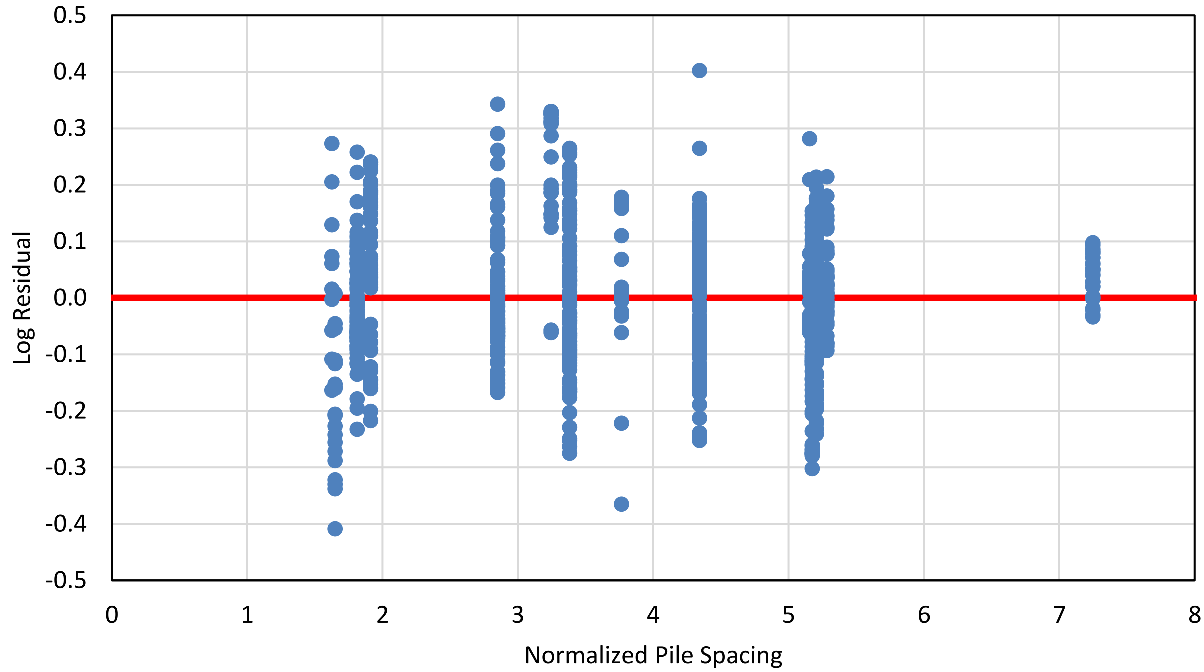

Figure 5-23: Log residual of the normalized pile spacing variable for the multiple regression analysis.

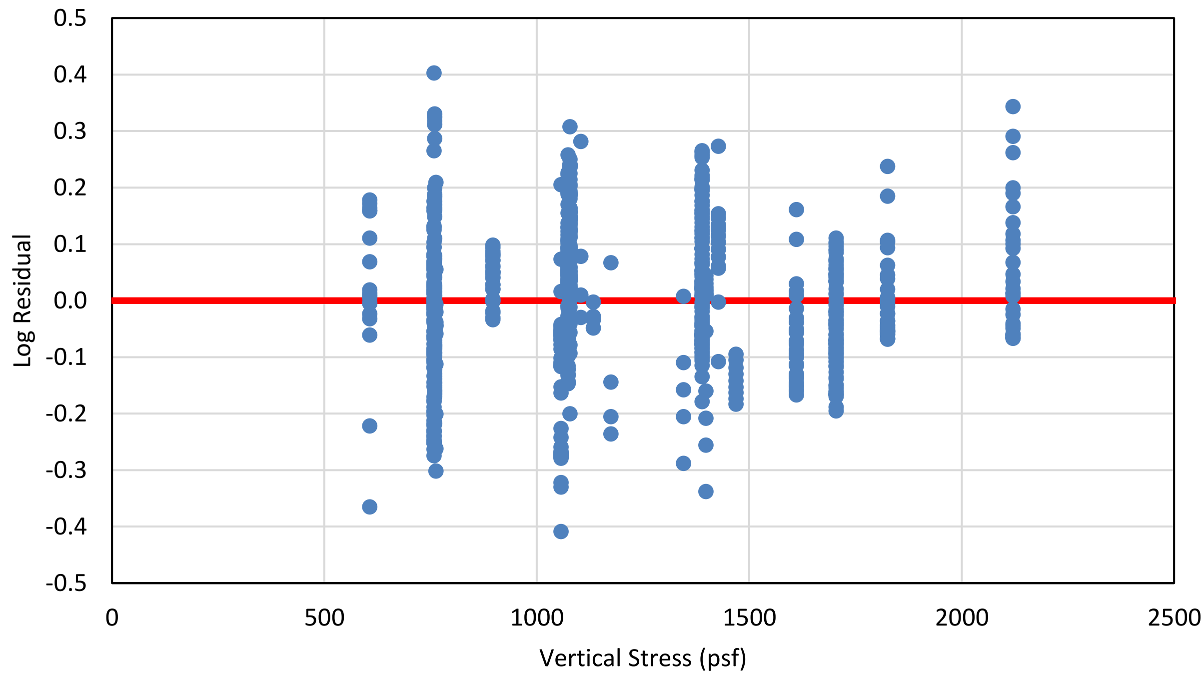

Figure 5-24: Log residual of the vertical stress variable for the multiple regression analysis.

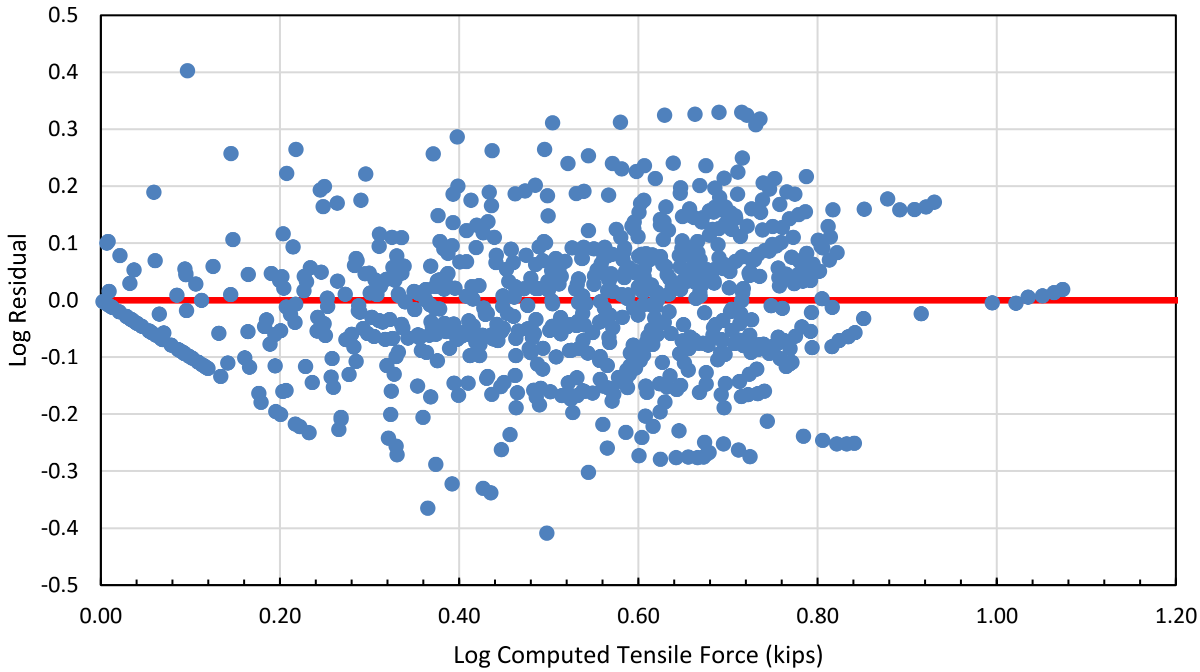

Figure 5-25: Log residual versus computed log tensile force.

Table 5-3 shows the minimum and maximum values that were included for each parameter. Values used out of this range may not yield accurate predicted tensile force when using the equation above.

Table 5-3. Numerical Range of Parameters for Welded Wire Reinforcement Statistical Analysis

Parameter	Range
Pile Load, P	0 kip – 54.7 kip
Normalized Transverse Distance, T/D	0.2 - 6.8
Vertical Stress, σ_V	607 psf- 2121 psf
Normalized Spacing, S/D	1.6 – 7.2
Reinforcement Length to Total Height Ratio, L/H	0.7 - 1.4
Pile Diameter, D	12.75 – 16 in.
Measured Tensile Force, F	0 – 11.7 kip

5.5 Ground Displacement

Vertical and horizontal ground movement occurred during each of the laterally loaded pile tests. Vertical displacement was measured using an optical survey level. Because of safety concerns during testing, vertical displacement measurements were taken before and after testing of the pile. Horizontal displacement was measured using string potentiometers attached to a stationary reference beam and connected to steel stakes driven into the ground between the pile and back face of the wall. Horizontal displacement measurements were taken at the rate of two readings per second.

Vertical ground displacement at 3 inches of pile head displacement and along 1-foot intervals for each test pile is shown in Figure 5-26. In general, vertical displacement is greatest directly in front of the test pile and tapers off to almost no heave near the wall face. The 1.8D and 3.4D tests are similar in their vertical displacement from the pile face to 1 foot in front of the pile. The 4.3D and 5.2D tests are similar in vertical displacement from the pile face to 2 feet in front of the pile. These similarities at different pile spacings could have occurred due to higher forces needed to achieve similar pile head deflection for farther spaced piles. In general, as pile spacing increases the vertical displacement increases when pile head deflection remains constant.

Horizontal ground displacement for the 3.4D pile test at various load increments is shown in Figure 5-27. Ground displacement figures for all test piles are located in Appendix E. Ground displacements for the 3.4D test increases as the pile load increases. In general, the following is true for horizontal ground displacement for each test pile: as pile load increases the horizontal ground displacement increases; horizontal displacement is greatest at the pile face; and horizontal displacement decreases as distance from the pile face increases. Results from this test are in agreement with other pile load tests behind an MSE wall (Besendorfer 2015).

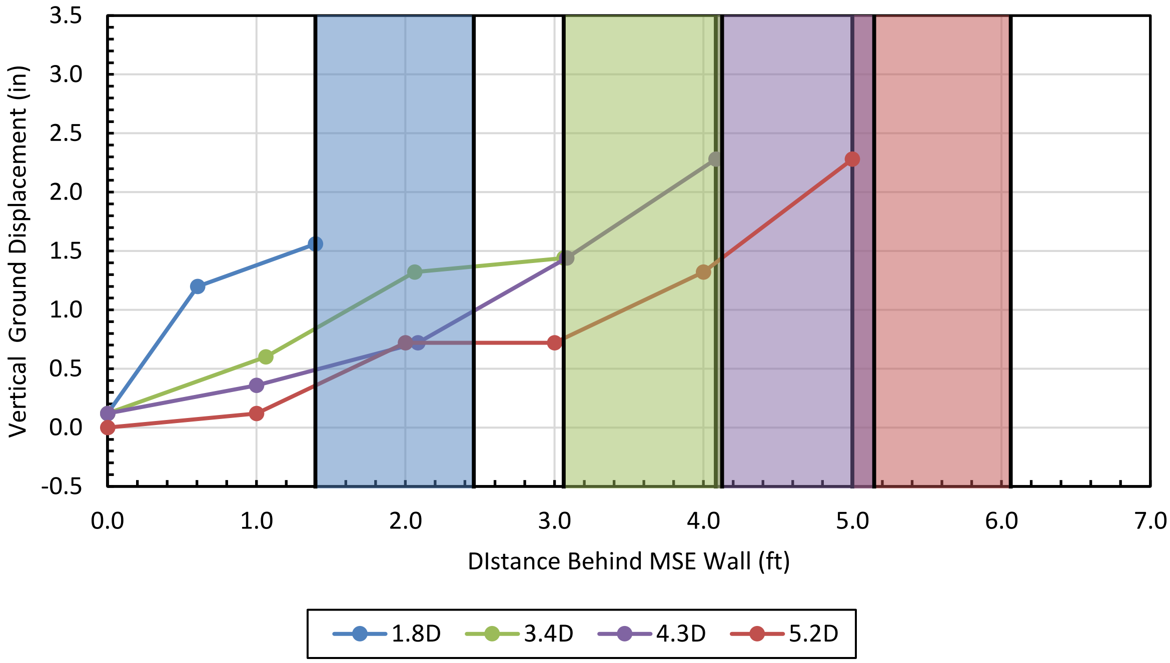

Figure 5-26: Vertical ground displacement for each test pile.

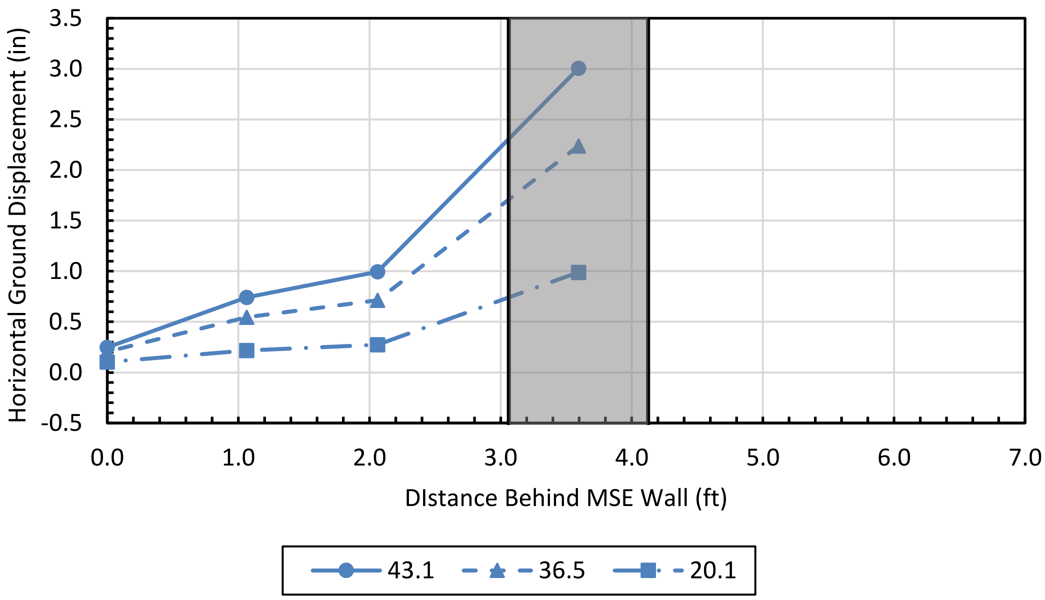

Figure 5-27: Horizontal ground displacement of 3.4D test pile at different loads.

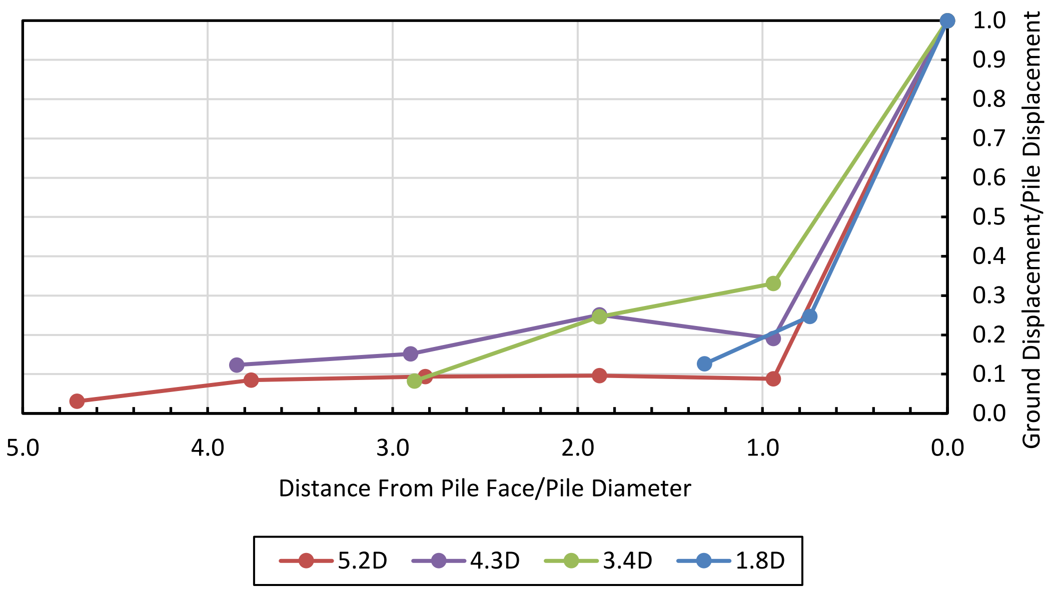

Figure 5-28: Normalized horizontal ground displacement for each pile test.

Figure 5-28 shows the normalized distance intervals and normalized ground displacement at 3 inches of pile head deflection for each test. The pile spacing was normalized by the pile diameter while the ground displacement measurements were normalized by pile head displacement. Typically, as the normalized distance from the pile face increases, the normalized ground displacement decreases. The figure also indicates that the ratio of ground displacement to pile displacement drops dramatically within a normalized distance of 1D from the pile face and thereafter decreases from 0.35 to 0.

5.6 Wall Panel Displacement

Wall panel displacement was measured primarily by digital imagery correlation (DIC). Secondary measurements were obtained using a string potentiometer and shape arrays. The DIC cameras were placed approximately 25 feet in front of the test section of wall, the string potentiometer was attached to the top of the wall, and the four shape arrays were attached to the back face of the wall.

Figure 5-29 and Figure 5-30 show the wall deflection for each load test at 0.5 and 3 inches of pile head deflection. As seen in the figures, very little wall deflection occurred at 0.5 inches of pile head deflection. 5.2D shows more deflection than the other test piles, which is likely caused by camera movement or anomalies and will be discussed later in this section. At 3 inches of pile head displacement for DIC measurements, maximum wall deflections of 0.34 and 0.27 occurred in the 1.8D and 4.3D piles, respectively. In general, the test piles located at a wall joint experienced roughly two times the deflection as the test piles located in the center of the wall panel as shown in Figure 5-30. However, the area of wall panel that experienced large deflection was much smaller on the tests behind joints than the tests in the center of the panel. The tests at the center of the panel had smaller deflections that were more evenly distributed across the panel. Figure 5-30 also shows that as the pile spacing increases, the depth to maximum wall deflection typically increases.

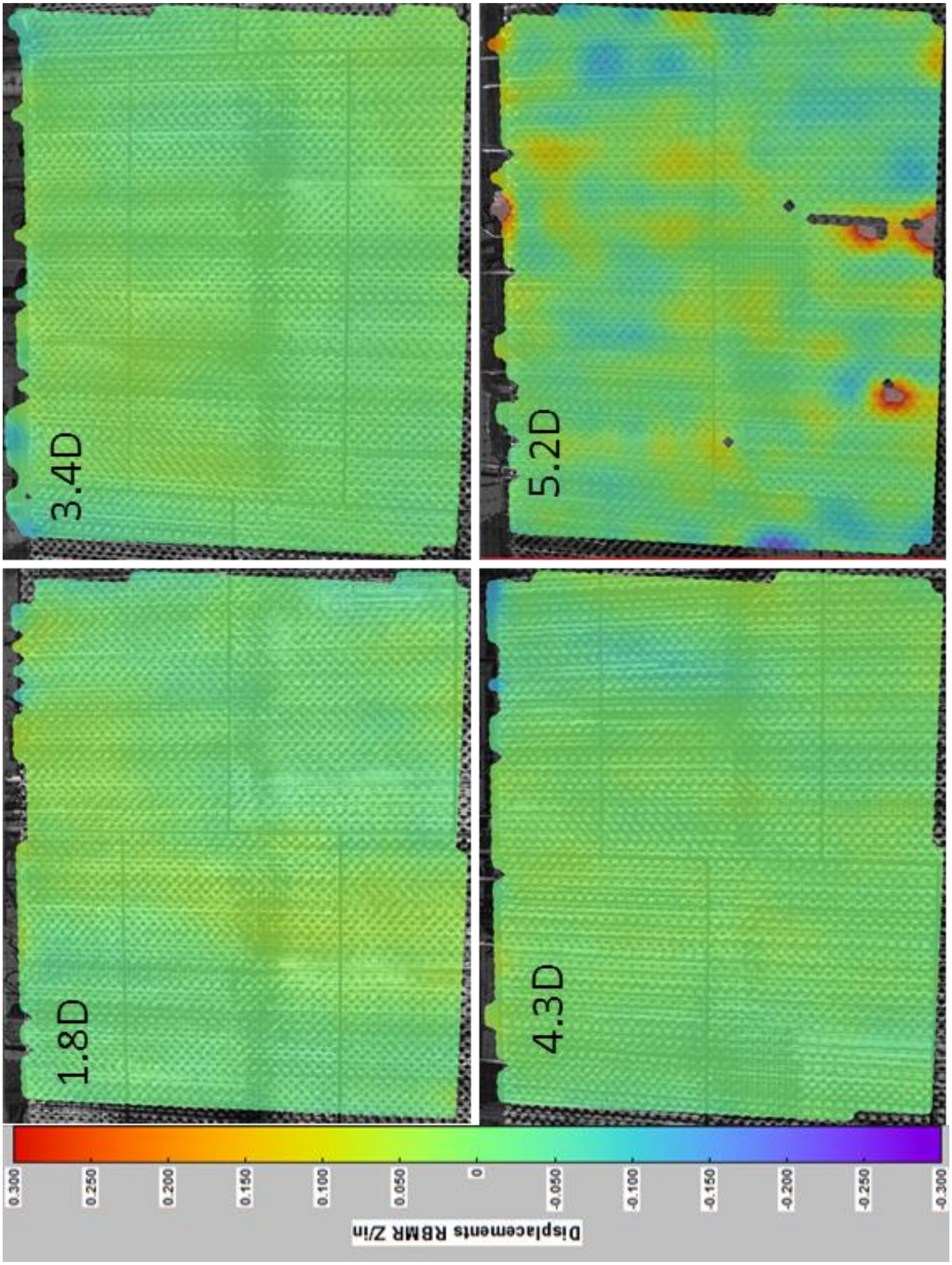

Figure 5-29: Wall panel displacement at 0.5" of pile head deflection.

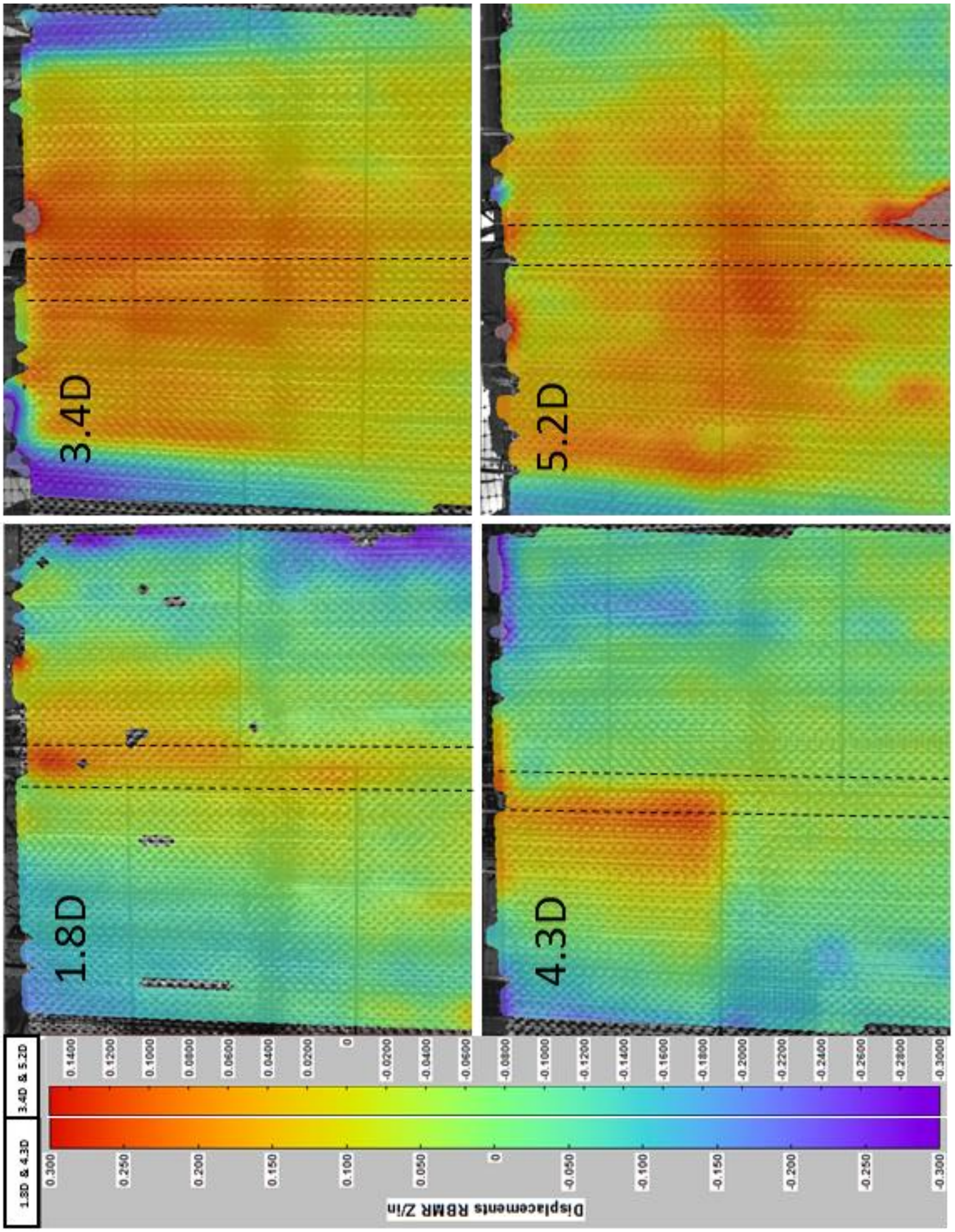

Figure 5-30: Wall panel displacement at 3” of pile head deflection. Note the different scales used for different pile distances.

The data shown in the figures were based on a Z-direction Rigid Body Motion Removed (RBMR) analysis, which only calculates displacements based on the bending or distortion of the wall in the Z (out-of-plane) direction. The regular Z displacement option accounts for all movement in the Z direction that the cameras detect, regardless if the movement is from the wall moving or from the cameras moving. Because of camera movement during testing, caused by wind or other external forces, the RBMR option was chosen for the analyses. However, for the RBMR option to be completely effective, a large area of wall needs to be used for the software to accurately remove rigid body motion. Ideally, wall panels that aren't affected by the testing should be included in the masked portion of the DIC analyses in order to test the accuracy of the RBMR option. The area of the wall that the DIC setup covered for each test was roughly 10'x12' and was likely not sufficient for the RBMR option to be completely accurate. For this project, points at the two bottom corners of each test pile picture at a given deflection were averaged and added to the RBMR deflection to account for any error that was left over in the original RBMR data. The displacements were then compared to the string potentiometer data as shown in Figure 5-31 through Figure 5-34.

In general, the data from the DIC and string potentiometers agree fairly well with the exception of the 4.3D test pile. The 4.3D pile has a deflection of approximately 0.2 inches near the top of the wall, whereas the string potentiometer measured a deflection of approximately 0.37 inches. A possible explanation for the large difference in deflection could be that the RBMR option for the 4.3D pile may not be accurate since all of the panels in the masked section of the wall (see Figure 5-30) were in movement from the pile loading.

Three of the four shape arrays were malfunctioning at the time of testing for this portion of the project. The working shape array was not always installed in front of the pile and so the data collected cannot accurately be correlated with the displacement data. Typically, the shape array data showed much larger deflections than the DIC or string potentiometer data. This is most likely caused from the shape array conduit detaching from the back of the wall panel creating a gap that was filled with backfill during wall construction. The shape array conduit would deflect much more with soil between it and the wall by pushing the soil out of the way as the pile load increased. It is likely that, had the conduit been firmly attached to the wall throughout the whole construction process, the measured deflection from the working shape array would have been much closer to the values from the DIC and string potentiometer.

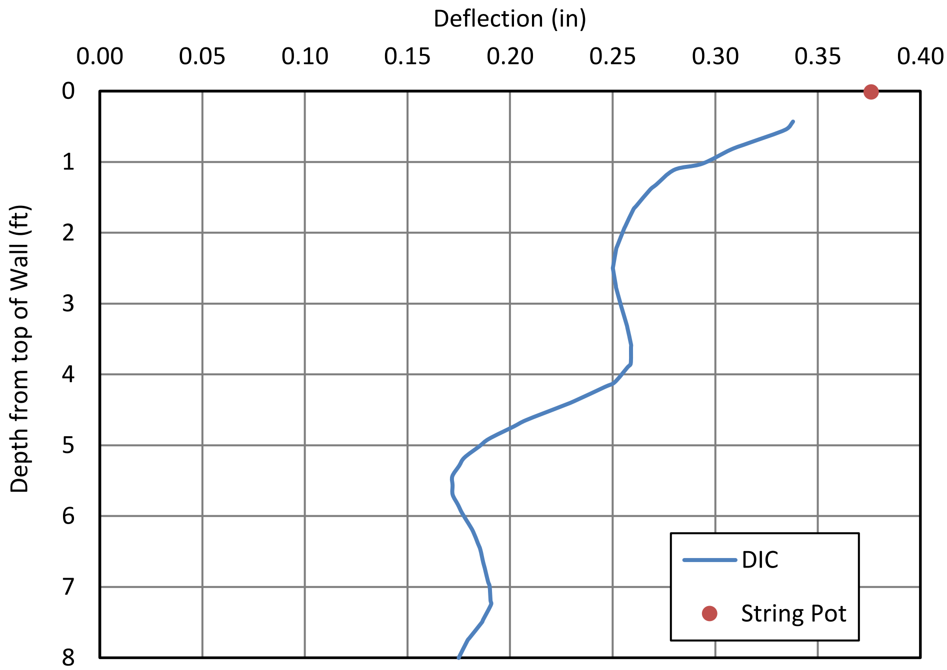

Figure 5-31: Wall displacement profile at 3 inches of pile head displacement for the 1.8D test pile.

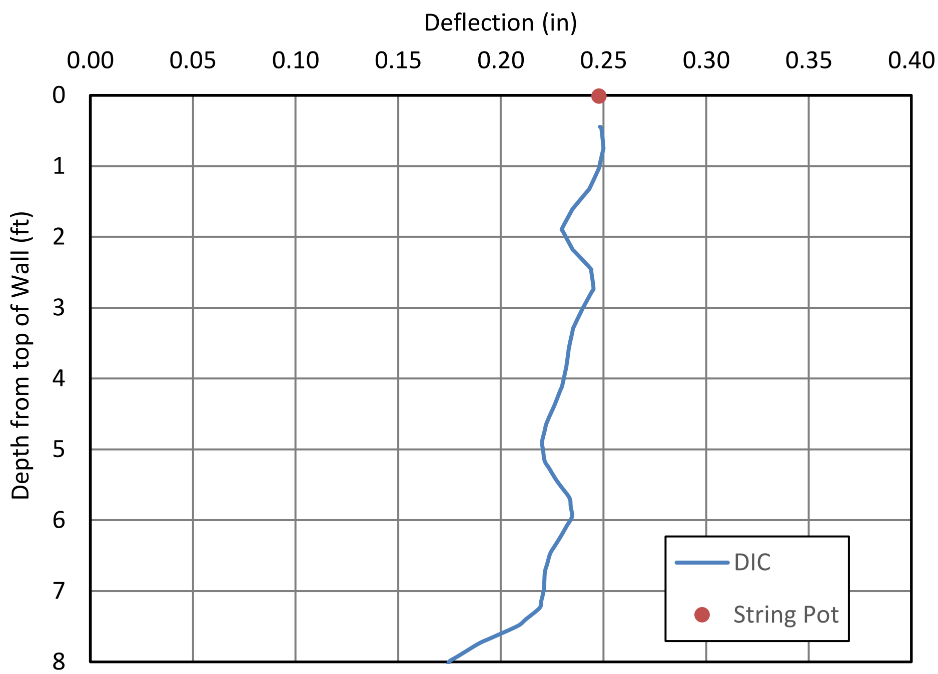

Figure 5-32: Wall displacement profile at 3 inches of pile head displacement for the 3.4D test pile.

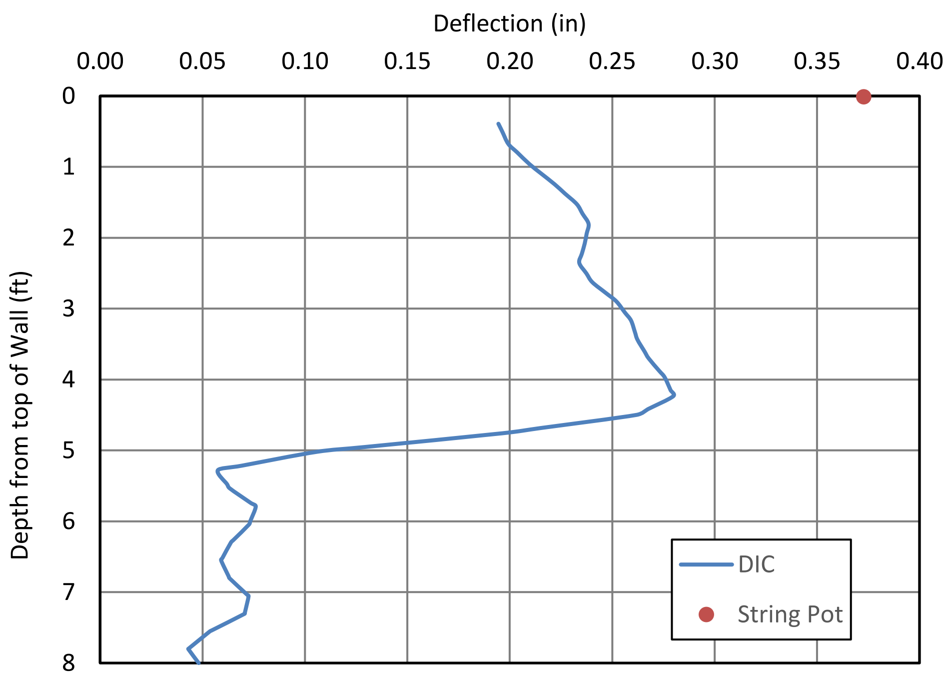

Figure 5-33: Wall displacement profile at 3 inches of pile head displacement for the 4.3D test pile.

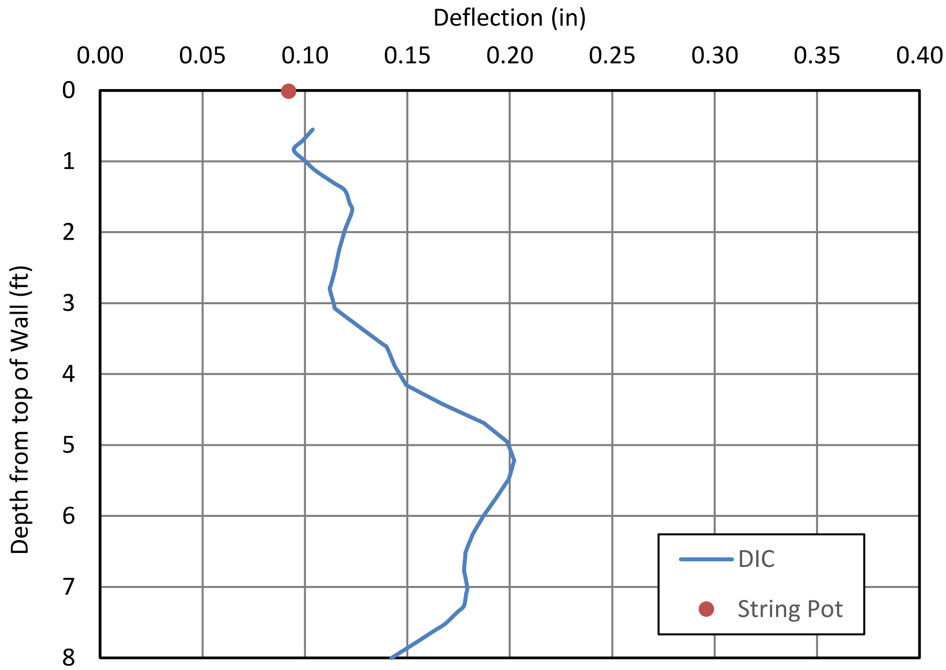

Figure 5-34: Wall displacement profile at 3 inches of pile head displacement for the 5.2D test pile.

5.7 Pile Performance

As indicated previously, strain data for each pile was measured using strain gauges that were placed on opposite sides of the pile at distances of 2, 4, 6, 9, 12, 15 and 18 feet below the ground surface. The strain data was used to find the bending moment, M, in inch-kips for each test pile using the equation:

$$\boldsymbol{M_i = \frac{EI}{2y}((\mu\varepsilon_{it} - \mu\varepsilon_{0t}) - (\mu\varepsilon_{ic} - \mu\varepsilon_{0c}))(10^{-6})} \qquad \textbf{(5-4)}$$

where

E is the pile modulus of elasticity (29,000 ksi),

I is the moment of inertia of the pile (including angle iron) in in^3,

$\mu\varepsilon_{it}$ is the micro strain for the i^{th} data due to tension,

$\mu\varepsilon_{ic}$ is the micro strain for the i^{th} data due to compression,

$\mu\varepsilon_{ot}$ is the initial micro strain caused by tension,

$\mu\varepsilon_{oc}$ is the initial micro strain caused by compression, and

y is the distance in inches separating the two strain gauges along the line of loading.

It should be noted that after testing in the field was completed, further laboratory testing indicated that the strain gauges used on the test piles were installed with the incorrect surface attached to the piles. Ten laboratory tests were performed on plate steel to verify the correct strain gauge surface by applying strain gauges with the correct and incorrect sides adhered to the steel. The measured strain values were compared with the data from the laboratory compression equipment and the appropriate strain gauge side was determined. Correction factors were determined by dividing the measured values of the correctly placed strain gauges by the incorrectly placed strain gauges. Laboratory testing showed that the correction factor for the strain gauges was approximately 3. This correction factor was then applied to Equation 5-4 before plotting the results.

The test piles were driven with the intention of having the strain gauges perpendicular to the wall face. However, all of the piles used on this portion of the project rotated somewhat during installation. Pile rotation was measured by taking the distance of the strain gauges to the center of the pile where the load was applied and using geometry to find the change in y, as shown in Figure 5-35. The corrected y value was used in calculating the bending moment in Equation 5-4.

In locations where one strain gauge was damaged during construction the other strain gauge value was doubled in Equation 5-4. If both strain gauges at a given depth were damaged or faulty the data point was omitted from the chart, as mentioned in section 4.3.2.

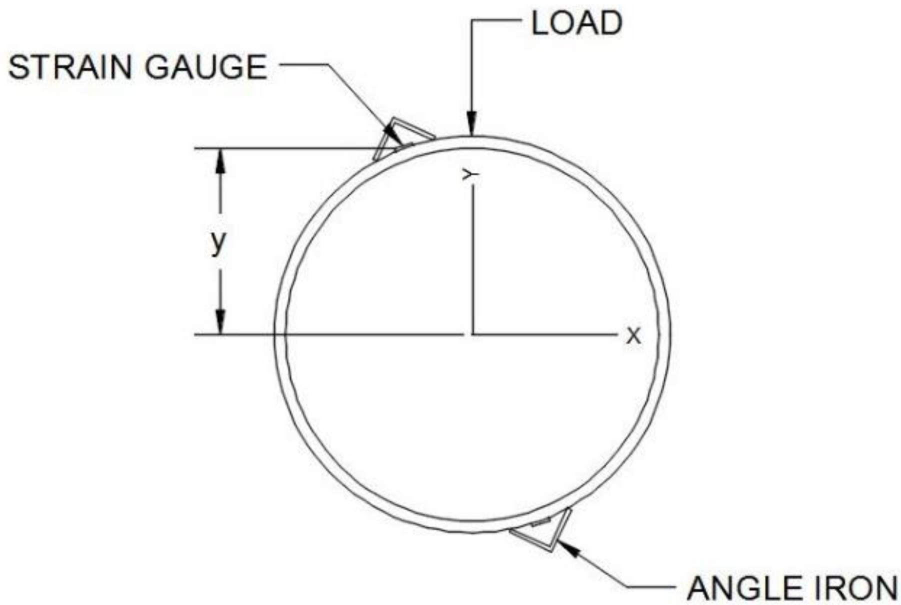

Figure 5-35: Corrected y measurement to account for pile rotation.

Bending moment is plotted versus depth below the surface for each pile at several pile head loads in Figure 5-36 through Figure 5-39. The moments are taken from the one-minute time hold readings for each test. Maximum moments for 3 inches of pile head deflection range between 2,300 kip-in and 4,200 kip-in and are located between 9 feet and 4 feet below ground surface, respectively. Typically, as pile spacing from the wall increases the depth to the maximum moment decreases, with the exception of the 4.3D test. The 4.3D test had two bad strain gauges for the 6 foot interval and one bad strain gauge for the 9 foot interval, therefore the location of the maximum moment is poorly constrained. Based on the other pile tests and an LPILE moment analysis (discussed in Chapter 6), it is likely that the maximum moment for the 4.3D test was much greater and at a depth between 5 feet and 7 feet below the surface. The lack of good data caused key points on the graph to be omitted and therefore skewed the results.

Maximum moments generally increased with pile spacing, but this is likely due to the increased pile head loads to create similar pile head deflections. Based on the data from the figures, maximum moments for similar pile head load values were similar. For example, at loads ranging from 20.1 and 21 kips, the maximum moment was 1,300 to 1,500 in-kips. Note that 5D data was interpolated using Figure 5-39 to get a load of 21 kips and a moment of approximately 1,500 in-kips. Again, the 4.3D pile is the exception and it is likely that the induced maximum moment was actually higher than measured data indicates as discussed previously.

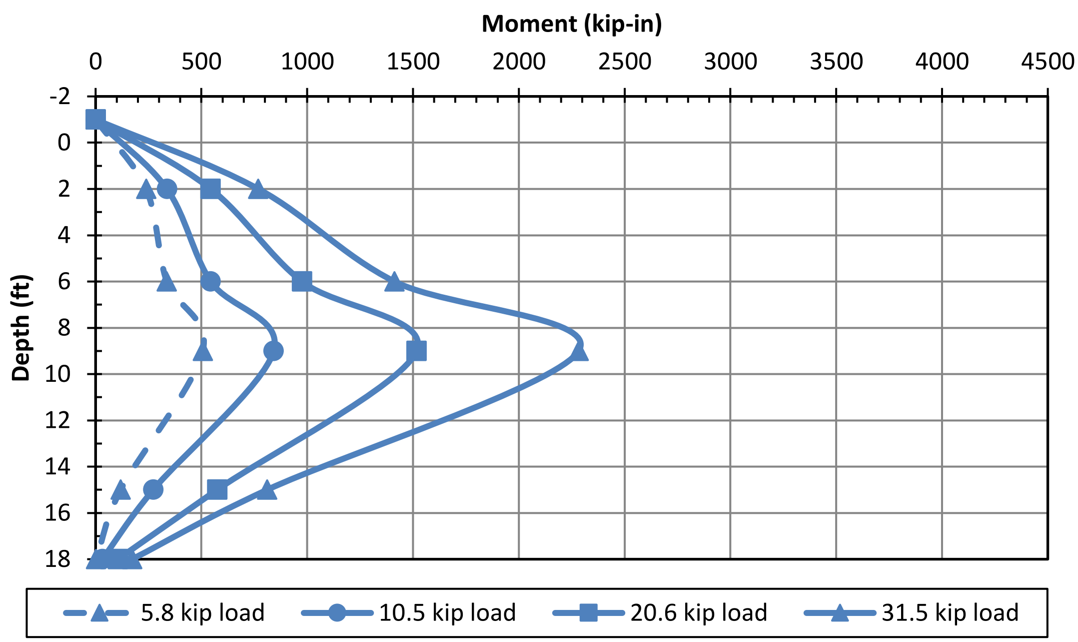

Figure 5-36: Bending moment versus depth of several pile head loads for the 1.8D test.

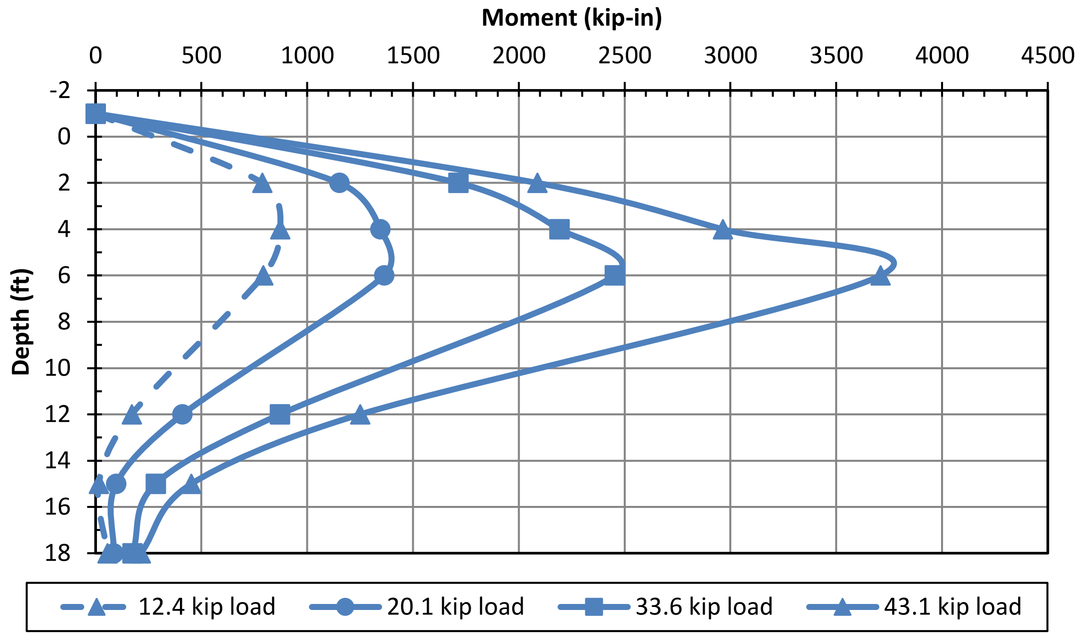

Figure 5-37: Bending moment versus depth of several pile head loads for the 3.4D test.

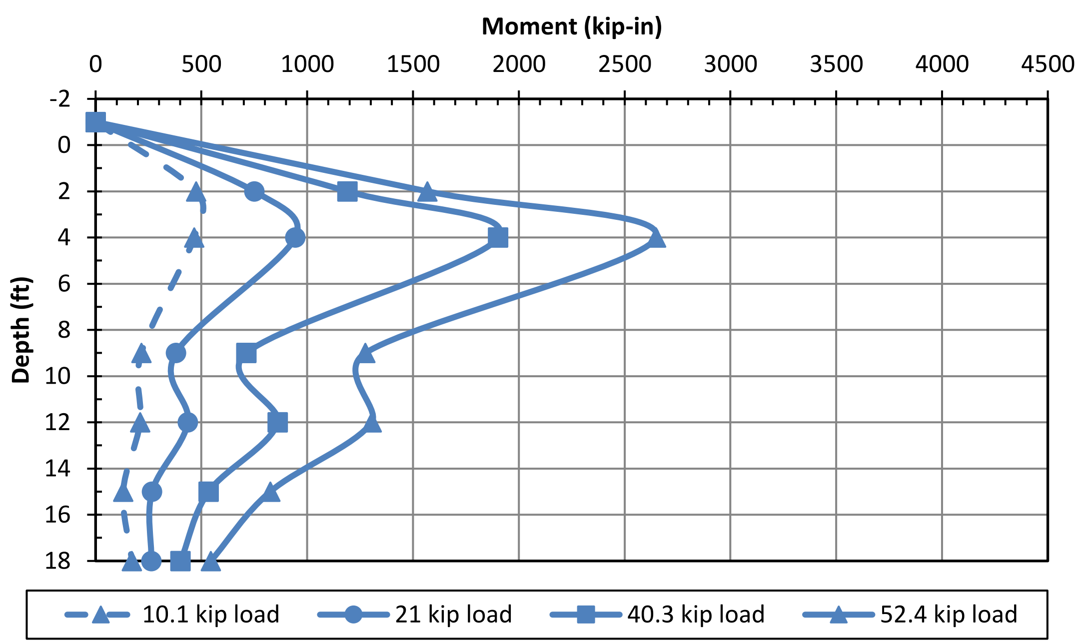

Figure 5-38: Bending moment versus depth of several pile head loads for the 4.3D test.

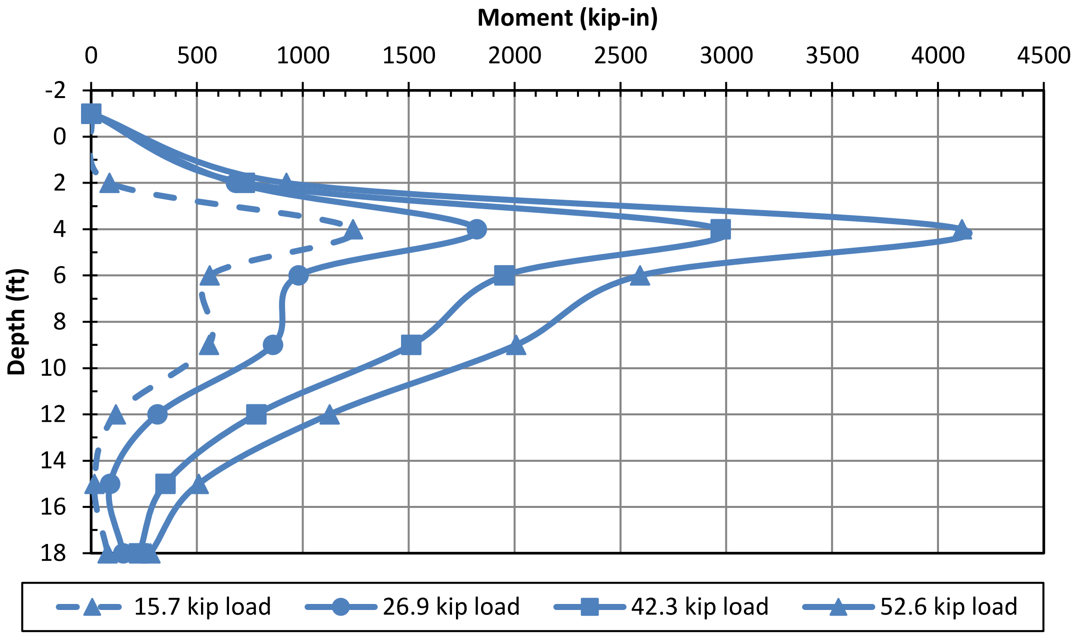

Figure 5-39: Bending moment versus depth of several pile head loads for the 5.2D test.

6 LATERAL LOAD TESTING FOR RIBBED STRIP REINFORCEMENT

Lateral load testing of the four piles began on August 4th, 2014 and was complete by August 6th, 2014. For an additional reference, a reaction pile located outside of the reinforced mass but still in the compacted backfill was tested on August 20th, 2014. Displacement control criteria governed the loading procedure. Lateral load was applied to the pile until the target displacement was reached. Target displacement ranged from 0.25 to 3.0 inches, with each loading increment being 0.25 inches. Each target displacement was maintained for a five-minute period between loading increments. The same test approach was used for all of the piles.

6.1 Load Displacement Curves

Pile head load versus deflection plots for the four tests and the reaction pile are shown in Figure 6-1 and Figure 6-2. The load curves are based on the hydraulic pressure gauge monitoring the pressure in the hydraulic jack line. Figure 6-1 shows the peak load applied to the pile versus pile deflection. The pressure in the pump spiked briefly after reaching the target displacement for each load cycle. The peak load at each loading increment is the average of several seconds of data after the highest load was applied. The peak load is likely to only be encountered in situations such as an earthquake but is probably not representative of static loading conditions. Figure 6-2 shows the pile head load versus deflection after a five-minute relaxation period and is more likely representative of static loading conditions caused by thermal expansion and contraction.

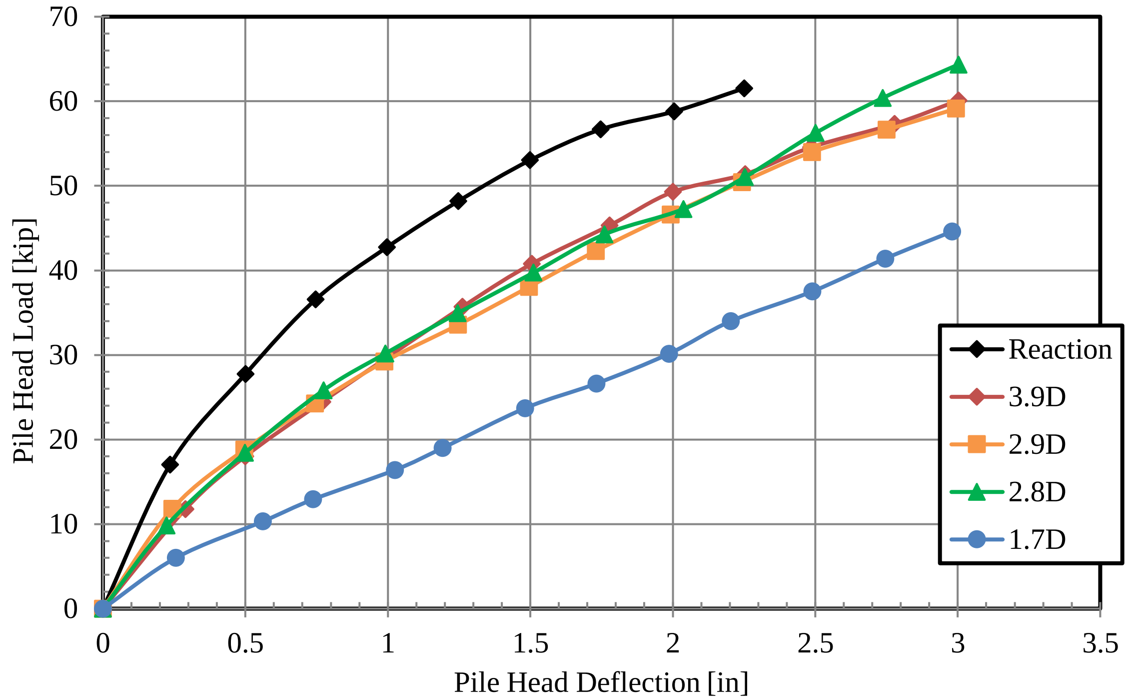

Figure 6-1: Peak pile load versus displacement.

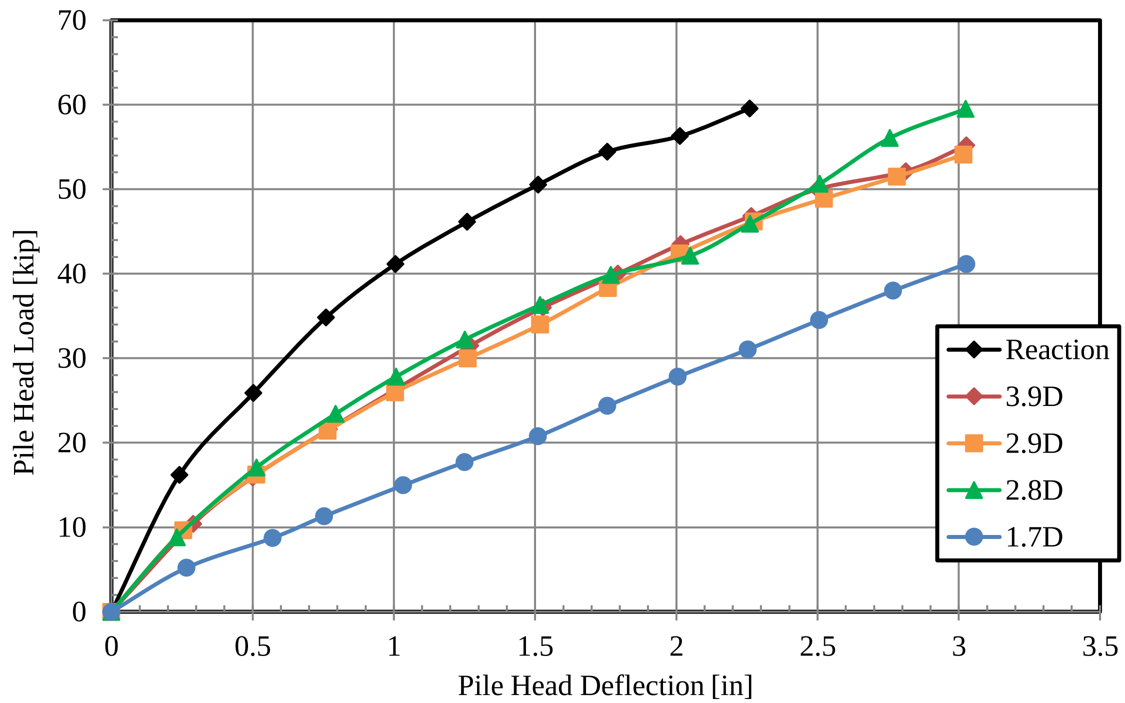

Figure 6-2: Final pile head load versus displacement.

A general comparison of the curves shows that the lateral resistance of the 3.9, 2.9 and 2.8D piles is approximately equal and the resistance of the 1.7D pile is about 70% less than these piles. The spacing of the 2.9D and 2.8D piles is approximately the same so similar load-deflection curves are not unexpected. However, the resistance of the 3.9D pile being similar to that of the 2.9 and 2.8D piles is unexpected based on previous testing and research performed by Hatch (2014), Han (2014), Price (2012), and Nelson (2013). Figure 2-16 indicates that lateral resistance of piles spaced greater than 3.8D should be approximately the same. Based on the testing, either the resistance of the 3.9D pile was lower than expected or the resistance of 2.9 and 2.8D piles was higher than expected. There are several possible explanations for this discrepancy. The night before the 2.8 and 2.9D piles were tested, a significant rainstorm occurred at the site. The USCS material classification of SP-SM indicates that there are some fines in the soil (See section 3.3.1) so perhaps the resistance of the 2.8 and 2.9D tests was increased due to cohesion that added to the strength of the soil. Both of the tests were performed on the day following the rainstorm. Furthermore, the water that infiltrated the soil would increase the unit weight of the soil and may have caused some natural compaction. Another possibility is that the panel configuration varies from test to test. There is a joint directly in front of the 1.7D and 2.9D piles while the 2.8D and 3.9D piles are located in the center of a panel. Also, the size of the panels varies at the top of the wall from tests to test. Perhaps the panel configuration of the 3.9D pile does not provide as much strength as the panel configuration in the vicinity of the 2.9 and 2.8D piles. Another possibility is that the compaction around the piles differed. Compaction between the piles and the wall was done using a vibratory plate compactor. The path of compaction generally was around the pile, next to the wall, and then in-between piles. Assuming the same number of passes of the plate compactor occurred between each pile and the wall, the soil between the wall and piles on the 2.8 and 2.9D piles would have received more compaction effort than the soil around the 3.9D pile. Although nuclear density testing was performed throughout construction as outlined in section 3.3.1 of this report, the exact location of all tests is not known and cannot be used to verify this. We do know; however, that the compaction tests indicated substantial variation in relative compaction within the zone between the piles and wall panels in comparison with the soil behind the piles as shown in Table 3-3 and Table 3-4. This variation could account for the observed inconsistencies.

6.2 Soil Reinforcement Performance

The load in the soil reinforcement was calculated using the strain data. Strain gauges were applied to both sides of the reinforcement and the average of the values was used. In the case where one of the gauges was damaged, the strain from the working gauge was used and in cases where both were damaged, the data point was omitted. The induced load in the reinforcement was calculated using the following equation:

$$T_i = EA(\mu\varepsilon_i - \mu\varepsilon_o)(10^{-6}) \qquad (6\text{-}1)$$

where

T_i is the equivalent induced force in kips for the wire strip at the ith data point,

E is the modulus of elasticity of the steel strip (29,000 ksi),

A is the cross sectional area of the steel strip (0.31 in^2),

$\mu\varepsilon_i$ is the micro strain for the ith data point, and

$\mu\varepsilon_o$ is the micro strain for the initial data point just before loading the pile.

The measured tensile force represents only the force induced by the lateral load on the pile and does not account for the force induced by earth pressure during construction of the wall itself.

For depths of 45 and 75 inches, the measured load in the soil reinforcement at various distances behind the back face of the MSE wall is shown in Figure 6-3 and Figure 6-4, respectively. The load on the reinforcement is shown at several load levels. Both plots are for the 2.9D test and the transverse distance from the center of the pile to the center of the reinforcement is approximately 38 in. in both cases. As an additional reference, the nominal tensile resistance based on FHWA equations (2009) described in section 2.1 has been added to the plots. The tensile force in the reinforcement tends to peak approximately near the center of the pile. The tensile force increases between the wall and pile and tends to decrease between the pile and the back end of the reinforcement. Similar plots for the other reinforcements monitored during each test can be found in Appendix F.

The maximum measured induced load in the reinforcement at each pile head load for the piles at 1.7, 2.8, 2.9, and 3.9D from the wall is shown in Figure 6-5 through Figure 6-12. In these figures, Layer 1 designates the shallowest level of reinforcement while Layer 4 indicates the deepest. Separate figures are provided for strip reinforcements located at close and far distances measured transverse to the direction of loading relative to the center of the test pile. Transverse distance for each of the reinforcements relative to the pile is summarized in Table 4-2. All of the reinforcements underwent testing multiple times and occasionally a residual load was observed in the reinforcement after unlading the pile. Hence, the non-zero load at zero pile head load is due to the residual load from previous tests. In general, the following trends in the soil reinforcement have been observed. The induced tensile force on the reinforcement increases as the load on the pile increases. The load on the reinforcement increases with depth to the second or third layer, after which it again decreases. The induced load on the reinforcement decreases as the transverse distance between the pile and the reinforcement increases. At a given pile load, the induced tensile force in the reinforcement increases as pile spacing decreases. These trends seem to be somewhat dependent on whether there is a vertical joint between the panels directly in front of the pile and also on the size of the panels at the top of the wall in front of the pile being tested.

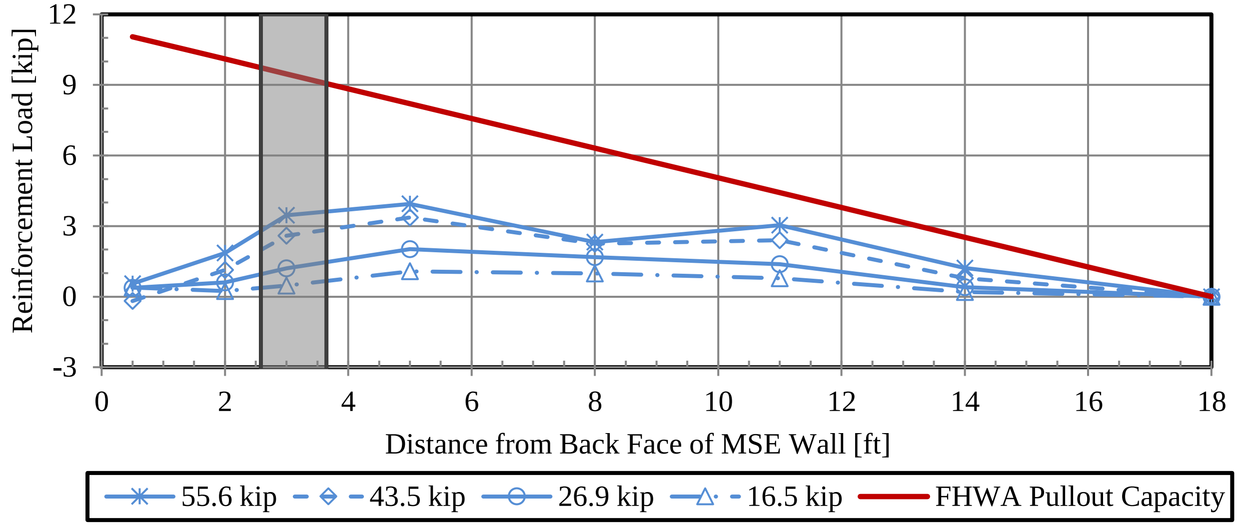

Figure 6-3: Induced loads in the second layer of soil reinforcement at various pile head loads and distances from the wall. (2.9D test, 38 in. reinforcement transverse spacing).

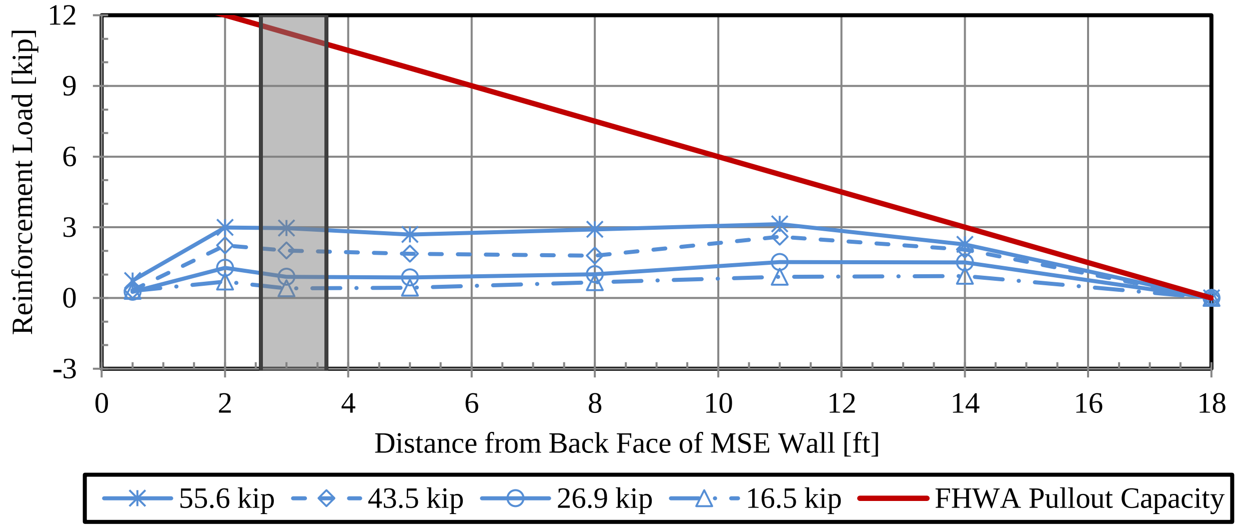

Figure 6-4: Induced loads in the third layer of soil reinforcement at various pile head loads and distances from the wall. (2.9D test, 37 in. reinforcement transverse spacing).

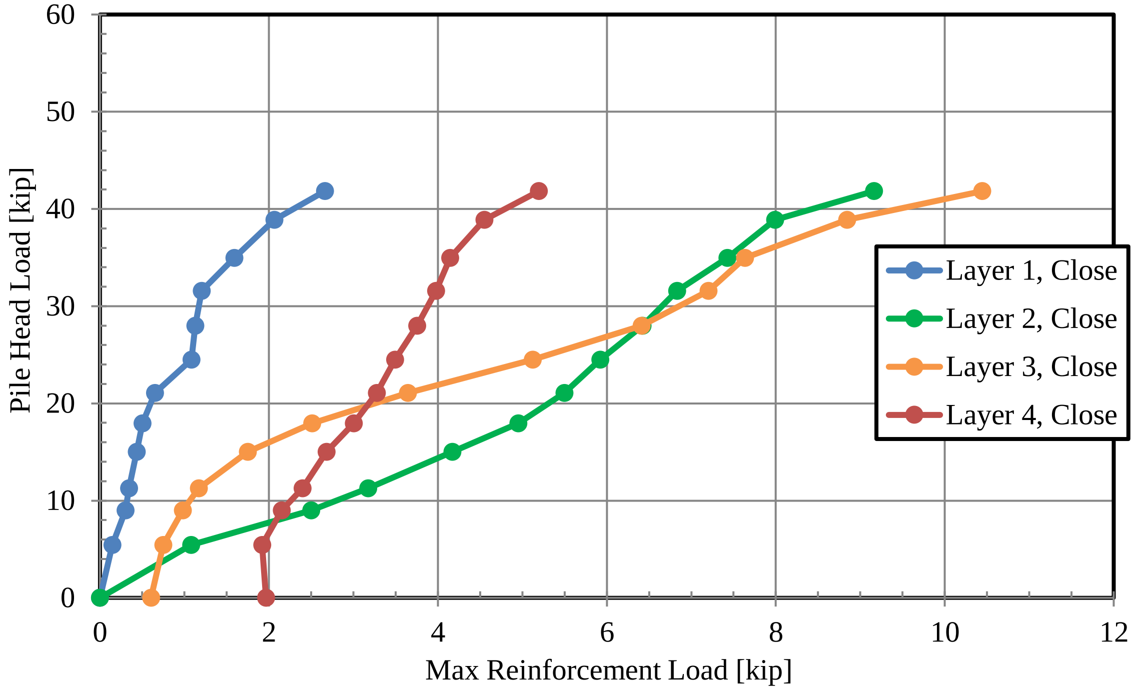

Figure 6-5: Max tensile force in close soil reinforcement at each pile head load for 1.7D test.

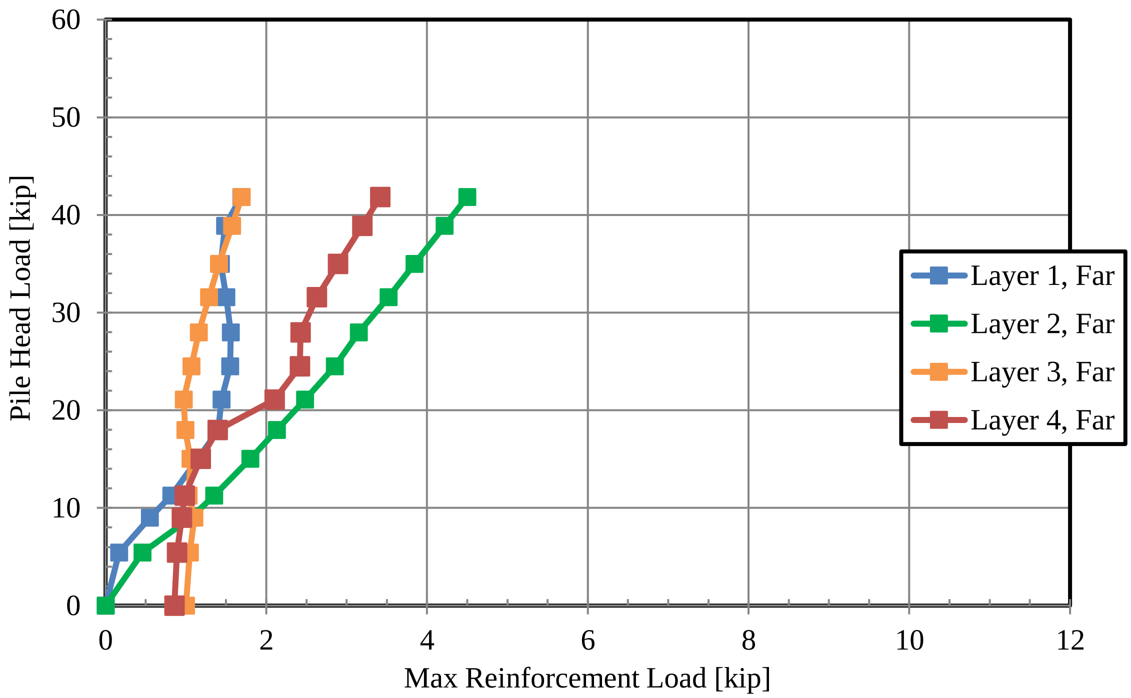

Figure 6-6: Max tensile force in far soil reinforcement at each pile head load for 1.7D test.

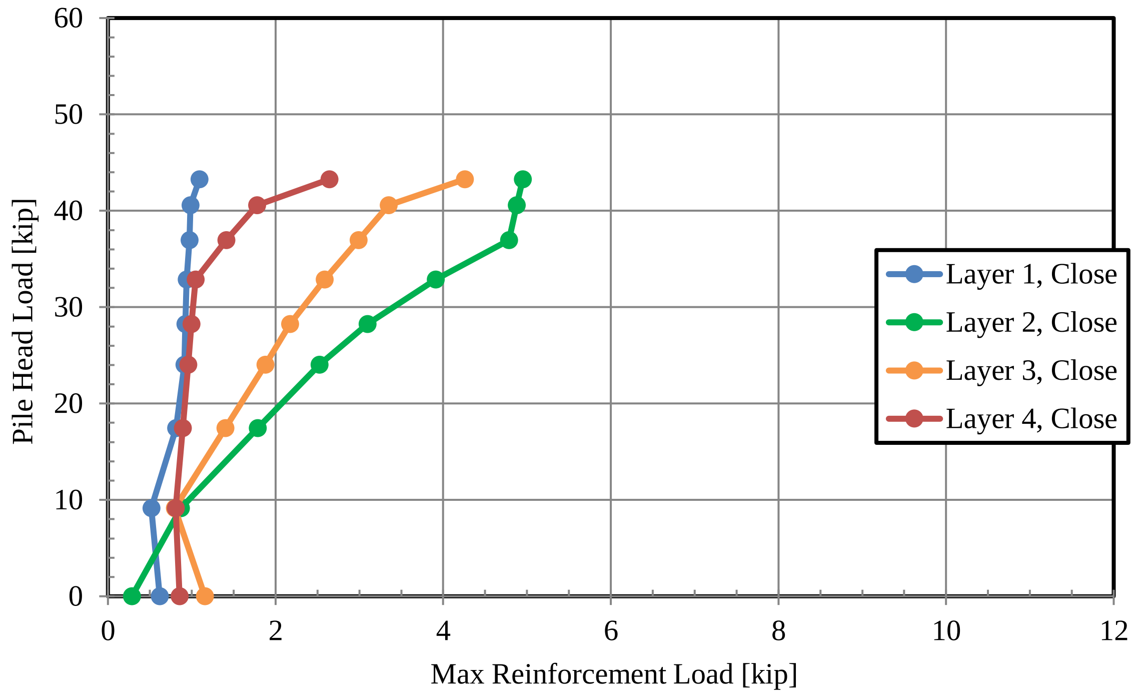

Figure 6-7: Max tensile force in close soil reinforcement at each pile head load for 2.8D test.

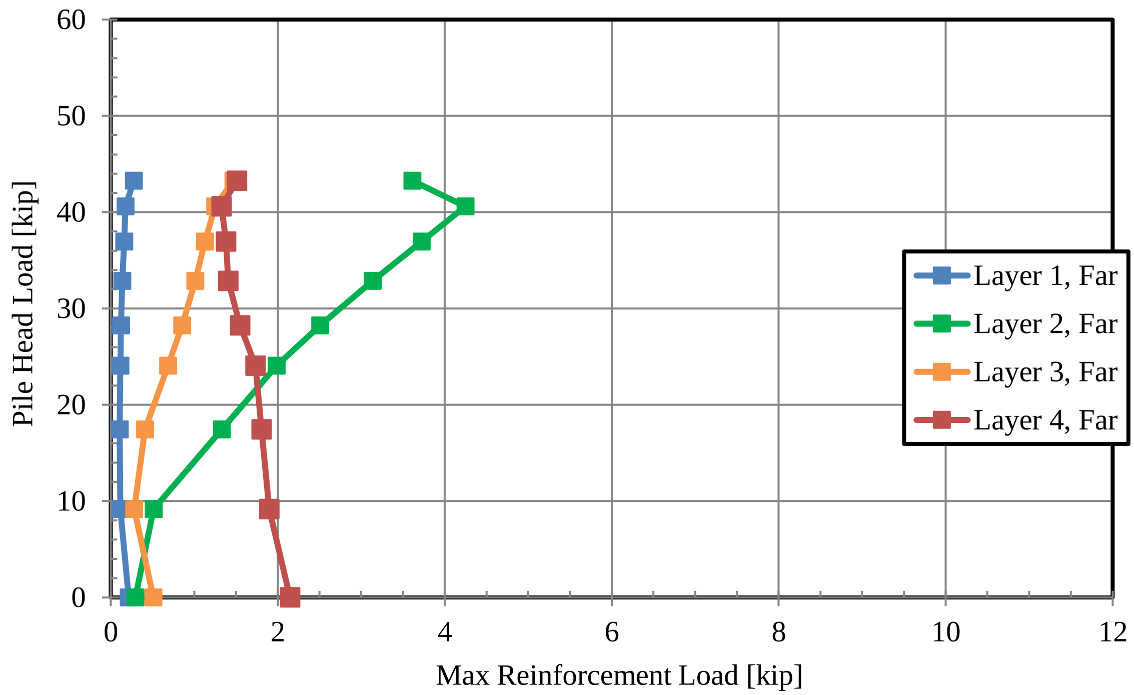

Figure 6-8: Max tensile force in far soil reinforcement at each pile head load for 2.8D test.

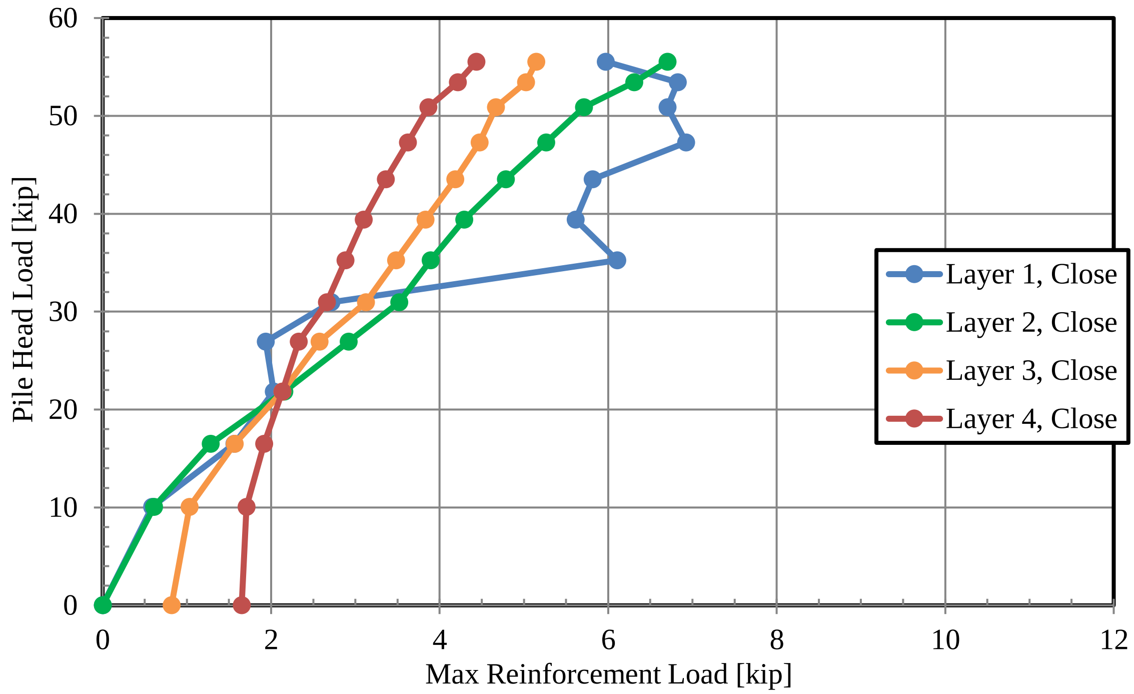

Figure 6-9: Max tensile force in close soil reinforcement at each pile head load for 2.9D test.

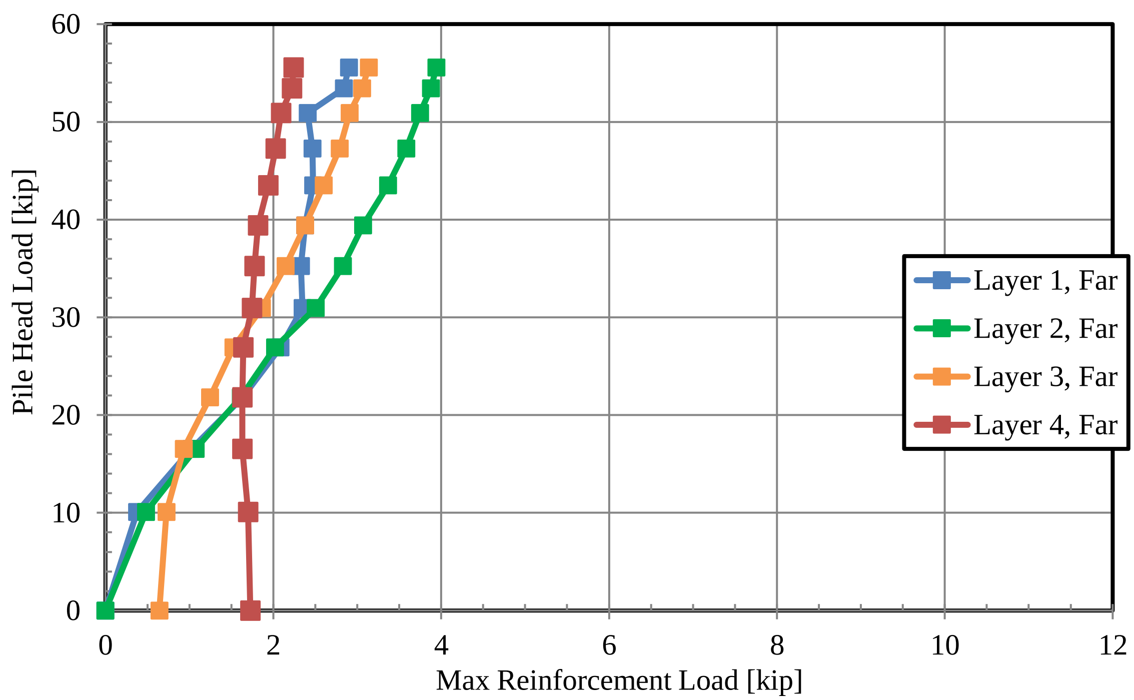

Figure 6-10: Max tensile force in far soil reinforcement at each pile head load for 2.9D test.

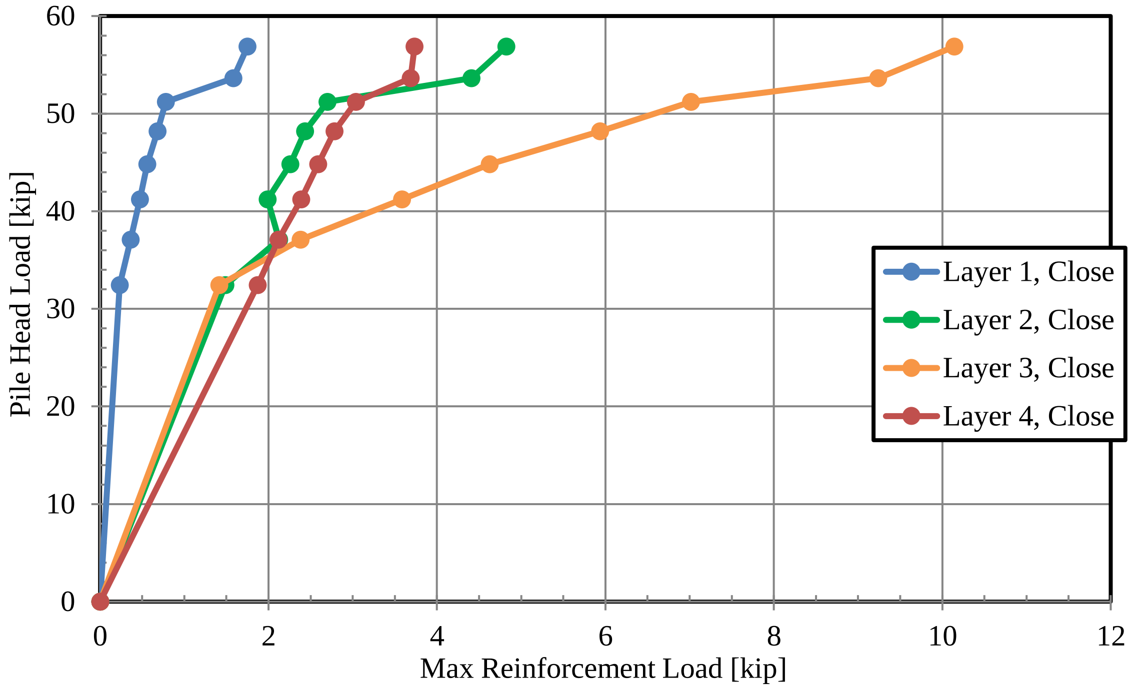

Figure 6-11: Max tensile force in close soil reinforcement at each pile head load for 3.9D test.

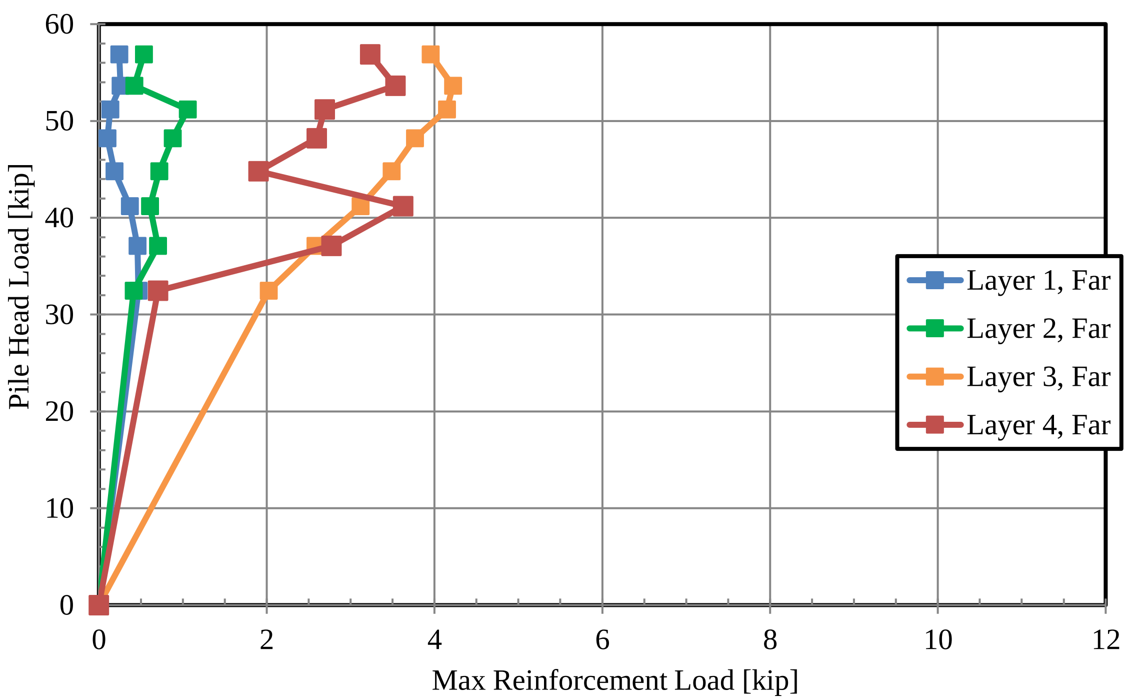

Figure 6-12: Max tensile force in far soil reinforcement at each pile head load for 3.9D test.

Figure 6-13 shows an idealized model of what is likely occurring in the reinforcement. The measured force distribution in the reinforcement suggests that soil in front of the pile is being pushed forward as the pile is loaded and the soil behind the pile is acting as an anchor for the reinforcement. Behind the pile, the strip is moving toward the wall relative to the soil. This leads to decrease tension in the strip behind the pile as load is transferred to the surrounding soil by skin friction. In front of the pile, forward movement of the soil relative to reinforcement increases the force in the reinforcement. Positive tensile force in the reinforcement at the wall face is likely a result of the increased earth pressure on the wall from the pile loading. Occasionally negative values were observed indicating that the reinforcement is in compression rather than tension. This is likely the result of bending in the reinforcement caused by uneven movement of the soil.

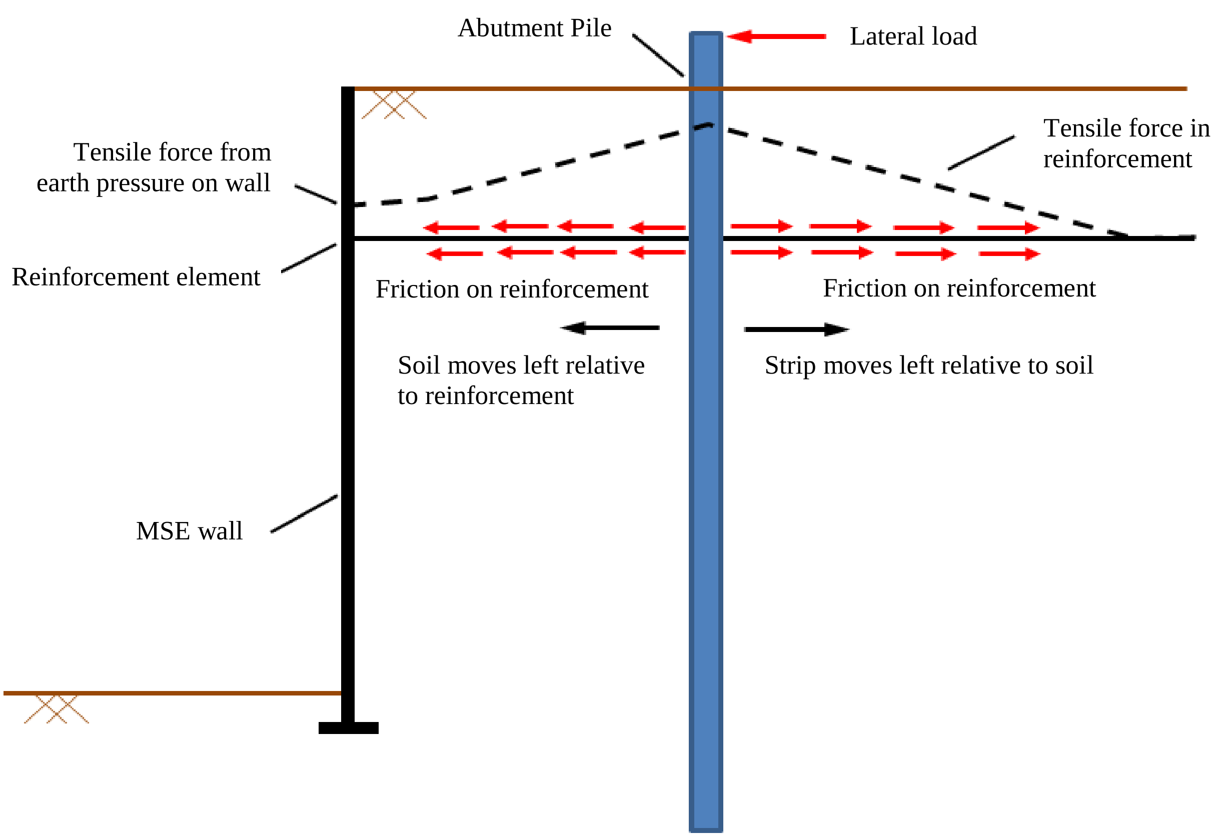

Figure 6-13: Interaction of soil and MSE wall reinforcement when pile is laterally loaded.

6.3 Statistical Analysis of Load in Reinforcement

The development of tensile force owing to lateral pile loading adjacent to an MSE wall is a relatively complicated soil structure interaction problem. The pile is interacting with the soil, soil is interacting with the reinforcements, and the reinforcements are interacting with the wall. As a result, it was not possible to develop any meaningful simple models to describe the observed behavior. With the help of Dr. Dennis Eggett (BYU Statistics Department), a multiple regression statistical analysis was performed using data from Phase II (Besendorfer, 2015), Phase I (Han, 2014), and data previously collected from UDOT bridge construction (Nelson, 2013). The Statistical Analysis System (SAS) software program was used to run the regression analysis using the general linear modeling (GLM) procedure. SAS was used to determine the statistically significant parameters in the model, after which the Data Analysis pack for Microsoft® Excel was used to fine tune the model by eliminating parameters and thereby simplifying the model without decreasing the R^2 value significant.

The regression analysis was performed by assigning the maximum tensile stress on the soil reinforcement as the dependent variable. Data was obtained for each load increment for each pile load test. The independent variables tested in this analysis were pile head load, normalized transverse distance from the pile center (T/D) where D is the pile diameter, vertical stress (σ_v) in lbs/ft^2, normalized spacing of the pile behind the MSE wall (S/D), and the reinforcement length to height ratio (L/H). In computing the vertical stress, the weight of the surcharge was considered and the surcharge height was also considered to increase the effective wall height H in accordance with AASHTO code requirements.

After the SAS analysis was completed, the relevant parameters were all of the independent variables and the following two-way interactions: vertical stress by L/H ratio, load by load, vertical stress by transverse distance, and load by transverse distance. Table 6-1 presents the R^2 value after the SAS analysis, and subsequent R^2 values after removing the next least significant term. Terms were removed from top to bottom in order of least significance to most significance, where the final R^2 value is the result of load as the final parameter. As seen in Table 6-2, two terms could be eliminated without markedly decreasing the R^2 value; however, removing additional terms would reduce the R^2 value by 3 to 5% for each term eliminated. Therefore, a somewhat more complicated equation was accepted to maintain a higher R^2 value.

Table 6-1: Effect of term elimination on R^2 values.

Term Removed	Adjusted R^2	Decrease in Adjusted R^2	R^2	Decrease in R^2
None	80.67%	None	81.03%	None
$(T/D)*(S/D)^+$	80.42%	0.25%	80.76%	0.27%
$\sigma_V*(T/D)^+$	80.13%	0.29%	80.45%	0.31%
$(L/H)^{2+}$	79.62%	0.51%	79.92%	0.53%
$P*(S/D)^+$	78.71%	0.91%	78.99%	0.93%
$P*(L/H)^+$	77.35%	1.36%	77.62%	1.37%
$\sigma_V*(L/H)$	75.86%	1.49%	76.12%	1.51%
σ_V^2	74.59%	1.27%	74.83%	1.29%
L/H	73.18%	1.41%	73.39%	1.43%
σ_V	72.61%	0.57%	72.79%	0.60%
S/D	70.96%	1.65%	71.11%	1.68%
P*(T/D)	68.53%	2.43%	68.65%	2.46%
P^2	64.78%	3.74%	64.88%	3.77%
T/D	51.45%	13.33%	51.52%	13.36%

$^+$Terms removed for the prediction equation.

Table 6-2: Final results of the statistical analysis with tensile force as the dependent variable.

Parameter	Coefficient	Standard Error	t-stat	P-value	Lower 95%	Upper 95%
Intercept	-1.8959204180	0.20553	-9.22469	<0.00001	-2.29941	-1.49243
Pile Load, P	0.0284582504	0.00115	24.68453	<0.00001	0.02619	0.03072
Normalized Transverse Distance, T/D	-0.0232492106	0.00707	-3.28707	0.00106	-0.03713	-0.00936
Vertical Stress, σ_V	0.0025190053	0.00028	8.93580	<0.00001	0.00197	0.00307
Normalized Spacing, S/D	-0.0343075454	0.00396	-8.66478	<0.00001	-0.04208	-0.02653
Length to Height Ratio, L/H	1.4642771789	0.16072	9.11065	<0.00001	1.14875	1.77980
σ_V(L/H)	-0.0012644575	0.00018	-7.04195	<0.00001	-0.00162	-0.00091
σ_V^2	-0.0000006085	<0.00001	-9.32383	<0.00001	<0.00001	<0.00001
P(T/D)	-0.0020748413	0.00024	-8.78667	<0.00001	-0.00254	-0.00161
P^2	-0.0002084736	0.00002	-11.44068	<0.00001	-0.00024	-0.00017

Data for the measured maximum tensile force and computed maximum tensile force were not normally distributed but were log normally distributed. Therefore, a base 10 log transformation was applied to the tensile force before running the analysis to account better for scatter in the data. A total of 746 data observations were used in the regression analysis resulting in an R^2 value of 0.776. An R^2 of 0.78 indicates that the equation accounts for approximately 78 percent of the observed variation in the tensile force for the welded-wire grid reinforcements. P values are used to understand the statistical significance of a variable, with lower values being more significant. P values for this regression analysis were all less than 0.001 as shown in Table 6-2 indicating that all of the terms in the final equation are statistically significant. The final results of the log form regression analysis are presented in Table 6-2.

Based on the regression analysis, the maximum tensile force, F, in kips is given by the equation:

$$\boldsymbol{F}\text{=}\mathbf{10}\wedge\left(-\mathbf{1.9}+\mathbf{0.028}\boldsymbol{P}-\mathbf{2.1}\boldsymbol{x}\mathbf{10}^{-4}\boldsymbol{P}^{2}-\mathbf{0.0023}\left(\frac{\boldsymbol{T}}{\boldsymbol{D}}\right)-\mathbf{0.0021}\boldsymbol{P}\left(\frac{\boldsymbol{T}}{\boldsymbol{D}}\right)-\mathbf{0.034}\left(\frac{\boldsymbol{S}}{\boldsymbol{D}}\right)+\mathbf{1.5}\left(\frac{\boldsymbol{L}}{\boldsymbol{H}}\right)+\mathbf{0.0025}\boldsymbol{\sigma_{v}}-\mathbf{6.1}\boldsymbol{x}\mathbf{10}^{-7}\boldsymbol{\sigma_{v}}^{2}-\mathbf{0.0013}\boldsymbol{\sigma_{v}}\left(\frac{\boldsymbol{L}}{\boldsymbol{H}}\right)\right)-\mathbf{1} \qquad \textbf{(6-2)}$$

where

P is the pile head load (kips),

T is the transverse distance from the reinforcement to the pile center (in.),

D is the outside pile diameter (in.),

σ_v is the vertical stress (psf),

S is the spacing from the pile center to the back face of the wall (in.),

L is the length of the reinforcement (ft.), and

H is the combined height of the wall and equivalent height of surcharge (ft.).

Parameter coefficients from Table 6-2 were limited to two significant figures in Equation 6-2. Note that reducing the coefficients to two significant figures simplifies the statistical regression equation without any significant loss in accuracy or change in R^2.

Predicted maximum tensile forces were then computed by taking the field data for the above parameters and plugging them into Equation 6-2. A comparison of the predicted and measured maximum tensile forces in log form is shown in Figure 6-14. Data on the red 1:1 line indicates that the measured and predicted values are equal. The red dashed lines are associated with plus or minus one standard deviation which encloses approximately 68% of the data points. The black dashed lines indicate plus or minus two standard deviations which enclose approximately 95% of the data points. For convenience in showing measured and computed tensile forces directly, the data was transformed out of log form and is shown in Figure 6-15.

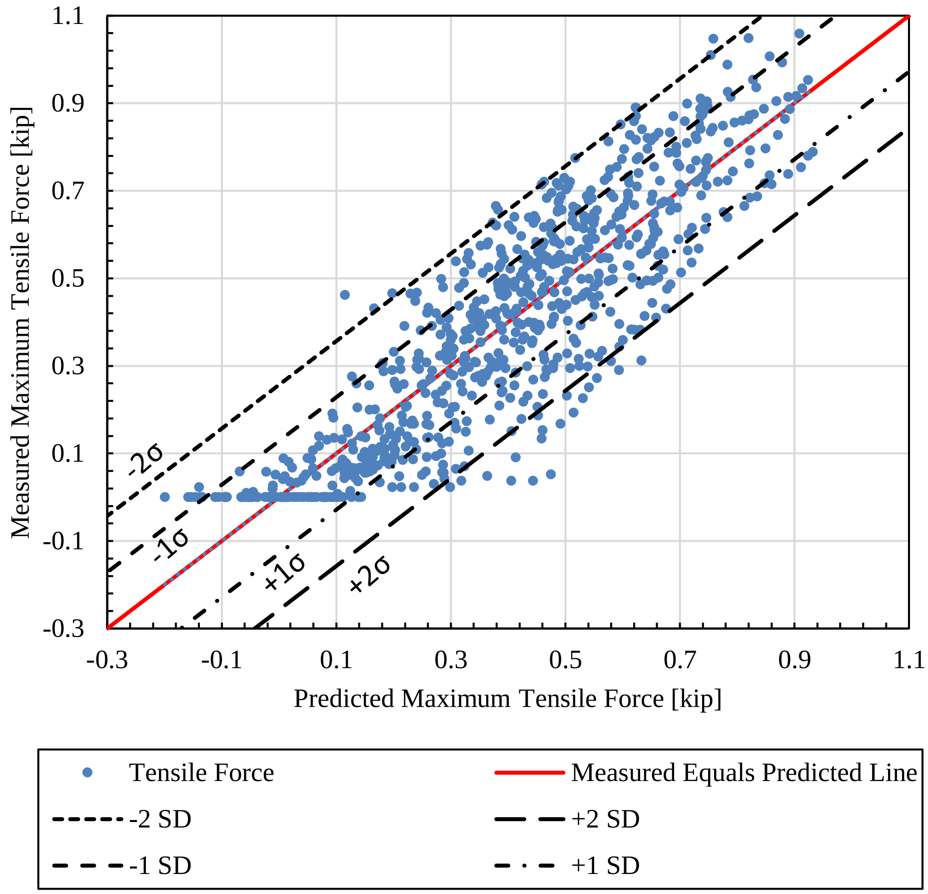

Figure 6-14. Measured versus computed logarithmic tensile force results.

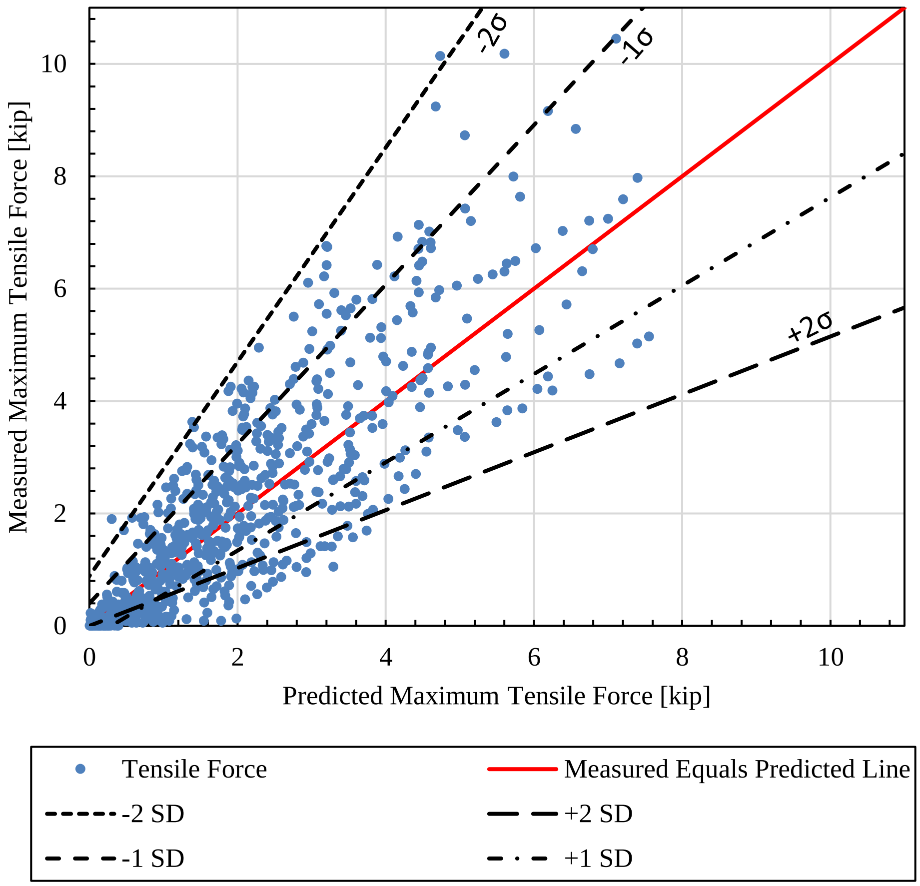

Figure 6-15. Measured versus computed tensile force results.

Data that is not located on the 1:1 red line in Figure 6-14 and Figure 6-15 demonstrates the difference (or residual) of the predicted data from the measured data. The residual for the data was calculated by using the following equation:

$$\boldsymbol{R = log(F_{measured} + 1) - log(F_{predicted} + 1)} \qquad \textbf{(5-3)}$$

where

R is the residual,

$F_{measured}$ is the measured maximum tensile force, and

$F_{predicted}$ is the predicted maximum tensile force.

The log residual is plotted against each independent variable in Figure 6-16 through Figure 6-20. If the regression equation is adequately capturing the influence of a variable, then the residuals will be uniformly distributed about zero with respect to the independent value. However, if the residuals trend upwards or downwards as the independent value increases, then the regression equation may need to be revised over some data range. In general, the residuals fall within the range of -0.3 to 0.4 and appear to be uniformly scattered with respect to zero for all the independent variables. Generally, these results indicate that the regression equation is adequately accounting for the influence of the variables in the equation. However, there is a slightly upward trend towards positive residuals at greater stress levels in Figure 6-20. To further illustrate the uniformity of the scatter about zero and the validity of the equation, residuals were plotted as a function of computed log force as shown in Figure 6-21. The linear regression line from Figure 6-21 is centered on zero along the x-axis, demonstrating there is no bias in the regression equation based on residuals.

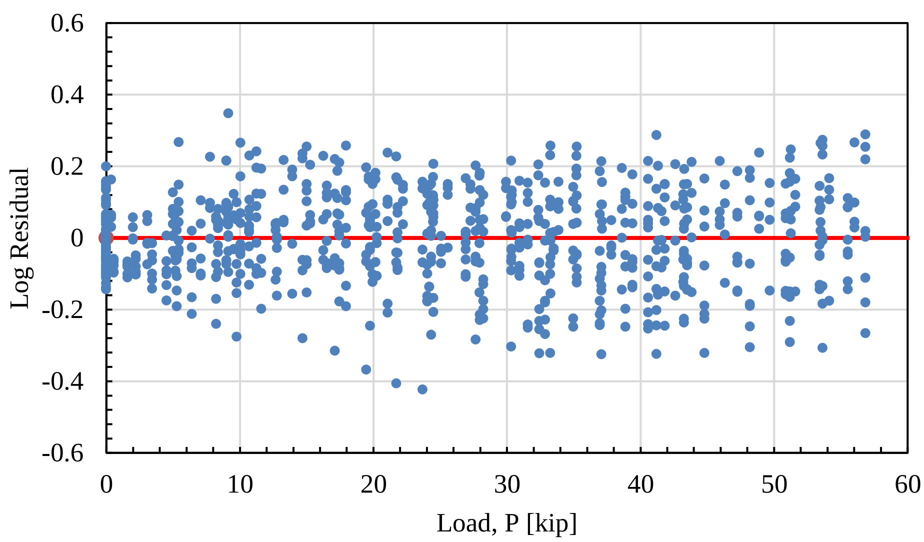

Figure 6-16. Log residual of the pile head load variable for the multiple regression analysis.

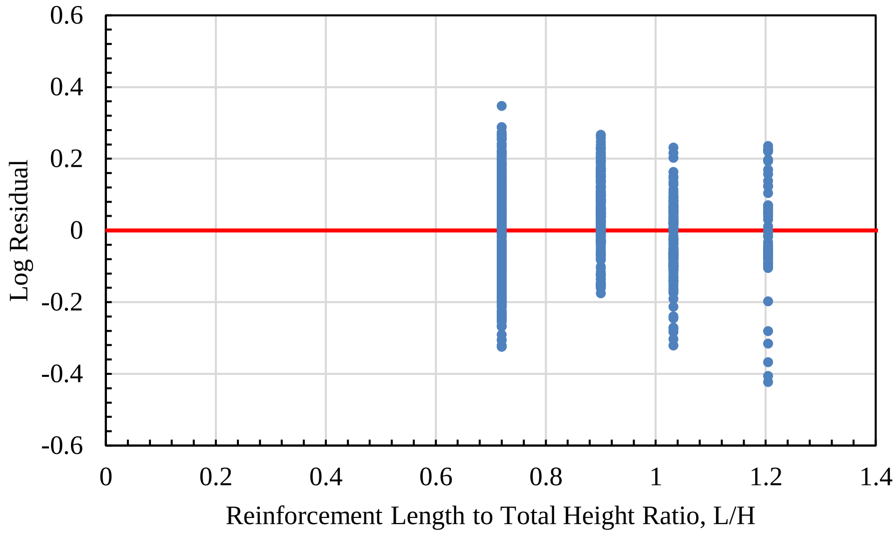

Figure 6-17. Log residual of the L/H ratio variable for the multiple regression analysis.

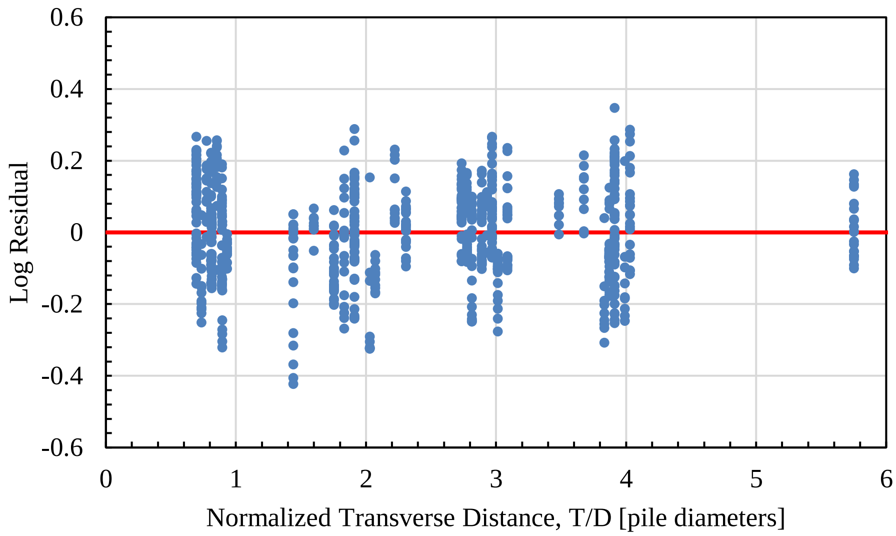

Figure 6-18. Log residual of the normalized transverse distance variable for the multiple regression analysis.

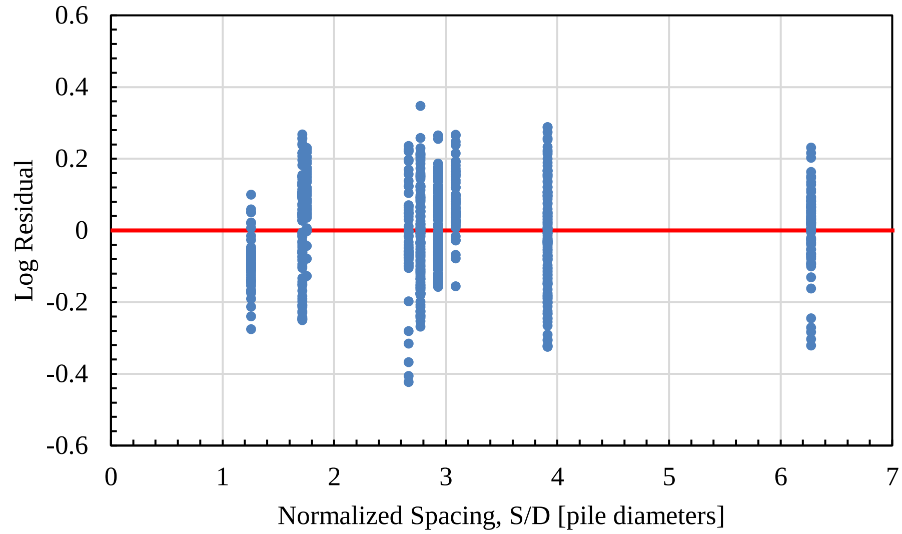

Figure 6-19. Log residual of the normalized pile spacing variable for the multiple regression analysis.

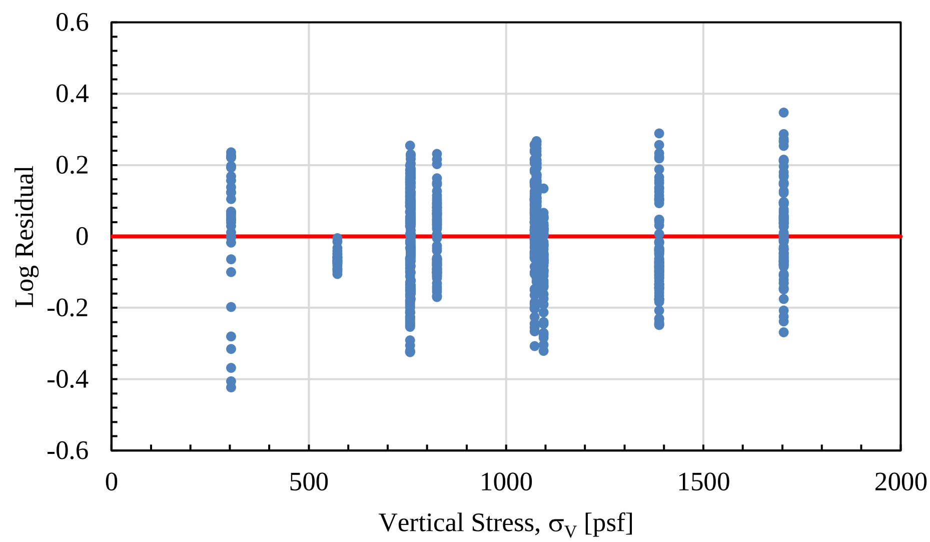

Figure 6-20. Log residual of the vertical stress variable for the multiple regression analysis.

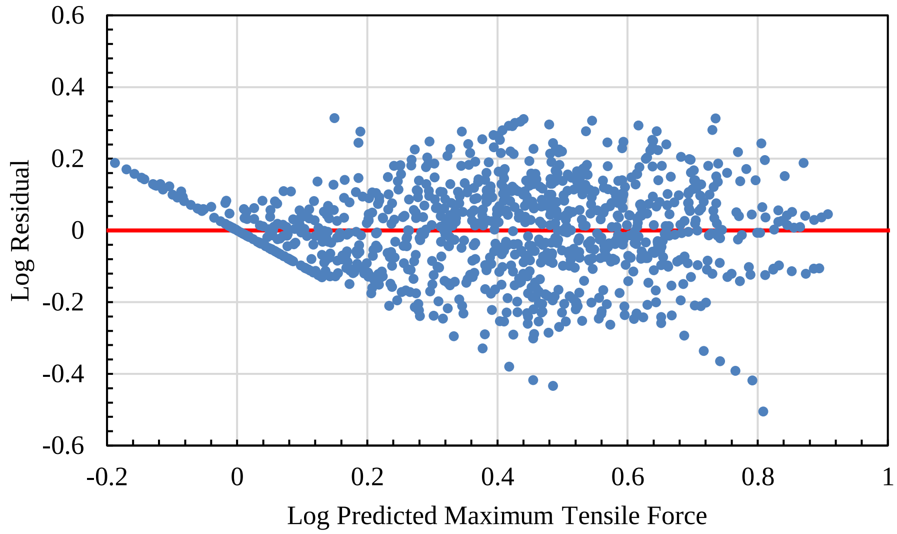

Figure 6-21. Log residual versus computed log tensile force.

Table 6-3 shows the minimum and maximum values that were included for each parameter. Values used out of this range may not yield accurate predicted tensile force when using the equation above.

Table 6-3. Numerical Range of Parameters for Strip Reinforcement Statistical Analysis

Parameter	Range
Pile Load, P	0 kip - 56.9 kip
Normalized Transverse Distance, T/D	0.7 - 5.8
Vertical Stress, σ_V	304 psf- 1704 psf
Normalized Spacing, S/D	1.3 - 6.3
Reinforcement Length to Total Height Ratio, L/H	0.7 - 1.2
Pile Diameter, D	12.75 in.
Measured Tensile Force, F	0 – 10.4 kip

6.4 Ground Displacement

The lateral load applied to the pile caused displacement of the ground surface between the pile and the MSE wall. The horizontal movement of the ground surface was monitored throughout testing using string potentiometers attached to steel stakes pounded into the ground between the pile and the wall. Vertical ground displacement was also measured using an optical surveying level and rod. Vertical ground displacement was measured at 3.0 in. pile head deflection but was not measured throughout the test for safety reasons.

Figure 6-22 shows the measured vertical ground displacement at 3.0 in. pile head deflection for all of the tests. In general, the heave at the wall tends to increase as the pile is loaded closer to the wall. In addition, the general trend is that vertical ground displacement is highest near the pile face and decreases with distance from the pile face. The 2.8D test is the exception. According to measurements taken, the soil displaced very little near the pile face and the greatest displacement was approximately 1 ft. from the pile face. There are several possible explanations for this. Because the pile was at 3 in. of displacement during the second measurement, the level rod may have been held at an angle while the second measurement was taken or perhaps the measurement was read from the rod incorrectly. Assuming the measurement is correct, this discrepancy could be due to the different panel configuration of the wall in front of the pile. A smaller 2.5x10 ft. panel is located at the top of the wall for this test. Rotation of the top of the panel towards the pile was observed as lateral loading occurred. This may have caused additional compression of the soil between the pile and the wall and an increase in the soil heave further from the pile. Furthermore, it rained during this test increasing the uncertainty of the measurement.

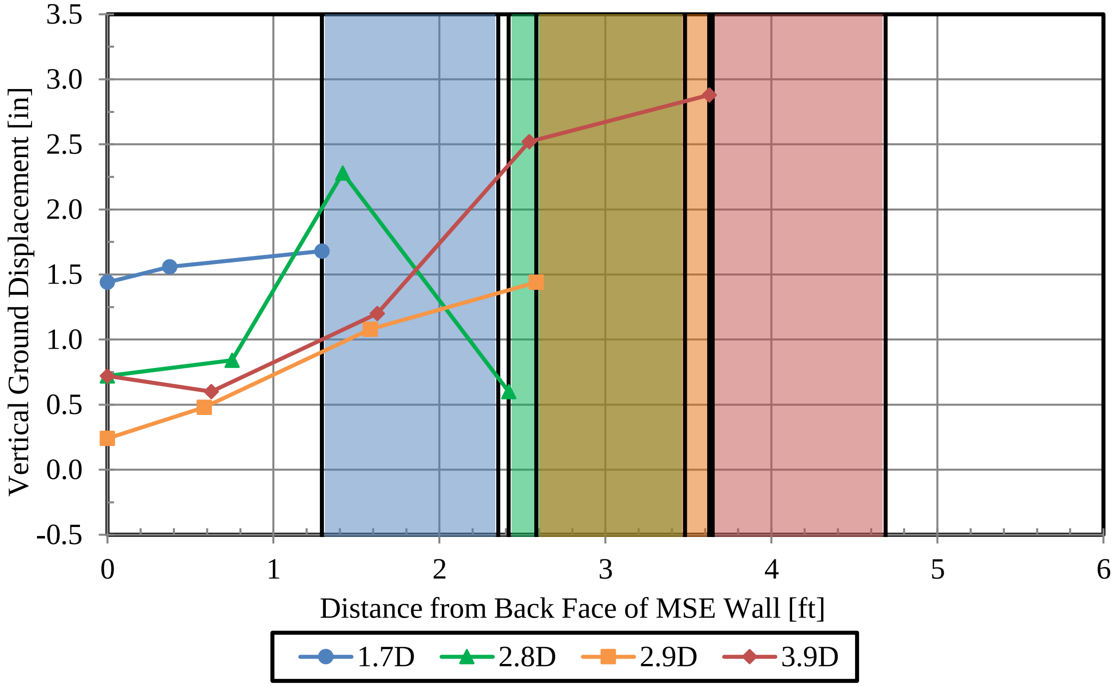

Figure 6-22: Vertical ground displacement for all test piles.

Horizontal ground displacement was greatest near the pile and decreased in a non-linear fashion with increased distance from the pile to relatively small values at the back face of the wall. Figure 6-23 is an example of the horizontal ground displacement between the pile and the back face of the MSE wall for the 2.9D test at several load levels. Horizontal ground displacement curves for the rest of the tests can be found in Appendix E. As expected, horizontal ground displacement tends to increase as the displacement of the pile increases. For each of the tests, the distance from the pile where each measurement was taken was normalized by the pile diameter and the measured horizontal ground displacement was normalized by the pile displacement. Figure 6-24 is a plot showing these normalized curves at 3.0 in. of pile displacement. The curve for the pile at 3.9D suggests that a distance of 3.5 to 4 pile diameters might normally be required to reduce normalized horizontal displacements to near zero. However, at closer pile spacings, the reinforcing members appear to resist additional applied forces to reduce displacement at the wall.

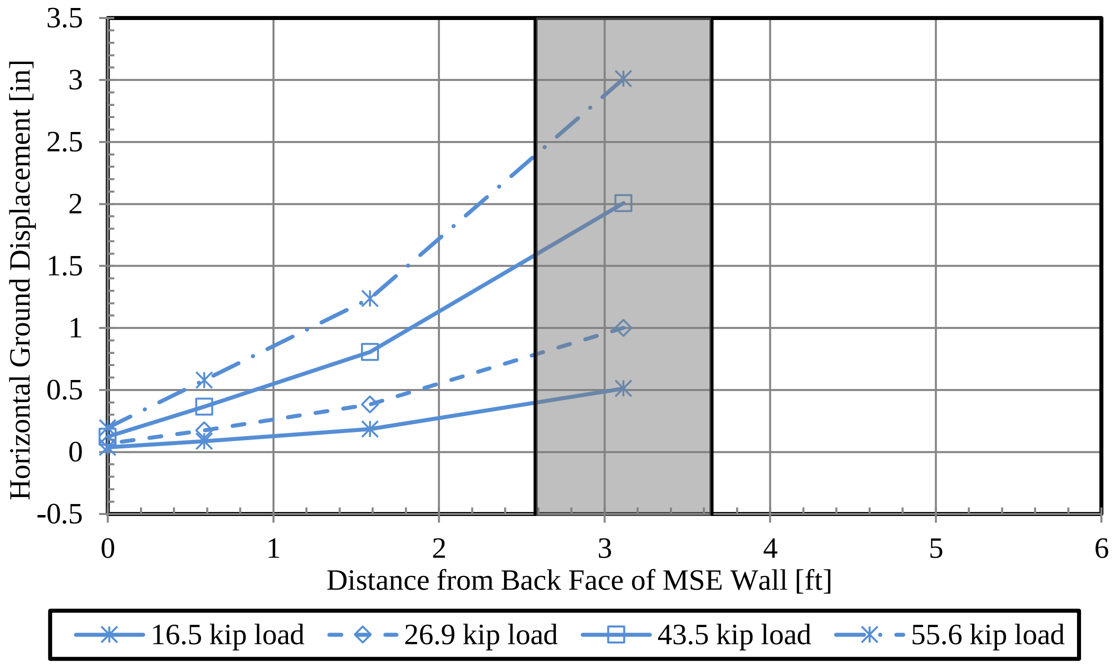

Figure 6-23: Horizontal ground displacement for 2.9D test at several pile head load levels.

Both the 2.8D and 3.9D curves show that normalized ground displacement dropped to near zero about one pile diameter (1 ft.) from the pile face, followed by a slight increase and then decrease to approximately zero at the back face of the wall. Both of these piles are located at the center of a wall panel while the other two are at a joint. A likely explanation is that the steel stakes that the string potentiometers were attached to rotated backwards slightly due to passive shear plane development in front of the pile causing a decrease in measured displacement. The lines connecting the string potentiometers to the stakes could not be attached at ground level because space was needed to ensure string potentiometer function was not hindered by ground heave.

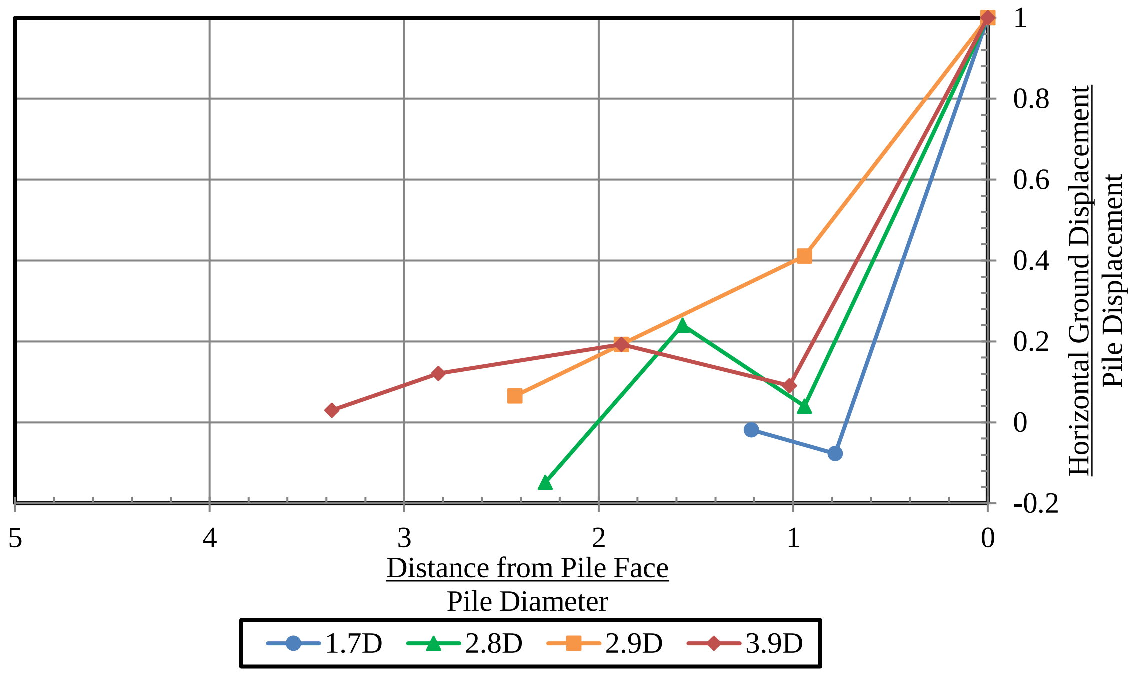

Figure 6-24: Normalized ground displacement.

6.5 Wall Panel Displacement

DIC was used as the primary method of monitoring wall panel displacement. Additionally, a string potentiometer was attached to the top of the wall to monitor the deflection of the top of the panel. Four shape arrays placed against the back side of the wall located at various transverse distances from the pile center were used as an additional method of measuring the deflection of the wall.

Figure 6-25 and Figure 6-26 show the respective results of the DIC analysis of wall panel displacement at 0.5 in. and 3.0 in. pile head deflection.

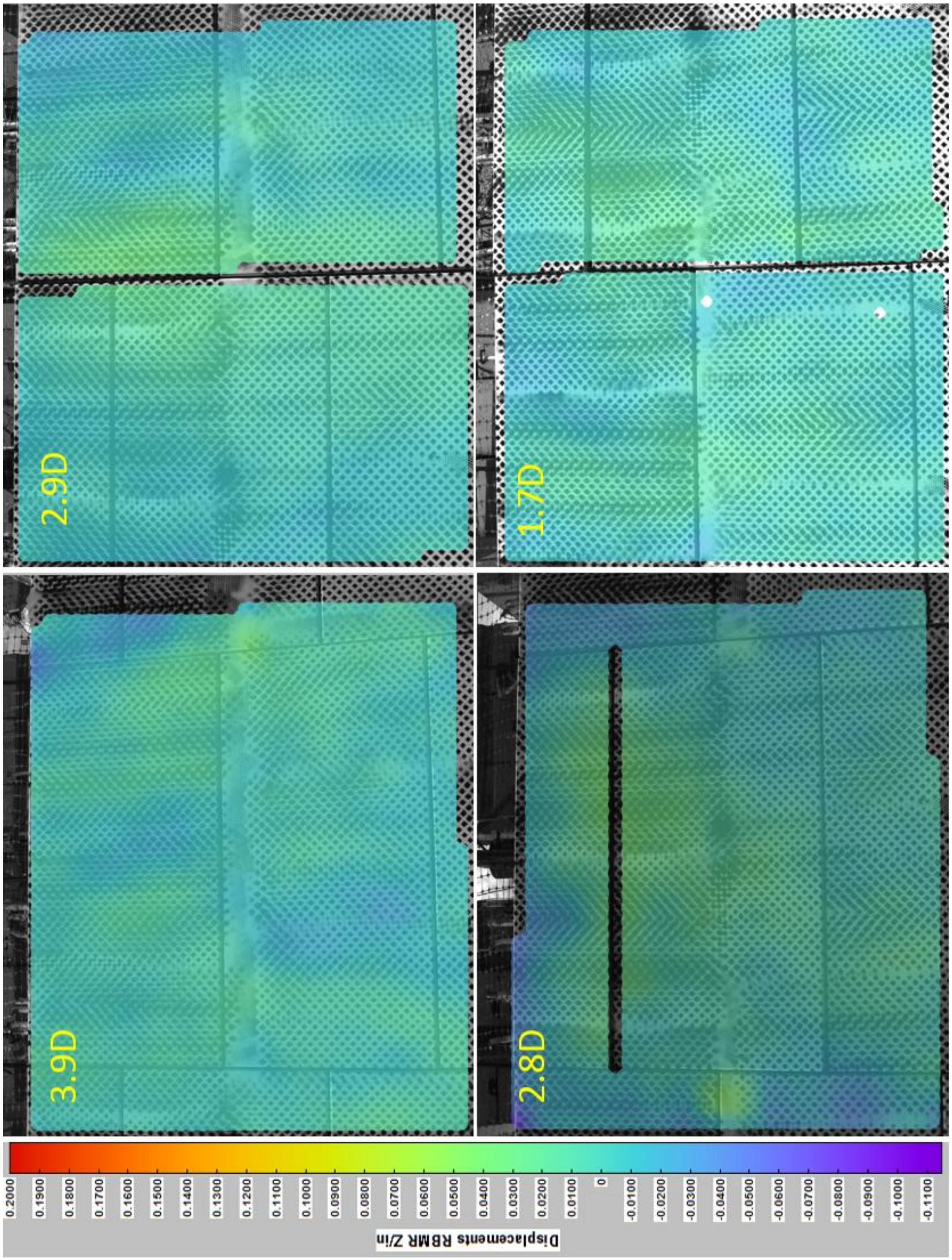

Figure 6-25: Wall panel displacement at 0.5 in. pile head displacement for all piles tested.

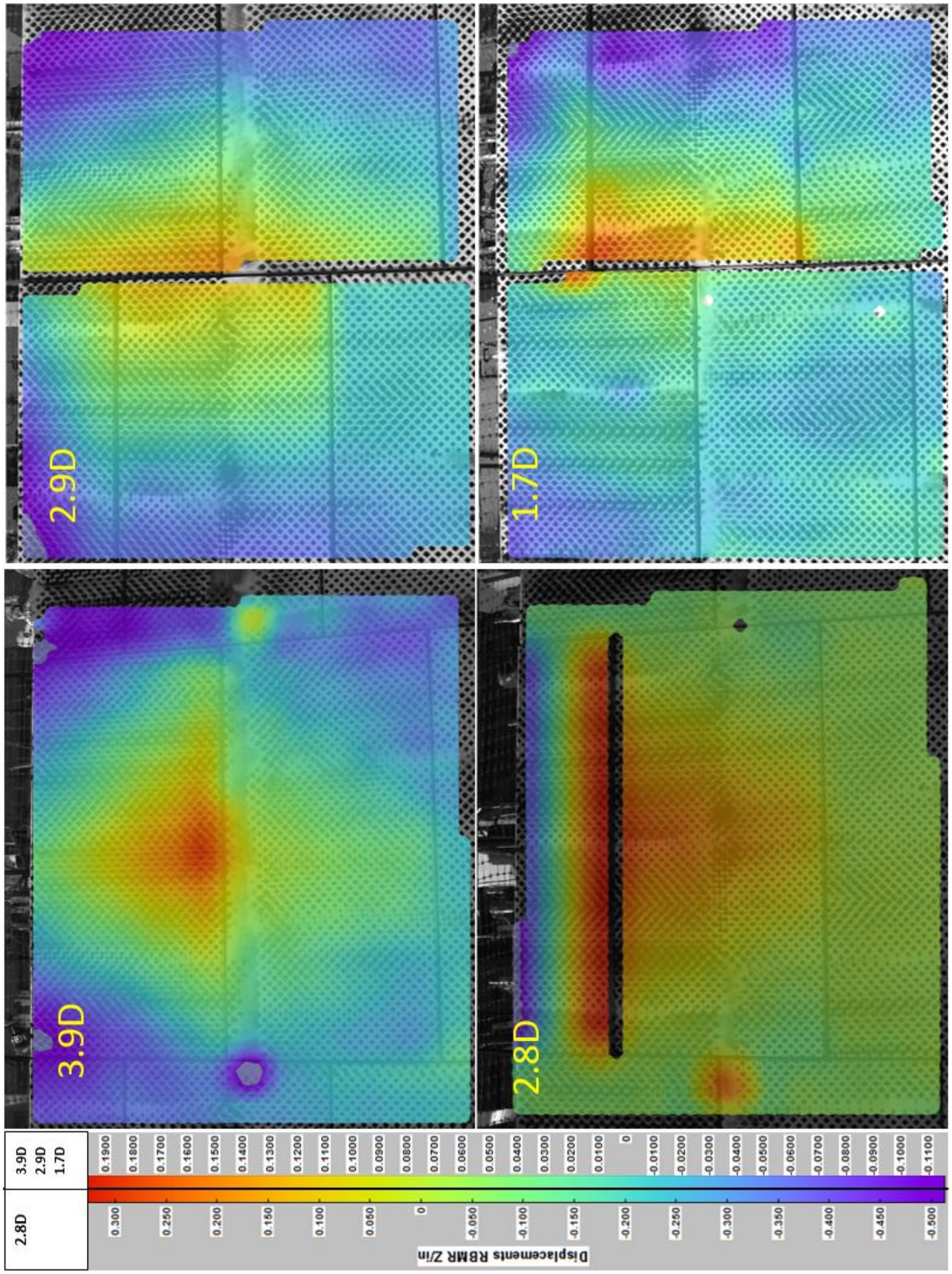

Figure 6-26: Wall panel displacement at 3.0 in. pile head deflection. Note different scale on 2.8D.

In both cases, the lateral load of the 2.8D test causes the greatest wall panel displacement. The higher displacement of the wall panels experienced by the 2.8D test is likely a result of the smaller 2.5 ft. tall by 10 ft. wide panel located at the top of the wall closest to this pile. This panel has only one layer of reinforcement located in the middle of the panel. The top of this panel rotated back towards the pile while the bottom rotated away from the pile, with the reinforcement acting as a horizontal neutral axis. At 0.5 in. pile head deflection, the maximum displacement observed for each of the four tests is approximately 0.050 in., and there is little evidence of any distinctive displacement pattern. This displacement level is likely near the threshold of the DIC system's ability to resolve displacement at the distance the cameras were placed from the wall. Based on the RBMR data, at 3.0 in. pile head deflection, the maximum panel displacement for the 3.9, 2.9, 2.8, and 1.7D tests was 0.18, 0.13, 0.35, and 0.19 in., respectively. The maximum wall deflection generally occurs near the second layer of soil reinforcement which also generally experienced the highest induced load.

With the data collected, it is difficult to determine the extent of the zone of influence on wall displacement caused by the lateral loading of the pile. The cameras for the DIC analysis were focused on an area of the wall approximately 10 ft. tall by 12 ft. wide. However, the results suggest that displacement is relatively insignificant beyond 5 to 6 ft. on either side of the loaded pile and below a depth of about 10 to 12 ft. A review of the displacement contours, suggests that displacement forms a narrower "columnar" horizontal band for piles loaded at a joint between panels, but is somewhat broader for the piles loaded in the center of a wall panel. In addition, for a pile loaded at a joint, the displacement pattern is not always uniform across the joint and one side will often experience greater displacement than the other. Similarly, the displacements do not always transfer uniformly with depth and offsets in displacement are also seen across horizontal joints. The measurements indicate that the panels also rotated around a vertical axis but it is difficult to determine if part of the panel went backward or if it all came forward. There are different options in the software used to reduce the DIC images that allows different types of displacement to be calculated. One option is to calculate raw displacement in the x, y, or z-direction, with the z-direction being out-of-plane. It should be noted that when using this option, any movement relative to the initial position of the cameras is added to the total displacement, even if the movement is caused by the camera being moved. Another possibility is to use the Rigid Body Motion Removed (RBMR) option. This option only calculates displacements that are due to bending or distortion of an object. For example, if the camera were moved towards the wall but no bending or distortion of the wall occurred, this would show up as zero displacement. While this option seems like the best available option within the software to correct movement caused by wind or the camera settling, we observed that the cameras were not focused on a large enough area of the wall for the software to properly remove any rigid body motion and near the corners of the images negative deflections may be shown. These deflections are likely a result of the correction algorithm and not real. Hence, it is difficult to determine the extent of negative deflection that actually occurred when panels rotated. As shown in Figure 4-7, the DIC cameras were hooked to a tripod and there was wind blowing during most of the tests. Additionally, there was rain that caused some settlement of the tripod legs that were resting on the native soil. It would likely have been best to attach the camera to a more secure reference frame such as a concrete block that had been allowed to settle prior to testing so that the total z-displacement option could be used without the need of removing displacements caused by movement of the cameras. However, because some movement of the cameras did occur, a correction was determined for each time step. To determine the amount of deflection caused by movement of the camera versus actual deflection of the wall, the z-displacement at each of the corners of the DIC images was analyzed. At a transverse distance of approximately 5.5 ft., very little movement of the wall should actually be occurring so any deflection measured by the DIC is probably due to the cameras moving rather than movement of the wall and could be used as a correction. Furthermore, the deflection should be similar at these locations if the movement is due to the cameras moving. This behavior was observed for all of the tests. Within the software used to compute the DIC deflections, there is no option available to apply this correction however so the RBMR option was used in computation of the wall deflections shown in Figure 6-25 and Figure 6-26. However, this correction is applied to other displacements calculated using the DIC data.

The displacement at the location of each instrumented soil reinforcement was extracted from the DIC data and corrected for any movement of the cameras caused by wind as outlined in the previous paragraph. Plots of pile head displacement versus the displacement at each of the instrumented reinforcement locations for the 1.7, 2.8, 2.9, and 3.9D tests are shown in Figure 6-27 through Figure 6-30, respectively. The displacement is shown for both the reinforcement which is located close to the pile and the one located further from the pile. Additionally, the displacement at the top of the wall measured by the attached string potentiometer is shown in these plots. The transverse distance from the center of the pile to the center of the reinforcement can be found in Table 4-2. The second and third layers of reinforcements generally experienced the highest displacement at the higher pile head deflections, rather than the top layer. In addition, the reinforcements closer to the pile deflected somewhat more than the reinforcements further away in the transverse direction.

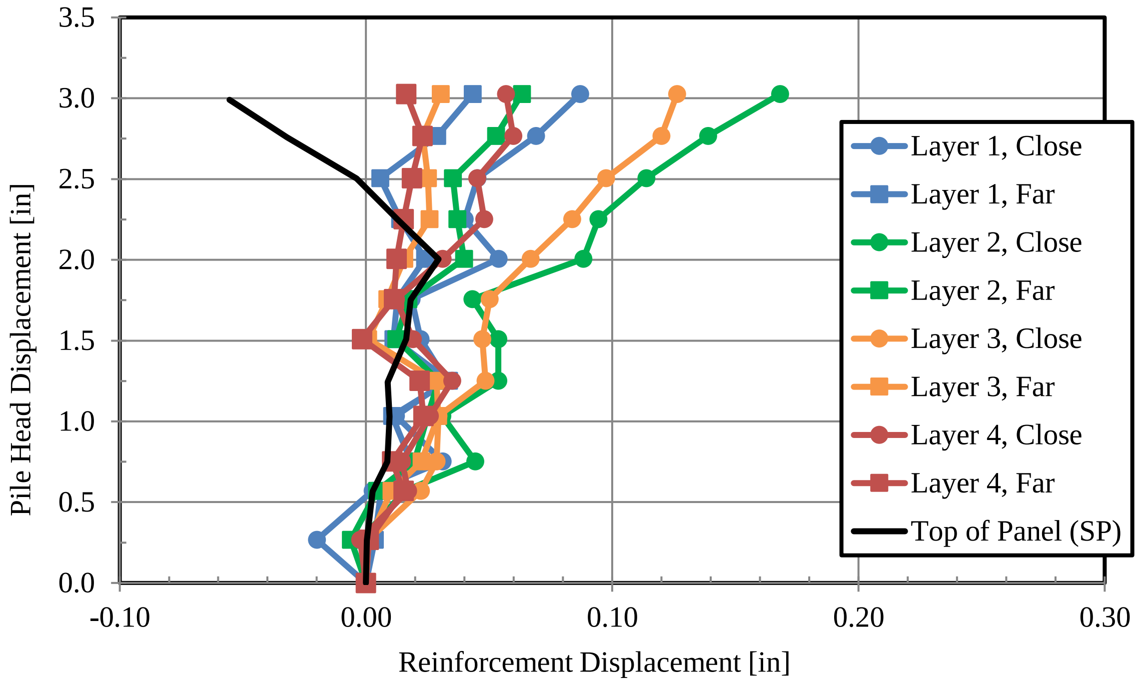

Figure 6-27: Panel displacement at the reinforcement connection location for the 1.7D test.

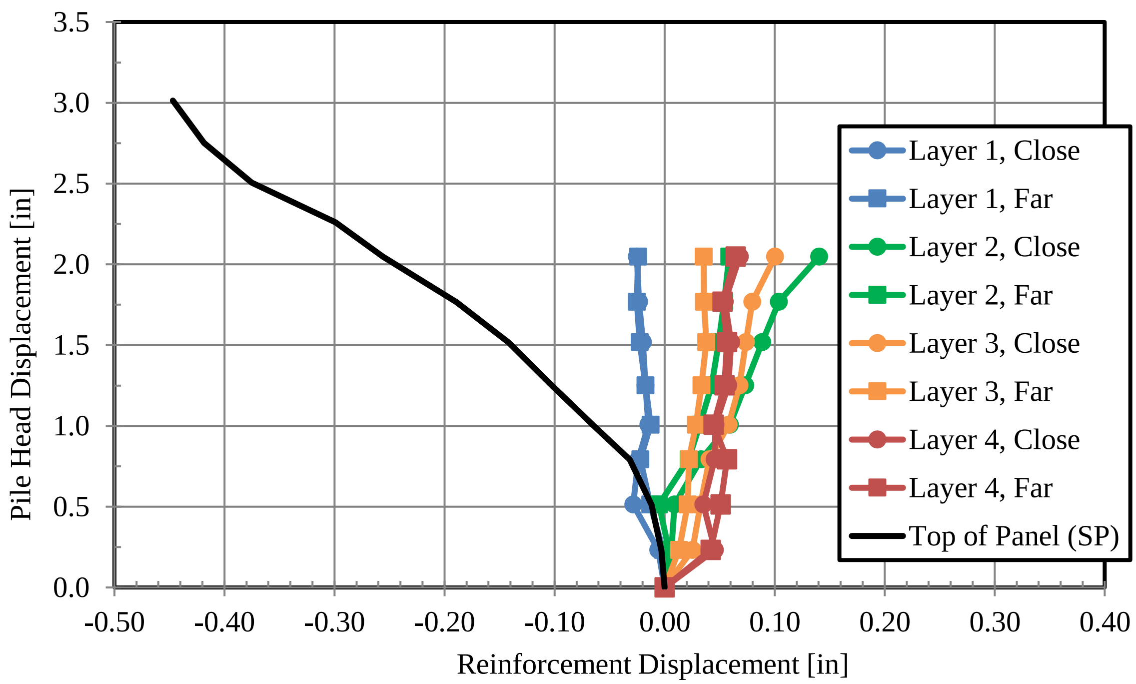

Figure 6-28: Panel displacement at the reinforcement connection location for the 2.8D test.

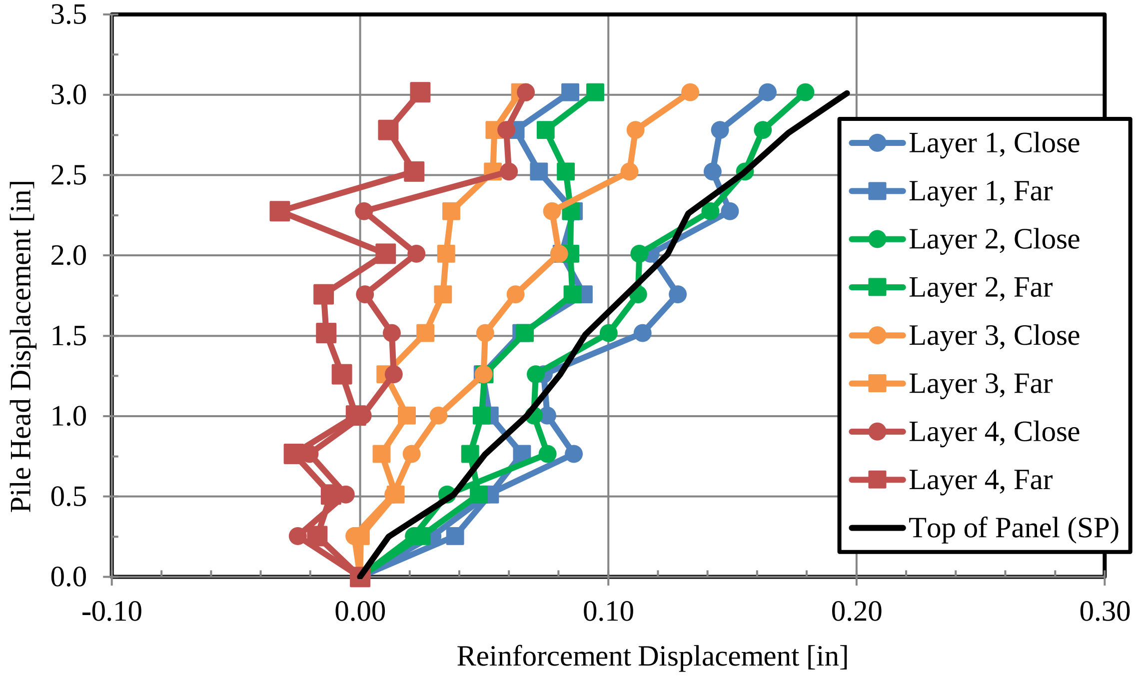

Figure 6-29: Panel displacement at the reinforcement connection location for the 2.9D test.

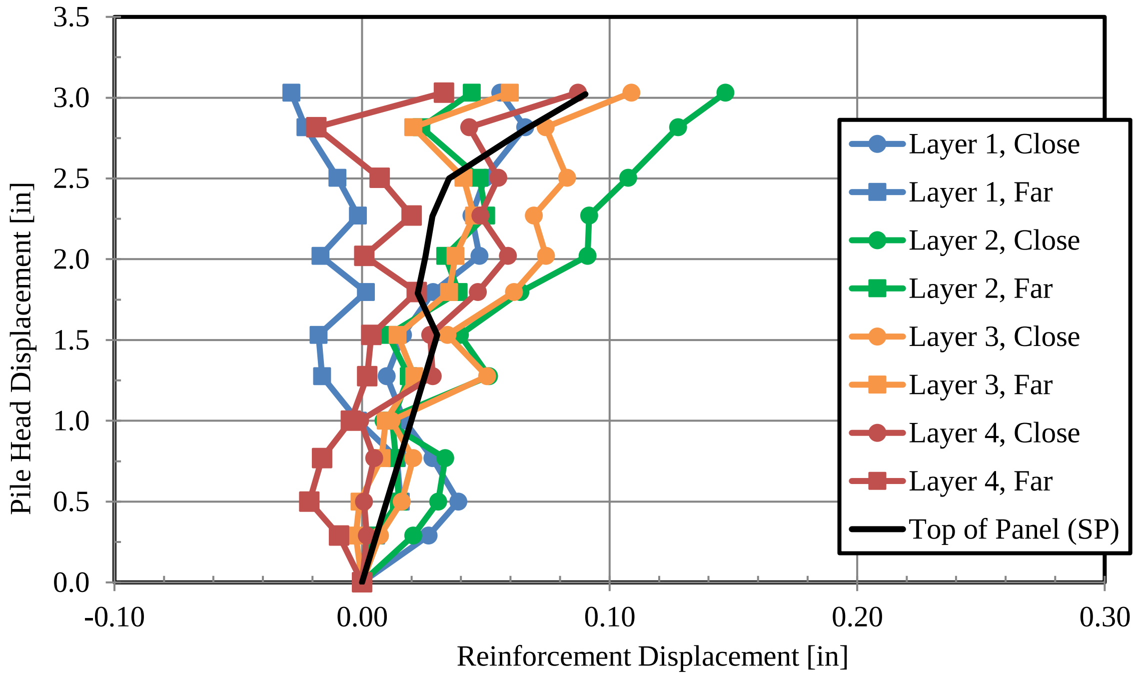

Figure 6-30: Panel displacement at the reinforcement connection location for the 3.9D test.

Although the curve shapes extracted from the DIC show some unexpected decreases in reinforcement deflection with increasing pile deflection the reinforcement deflection generally increases with increasing pile head deflection. The curve shapes do not appear to be flattening out at higher deflections as would be expected if the reinforcements were reaching their frictional capacity and pulling out. Despite the large lateral loads (and displacements) imposed on the piles, the reinforcement displacements were typically less than 0.25 in. in all cases and distress to the wall face was minimal even for the pile located 1.7D from the wall face.

Shape arrays were also used to monitor the deflection of the wall. Four shape arrays were placed in electrical conduit running vertically up the back face of the MSE wall at various transverse distances from the pile for each test. The conduit was secured against the back face of the MSE wall with duct tape during construction, but some separation of the conduit from the wall occurred during placement of the backfill. Additionally, the displacement of the top of the wall was measured by a string potentiometer that was attached to the top of the wall using an eye-bolt. The displacement measured by the shape array installed approximately in front of each pile being loaded is compared to the wall displacement at the same location calculated using the DIC data and to the displacement of the top of the wall measured by the string potentiometers. Figure 6-31 through Figure 6-34 shows this comparison for the 1.7, 2.8, 2.9, and 3.9D tests, respectively.

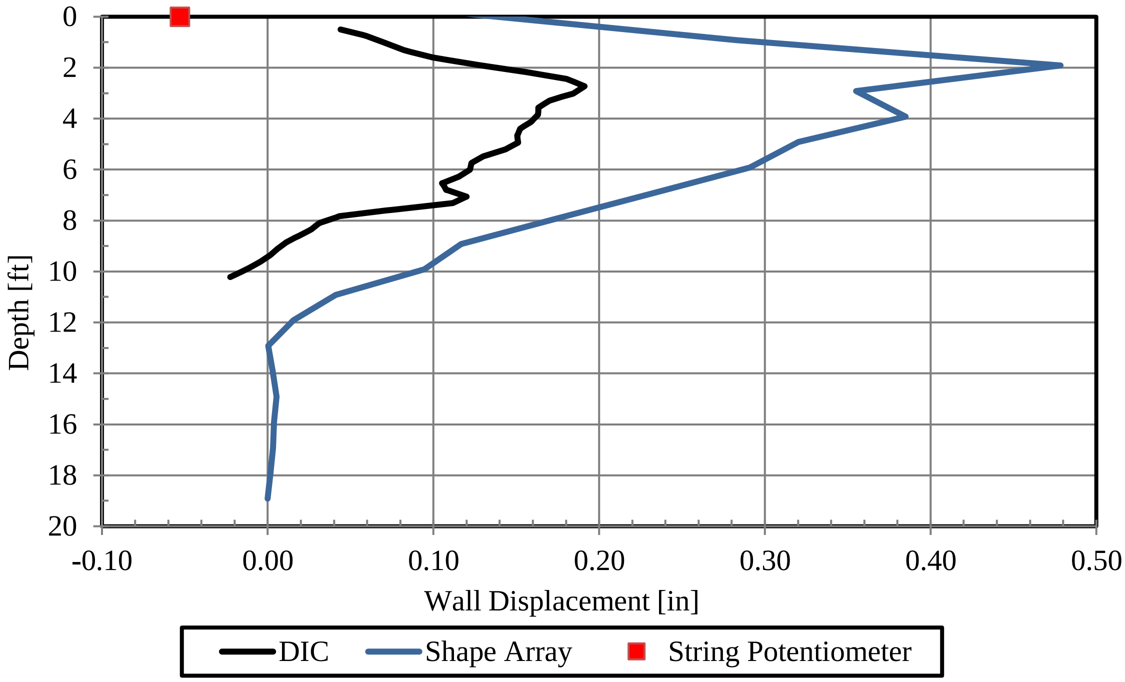

Figure 6-31: Comparison of wall displacement measured by the shape arrays to DIC and string potentiometer data for the 1.7D test at 3.0 in. pile head deflection.

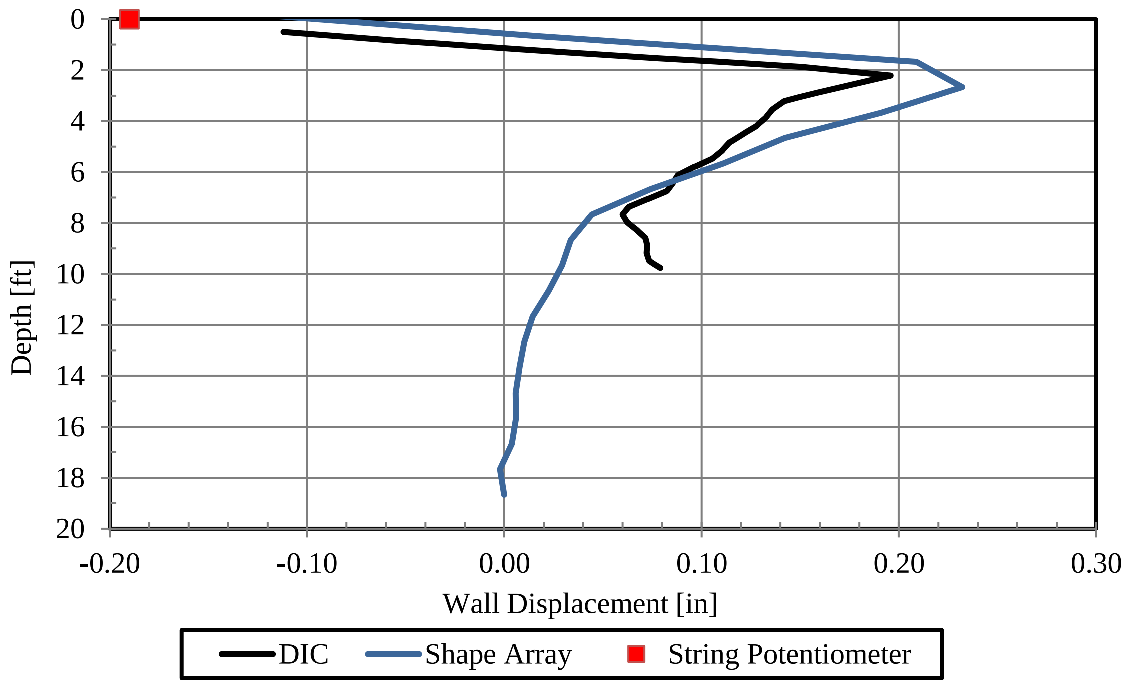

Figure 6-32: Comparison of wall displacement measured by the shape arrays to DIC and string potentiometer data for the 2.8D test at 1.75 in. pile head deflection.

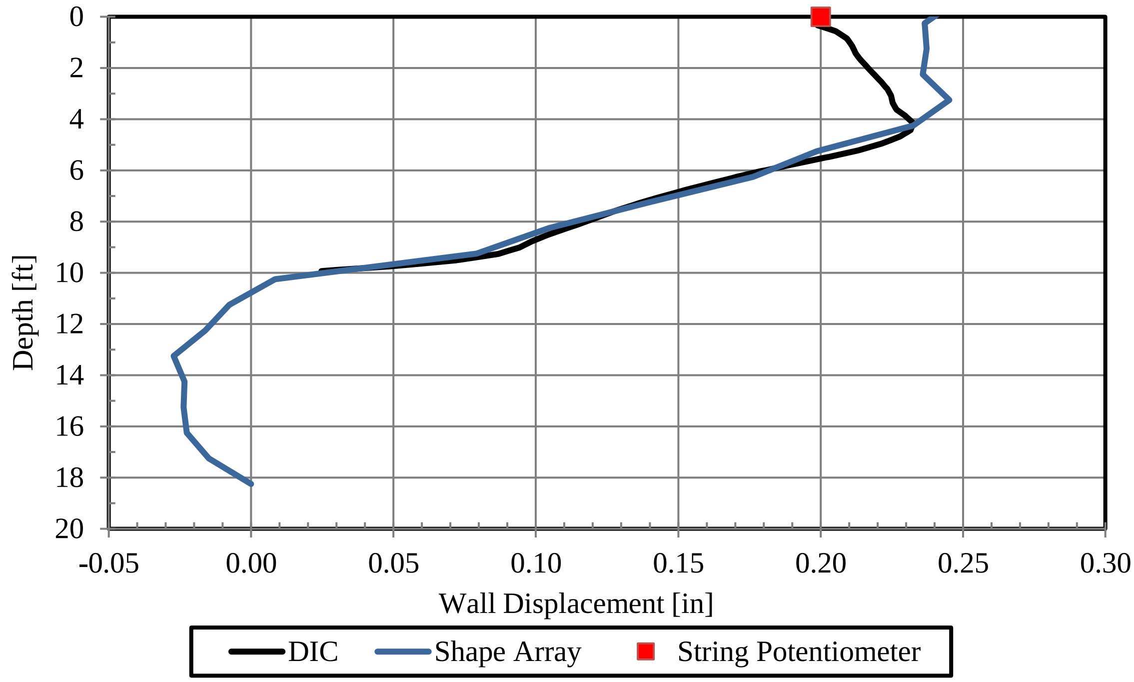

Figure 6-33: Comparison of wall displacement measured by the shape arrays to DIC and string potentiometer data for the 2.9D test at 3.0 in. pile head deflection.

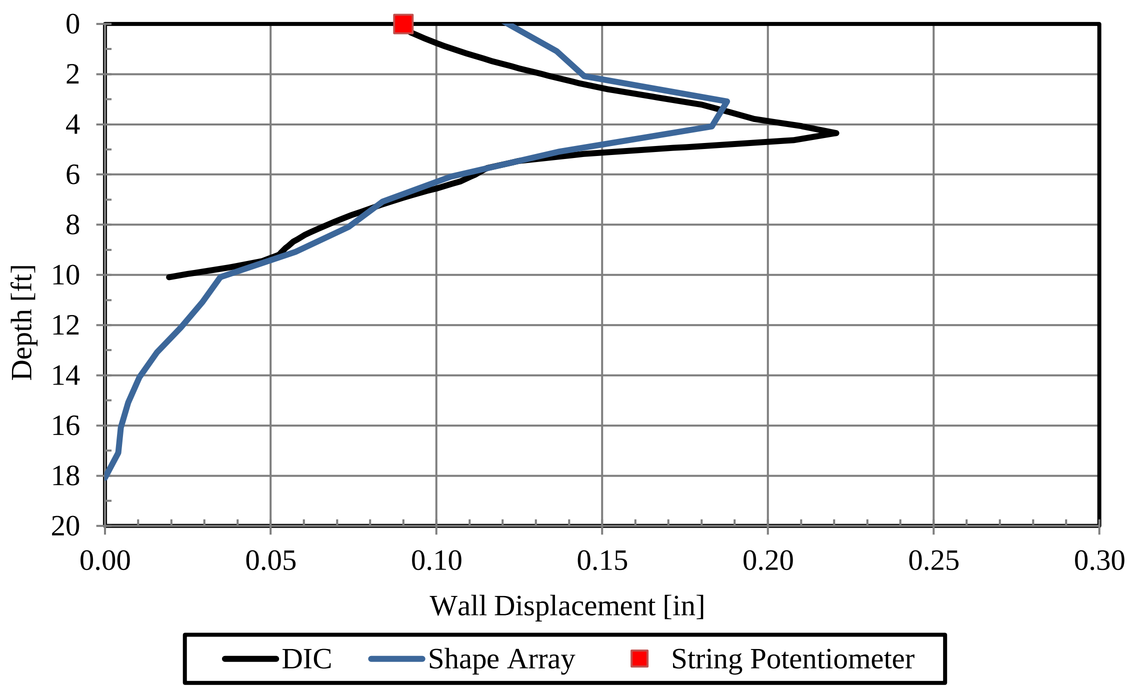

Figure 6-34: Comparison of wall displacement measured by the shape arrays to DIC and string potentiometer data for the 3.9D test at 3.0 in. pile head deflection.

Overall, the displacements are in good agreement and are likely within the accuracy of the respective systems. The DIC data has the correction applied as discussed previously in this section. The worst agreement was for the 1.7D test, with maximum wall displacement being measured as 0.48 in. using the shape arrays and 0.19 in. using DIC. This is likely due to separation of the PVC conduit from the wall in front of the pile, which allowed additional movement of the conduit with respect to the wall.

6.6 Pile Performance

Strain on the pile was measured at depths of 2, 4, 6, 9, 12, 15 and 18 ft. At these depths, gauges were applied to the side of the pile being loaded and the opposite side. The pile moment was estimated using the data. In the case where one of the gauges was damaged, the strain from the working gauge was used and in cases where both were damaged, the data point was omitted. The bending moment in the pile was calculated using the equation

$$M_i = \frac{EI}{2y}((\mu\varepsilon_{it} - \mu\varepsilon_{ot}) - (\mu\varepsilon_{ic} - \mu\varepsilon_{oc}))(10^{-6}) \qquad (5\text{-}4)$$

where

M_i is the bending moment in inch-kips for the pile at the ith data point,

E is the modulus of elasticity of the pile (29,000 ksi),

I is the moment of inertia of the pile and the attached angle iron (314 in^4),

$\mu\varepsilon_{it}$ is the micro strain for the ith data point, on the tension side of the pile,

$\mu\varepsilon_{io}$ is the initial micro strain for the tension side of the pile prior to loading,

$\mu\varepsilon_{it}$ is the micro strain for the ith data point, on the compression side of the pile,

$\mu\varepsilon_{oc}$ is the initial micro strain for the compression side of the pile prior to loading, and

y is the distance separating the two strain gauges measured along the line of loading.

Several of the piles rotated during driving so the strain gauges were not directly in line with the load. As shown in Figure 6-35, the rotation of the pile was measured and the distance separating the gauges in line with the load was calculated and applied to y in Equation (5-4) to account for the reduced measured strain.

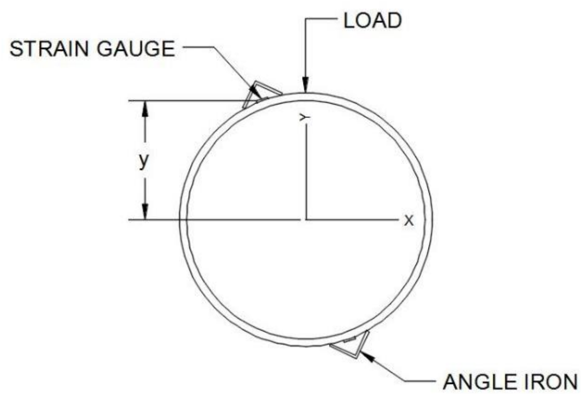

Figure 6-35: Measurement of y to correct strain measurement for pile rotation.

In spite of the angle iron covering the strain gauges and lead wires on the piles, some of the lead wires were cut during construction. This occurred for all of the strain gauges on one side of the 2.8D and 2.9D piles. For both of these piles, multiple wires were cut and it was not possible to determine their proper match through inspection of the wires. In this case, the strain of the gauges at unknown locations was compared to the strain measured by gauges at known depths and the gauges were assigned a location where opposing strains were approximately equal. There were several instances where both gauges at a given depth were not functioning properly and in this case, the moment at that depth was not calculated. When only one gauge was functioning, the strain at that location was doubled.

Figure 6-36 through Figure 6-39 are plots of bending moment in the pile versus depth below the ground surface for the four piles tested. The moment is given at several pile head loads for each test. The moment peaks at various depths ranging from 4 to 7 ft. The peak moment generally occurs at deeper depths as pile spacing decreases with the exception of the 1.7D test. This may be due to damaged strain gauges. Only one gauge was functioning at depths of 2, 6, and 9 ft., and neither gauge at 4 ft. was functioning. For a given load, the moment tends to be highest for the pile spaced furthest behind the wall and decreases as spacing of the piles decreases. This may be due to a softer response of the soil and wall as spacing decreases. The load applied to the pile may be distributed deeper in the profile rather than being focused at the top of the pile, causing less and a lower moment. This is also consistent with the observation that the observed moment tends to occur deeper as pile spacing decreases.

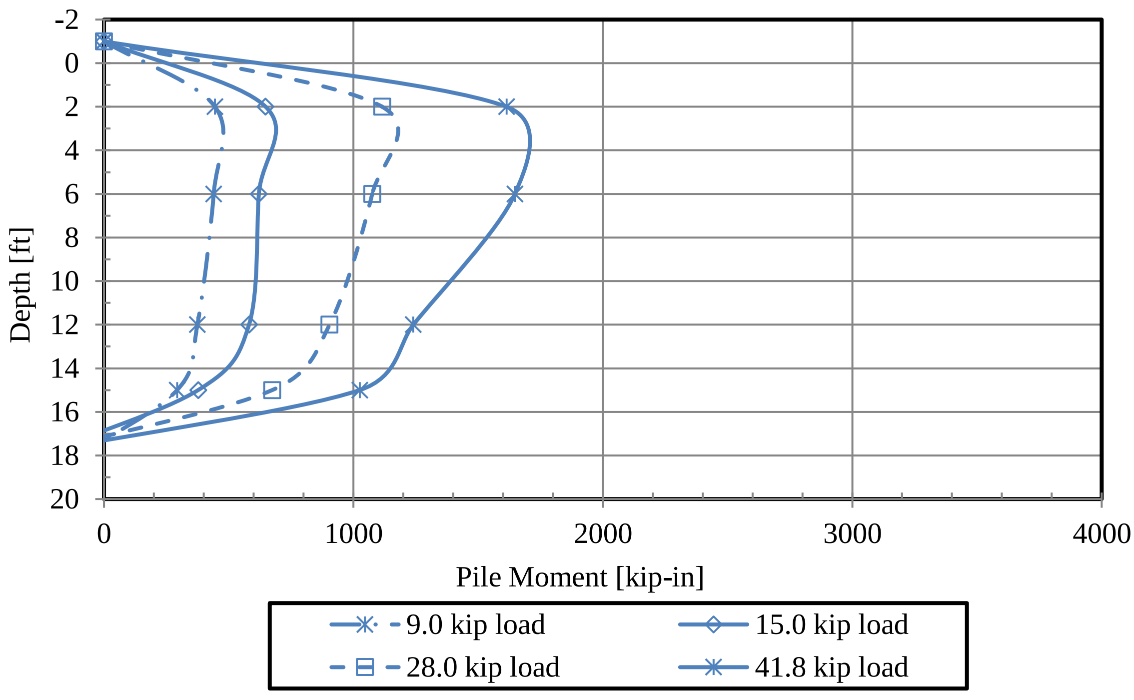

Figure 6-36: Moment versus depth for various loads on the 1.7D test.

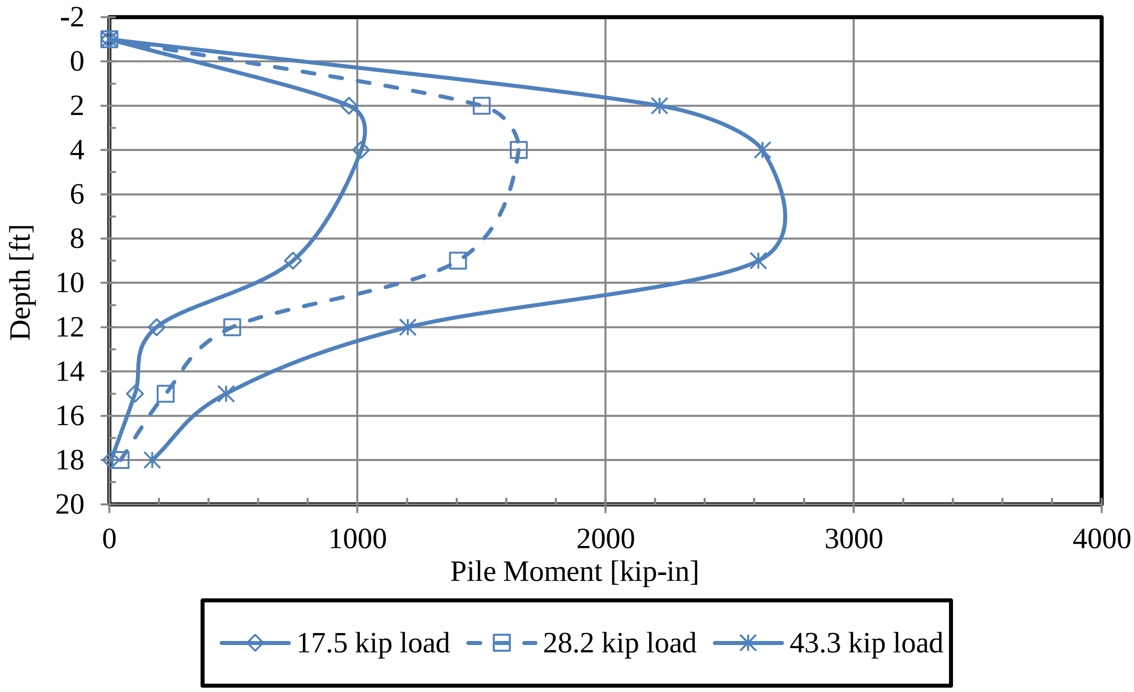

Figure 6-37: Moment versus depth for various loads on the 2.8D test.

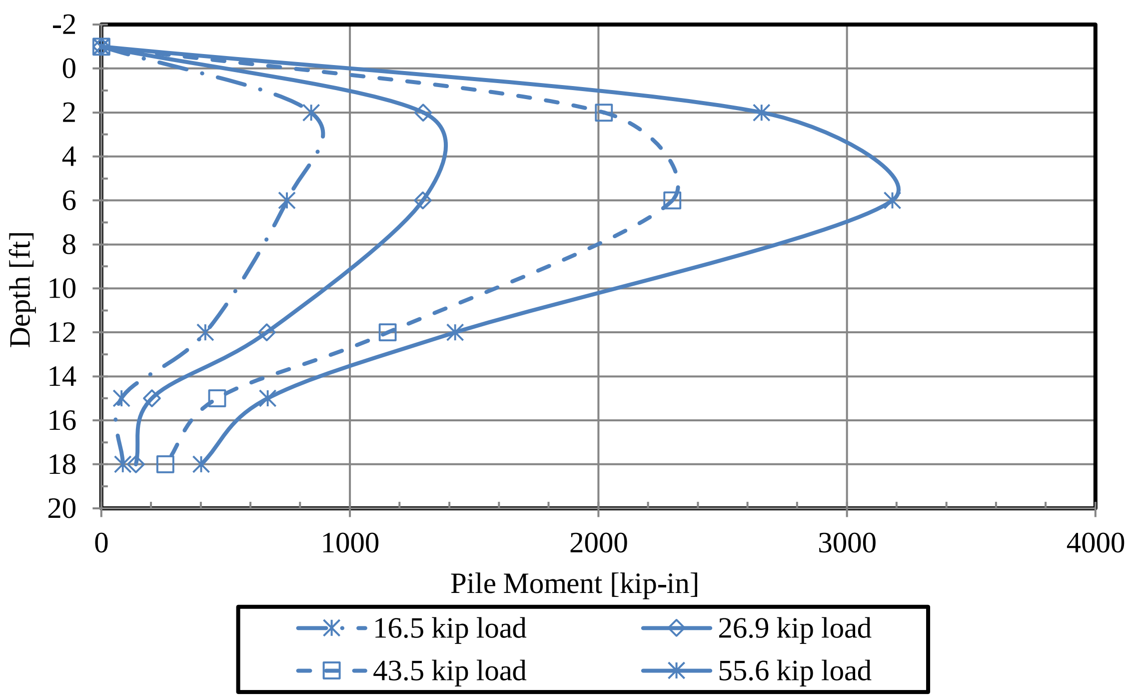

Figure 6-38: Moment versus depth for various loads on the 2.9D test.

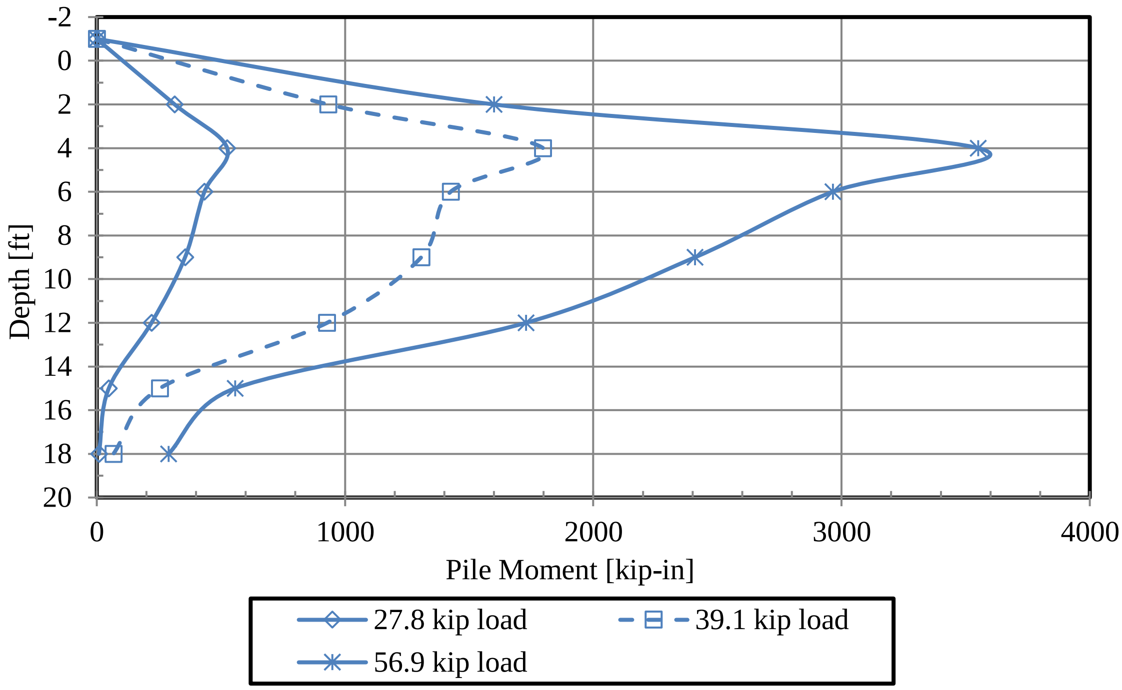

Figure 6-39: Moment versus depth for various loads on the 3.9D test.

Curves showing pile head load versus rotation of the tip of the pile for the four tests and the reaction pile are shown in Figure 6-40. The load for the curves is based on the hydraulic pressure gauge monitoring the pressure in the hydraulic jack line one minute after the target displacement was reached. The rotation of the pile head was calculated based on the string potentiometers at the load point and 3 ft. above the load point using the equation

$$\theta = \sin^{-1}\left(\frac{d_{3ft} - d_{lp}}{36in}\right) \tag{5-5}$$

where

θ is the pile head rotation,

d_{3ft} is the pile displacement 3 ft. above the load point, and

d_{lp} is the pile displacement at the load point.

The rotation of the pile tended to increase as the load increases for all of the tests. The pile head load versus pile head rotation curves are all very similar for the 3.9, 2.9, and 2.8D tests, just as the load displacement curves are for these tests. At a given load, the rotation of the pile tends to be lower for the 1.7D test indicating that less bending of this pile is occurring than it is for the other tests which is also consistent with the lower observed pile moment.

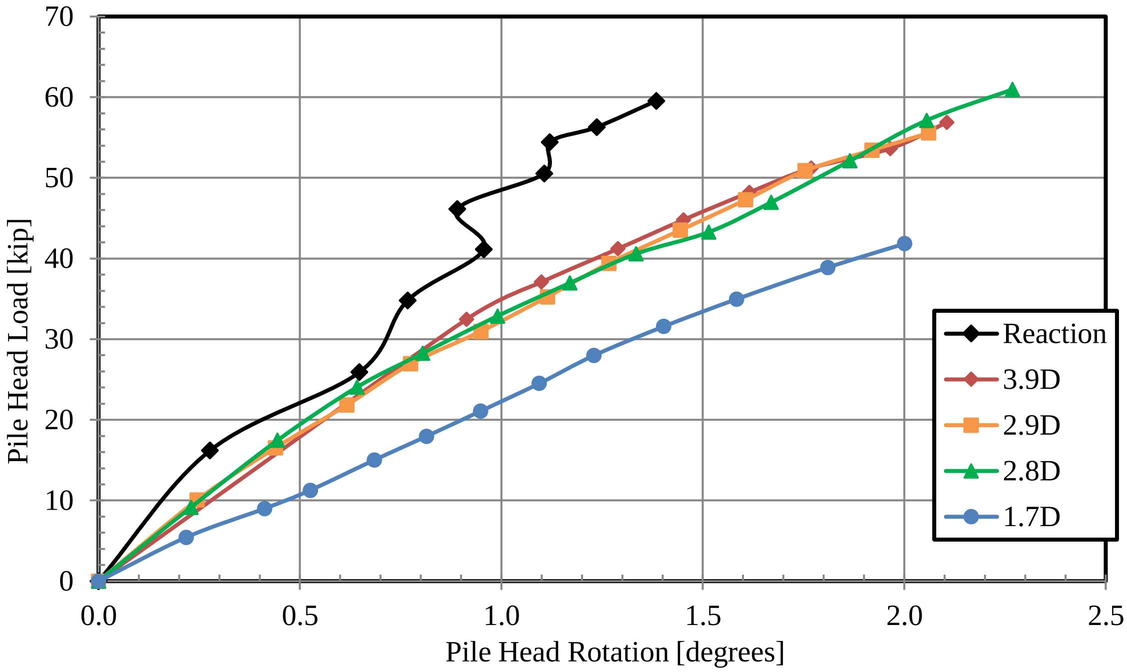

Figure 6-40: Pile head load versus rotation of the tip of the four test piles and the reaction pile.

7 LATERAL PILE LOAD ANALYSES FOR WELDED WIRE REINFORCEMENT

Lateral pile load for this project was analyzed using the computer program LPILE 2015. As discussed in Chapter 2, LPILE is a finite difference program that models the pile as a beam and iteratively solves for deflection using the p-y method. In this method, the soil is modeled using p-y springs which account for horizontal soil resistance (p) and horizontal deflection (y). Input parameters for LPILE include the pile material, size and type as well as the soil layering and properties. Different soil types were programmed into LPILE based on previously researched full-scale load tests including clay, sand and a number of specialty soils. The program also allows manual entry of soil parameters.

The LPILE program was used to produce plots of pile head load vs. deflection, pile head load vs. rotation, and bending moment vs. depth for comparison with the measured curves. After calibration of the LPILE model based on performance of the pile furthest from the wall, p-multipliers were back-calculated in an effort to account for the reduction in lateral soil resistance owing to the presence of the MSE wall. The following sections will describe the material properties used as input parameters in LPILE and will discuss a comparison of the test results with the curves computed by LPILE.

LPILE was used to model the test piles as elastic, non-yielding steel pipe piles with an outside diameter of 12.75-inches. A moment of inertia of 314 in^4 was used to account for the pile section with the steel angle iron welded onto the sides of each pile. The soil plug in the bottom 10 to 11 feet of the pile was neglected as it had little impact on the pile response.

As mentioned in previous chapters, the piles were driven about 18 feet into native soil and granular backfill was compacted to a depth of approximately 20 feet around the piles leaving a two foot length of pile above the ground surface. API Sand (O'Neill) was used to model the compacted backfill in the upper 20 feet and the native soil in the bottom 18 feet. Because the pre-cast concrete blocks only imposed a surcharge on the soil behind the test piles, this surcharge effect could not be modeled accurately using LPILE. LPILE can only model a continuous, uniform surcharge. To provide bounds on the computed behavior, two analyses were performed for each test pile. One analysis employed a continuous surcharge and one did not account for any surcharge. To account for surcharge in an LPILE model, a user must define a thin soil layer with no shear strength, but having a unit weight that produces a weight equal to the desired surcharge. In this case, the surcharge was modeled with a layer of soil 3-inches thick with a unit weight of 2,400 pcf to produce the surcharge pressure (q) of 600 psf. Friction angle and stiffness parameters were set to zero.

Input parameters for each soil layer consisted of an effective unit weight (γ), friction angle (φ), and the modulus of subgrade reaction (k). Each input parameter and associated soil layer is shown in Table 7-1 for the non-surcharge analysis and in Table 7-2 for the applied surcharge analysis. The soil unit weight was based on the average moist unit weight obtained from the nuclear density tests described previously. Friction angle, ϕ, and stiffness, k, were determined from the back analysis as described subsequently. Material properties in the native soil layer had relatively little effect on computed pile performance.

Table 7-1: Soil layers and input parameters without surcharge.

Soil Type	Layer Thickness (ft)	Unit Weight, γ (pcf)	Friction Angle, ϕ (degrees)	Modulus of Subgrade Reaction, k (pci)
API Sand (O'Neill)	20	126.8	38	220
API Sand (O'Neill)	18	125	34	115

Table 7-2: Soil layers and input parameters with surcharge.

Soil Type	Layer Thickness (ft)	Unit Weight, γ (pcf)	Friction Angle, ϕ (degrees)	Modulus of Subgrade Reaction, k (pci)
User-Defined	0.25	2,400	-	-
API Sand (O'Neill)	20	126.8	30	38
API Sand (O'Neill)	18	125	34	115

In LPILE the load was applied at the top of the model pile one foot above the ground surface with a pinned-head boundary condition to match field loading conditions. Loads were input for each deflection interval and the LPILE model was used to compute deflection.

7.1 LPILE Analysis Results

LPILE was used to back-calculate appropriate p-multipliers for each pile load test. Initially, the pile furthest from the wall (5.2D) was analyzed and the soil properties necessary to match the measured load-deflection curve were determined. Based on the assumption that the pile furthest from the MSE wall would be relatively unaffected by the presence of the wall, a p-multiplier of 1.0 was assumed for this case indicating no wall interaction. In calibrating the soil model, both ϕ and k affect the computed load-deflection curve; however, k has more effect on the curve at small deflection levels while ϕ has a greater effect at larger deflections as the soil layers begin to reach failure. Generally, the k value was selected based on the correlation with friction angle for soil above the water table shown in Figure 7-1 as specified by API. However, some adjustment was allowed to improve agreement with the measured curve.

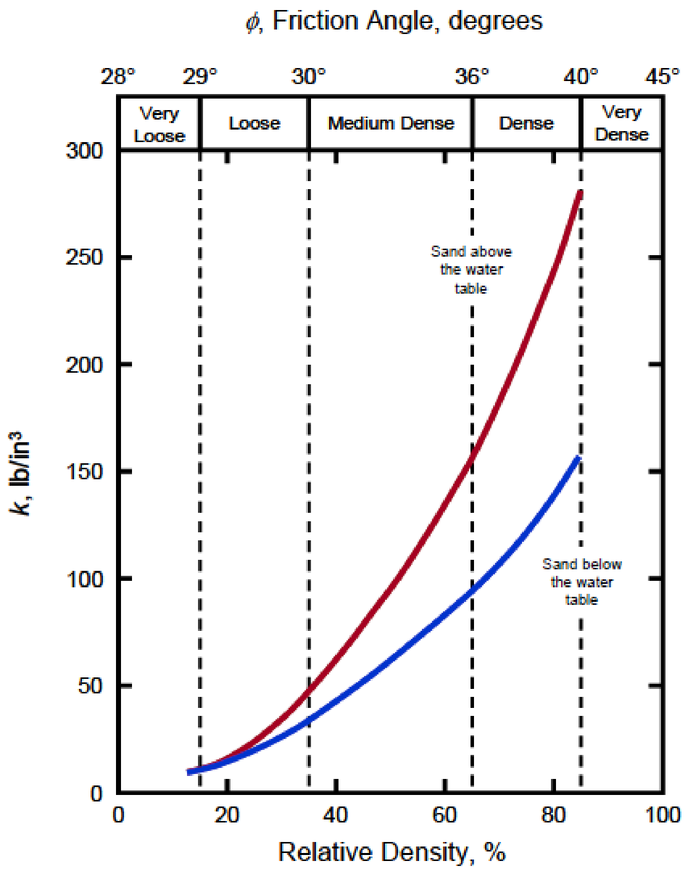

Figure 7-1: Soil modulus reaction based on friction angle or relative density of soil (API, 1982).

For piles located closer to the wall, these back-calculated soil parameters were then held constant for each pile and a constant p-multiplier was back-calculated to produce agreement with the measured load-deflection curve for that pile. P-multipliers are factors that are multiplied by the normal lateral soil resistance to account for the reduced lateral soil resistance for piles near an MSE wall. Separate analyses were performed with LPILE using both the no-surcharge and surcharge models. Once the appropriate soil parameters and p-multipliers had been determined, computed pile load versus pile rotation and pile bending moment versus depth curves were also compared with measured curves.

7.1.1 Load Deflection Curves

As mentioned previously, load-deflection curves were calculated in LPILE by inputting soil and load parameters from the 5.2D test into LPILE to get a load-deflection curve similar to the measured load-deflection curve. A best fit curve was found by back-calculating ϕ and k values, which are found in Table 7-1 and Table 7-2. Load-deflection curves were generated with LPILE to account for both surcharge loading (q=600 psf) and non-surcharge loading (q=0 psf) and are shown in Figure 7-2 with the measured load-curve for the 5.2D pile. A p-multiplier of 1.0 was assigned to the 5.2D test with the assumption that it is spaced far enough behind the wall to not be affected by the walls presence. Best-fit load-deflection curves were then assigned to the measured load-deflection curves for the 4.3D, 3.4D and 1.8D tests, as shown in Figure 7-3 through Figure 7-5, by assigning different p-multipliers in LPILE until the desired curve was found for each test. P-multipliers for each test are shown in Table 7-3. LPILE curves were matched to the measured load-deflection curves by matching the top three deflection points of each curve. The top three points used as the criteria for the best fit line because the 4.3D test had bad data for the first 1.5 inches of deflection and the 1.8D load-deflection curve would have more realistic values at higher deflections after the loosely placed fill had time to mobilize and compact from axial pile loading.

Table 7-3: P-multiplier for each test pile

Pile	P-mult (q=0 psf)	P-mult (q=600 psf)
5.2D	1.00	1.00
4.3D	0.95	0.95
3.4D	0.68	0.71
1.8D	0.30	0.38

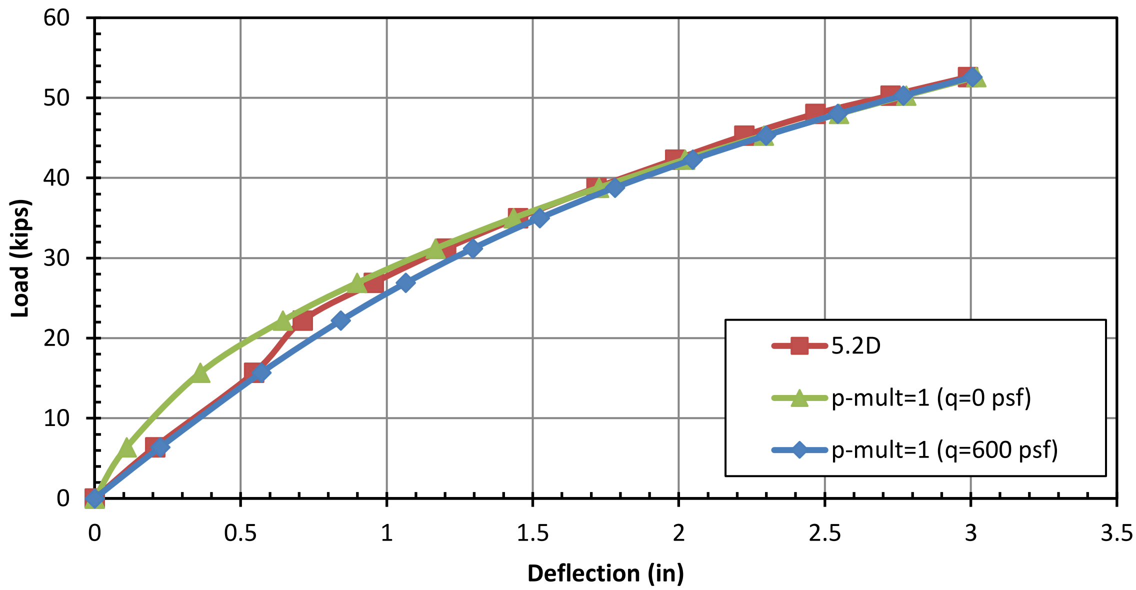

Figure 7-2: Comparison of load-deflection curves between measured and calculated results for the 5.2D test.

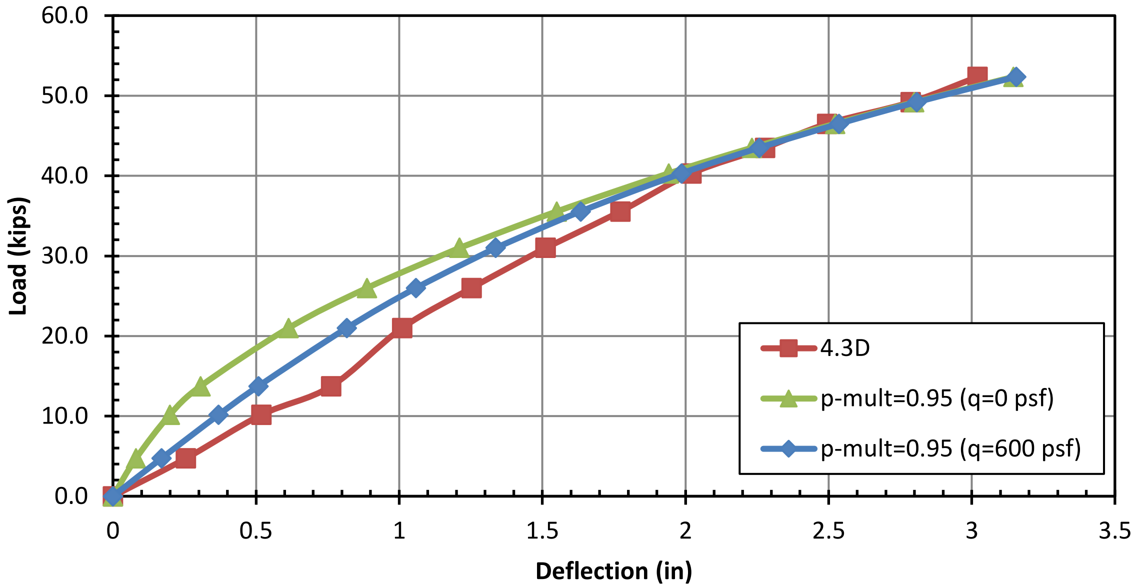

Figure 7-3: Comparison of load-deflection curves between measured and calculated results for the 4.3D test.

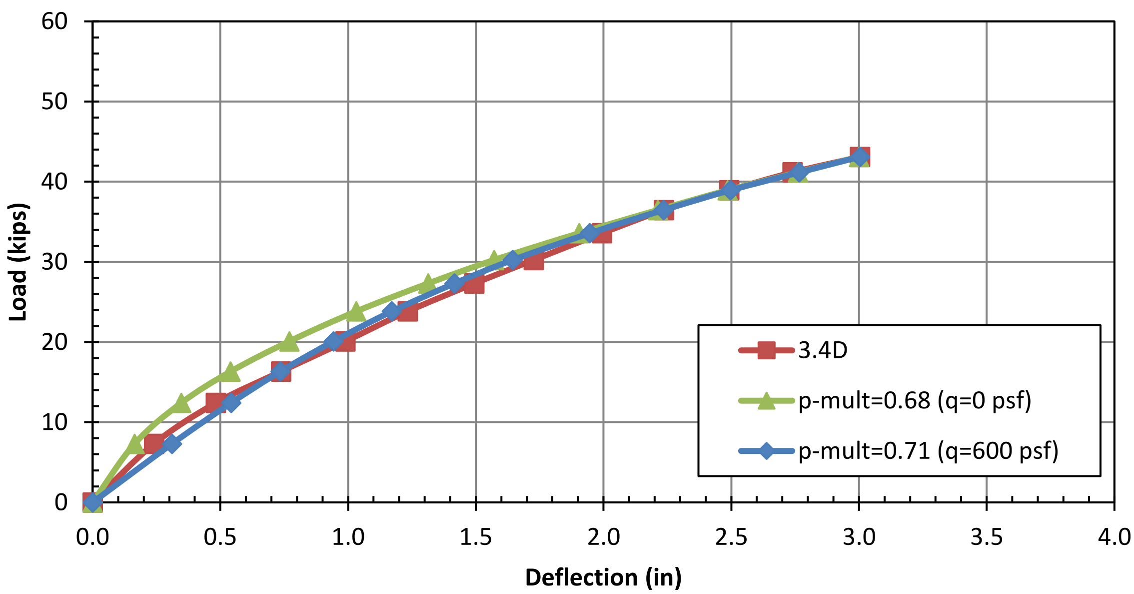

Figure 7-4: Comparison of load-deflection curves between measured and calculated results for the 3.4D test.

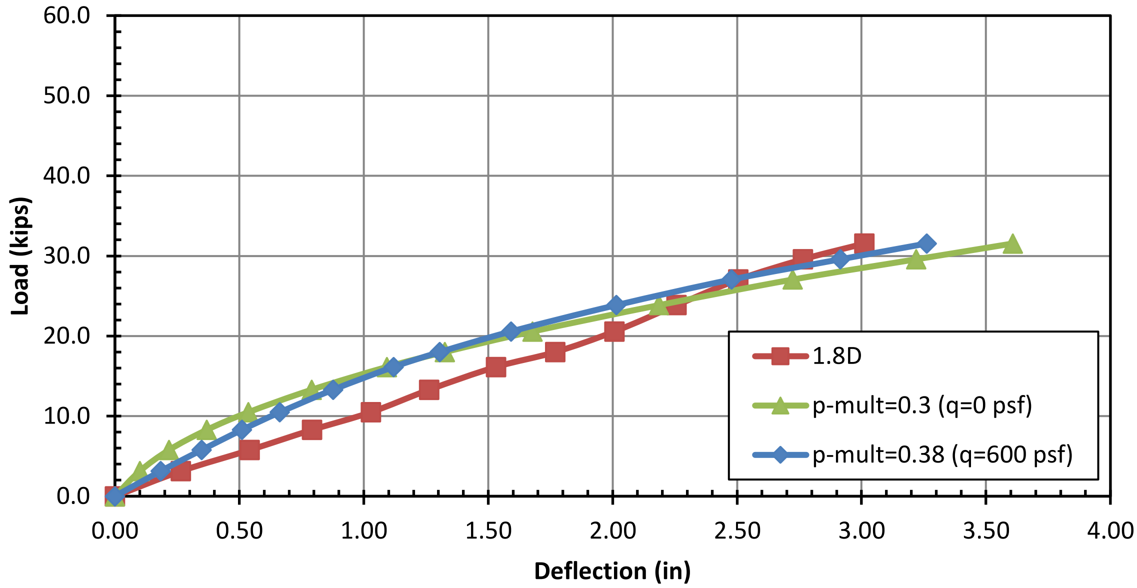

Figure 7-5: Comparison of load-deflection curves between measured and calculated results for the 1.8D test.

In general, the p-multiplier curves with surcharge fit the measured curves better than the non-surcharge curves. However, the field test curve should fit somewhere between the non-surcharge and surcharge curves since the surcharge load was only in a limited area whereas LPILE models the surcharge load as an infinite layer. Both of the LPILE curves fit the measured load-deflection curves reasonably well for the 5.2D and the 3.4D tests. As mentioned previously, the 1.8D test was close enough to the wall that compaction was difficult. As a result, the soil resistance was lower and was likely the reason for lower than expected pile loads. As discussed in section 5.1, low pile loads on the 4.3D test were caused by the hydraulic pump malfunctioning during the first half of the test. Loads from 0 to 1.5 inches of deflection were recorded much lower than what was actually produced. Figure 7-6 shows a comparison of the 15-foot and 20-foot SSL tests for the 4.3D pile and demonstrates that higher loads than those recorded likely occurred during the first half of the 20-foot test. The dashed lines in the figure represent the portion of the 4.3D test that were recorded low and manually adjusted, but which likely need adjusted to match closer to the 15-foot test.

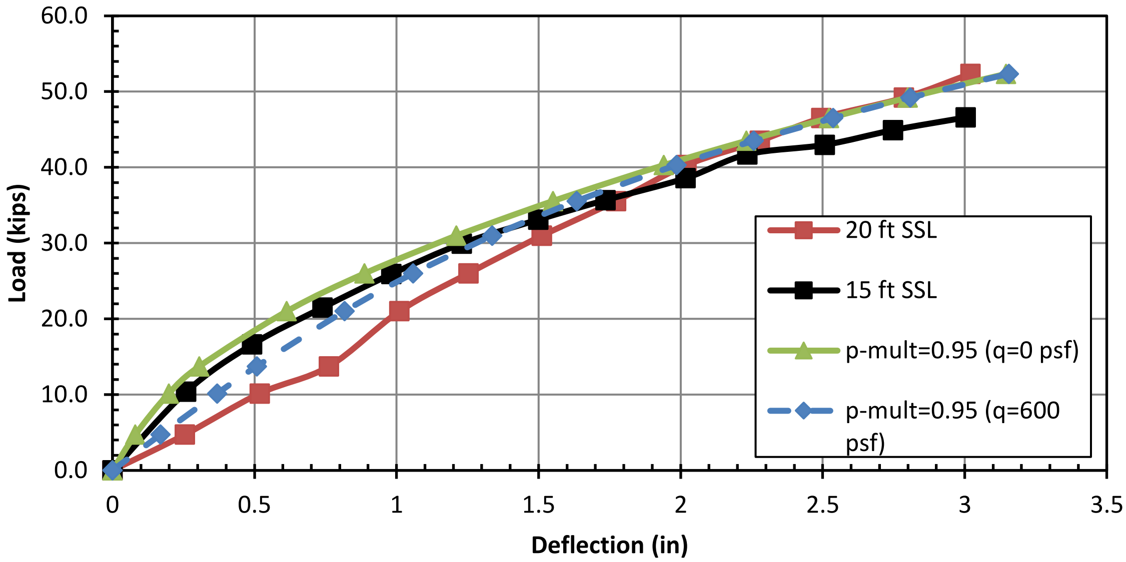

Figure 7-6: Comparison of 4.3D pile load-deflection tests for the 15-foot and 20-foot tests.

7.1.2 P-Multipliers and Pile Spacing Curves

P-multipliers are plotted versus distance from the wall in Figure 7-7 for all load tests on steel piles published to date. P-multipliers used in Figure 7-7 are of the non-surcharge condition to be consistent with other studies. However, this would not change the figure too much because the difference of the p-multiplier values for the different surcharge conditions is relatively small. The piles used for these tests were all round pipe piles ranging in diameter from 12.75 inches to 16.0 inches. A total of 24 p-multiplier points were used in Figure 7-7. The red data points (Nelson 2013, Han 2014, Besendorfer 2015) are test results using galvanized steel strip reinforcement. The blue data points (Price 2012, Hatch 2014, and this test) are test results using the galvanized welded-wire grid reinforcement. All tests have an L/H ratio ranging between 0.72 and 1.42. In general, neither the L/H ratio nor the type of steel reinforcement used appears to affect the p-multiplier for steel pipe piles behind an MSE wall.

A linear regression analysis was performed to evaluate the p-multiplier as a function of normalized pile spacing data that was a distance of less than four diameters from the wall. The best fit relationship for P_{mult} is given by the equations:

$$P_{mult} = 0.32\frac{S}{D} - 0.23 \qquad \text{for S/D} < 3.9 \qquad (6\text{-}1)$$

$$P_{mult} = 1.0 \qquad \text{for S/D} > 3.9$$

where

S is the distance from the back face of the wall to the center of the pile; and

D is the outside diameter of the pile.

The linear regression equation indicates that a p-multiplier of 1.0 will result from a normalized spacing greater than 3.9. A p-multiplier of 1.0 indicates that the presence of the wall has no effect on the lateral resistance or alternatively that the reinforcement is sufficient to provide as much lateral restraint as if the wall were not present. For normalized spacings less than 3.9 the p-multipliers appear to decrease nearly linearly with normalized distance. The equation for a p-multiplier of less than 3.9 was generated by taking a linear regression of all but two points in Figure 7-7 that were less than 4.0 pile diameters away from the wall. The 2.8D and 2.9D tests by Besendorfer were considered outliers and removed from the equation. By removing the two outliers, the R^2 value increases from 0.79 to 0.89 and the equation is nearly identical to that developed initially. As more data from testing is completed the linear regression equation will be refined and become more accurate.

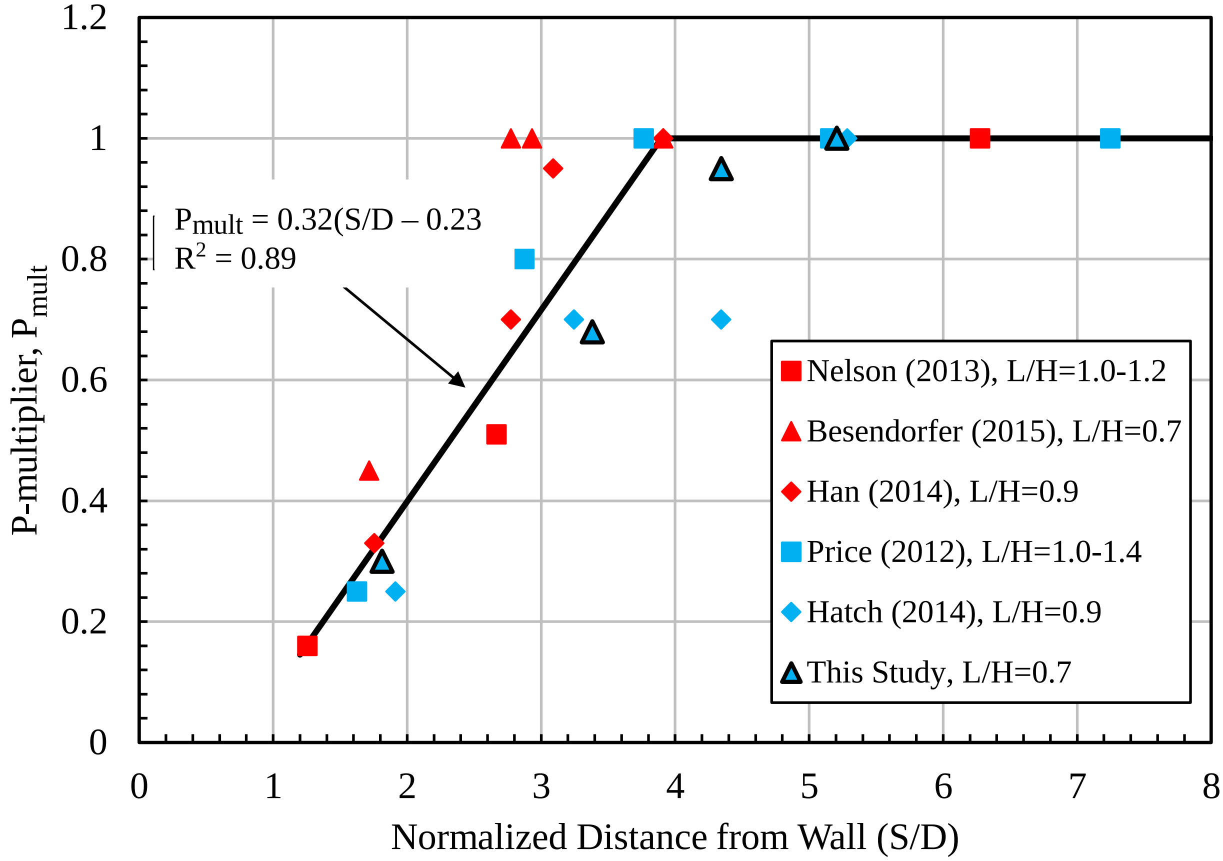

Figure 7-7: P-multiplier curve versus normalized distance for all known steel piles to date.

7.1.3 Pile Head Load versus Rotation Curves

As discussed in Section 5.2, pile head rotation was measured by taking the difference of the deflection measured by the two string potentiometers and using simple trigonometry to solve for the angle of rotation at the load point. The load vs. rotation curves from each test are compared with curves obtained with an LPILE analysis with and without an applied surcharge load in Figure 7-8 through Figure 7-11. In general, the measured curve for each test pile agrees reasonably well with the curves computed by LPILE, with the exception of the 4.3D pile. The 4.3D pile matches well with LPILE analyses after approximately 40 kips of load or 2 inches of pile deflection. As mentioned in earlier sections, complications were encountered during the 4.3D pile load test when the hydraulic pump yielded unrealistically low normal pressure readings which appear to be in error. Although the load readings were manually corrected for pile head deflections of 1.0 through 1.5 inches, errors in other deflection intervals likely occurred causing lower deflection readings. It should be noted that the 3.4D pile showed negative rotation for the first 0.75 inches of pile deflection. Since this was not the case, 0.25 inches was added to the deflection difference in order to account for the error in the pile rotation. In general, as the distance from the pile to the wall increases the soils ability to resist pile head rotation increases.

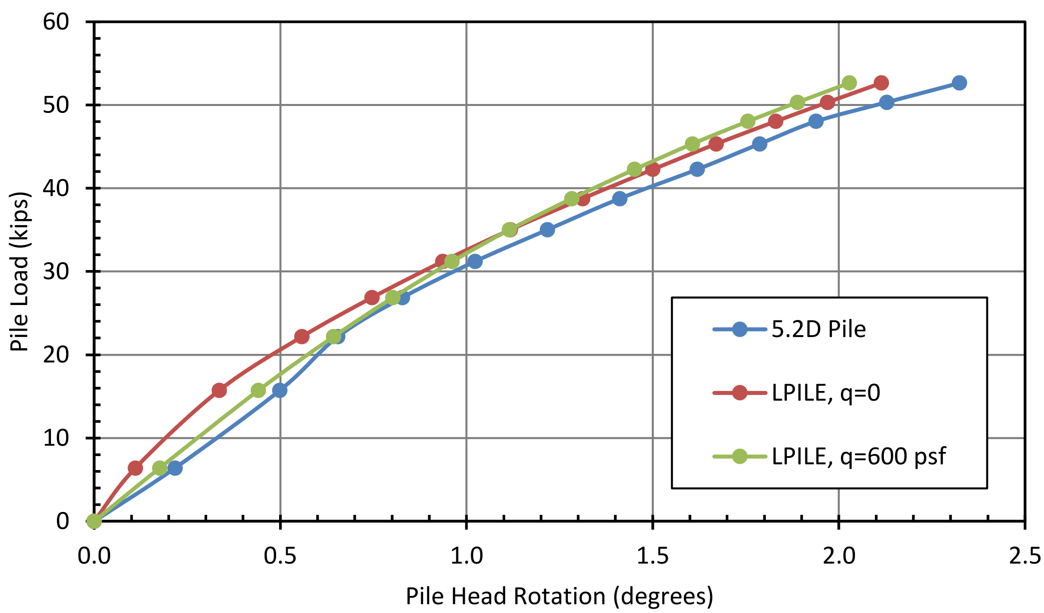

Figure 7-8: Comparison of the pile head load versus pile head rotation for the 5.2D test and LPILE analyses with and without surcharge.

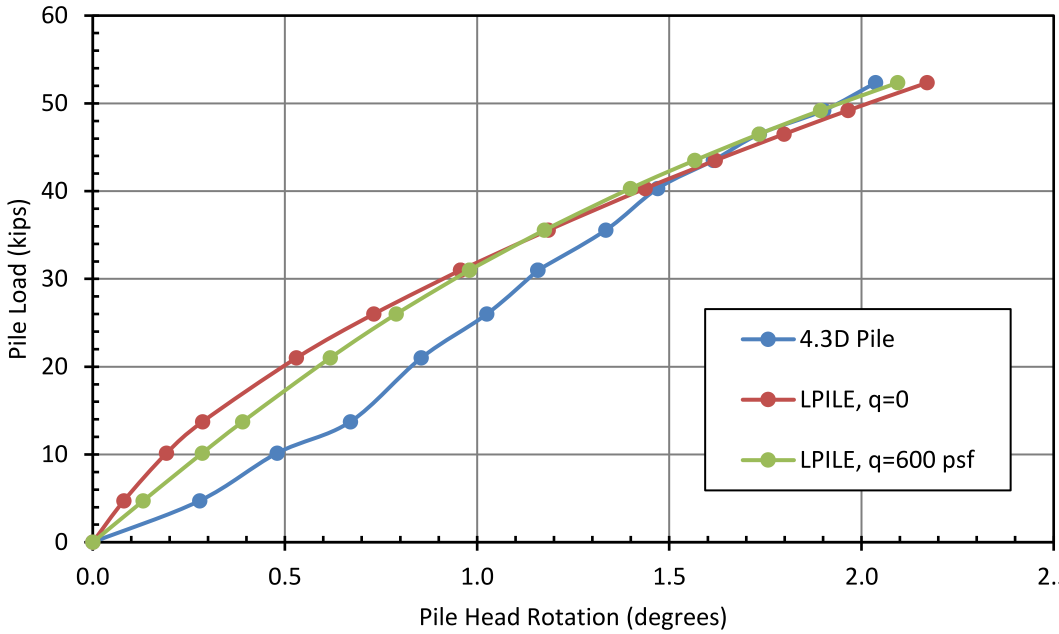

Figure 7-9: Comparison of the pile head load versus pile head rotation for the 4.3D test and LPILE analyses with and without surcharge.

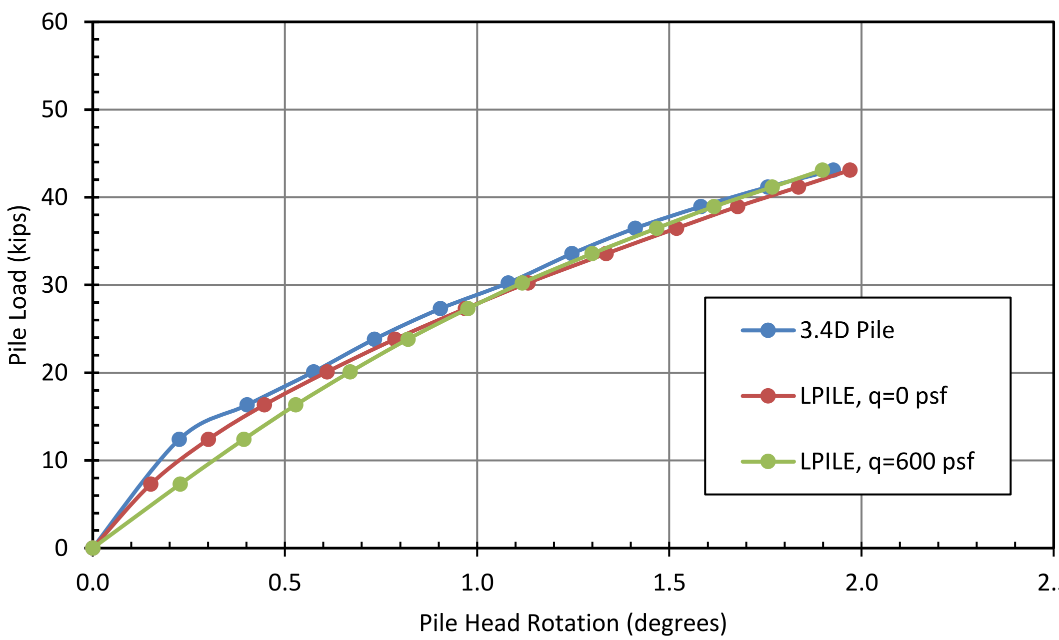

Figure 7-10: Comparison of the pile head load versus pile head rotation for the 3.4D test and LPILE analyses with and without surcharge.

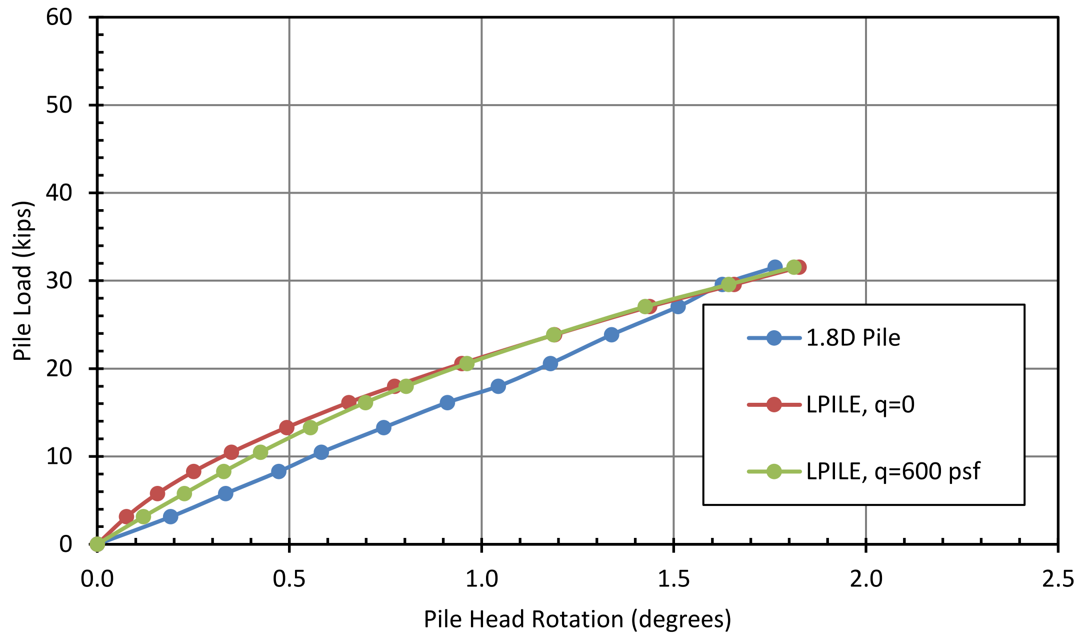

Figure 7-11: Comparison of the pile head load versus pile head rotation for the 1.8D test and LPILE analyses with and without surcharge.

7.1.4 Bending Moment versus Depth Curves

Bending moments along the length of the pile were determined using data from strain gauges obtained during testing and Equation 5-4 as described previously in Section 5.7. LPILE with the back-calculated p-multipliers described previously was also used to calculate bending moment versus depth curves for each pile test with and without surcharge load applied. Bending moment versus depth curves obtained from the strain gauge measurements for the 0.5-inch and 3.0-inch pile head deflection increments are shown in Figure 7-12 through Figure 7-15 along with the curves from the LPILE analyses with and without the applied surcharge load.

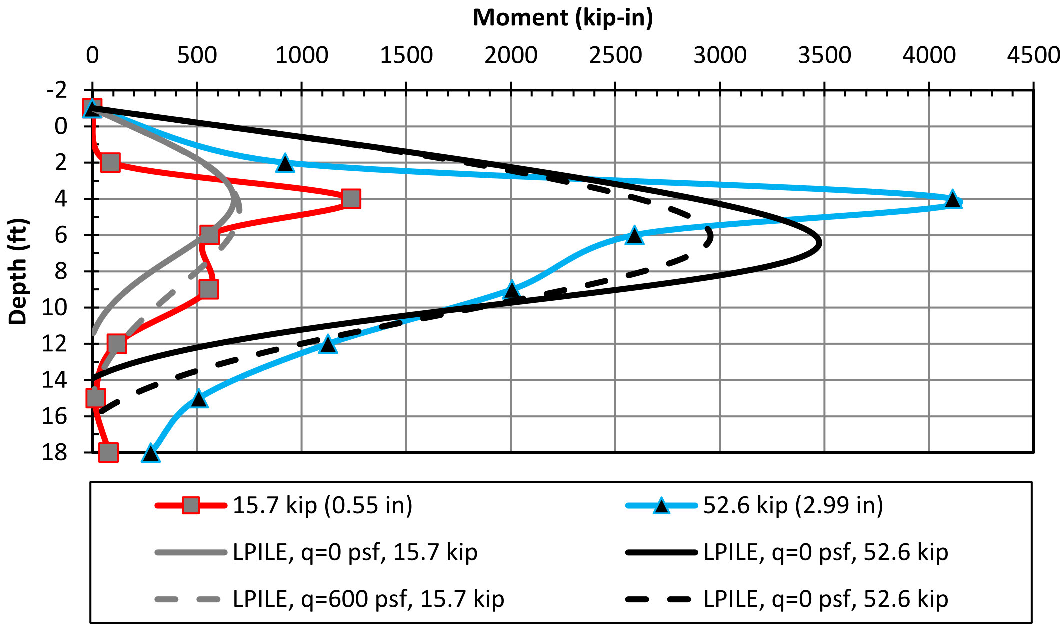

Figure 7-12: Measured and computed pile bending moment for the 5.2D test pile.

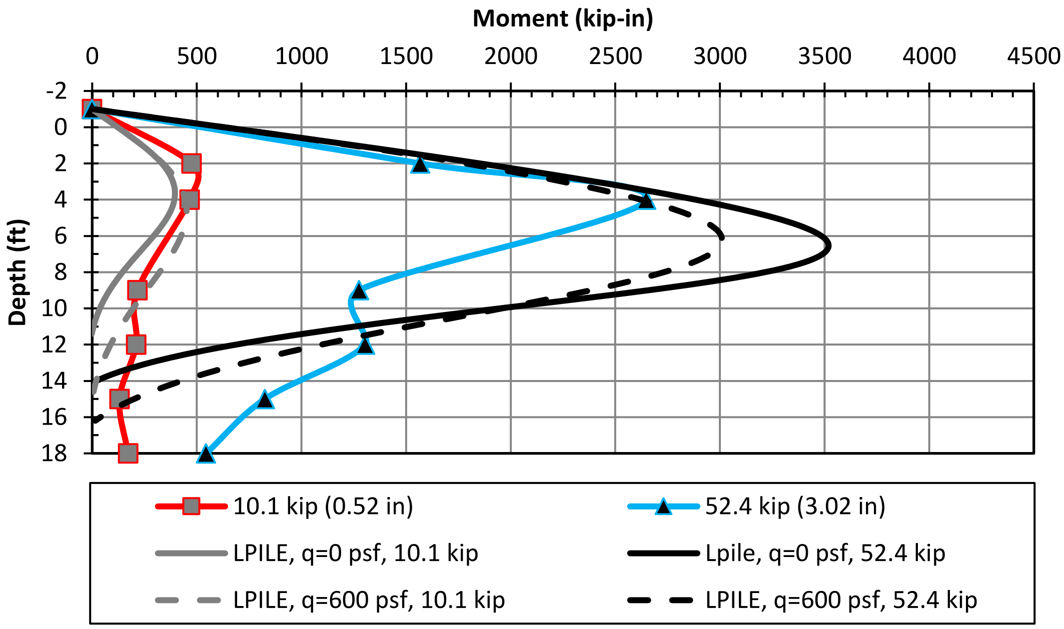

Figure 7-13: Measured and computed pile bending moment for the 4.3D test pile.

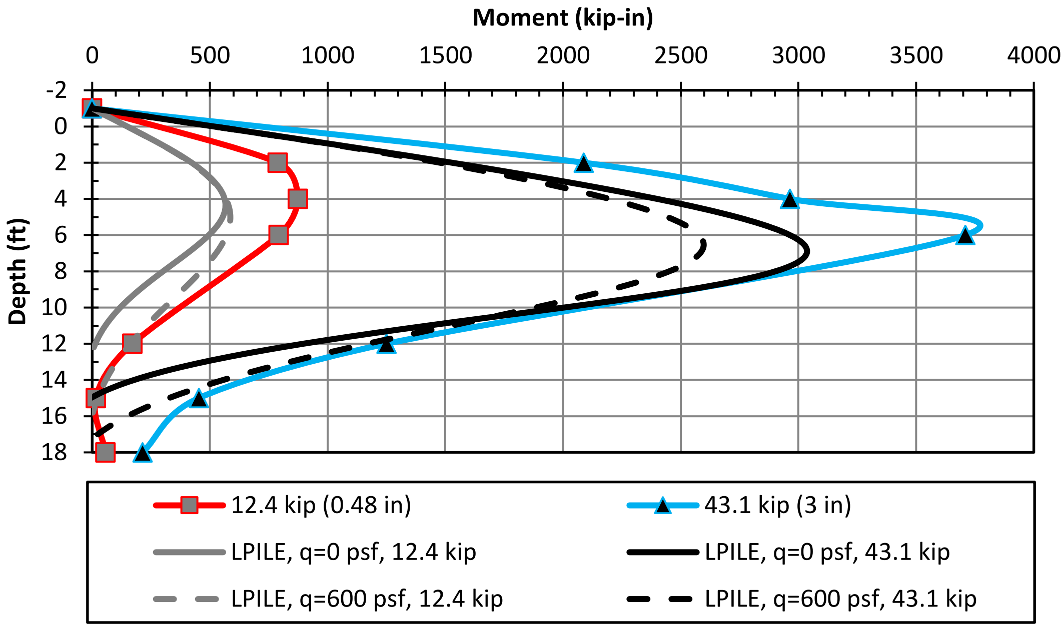

Figure 7-14: Measured and computed pile bending moment for the 3.4D test pile.

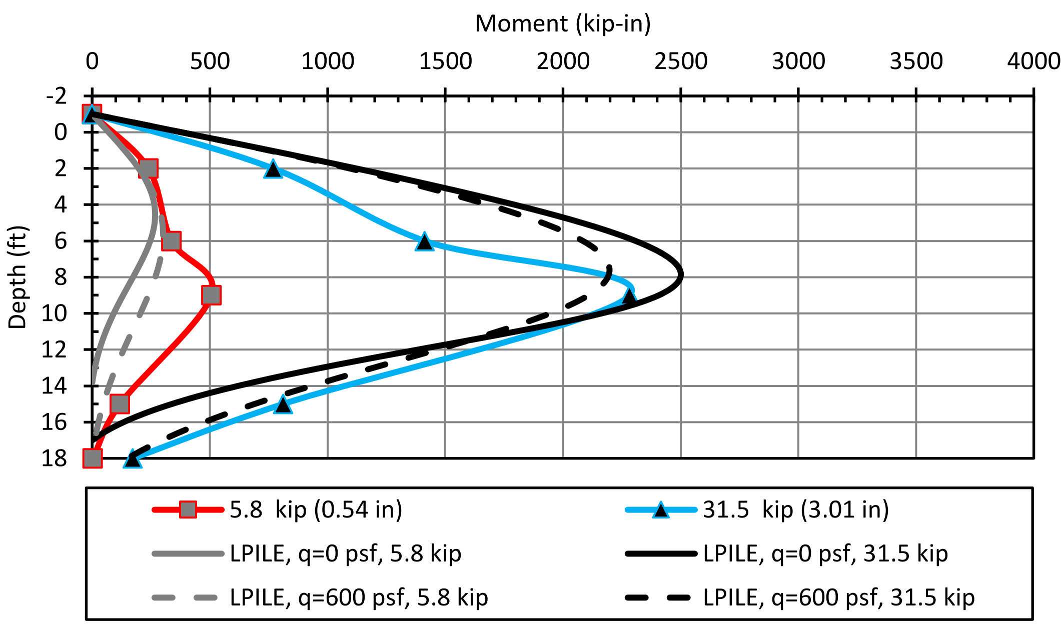

Figure 7-15: Measured and computed pile bending moment for the 1.8D test pile.

In general, the measured maximum bending moment agrees well with the maximum bending moment data calculated by LPILE. The maximum moment depth is defined as the depth where the maximum moment occurs. At three inches of pile head deflection for each test, the measured maximum bending moment is typically within 25% of the LPILE moment envelope created using q=0 psf and q=600 psf for the surcharge load. In addition, the measured depth to the maximum moment is within 2.5 feet of the calculated maximum moment depth for the load associated with three inches of pile head deflection. In cases such as the 4.3D pile, erroneous strain gauge data occurred in the location where LPILE predicted the maximum moment would occur. Therefore, it is likely that the measured maximum moment would be greater and the depth to the maximum moment would be deeper. For the 3.4D and 5.2D tests, both maximum moments are approximately 25% higher than the calculated moments from LPILE. Higher recorded moments could be the result of pile locations being directly behind the center of the panels. The combined panel and soil reinforcement resistance could have caused a higher resistance than the normal soil conditions that LPILE models. Although the difference in the LPILE calculations with and without surcharge loads does not affect the results by much, it gives a good range of where the test pile data should be theoretically, assuming all other variables are constant.

At 0.5 inches of pile head deflection, the measured maximum bending moment for the 1.8D, 3.4D, 4.3D and the 5.2D test piles are 68%, 48%, 5% and 76% more than that calculated by LPILE. The 1.8D measured and calculated maximum bending moments are within 5% of each other to a depth of approximately 6 feet below ground surface, after which the measured forces are much higher. The larger measured bending moment at a depth of nine feet is likely because one of the strain gauges was not reading correctly, so the measured value of the working strain gauge was used as the average value. Measured and calculated bending moments for the 5.2D test pile varied by as much as 76% in the upper 5 feet, after which the measured and calculated values typically remained within 20% of each other. The depth of the maximum moment is generally within 1.5 feet of the calculated maximum moment depth, with the exception of the 1.8D test which varied by approximately 4 feet. The difference between the measured and calculated maximum moment could be caused by limitations in LPILE to account for soil reinforcement.

8 LATERAL PILE LOAD ANALYSIS FOR RIBBED STRIP REINFORCEMENT

To be more useful for a broad range of applications, the results of these tests were modeled in LPILE, a computer program commonly used to analyze laterally loaded piles. LPILE is a finite difference program that uses the p-y method. With the p-y method, the soil surrounding the pile is modeled as a series of springs at various depths along the pile. The spring stiffness varies nonlinearly with displacement. The displacement of a pile at any depth at a given lateral load can be determined through an iterative approach using this method. Soil type and state, pile geometry, and loading method can all cause variation of the pile displacement at any given lateral pile load. Hence, various p-y curves are necessary for different types of soil. LPILE computes deflection, bending moment, shear force, and soil response over the length of the pile. Various options are available within the program for determining p-y curves based on different soil types. The accuracy of the analysis depends on how accurately the reaction of the soil is modeled by the p-y curve. The API Sand (1982) method built into LPILE seems to model the backfill used for the wall reasonably well and is used for lateral load analysis of the piles in these tests. The API method was also the method used by Price (2012), Nelson (2013), Hatch (2014), and Han (2014) in their analyses so this approach is consistent with their work.

The pile located 3.9 pile diameters from the wall was assumed to have no interaction with the wall based on previous research performed by Price (2012) and Nelson (2013). This pile was used to calibrate the soil parameters used in the LPILE model. The displacement of the pile head at any given load is dependent on the soil moist unit weight, γ; friction angle, ϕ; and the modulus of subgrade reaction, k; all of which are assumed to be the same for all tests. The unit weight was known from field testing described previously. Initial estimates of friction angle and subgrade reaction were made based on relative density estimated from the relative compaction. The friction angle and subgrade reaction were then varied until the predicted load versus displacement of the pile head matched the measured load versus displacement. After the soil friction angle and subgrade reaction which modeled the soil correctly were determined, a p-multiplier (less than 1) was applied to the p-y curve to account for the reduced resistance of the piles closer to the wall.

This analysis allows the results of these tests to be more useful for a broad range of applications. Designers can create an LPILE model based on their soil and pile type and use the reduction curves to determine proper multipliers to use based on the distance of the pile behind the wall. The use of this approach is based on the assumption that a similar reduction in lateral resistance is expected for other pile sizes and types, soil types, wall panel types, and so on. Additional tests with larger diameter piles will likely be necessary to confirm this assumption in the future.

8.1 Material Properties

Table 8-1 is a list of input parameters for the pile and their respective values used in the LPILE analysis. The pile was modeled as a linear elastic material. After running the analysis, this assumption was checked and it was found that the stress on the piles reached the yield point from 2.5 to 3.0 in. pile head deflection depending on the pile. However, after updating the model for the 3.9D pile, the analysis showed that the predicted deflection changes less than 2% at 3.0 in. pile head deflection so the linear elastic model of the pile was still used. The pile moment of inertia and cross-sectional area were calculated for the pile including the angle iron tack welded to the pile to protect the strain gauges. A pinned head load condition was used in the analysis consistent with the field loading condition. Loads were applied 12 in. above the ground surface and were the measured loads from the analysis. The piles were modeled as hollow sections despite being driven open ended. The piles eventually plugged with soil; however, the soil plugs were generally limited to a zone about 12 ft. from the pile tip leaving the upper 28 ft. of the pile hollow. Therefore, for practical purposes, the section of the pile interacting with soil was acting as a hollow section and the plugged section was deep enough to have no effect on the results.

Table 8-1: Pile properties for LPILE analysis

Pile Shape	**Total Length [ft]**	**Load point above ground [in]**	**Outside diameter [in]**	**Wall thickness [in]**	**Moment of inertia [in^4]**	**Cross-sectional Area [in^2]**	**Modulus of Elasticity [psi]**	**Yield Stress [psi]**
Circular	40	12	12.75	0.375	314	15.3	29000000	Elastic (57,000)

The soil friction angle, modulus of subgrade reaction, and soil effective unit weight are the required inputs for the API Sand method in LPILE. Figure 8-1 shows the API soil subgrade reaction correlated to relative density or to soil friction angle. Curves are provided for sand above and below the water table. The backfill was above the water table so the curve representing sand above the water table was used. To determine the correct friction angle and subgrade reaction to represent the soil, a friction angle was initially estimated and the corresponding subgrade reaction was read from Figure 8-1. If the displacements were too high for a known pile load based on measured load deflection curves, a higher friction angle and subgrade reaction were chosen and vice versa. This process was repeated until the predicted deflection at measured loads matched the measured deflection.

As described in section 3.3.2, a 600 psf surcharge was applied behind each pile using concrete blocks to simulate a 5-ft. high bridge abutment behind the wall. LPILE does not have the option to apply an asymmetric soil profile, so there was no way to model the surcharge as it was applied during the testing. Although the surcharge was not in front of the pile during loading, the spreading of the load with depth is likely to have caused additional resistance deeper in the profile. In an attempt to model the surcharge, a layer of soil with a 2400 pcf unit weight, 3 in. thick, was applied to the top of the profile. The user defined p-y option was applied to this layer in a manner that the layer would provide no lateral resistance but only additional vertical stress on the underlying layers. The reinforced backfill was modeled using the API Sand approach, and the friction angle was found to be 31 degrees with a modulus of subgrade reaction of approximately 60 pci. The underlying native soil was also modeled using the API sand approach with a friction angle of 34 degrees, however, the analysis is unaffected by the soil properties at this depth. Table 8-2 summarizes the soil properties used in the analysis when the surcharge was modeled in LPILE. Two LPILE models of each of the piles were created, one attempting to simulate the 600 psf applied surcharge and one in which no attempt to simulate the surcharge was made. Table 8-3 summarizes the soil properties used in the analysis when no attempt was made to model the surcharge. The same analysis was performed as described previously and the back-calculated friction angle for the reinforced soil was found to be 39 degrees with a subgrade reaction of 260 pci. In reality, the actual stress in the soil profile caused by the 600 psf surcharge would be somewhere between these two cases so the friction angle is somewhere between 31 and 39 degrees and the subgrade reaction is between 60 and 260 pci. This range of friction angles is reasonable for the backfill material based on the backfill estimated relative density of 50% and the friction angles corresponding to various relative density values shown in Figure 8-1.

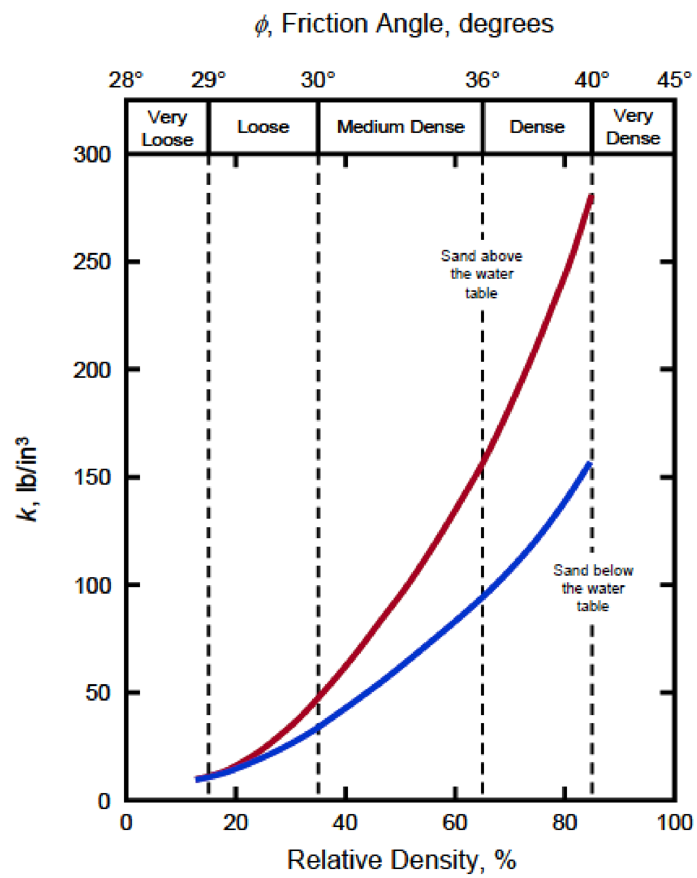

Figure 8-1: Soil modulus reaction based on soil friction angle or relative density (API, 1982).

Table 8-2: Soil properties used in LPILE analysis with simulated surcharge

Depth [ft]	**Description**	**Soil type (p-y model)**	**Eff. Unit weight, γ [pcf]**	**Friction angle, ϕ [deg]**	**p-y modulus, k [pci]**
0.75 - 1	Surcharge	User defined	2400	0	0
1 - 21	Reinforced fill	API Sand (O'Neil)	127.8	31	60
21 - 40	Underlying native soil	API Sand (O'Neil)	125	34	100

Table 8-3: Soil properties used in LPILE analysis with surcharge not simulated

Depth [ft]	Description	Soil type (p-y model)	Eff. Unit weight, γ [pcf]	Friction angle, ϕ [deg]	p-y modulus, k [pci]
1 - 21	Reinforced Fill	API Sand (O'Neil)	127.8	39	260
21 - 40	Underlying native soil	API Sand (O'Neil)	125	34	100

8.2 Results of LPILE Analysis

The computed load-deflection curves were compared to measured load-deflection curves for each pile and used to calibrate an LPILE model for each pile tested and determine appropriate p-multipliers for the piles spaced closer to the wall than approximately 3.8D. LPILE also computes pile bending moment and rotation, both of which are compared to measured results as another check to ensure that the LPILE model is correct.

8.2.1 Load-Deflection Curves

Figure 8-2 shows the final load-deflection curves computed by LPILE compared to the measured load-deflection curves. Two LPILE predicted curves are shown, one for the case without the surcharge modeled (q=0 psf) and one for the case when the surcharge is modeled (q=600 psf). The measured load-deflection curves are based on the average of 30 seconds of data starting one minute after the peak load was reached for each target deflection. Table 8-4 gives the back-calculated p-multiplier determined for each test based on the LPILE model without the surcharge modeled, as has been done in previous research. It was found that a p-multiplier of 1 was most appropriate for the 3.9, 2.9 and 2.8D tests and a p-multiplier of 0.5 was used for the 1.7D test. Although the load deflection curve predicted by LPILE does not fit the measured curve very well, the R^2 value was lowest using a p-multiplier of 0.5 (R^2=0.86). Only one computed curve is shown for the 3.9 through 2.8D tests because the p-multiplier is 1 and the load-deflection curves are all approximately identical. For all four of the piles tested, the LPILE model with the surcharge simulated matches the measured results slightly better than the model without the surcharge. Overall, the predicted and measured load-deflection curves match very well. For the 1.7D test, the predicted LPILE curve with the simulated surcharge only matches for the first 0.25 in. of pile displacement. After that, LPILE predicts a stiffer response out to approximately 1.5 in. of pile displacement, after which the response softens and the curve begins to level out. The measured curve shows that the response is approximately linear, at least to the extent of the displacements measured. This may be an indication that the actual response is governed by the resistance the soil reinforcement is providing rather than by the resistance of the soil. This would indicate that the full resistance of the soil reinforcement has not been mobilized at the peak measured displacement. Another possibility is that the soil around the pile was loose and compacted due to the pressure applied from the lateral pile load causing the soil to become progressively stronger which could also lead to the more linear curve shape.

Table 8-4: P-Multipliers for each test

Pile	P-multiplier
1.7D	0.5
2.8D	1.0
2.9D	1.0
3.9D	1.0

.

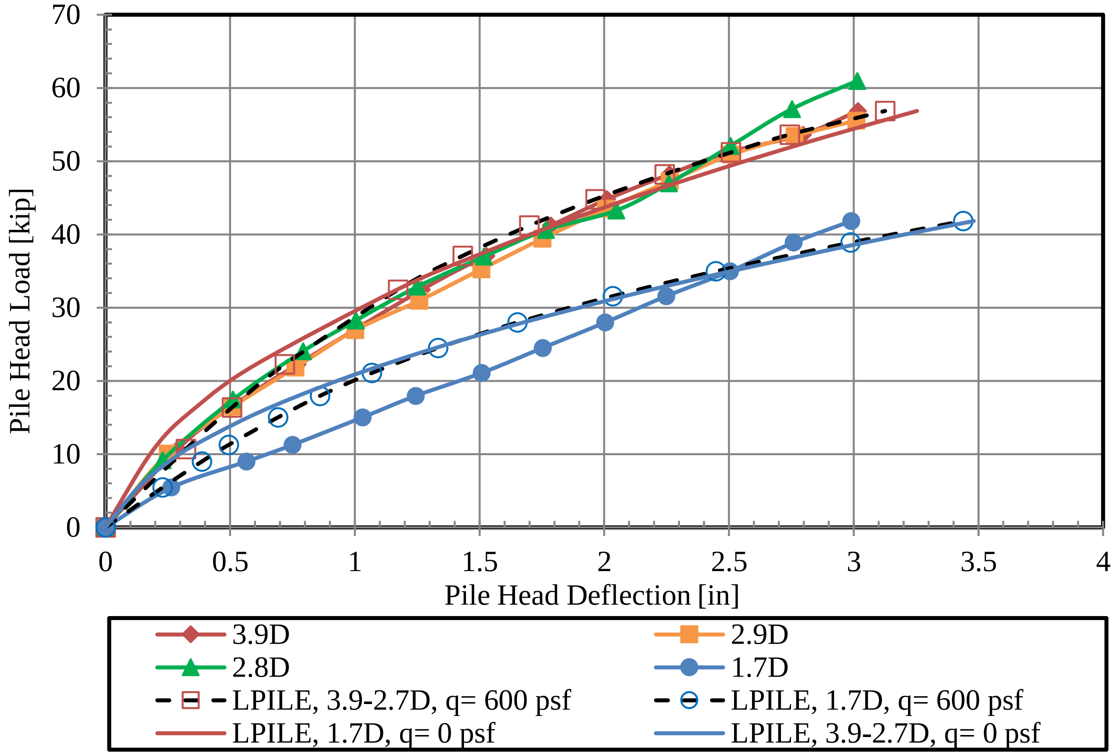

Figure 8-2: Comparison of load versus deflection curves computed by LPILE to measured load-deflection curves.

The reason why the load deflection curves are nearly identical for the 3.9, 2.9, and 2.8D tests is unknown. The spacing of the 2.9 and 2.8D piles behind the wall is similar enough that similar load deflection curves are expected. However, according to previous research, the p-multiplier for a pile spaced at these distances should be approximately 0.9 compared to the pile spaced at 3.8D (See Figure 2-16). The p-multiplier for the 1.7D test is also higher than expected. A p-multiplier of 0.5 provided the best overall calibration of the model while a multiplier of 0.3 is expected based on previous research. If the lateral resistance of the 3.9D pile had been higher, the p-multipliers for the other tests would have been reduced. A comparison of all the pipe piles tested during this research indicates that the strength of the 3.9D test is similar to the other pipe piles at similar distances behind the wall as shown in Figure 8-3 while the three piles spaced at 2.9, 2.8, and 1.7 diameters have a higher lateral resistance than other pipe piles tested at similar spacing as shown in Figure 8-4 and Figure 8-5. The reason for the higher resistance of the 2.9, 2.8, and 1.7D may be the soil compaction was higher for these piles. Compaction between the piles and the wall was performed using a vibratory plate compactor. The path of compaction generally was around the pile, next to the wall, and then in-between piles. Assuming the same number of passes of the plate compactor occurred between each pile and the wall, the soil between the wall and piles on the 1.7, 2.8, and 2.9D piles would have received more compaction effort than the soil around the 3.9D pile. Although nuclear density testing was performed throughout construction as outlined in the section 3.3.1 of this report, the exact location of all tests is not known. In addition, as indicated in section 3.3.1, the scatter in the relative compaction data for the zone between the piles and the wall exhibited considerable variation. Another possible reason for the higher resistance of these piles is the night before the 2.8 and 2.9D piles were tested, a significant rainstorm occurred at the site. The USCS material classification of SP-SM indicates that there are some fines in the soil, (See Appendix C. Geneva Rock Laboratory Test Reports) so perhaps the resistance of the piles at 2.8D and 2.9D tests was increased due to cohesion that added to the strength of the soil. Both of the tests were performed on the day following the rainstorm. Furthermore, the water that infiltrated the soil would increase the unit weight of the soil and may have caused some natural compaction.

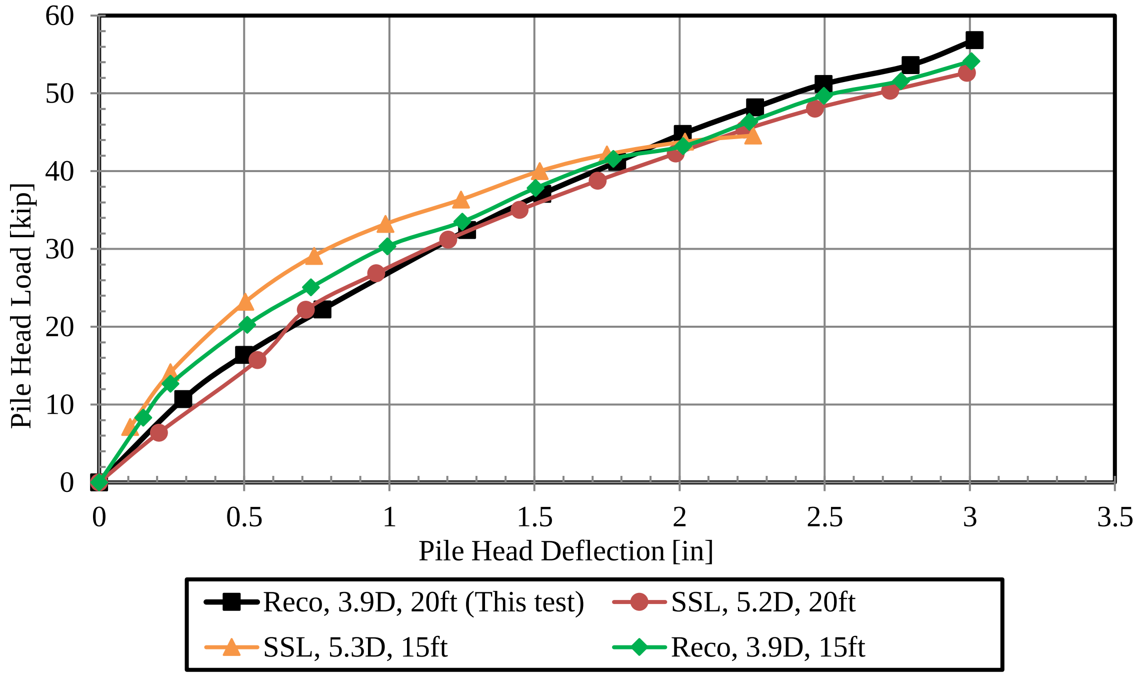

Figure 8-3: Comparison of load versus displacement curves for the 3.9D pile to other piles at similar spacings tested during this study.

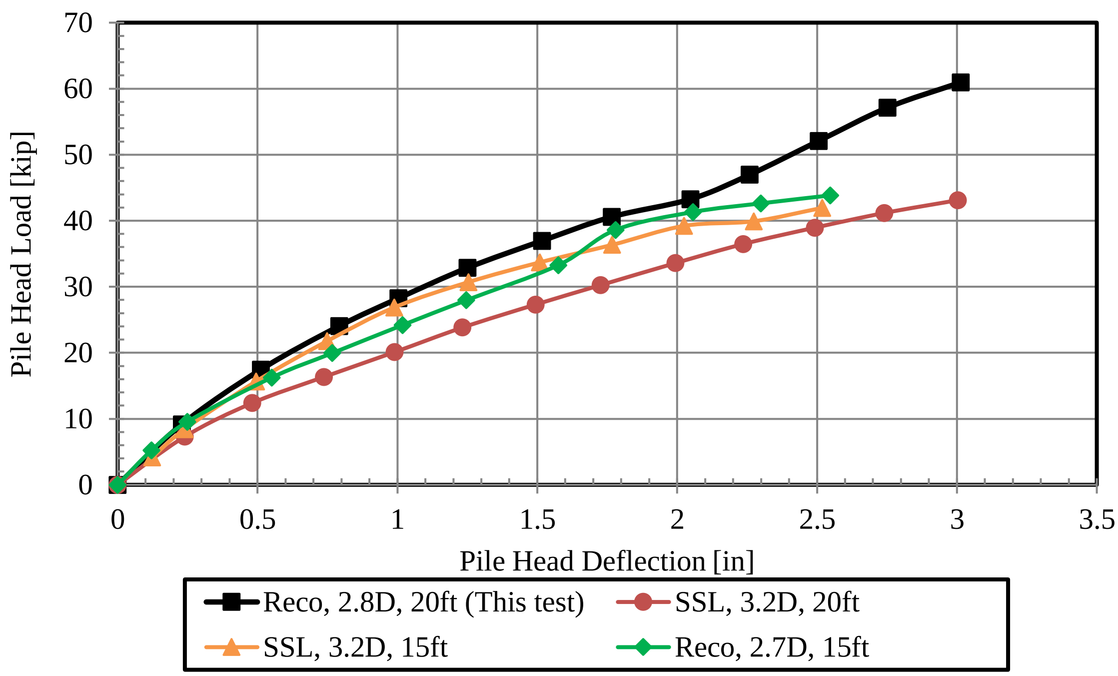

Figure 8-4: Comparison of load versus displacement curves for the 2.8D pile to other piles at similar spacings tested during this study.

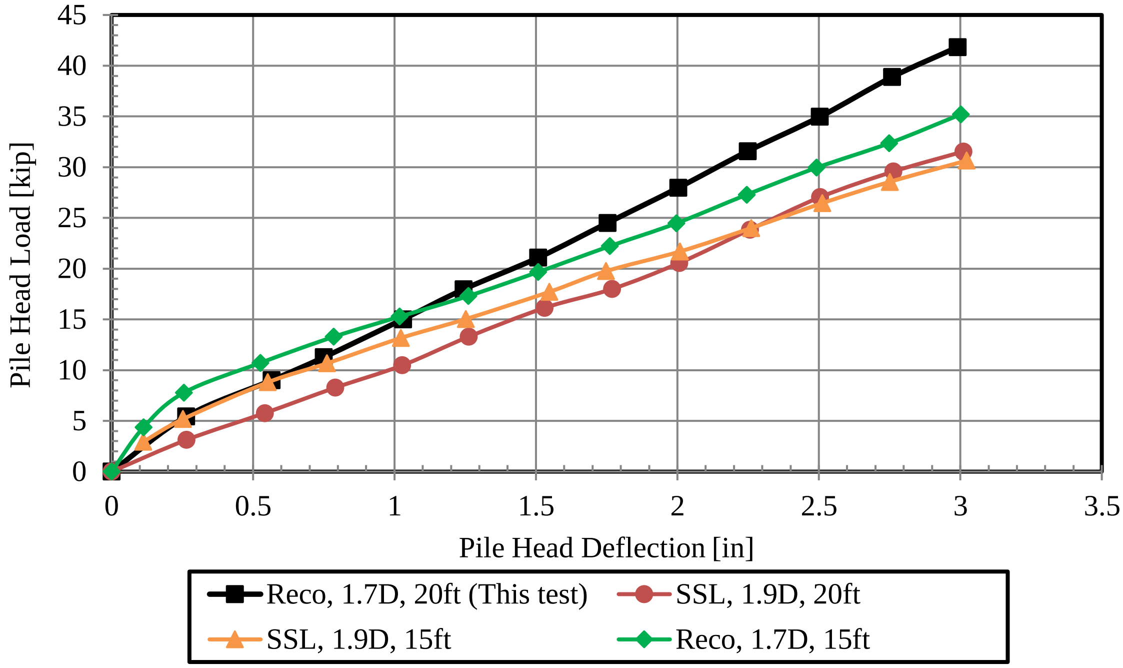

Figure 8-5: Comparison of load versus displacement curves for the 1.7D pile to other piles at similar spacings tested during this study.

8.2.2 Pile Head Load versus Rotation Curves

The rotation of the pile was measured using data from string potentiometers attached to the pile as described in section 5.2. Figure 8-6 and Figure 8-7 show the measured values compared to those predicted by LPILE for the 1.7 and 2.9D tests. The results are shown for the LPILE model with and without the simulated surcharge. The results of the pile head rotation predicted by LPILE are very close to measured values. The worst agreement is for the 1.7D test. This is expected because the predicted load-displacement curve was also the worst for the 1.7D pile. The agreement between the 2.8D and 3.9D tests is very similar to that of the 2.9D test.

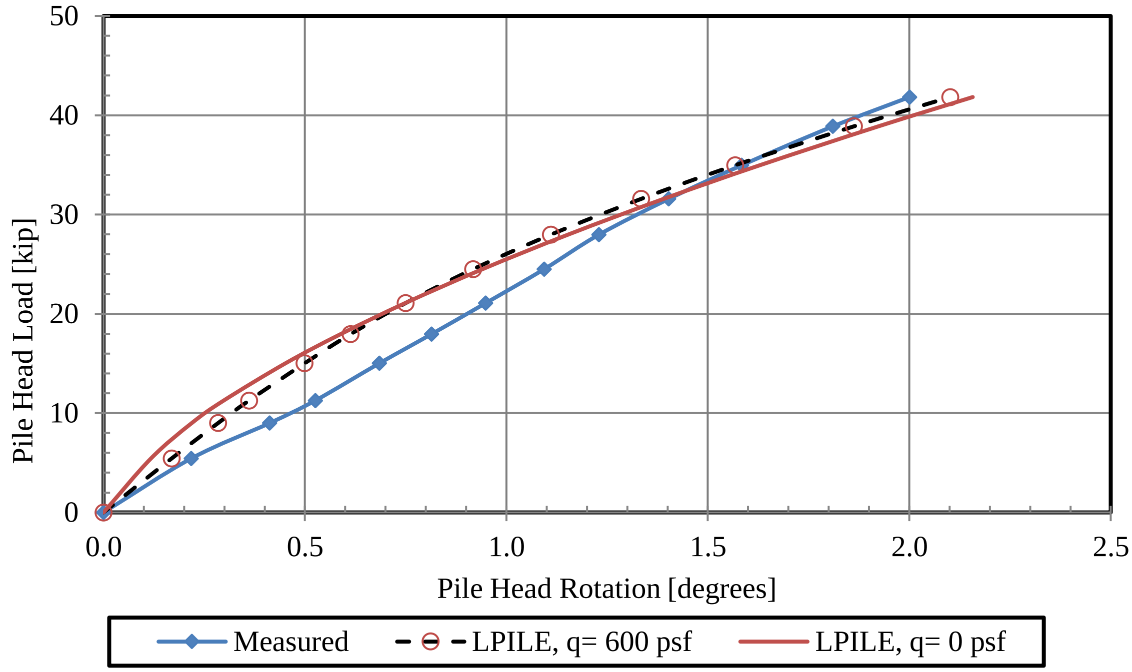

Figure 8-6: Comparison of pile head load versus rotation curves computed by LPILE to measured pile head load versus rotation curves for the 1.7D test.

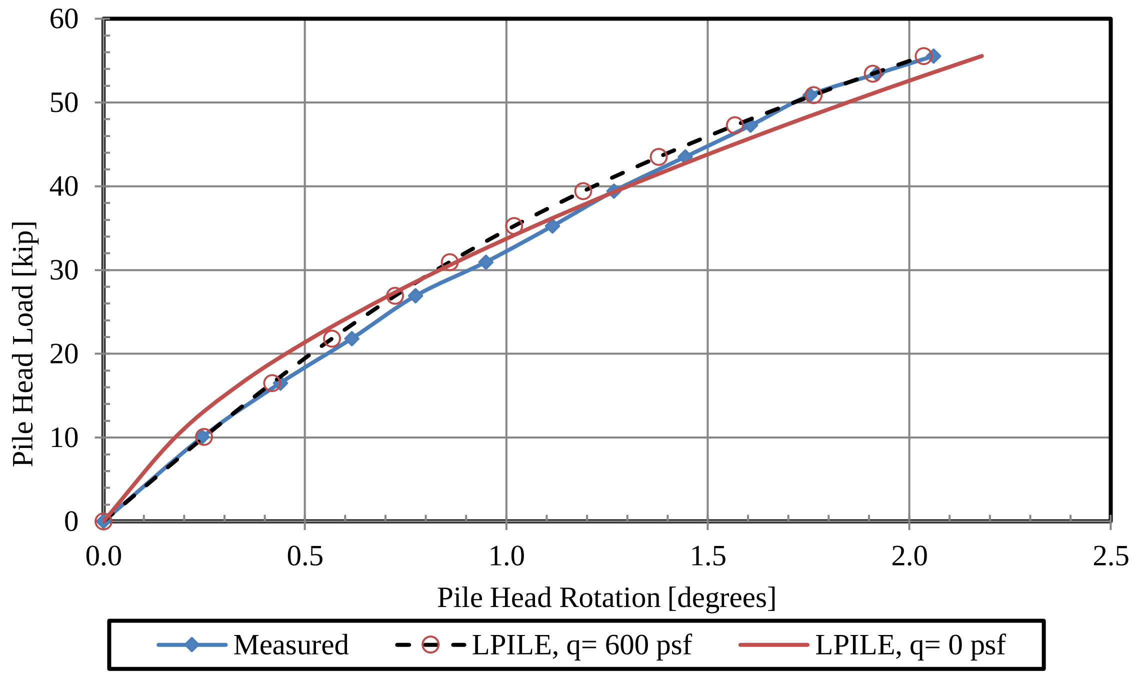

Figure 8-7: Comparison of pile head load versus rotation curves computed by LPILE to measured pile head load versus rotation curves for the 2.9D test.

8.2.3 Bending Moment versus Depth Curves

Bending moment versus depth curves for each of the piles was computed using strain gauge data as described previously. The measured bending moment is compared to the bending moment computed by the LPILE model with and without the simulated surcharge, q, for each of the test piles. Figure 8-8 through Figure 8-11 show this comparison at two different pile head loads for each test. The same soil profiles were used in LPILE as discussed in section 8.1.

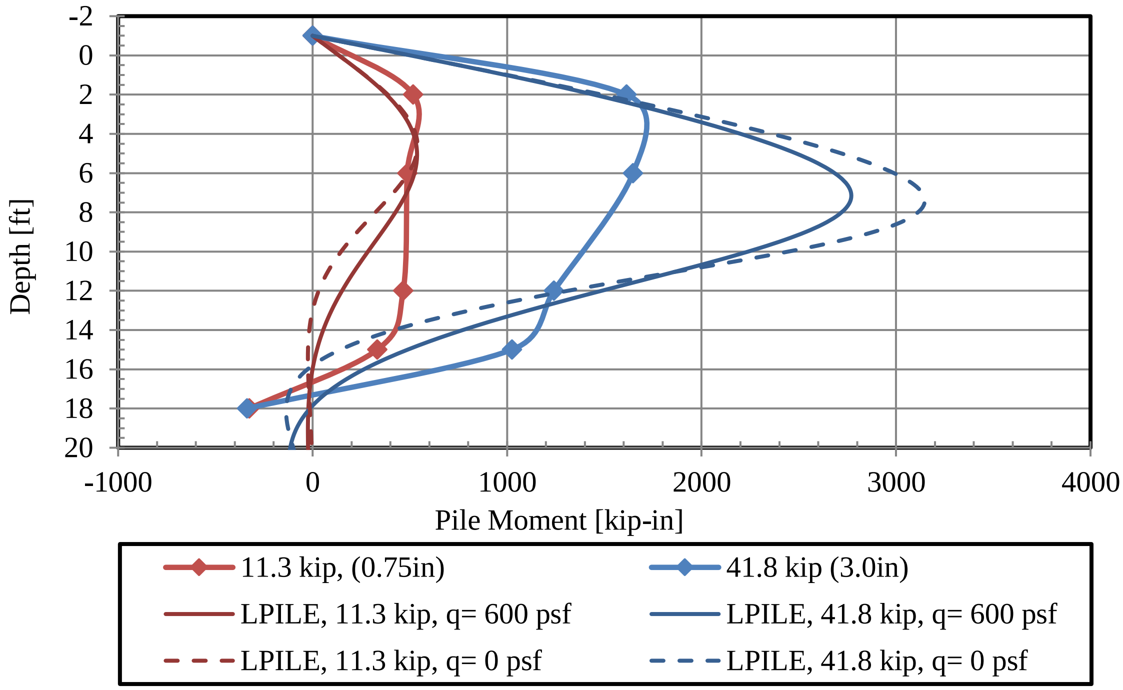

Figure 8-8: Measured and computed pile bending moment at multiple pile head load levels for the 1.7D test.

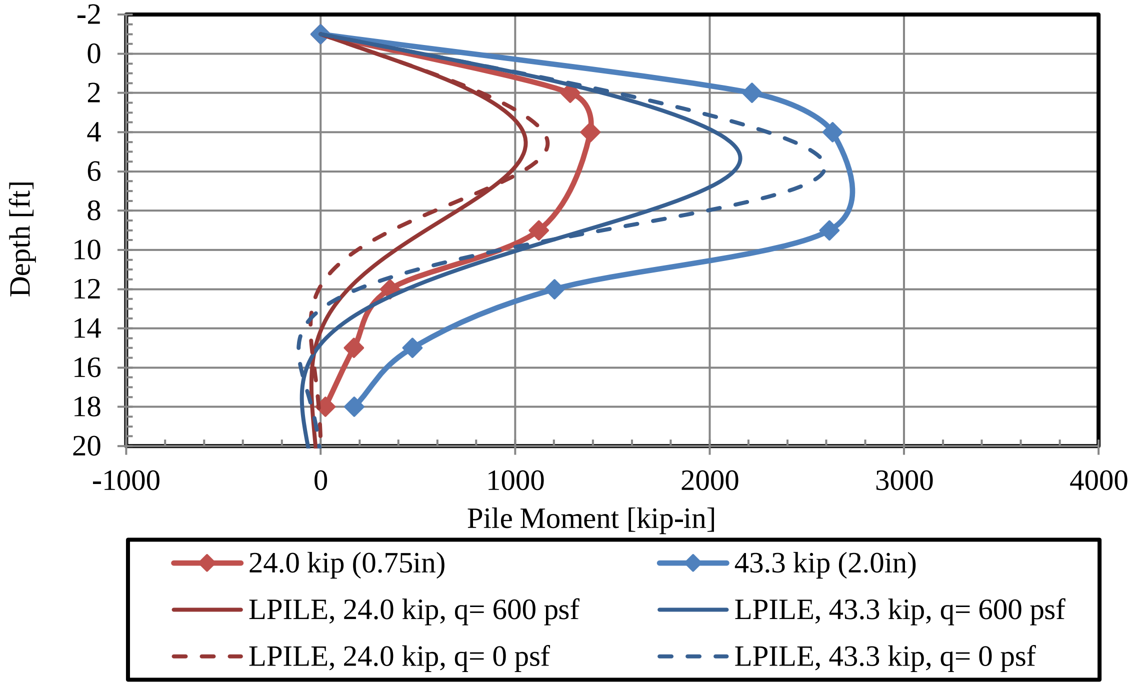

Figure 8-9: Measured and computed pile bending moment at multiple pile head load levels for the 2.8D test.

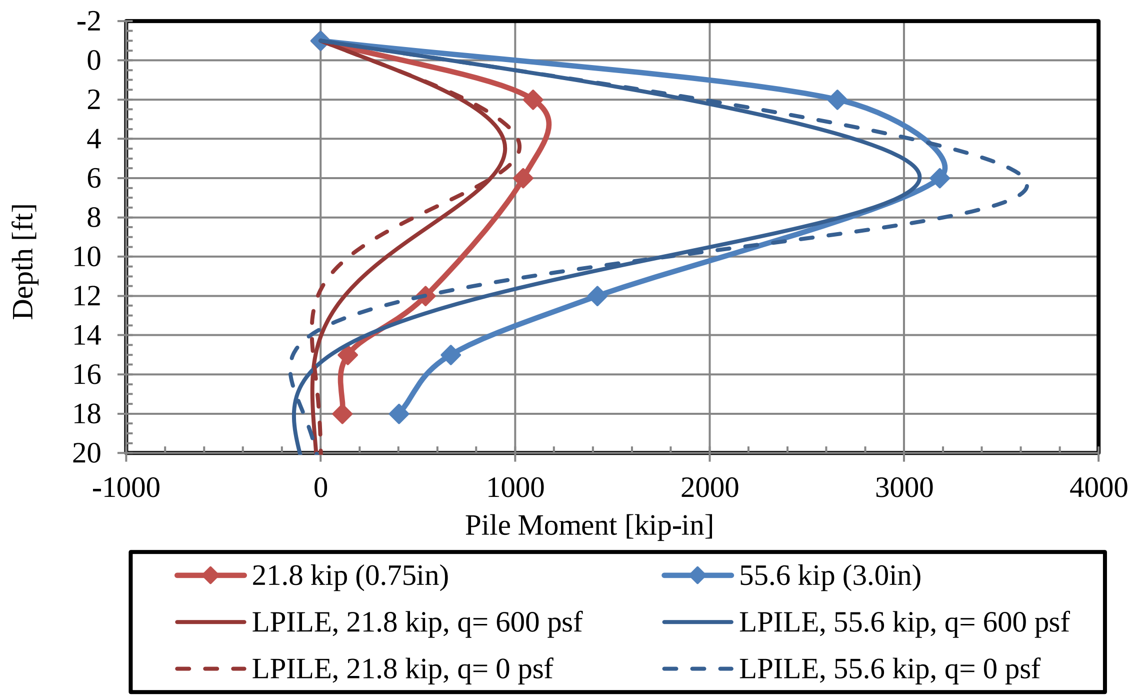

Figure 8-10: Measured and computed pile bending moment at multiple pile head load levels for the 2.9D test.

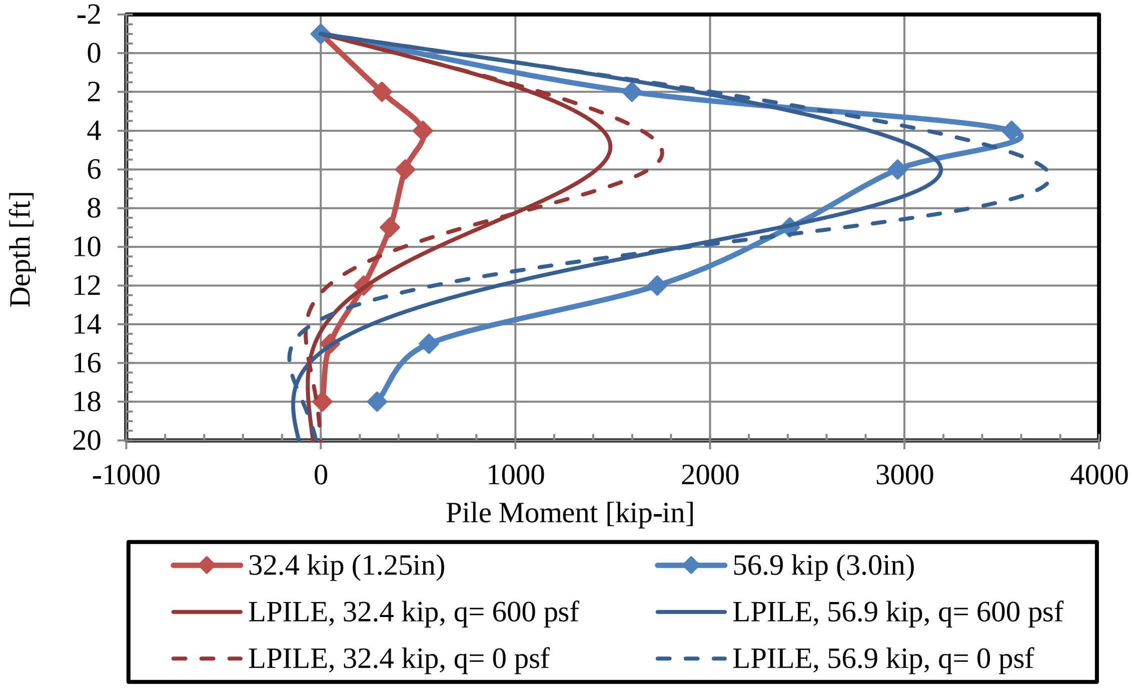

Figure 8-11: Measured and computed pile bending moment at multiple pile head load levels for the 3.9D test.

The agreement of the results varies between each test and pile head load. The depth of the maximum moment predicted by LPILE is within 2 ft. of the measured for all the tests except the 1.7D test and the predicted maximum moment is within 25% of the computed maximum moment for the 2.8D, 2.9D, and 3.9D tests and within 40% of 1.7D test. The relatively poor prediction of maximum moment is consistent with the fact that the load-deflection curve for this case was not well predicted in comparison with the other test piles. Overall, the LPILE model with the simulated surcharge does not seem to clearly match the measured curve better than the model without the applied surcharge.

9 CONCLUSION FOR WELDED WIRE REINFORCEMENT

Full-scale load tests were performed on four 12.75”x0.375” pipe piles spaced at distances of 1.8, 3.4, 4.3 and 5.2 pipe diameters behind a 20-ft high MSE wall. The purpose of this study was to measure reduced lateral pile load displacement curves for piles at varying distance from an MSE wall; measure the distribution of reinforcement tensile force induced by lateral pile loading; develop reduction factors to account for reduced pile resistance based on spacing and reinforcement type; and to develop a design approach to predict reinforcement loads induced by pile loading. This chapter addresses conclusions made from this study regarding lateral pile resistance and induced forces in soil reinforcement and provides recommendations for further research.

9.1 Conclusions Regarding Steel Pipe Pile and MSE Wall Interaction

1. Lateral pile resistance decreases as pile spacing behind the MSE wall decreases below about four pile diameters behind the wall. Relative to the pile furthest from the wall, average pile load decreased approximately 4, 21 and 51 percent for piles spaced at 4.3D, 3.4D and 1.8D from the MSE wall face, respectively.
2. For similarly loaded piles, pile head rotation also decreases as pile spacing increases.
3. Based on this study and previous test data, a simple p-multiplier approach provides reasonably accurate estimates of lateral load-displacement curves as well as bending

moment versus depth curves. Lateral soil resistance remains relatively constant (p-multiplier of 1.0) for piles located greater than approximately 3.9 pile diameters (3.9D) behind an MSE wall with inextensible reinforcements. For piles spaced closer than 3.9D, a linear reduction in the p-multiplier was observed.

4. Reinforcement length to height (L/H) ratios and inextensible reinforcement types do not appear to significantly affect p-multiplier relationships.
5. In contrast to tests involving extensible (geosynthetic) reinforcements, lateral wall deformation for the concrete MSE wall panels were generally less than 0.4 inches with the inextensible reinforcements even at large pile head loads (60 kips) and deflections (3 inches).

9.2 Conclusions Regarding Pile and Welded-Wire Grid Reinforcement Interaction

1. Maximum tensile forces occur in the soil reinforcement near the pile location.
2. Maximum induced tensile forces increase as pile loads and pile distance from the wall face increase.
3. Maximum tensile forces decrease as transverse distances between the soil reinforcement and the pile center increase.
4. The statistical regression equation developed in this study accounts for approximately 79% of the variation in maximum induced tensile force for all welded-wire grid reinforcements tested to date. Variables affecting maximum induced tensile force are pile load, transverse distance from the pile load, vertical stress, pile spacing and L/H ratio.

10 CONCLUSION FOR RIBBED STRIP REINFORCEMENT

Piles used to support bridge abutments are commonly located within the reinforced zone of MSE walls and are subject to lateral loading from earthquakes and thermal expansion and contraction. Full scale lateral load testing was performed on 12.75x0.375 pipe piles spaced at 3.9, 2.9, 2.8, and 1.7 pile diameters behind an MSE wall which was constructed for this research to determine appropriate reduction factors for lateral pile resistance based on pile spacing behind the back face of the wall. Galvanized ribbed steel strips were used as the reinforcement for the MSE wall in the vicinity of the four piles discussed in this report. The relationship between lateral pile load and induced load on the soil reinforcement was also investigated through instrumentation of four layers of soil reinforcement located near the laterally loaded piles. Based on data gathered in this research in combination with previous testing and research the following conclusions can be made. The conclusions are primarily limited to the type of wall tested but may be applied to other situations using engineering judgment.

10.1 Conclusions Relative to Lateral Pile Resistance

1. Lateral pile resistance tends to decrease as spacing from the back of the MSE wall decreases.
2. In general, piles spaced further than 3.8D behind the MSE wall can be assumed to have no reduction in lateral resistance because of interaction with the wall. However, the resistance of piles spaced closer to the wall than 3.8D can be modeled in LPILE using a p-multiplier less than 1.0 that varies linearly with spacing from the wall.

3. P-multipliers for the 3.9D, 2.9D, 2.8D, and 1.7D tests are 1.0, 1.0, 1.0, and 0.5, respectively. These multipliers are higher than expected based on previous testing and research and are likely a result of increased compactive effort near the 2.9D and 2.8D piles. These results indicate the importance of consistent compactive effort for the soil between the pile and the wall in evaluating lateral pile resistance.
4. The reinforced backfill can be modeled in LPILE using the API Sand (1982) method with a friction angle of 31 degrees and a subgrade modulus of approximately 60 pci when a uniform surcharge of 600 psf is applied. If no surcharge is applied, a friction angle of 39 degrees and subgrade modulus of 260 pci is more appropriate.

10.2 Conclusions Relative to Force Induced in the Reinforcements

1. Induced load in reinforcement tends to increase with depth to the 2nd or 3rd layer of reinforcement after which it decreases.
2. Induced load in the reinforcement tends to increase as pile spacing decreases.
3. Induced load in the reinforcement decreases rapidly with increased transverse distance from the pile.
4. The tensile force induced in the reinforcement can be estimate using a regression equation which considers the influence of pile load, pile spacing behind the wall, reinforcement depth or vertical stress on the reinforcement, and transverse spacing of the reinforcement. The R^2 value for the model is approximately 0.78, indicating that about 78% of the observed variation is accounted for by the equation.
5. Despite the relatively high applied lateral loads and pile displacements, the reinforcements were successful in reducing lateral wall displacements to acceptable levels for all of the tests. Maximum wall panel displacement was highest for the 2.8D

test and reached 0.35 in. at 3.0 in. of pile head displacement. The maximum wall displacement at 3.0 in. of pile head displacement was similar for all of the other tests but was only approximately 0.15 to 0.20 inches.

10.3 Recommendations for Further Research

Piles for this study were loaded laterally using a pinned head connection. However, a fixed head connection is more representative of real life construction as piles are grouped together by a pile cap supporting a bridge abutment. A fixed connection would hinder pile head rotation and would create a different load distribution induced in the soil reinforcement. Research has shown that laterally loaded pile groups have a reduced resistance capacity in comparison with single piles (Rollins et al. 2006). Therefore, a group pile test is recommended behind an MSE wall to understand the differences that fixed and pinned head connections have on the induced load capacities of the reinforcement and to understand if reduction factors for pile groups behind an MSE wall are similar to those previously studied.

Piles for this study were loaded at ¼ in. cumulative deflection intervals that represent static loading conditions. Lateral loading of piles supporting a bridge abutment typically comes from thermal expansion or earthquake loads, both of which are cyclic loads. It is recommended that further full-scale testing be performed on piles behind MSE walls representing cyclic loads and their effects on induced forces in soil reinforcement and wall deflection.

Backfill compaction was approximately 92% between the test piles and the back face of the wall. Compaction affects the lateral resistance of the loaded pile, as well as the soil's ability to resist pullout of the reinforcement. During construction of MSE walls it may be hard to achieve exact compaction of backfill according to specifications and it is more likely that a range of relative compaction actually occurs near the face. Therefore, it is recommended that further testing behind an MSE wall be performed on piles spaced equal distances behind the back face of the wall with varied relative compaction. Data from compaction tests could then be used to calculate a range of p-multipliers and reinforcement loads based on relative compaction for a specified pile spacing and correlations made for different pile spacings.

Piles located behind wall joints appeared to increase wall deflection and induced load in soil reinforcements compared with those located behind the center of the wall panel. Further research could be performed to better understand the relationship between pile location and wall joint location and to include a location reduction factor, if needed.

REFERENCES

API Recommended Practice for Planning, Designing, and Constructing Fixed Offshore Platforms. (1982). American Petroleum Institute, 13th Edition, Washington, D.C.

Berg, R.R., Christopher, B.R., and Samtani, N.C. (2009). "Design of Mechanically Stabilized Earth Walls and Reinforced Soil Slopes" *FHWA, Washington, D.C., Report No. FHWA-NHI-10-024.*

Besendorfer, J. (2015). "Lateral Resistance of Pipe Piles Near 20-ft Tall MSE Abutment Wall with Strip Reinforcements" MS Thesis, Department of Civil and Environmental Engineering, Brigham Young University, Provo, UT.

Han, J. (2014). "Lateral Resistance of Piles Near 15 Foot Vertical MSE Abutment Walls Reinforced with Ribbed Steel Strips" MS Thesis, Department of Civil and Environmental Engineering, Brigham Young University, Provo, UT.

Hatch, C. (2014). "Lateral Resistance of Piles Near Vertical MSE Abutment Walls" MS Thesis, Department of Civil and Environmental Engineering, Brigham Young University, Provo, UT.

Hild, F., and Roux, S. (2006). "Digital Image Correlation: from Displacement Measurement to Identification of Elastic Properties - a Review." Strain, 42(2), 69–80.

Isenhower, W.M., Wang S. (2015). "Technical Manual for LPILE 2015 (Using Data Format Version 8)", Ensoft Inc., Austin, TX.

Lawson, W., Jayawickrama, P., Wood, T., and Surles, J. (2013). "Pullout Resistance Factors for Inextensible Mechanically Stabilized Earth Reinforcements in Sandy Backfill." *Transportation Research Record: Journal of the Transportation Research Board*, 2363, 21–29.

"Measurement Principles of DIC." *Digital Image Correlation (DIC) Measurement Principles*, <http://www.dantecdynamics.com/measurement-principles-of-dic> (Aug. 11, 2015).

Nelson, K.R. (2013). “Lateral Resistance of Piles Near Vertical MSE Abutment Walls at Provo Center Street” MS Thesis, Department of Civil and Environmental Engineering, Brigham Young University, Provo, UT.

Parsons, R. L., Pierson, M., Han, J., Brennan, J. J., and Brown, D. A. (2009). “Lateral Load Capacity of Cast-in-Place Shafts behind an MSE Wall.” *Contemporary Topics in In Situ Testing, Analysis, and Reliability of Foundations*.

Pierson, M., Parsons, R. L., Han, J., Brown, D., and Thompson, W. R. (2009). “Capacity of Laterally Loaded Shafts Constructed Behind the Face of a Mechanically Stabilized Earth Block Wall”*, Kansas Department of Transportation, Report No. K-TRAN: KU-07-6.*

Pierson, M. C., Parsons, R. L., Han, J., Brennan, J. J., and Huang, J. (2011). “Influence of Geogrid Stiffness on Shaft Lateral Capacities and Deflections behind an MSE Wall.” Geo-Frontiers 2011.

Price, J.S. (2012). “Lateral Resistance of Piles Near Vertical MSE Abutment Walls” MS Thesis, Department of Civil and Environmental Engineering, Brigham Young University, Provo, UT.

Rollins, K. M., Olsen, K. G., Jensen, D. H., Garrett, B. H., Olsen, R. J., and Egbert, J. J. (2006). “Pile Spacing Effects on Lateral Pile Group Behavior: Analysis.” *J. Geotech. Geoenviron. Eng. Journal of Geotechnical and Geoenvironmental Engineering*, 132(10), 1272–1283.

Rollins, K.M., Price, J.S., and Nelson, K.R. (2013). “Lateral Resistance of Piles Near Vertical MSE Abutment Walls”, *Utah Department of Transportation, Report No. UT-13.04*.

Source: “Test Site.” 40°27’14.08” N and 111°53’53.60” W. GOOGLE EARTH. June 4, 2013. June 15, 2015.

APPENDIX A – PULLOUT CALCULATIONS

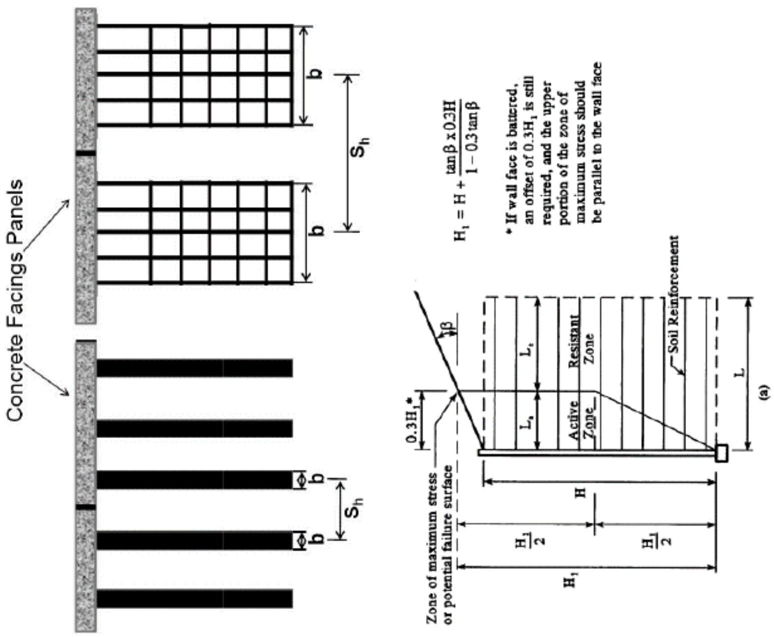

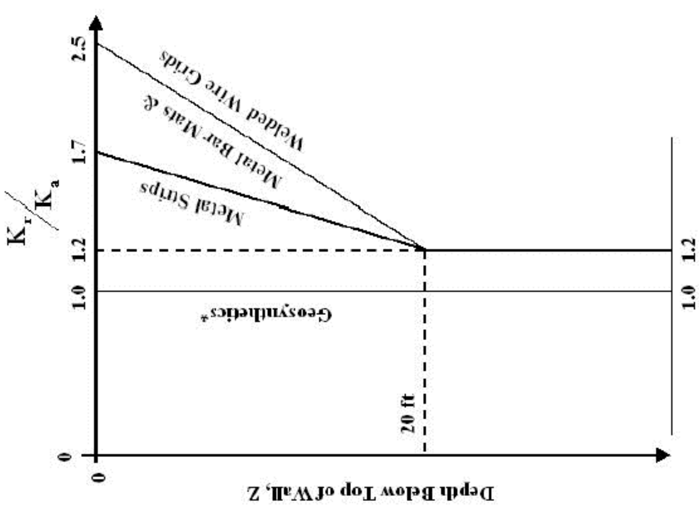

MSE Wall- Welded Wire Side

MSE Wall Properties

Wall Height	H	20	ft
Total Height	H_1	24.8	ft
Panel Width	w_p	9.94	ft
Panel Height	h_p	4.94	ft
Reinforcements per Panel Along Wall Length		2	

$$H_1 = H + H_{eq}$$

Soil Properties

Reinforced Backfill Moist Unit Weight	γ_r	126.2	pcf
Friction Angle	ϕ_r'	38	deg
		0.66	rad
Active Earth Pressure Coefficient	K_a	0.238	[Eqn. 4-25]

$$K_a = \tan^2\left(45 - \phi_r'/2\right)$$

Grid Reinforcement Properties

Approximate Vertical Spacing	S_v	2.5	ft
Approximate Horizontal Spacing	S_h	5	ft
Length of Reinforcement	L	18	ft
Longitudinal Grid Spacing	S_l	8	in
Scale Effect Correction Factor	α	1	[p. 3-16]
Reinforcement Effective Unit Perimeter	C	2	[pp. 3-16, 4-49]
Nominal Transverse Wire Thickness, W11	t	0.374	in

Depth, Z [ft]		orcement Length in Resistance Zone,	
at $Z = 0$	0	10.57	$L_e = L-0.3H_1$
at $Z = H_1/2$	12.38	10.57	$L_e = L-0.3H_1$
at $Z = H_1$	24.8	18	$L_e = L$

$$L = L_a + L_e$$

$$L_a = 0.3H$$

Top of Structure

$$F^* = 20(t/S_t)$$

Depth of 20 ft +

$$F^* = 10\,(t/S_t)$$

Boundaries for Pullout Friction Factor, F*			
Depth Below Top of wall, Z	K_r/K_a	F* (Top Layer)	F* (Other Layers)
0	2.5	1.247	0.623
20	1.2	0.623	0.312

Surcharge

Unit Weight of Surcharge	γ_{eq}	126.2	pcf
Equivalent Surcharge Height	H_{eq}	4.8	ft
Surcharge (Dead Load)	q	600	psf

Load Factor for Maximum Permanent Loads	$\gamma_{EV\text{-}MAX}$	1.35	[Table 4-2]
Resistance Factor for Pullout	ϕ_p	0.9	[Table 4-7]

Reinforcement Level	Wire Type	Depth to Layer, Z [ft]	K_r/K_a	Horizontal Earth Pressure Coefficient, K_r	Vertical Stress, $\sigma_V=\gamma_r(Z+H_{eq})$ [psf]	Factored Horizontal Stress, $\sigma_H=K_r(\gamma_r(Z+h_{eq}))\gamma_{EV\text{-}MAX}$ [psf]	Reinforcement Demand, $T_{max}=\sigma_H(Sv)$ [k/ft]	Transverse Grid Spacing, S_t [in]	Reinforcement Pullout Friction Factor, F*	Length of Reinforcement in Resistance Zone, L_e [ft]	Length of Reinforcement in Active Zone, L_a [ft]	Grid Reinforcement Width, b [ft]	Grid Reinforcement Coverage Ratio, $R_c=b/S_h$	Factored Pullout Resistance, $P_{rr}=\phi_p F^*\alpha\sigma_V L_e C R_c$ [k/ft]	Capacity to Demand Ratio, $CDR=P_{rr}/T_{max}$
				[Fig. 4-10]		[Sim. to Eqn. 4-30]	[Eqn. 4-32a]		[Eqns. 3-6, 3-7]	[Fig. 4-9 and Eqns. 4-37, 4-40]		[Fig. 3-3]	[Fig. 3-3]	[Sim. to Eqn. 4-35]	
1	6W11X0.50W11	1.25	2.42	0.58	758	589	1.47	6	1.208	10.57	7.43	3.33	0.667	11.61	7.89
2	5W11X1.00W11	3.75	2.26	0.54	1073	778	1.94	12	0.565	10.57	7.43	2.67	0.533	6.15	3.17
3	5W11X1.00W11	6.25	2.09	0.50	1389	934	2.33	12	0.526	10.57	7.43	2.67	0.533	7.41	3.18
4	5W11X1.00W11	8.75	1.93	0.46	1704	1057	2.64	12	0.487	10.57	7.43	2.67	0.533	8.42	3.19
5	5W11X1.00W11	11.25	1.77	0.42	2020	1147	2.87	12	0.448	10.57	7.43	2.67	0.533	9.19	3.20
6	6W11X1.00W11	13.75	1.61	0.38	2335	1205	3.01	12	0.409	11.40	6.60	3.33	0.667	13.07	4.34
7	6W11X1.00W11	16.25	1.44	0.34	2651	1229	3.07	12	0.370	12.90	5.10	3.33	0.667	15.18	4.94
8	6W11X1.00W11	18.75	1.28	0.30	2966	1221	3.05	12	0.331	14.40	3.60	3.33	0.667	16.97	5.56
														Average CDR:	**4.43**

MSE Wall- Ribbed Strip Side

MSE Wall Properties

Wall Height	H	20	ft
Total Height	H_1	24.8	ft
Panel Width	w_p	9.84	ft
Panel Height	h_p	4.92	ft
Reinforcements per Panel Along Wall Length		4	

$$H_1 = H + H_{eq}$$

Soil Properties

Reinforced Backfill Moist Unit Weight	γ_r	126.2	pcf
Friction Angle	ϕ_r'	39	deg
		0.68	rad
Active Earth Pressure Coefficient	K_a	0.228	[Eqn. 4-25]
Coefficient of Uniformity	C_u	60.0	$=D_{60}/D_{10}$
Grain Diameter at 60% Passing	D_{60}	3	mm
Grain Diameter at 10% Passing	D_{10}	0.05	mm

$$K_a = \tan^2\left(45 - \phi_r'/2\right)$$

Strip Reinforcement Properties

Approximate Vertical Spacing	S_v	2.5	ft
Approximate Horizontal Spacing	S_h	2.5	ft
Length of Reinforcement	L_t	18	ft
Scale Effect Correction Factor	α	1	[p. 3-16]
Reinforcement Effective Unit Perimeter	C	2	[pp. 3-16, 4-49]
Strip Width	b	50	mm
		1.969	in
Strip Thickness	t	4	mm
		0.157	in
Reinforcement Coverage Ratio	R_c	0.066	[Fig. 3-3]

Depth, Z [ft]		Reinforcement Length in Resistance Zone	
at Z = 0	0	10.57	$L_e = L-0.3H_1$
at Z = $H_1/2$	12.38	10.57	$L_e = L-0.3H_1$
at Z = H_1	24.8	18	$L_e = L$

$L = L_a + L_e$ $\quad$ $L_a = 0.3H$

Top of Structure

$$F^* = 1.2 + \log C_u \leq 2.0$$

Depth of 20 ft +

$$F^* = \tan \phi_r'$$

Boundaries for Pullout Friction Factor, F*		
Depth Below Top of Wall, Z	K_r/K_a	F*
0	1.7	2
20	1.2	0.810

Surcharge

Unit Weight of Surcharge	γ_{eq}	126	pcf
Equivalent Surcharge Height	H_{eq}	4.8	ft
Surcharge (Dead Load)	q	600	psf

Load Factor for Maximum Permanent Loads	$\gamma_{EV\text{-}MAX}$	1.35	[Table 4-2]
Resistance Factor for Pullout	ϕ_p	0.9	[Table 4-7]

Reinforcement Level	Depth to Layer, Z [ft]	K_r/K_a	Horizontal Earth Pressure Coefficient, K_r [Fig. 4-10]	Vertical Stress, $\sigma_V=\gamma_r(Z+H_{eq})$ [psf]	Factored Horizontal Stress, $\sigma_H=K_r(\gamma_r(Z+h_{eq}))\gamma_{EV\text{-}MAX}$ [psf] [Sim. to Eqn. 4-30]	Reinforcement Demand, $T_{max}=\sigma_H(Sv)$ [k/ft] [Eqn. 4-32a]	Strip Reinforcement Pullout Friction Factor, F* [Eqns. 3-6, 3-7]	Length of Reinforcement in Resistance Zone, L_e [ft] [Fig. 4-9 and Eqns. 4-37, 4-40]	Length of Reinforcement in Active Zone, L_a [ft]	Factored Pullout Resistance, $P_{rr}=\phi_p F^* \alpha \sigma_V L_e C R_c$ [k/ft] [Sim. to Eqn. 4-35]	Capacity to Demand Ratio, $CDR=P_{rr}/T_{max}$
1	1.25	1.67	0.380	758	388	0.97	1.926	10.57	7.43	1.82	1.88
2	3.75	1.61	0.365	1073	529	1.32	1.777	10.57	7.43	2.38	1.80
3	6.25	1.54	0.351	1389	658	1.65	1.628	10.57	7.43	2.82	1.72
4	8.75	1.48	0.337	1704	775	1.94	1.479	10.57	7.43	3.15	1.62
5	11.25	1.42	0.323	2020	880	2.20	1.331	10.57	7.43	3.36	1.53
6	13.75	1.36	0.309	2335	973	2.43	1.182	11.40	6.60	3.71	1.53
7	16.25	1.29	0.294	2651	1053	2.63	1.033	12.90	5.10	4.17	1.58
8	18.75	1.23	0.280	2966	1122	2.80	0.884	14.40	3.60	4.46	1.59
										Average CDR:	**1.66**

APPENDIX B – MSE WALL PLANS

SSL™

INNOVATIVE CONSTRUCTION PRODUCTS
4740 SCOTTS VALLEY DRIVE, SUITE E
SCOTTS VALLEY, CA 95066
PHONE: (831) 430-9300 FAX: (831) 430-9340
WWW.MSEPLUS.COM

INDEX OF DRAWINGS

SHEET	REV	DESCRIPTION
RW–01	0	TITLE & INDEX
RW–02	0	PLAN VIEW
RW–03	0	ELEVATION SSL BYU WALL
RW–04	0	TYPICAL CROSS SECTIONS
RW–05	0	STANDARD DETAILS: 1 OF 3
RW–06	0	STANDARD DETAILS: 2 OF 3
RW–07	0	STANDARD DETAILS: 3 OF 3
RW–08	0	PANEL REBAR DETAILS: 1 OF 5
RW–09	0	PANEL REBAR DETAILS: 2 OF 5
RW–10	0	PANEL REBAR DETAILS: 3 OF 5
RW–11	0	PANEL REBAR DETAILS: 4 OF 5
RW–12	0	PANEL REBAR DETAILS: 5 OF 5

DESIGN PARAMETERS

SOIL PARAMETERS:
INTERNAL DESIGN: $\phi = 34°$, $\gamma = 131$ PCF
EXTERNAL DESIGN: $\phi = 30°$, $\gamma = 125$ PCF
(FOUNDATION) $\phi = 30°$
DEAD LOAD: 600 PSF OF SOIL AT 1FT BEHIND TEST PILES

PRECAST CONCRETE PANELS:
$f'c = 4{,}000$ psi (28 DAYS)
$fy = 60{,}000$ psi (REINFORCEMENT)

SOIL REINFORCEMENT:
WELDED WIRE MESH $fy = 65{,}000$ psi

DESIGN CRITERIA

AASHTO 2012 LRFD:

DESIGN LIFE = 75 YEARS

ISSUED FOR REVIEW 5/12/14

CERTIFIED ONLY WITH RESPECT TO INTERNAL STABILITY OF REINFORCED EARTH STRUCTURES

SSL™
INNOVATIVE CONSTRUCTION PRODUCTS
4740 SCOTTS VALLEY DRIVE, SUITE E
SCOTTS VALLEY, CA 95066
PHONE: (831) 430-9300 FAX: (831) 430-9340

THIS DRAWING CONTAINS INFORMATION PROPRIETARY TO SSL AND IS FURNISHED FOR THE PROJECT SHOWN ONLY. THIS INFORMATION SHALL NOT BE TRANSMITTED TO ANY OTHER PERSON OR AGENCY WITHOUT WRITTEN CONSENT OF SSL.

THE DESIGN CONTAINED ON THESE DRAWINGS IS BASED ON INFORMATION PROVIDED BY THE OWNER. ON THE BASIS OF THIS INFORMATION, SSL HAS DESIGNED THE STRUCTURE(S) SHOWN AND IS RESPONSIBLE FOR INTERNAL STABILITY ONLY. THE OWNER REMAINS RESPONSIBLE FOR EXTERNAL STABILITY INCLUDING FOUNDATION (BEARING CAPACITY AND SETTLEMENT) AND SLOPE STABILITY (SLIDING AND ROTATION).

DRAWN BY: AJM	5/12/14
CHECK BY: GTF	5/12/14
DESIGN BY: AJM	5/12/14
CHECK BY: SVR	5/12/14
PROJ. ENGR: AJM	

NO.	DATE	REVISION DESCRIPTION	BY

TITLE & INDEX

BRIGHAM YOUNG UNIVERSITY
MSE TEST WALL
LATERAL PILE RESISTANCE

Scale: NTS
Job:
Sheet: RW–01
Sheet 01 of 12

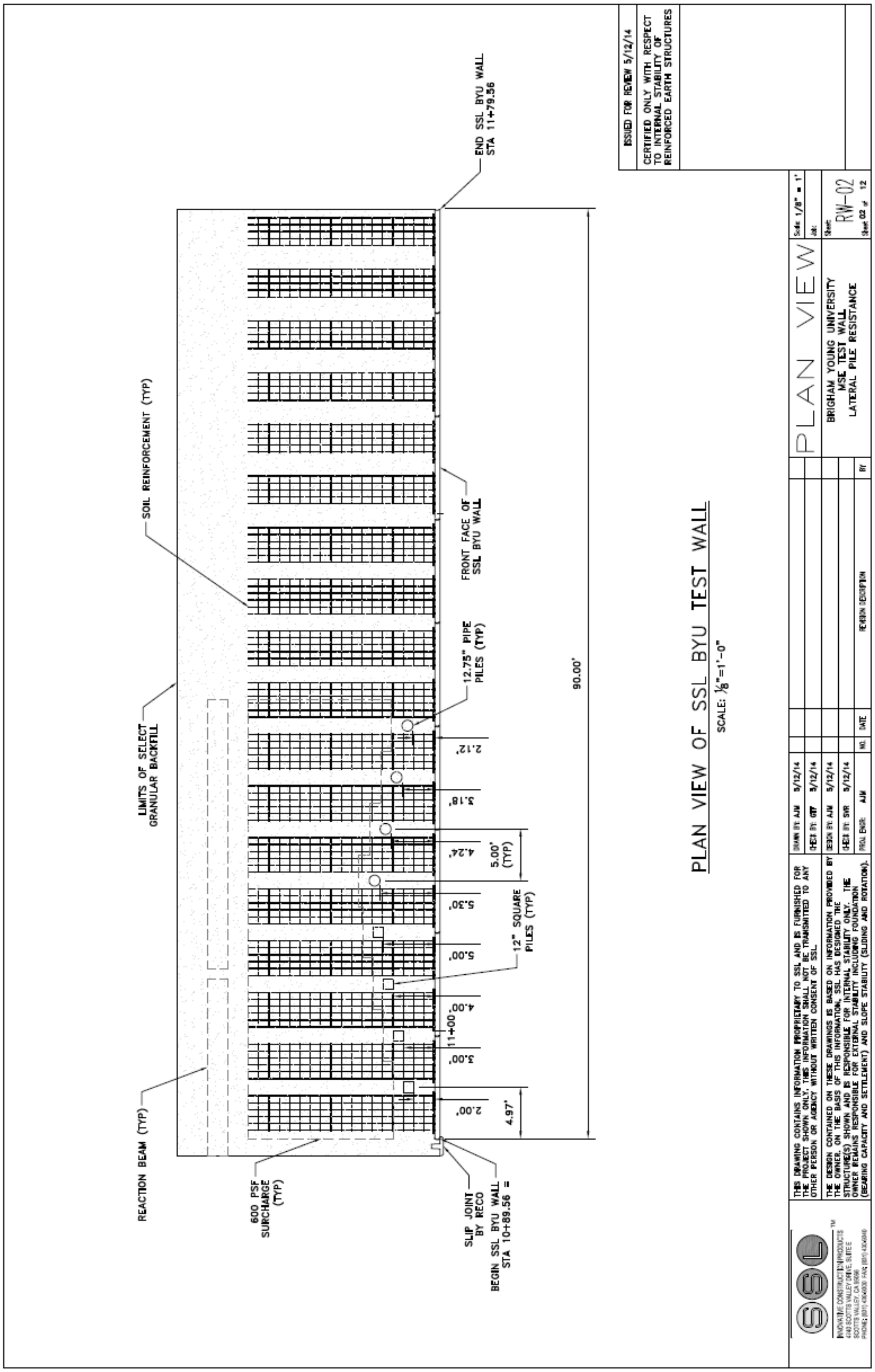
PLAN VIEW OF SSL BYU TEST WALL
SCALE: 1/8"=1'-0"
SOIL REINFORCEMENT (TYP)
LIMITS OF SELECT GRANULAR BACKFILL
REACTION BEAM (TYP)
600 PSF SURCHARGE (TYP)
SLIP JOINT BY RECO
BEGIN SSL BYU WALL STA 10+89.56 =
END SSL BYU WALL STA 11+79.56
FRONT FACE OF SSL BYU WALL
12.75" PIPE PILES (TYP)
12" SQUARE PILES (TYP)
90.00'
5.00' (TYP)
4.97'
11+00
2.00'
3.00'
4.00'
5.00'
5.30'
4.24'
3.18'
2.12'
ISSUED FOR REVIEW 5/12/14
CERTIFIED ONLY WITH RESPECT TO INTERNAL STABILITY OF REINFORCED EARTH STRUCTURES
PLAN VIEW
BRIGHAM YOUNG UNIVERSITY
MSE TEST WALL
LATERAL PILE RESISTANCE
RW-02
THIS DRAWING CONTAINS INFORMATION PROPRIETARY TO SSL AND IS FURNISHED FOR THE PROJECT SHOWN ONLY. THIS INFORMATION SHALL NOT BE TRANSMITTED TO ANY OTHER PERSON OR AGENCY WITHOUT WRITTEN CONSENT OF SSL.
THE DESIGN CONTAINED ON THESE DRAWINGS IS BASED ON INFORMATION PROVIDED BY THE OWNER. ON THE BASIS OF THIS INFORMATION, SSL HAS DESIGNED THE STRUCTURE(S) SHOWN AND IS RESPONSIBLE FOR INTERNAL STABILITY ONLY. THE OWNER REMAINS RESPONSIBLE FOR EXTERNAL STABILITY INCLUDING FOUNDATION (BEARING CAPACITY AND SETTLEMENT) AND SLOPE STABILITY (SLIDING AND ROTATION).
DRAWN BY: AJM 5/12/14
CHECK BY: GTF 5/12/14
DESIGN BY: AJM 5/12/14
CHECK BY: SVR 5/12/14
PROJ. ENGR: AJM
NO. DATE
REVISION DESCRIPTION
BY
Scale: 1/8" = 1'
Sheet 02 of 12
SSL

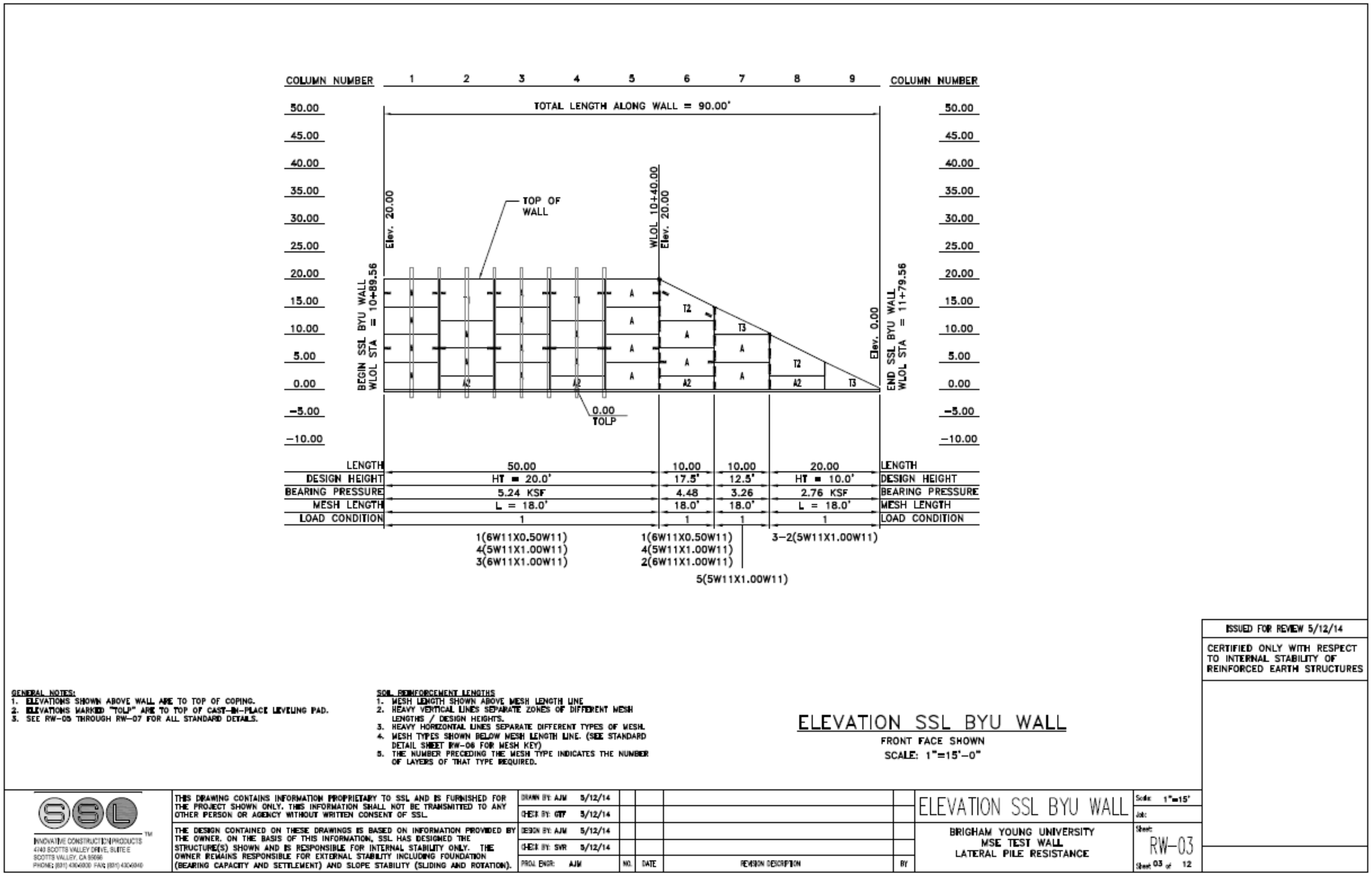
COLUMN NUMBER
1 2 3 4 5 6 7 8 9
TOTAL LENGTH ALONG WALL = 90.00'
50.00
45.00
40.00
35.00
30.00
25.00
20.00
15.00
10.00
5.00
0.00
-5.00
-10.00
BEGIN SSL BYU WALL
WLOL STA = 10+89.56
Elev. 20.00
TOP OF WALL
WLOL 10+40.00
Elev. 20.00
END SSL BYU WALL
WLOL STA = 11+79.56
Elev. 0.00
0.00
TOLP
A
A2
T2
T3
LENGTH
DESIGN HEIGHT
BEARING PRESSURE
MESH LENGTH
LOAD CONDITION
50.00
HT = 20.0'
5.24 KSF
L = 18.0'
1
10.00
17.5'
4.48
18.0'
1
10.00
12.5'
3.26
18.0'
1
20.00
HT = 10.0'
2.76 KSF
L = 18.0'
1
1(6W11X0.50W11)
4(5W11X1.00W11)
3(6W11X1.00W11)
1(6W11X0.50W11)
4(5W11X1.00W11)
2(6W11X1.00W11)
5(5W11X1.00W11)
3-2(5W11X1.00W11)
GENERAL NOTES:
1. ELEVATIONS SHOWN ABOVE WALL ARE TO TOP OF COPING.
2. ELEVATIONS MARKED "TOLP" ARE TO TOP OF CAST-IN-PLACE LEVELING PAD.
3. SEE RW-05 THROUGH RW-07 FOR ALL STANDARD DETAILS.
SSL REINFORCEMENT LENGTHS
1. MESH LENGTH SHOWN ABOVE MESH LENGTH LINE
2. HEAVY VERTICAL LINES SEPARATE ZONES OF DIFFERENT MESH LENGTHS / DESIGN HEIGHTS.
3. HEAVY HORIZONTAL LINES SEPARATE DIFFERENT TYPES OF MESH.
4. MESH TYPES SHOWN BELOW MESH LENGTH LINE. (SEE STANDARD DETAIL SHEET RW-06 FOR MESH KEY)
5. THE NUMBER PRECEDING THE MESH TYPE INDICATES THE NUMBER OF LAYERS OF THAT TYPE REQUIRED.
ELEVATION SSL BYU WALL
FRONT FACE SHOWN
SCALE: 1"=15'-0"
ISSUED FOR REVIEW 5/12/14
CERTIFIED ONLY WITH RESPECT TO INTERNAL STABILITY OF REINFORCED EARTH STRUCTURES
SSL
INNOVATIVE CONSTRUCTION PRODUCTS
THIS DRAWING CONTAINS INFORMATION PROPRIETARY TO SSL AND IS FURNISHED FOR THE PROJECT SHOWN ONLY. THIS INFORMATION SHALL NOT BE TRANSMITTED TO ANY OTHER PERSON OR AGENCY WITHOUT WRITTEN CONSENT OF SSL.
THE DESIGN CONTAINED ON THESE DRAWINGS IS BASED ON INFORMATION PROVIDED BY THE OWNER. ON THE BASIS OF THIS INFORMATION, SSL HAS DESIGNED THE STRUCTURE(S) SHOWN AND IS RESPONSIBLE FOR INTERNAL STABILITY ONLY. THE OWNER REMAINS RESPONSIBLE FOR EXTERNAL STABILITY INCLUDING FOUNDATION (BEARING CAPACITY AND SETTLEMENT) AND SLOPE STABILITY (SLIDING AND ROTATION).
DRAWN BY: AJM 5/12/14
CHECK BY: GTP 5/12/14
DESIGN BY: AJM 5/12/14
CHECK BY: SVR 5/12/14
PROJ. ENGR: AJM
NO. DATE REVISION DESCRIPTION BY
ELEVATION SSL BYU WALL
BRIGHAM YOUNG UNIVERSITY
MSE TEST WALL
LATERAL PILE RESISTANCE
Scale: 1"=15'
Sheet: RW-03
Sheet 03 of 12

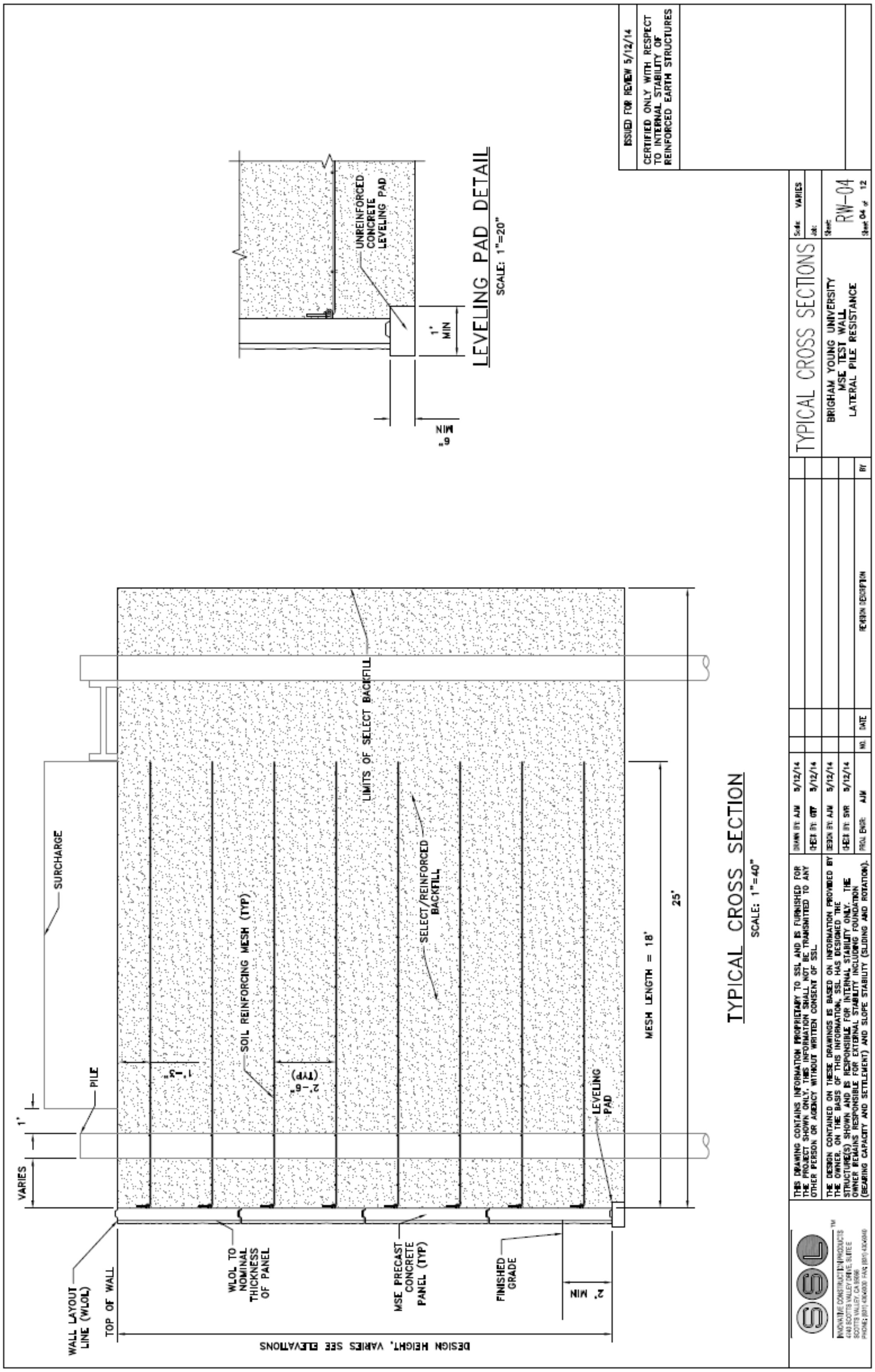
TYPICAL CROSS SECTION
SCALE: 1"=40"
LEVELING PAD DETAIL
SCALE: 1"=20"
UNREINFORCED CONCRETE LEVELING PAD
1" MIN
6" MIN
SURCHARGE
VARIES
1'
PILE
1'-3"
2'-6" (TYP)
SOIL REINFORCING MESH (TYP)
SELECT/REINFORCED BACKFILL
LIMITS OF SELECT BACKFILL
LEVELING PAD
MESH LENGTH = 18'
25'
WALL LAYOUT LINE (WLOL)
TOP OF WALL
WLOL TO NOMINAL THICKNESS OF PANEL
MSE PRECAST CONCRETE PANEL (TYP)
FINISHED GRADE
2' MIN
DESIGN HEIGHT, VARIES SEE ELEVATIONS
ISSUED FOR REVIEW 5/12/14
CERTIFIED ONLY WITH RESPECT TO INTERNAL STABILITY OF REINFORCED EARTH STRUCTURES
THIS DRAWING CONTAINS INFORMATION PROPRIETARY TO SSL AND IS FURNISHED FOR THE PROJECT SHOWN ONLY. THIS INFORMATION SHALL NOT BE TRANSMITTED TO ANY OTHER PERSON OR AGENCY WITHOUT WRITTEN CONSENT OF SSL.
THE DESIGN CONTAINED ON THESE DRAWINGS IS BASED ON INFORMATION PROVIDED BY THE OWNER. ON THE BASIS OF THIS INFORMATION, SSL HAS DESIGNED THE STRUCTURE(S) SHOWN AND IS RESPONSIBLE FOR INTERNAL STABILITY ONLY. THE OWNER REMAINS RESPONSIBLE FOR EXTERNAL STABILITY INCLUDING FOUNDATION (BEARING CAPACITY AND SETTLEMENT) AND SLOPE STABILITY (SLIDING AND ROTATION).
DRAWN BY: AJM 5/12/14
CHECK BY: GTF 5/12/14
DESIGN BY: AJM 5/12/14
CHECK BY: SVR 5/12/14
PROJ. ENGR: AJM
NO. DATE REVISION DESCRIPTION BY
TYPICAL CROSS SECTIONS
BRIGHAM YOUNG UNIVERSITY
MSE TEST WALL
LATERAL PILE RESISTANCE
Scale: VARIES
Sheet: RW-04
Sheet 04 of 12

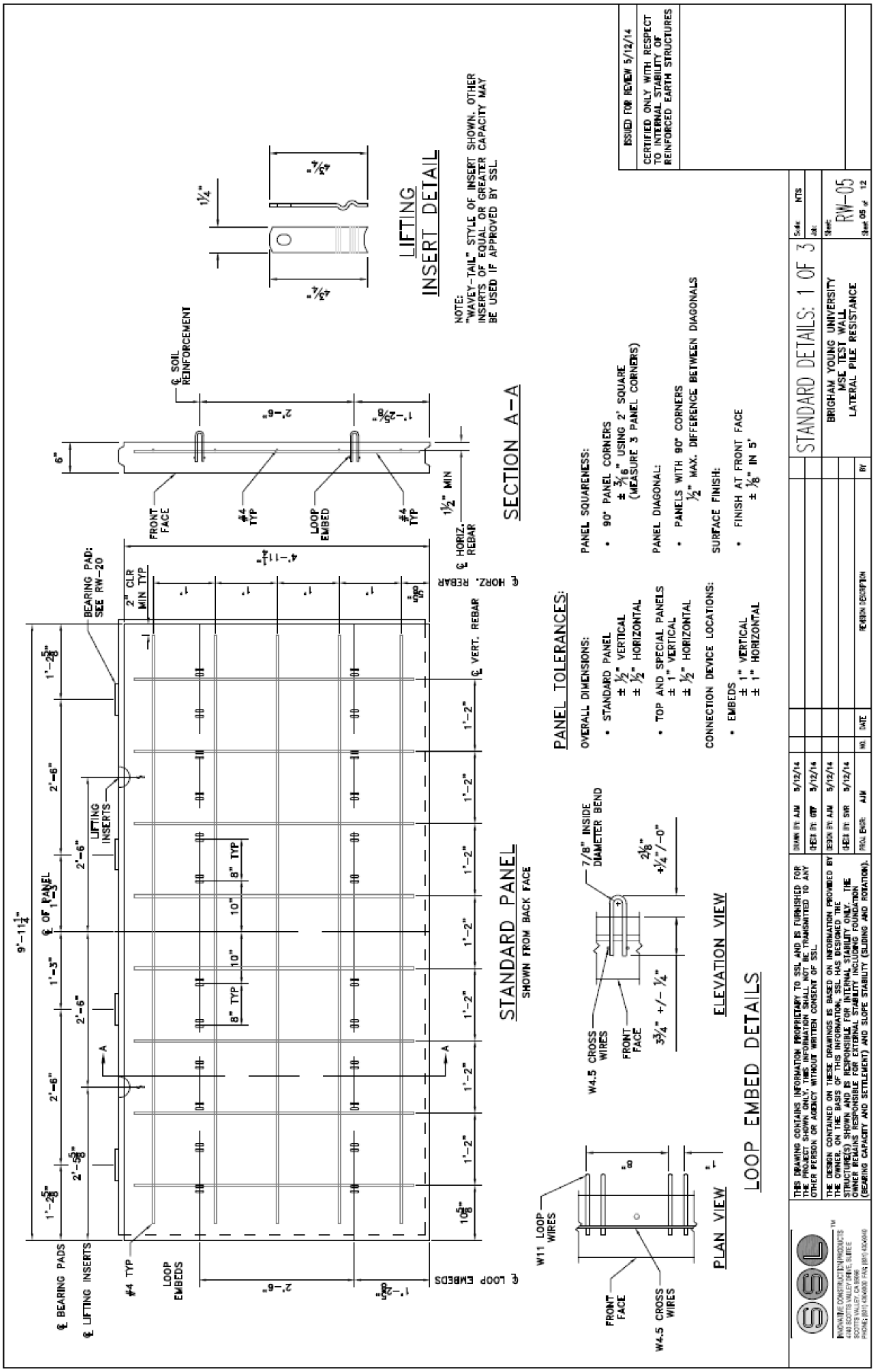

STANDARD PANEL
SHOWN FROM BACK FACE
SECTION A-A
LIFTING INSERT DETAIL
NOTE: "WAVEY-TAIL" STYLE OF INSERT SHOWN. OTHER INSERTS OF EQUAL OR GREATER CAPACITY MAY BE USED IF APPROVED BY SSL.
PANEL TOLERANCES:
OVERALL DIMENSIONS:
PANEL SQUARENESS:
PANEL DIAGONAL:
SURFACE FINISH:
CONNECTION DEVICE LOCATIONS:
LOOP EMBED DETAILS
PLAN VIEW
ELEVATION VIEW
ISSUED FOR REVIEW 5/12/14
CERTIFIED ONLY WITH RESPECT TO INTERNAL STABILITY OF REINFORCED EARTH STRUCTURES
STANDARD DETAILS: 1 OF 3
BRIGHAM YOUNG UNIVERSITY
MSE TEST WALL
LATERAL PILE RESISTANCE
RW-05

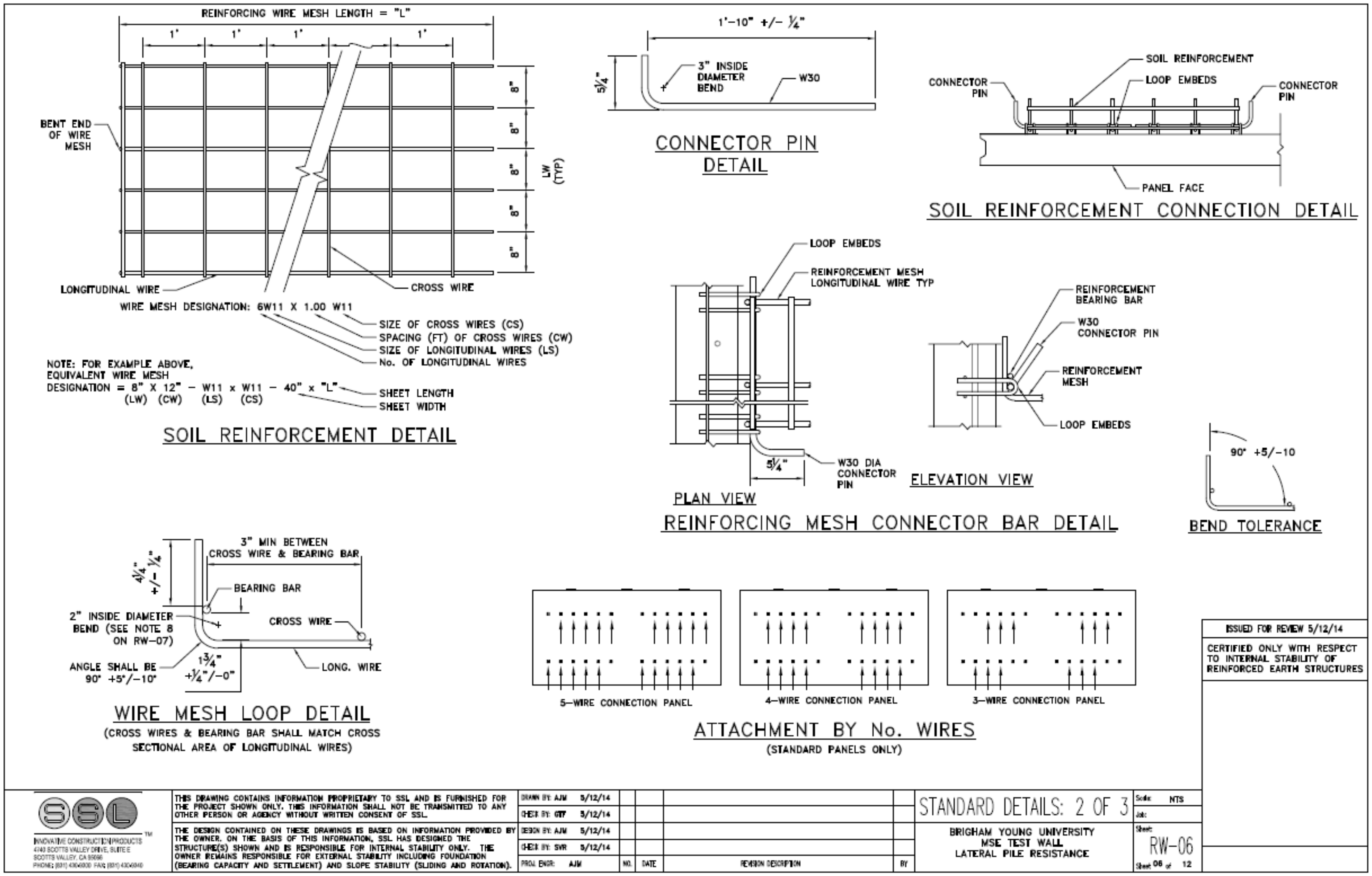
REINFORCING WIRE MESH LENGTH = "L"
BENT END OF WIRE MESH
LONGITUDINAL WIRE
CROSS WIRE
LW (TYP)
WIRE MESH DESIGNATION: 6W11 X 1.00 W11
SIZE OF CROSS WIRES (CS)
SPACING (FT) OF CROSS WIRES (CW)
SIZE OF LONGITUDINAL WIRES (LS)
No. OF LONGITUDINAL WIRES
NOTE: FOR EXAMPLE ABOVE, EQUIVALENT WIRE MESH DESIGNATION = 8" X 12" - W11 x W11 - 40" x "L"
(LW) (CW) (LS) (CS)
SHEET LENGTH
SHEET WIDTH
SOIL REINFORCEMENT DETAIL
1'-10" +/- 1/4"
3" INSIDE DIAMETER BEND
W30
CONNECTOR PIN DETAIL
SOIL REINFORCEMENT
LOOP EMBEDS
CONNECTOR PIN
PANEL FACE
SOIL REINFORCEMENT CONNECTION DETAIL
LOOP EMBEDS
REINFORCEMENT MESH LONGITUDINAL WIRE TYP
W30 DIA CONNECTOR PIN
PLAN VIEW
REINFORCEMENT BEARING BAR
W30 CONNECTOR PIN
REINFORCEMENT MESH
ELEVATION VIEW
REINFORCING MESH CONNECTOR BAR DETAIL
90° +5/-10
BEND TOLERANCE
3" MIN BETWEEN CROSS WIRE & BEARING BAR
BEARING BAR
CROSS WIRE
2" INSIDE DIAMETER BEND (SEE NOTE 8 ON RW-07)
ANGLE SHALL BE 90° +5°/-10°
LONG. WIRE
WIRE MESH LOOP DETAIL
(CROSS WIRES & BEARING BAR SHALL MATCH CROSS SECTIONAL AREA OF LONGITUDINAL WIRES)
5-WIRE CONNECTION PANEL
4-WIRE CONNECTION PANEL
3-WIRE CONNECTION PANEL
ATTACHMENT BY No. WIRES
(STANDARD PANELS ONLY)
ISSUED FOR REVIEW 5/12/14
CERTIFIED ONLY WITH RESPECT TO INTERNAL STABILITY OF REINFORCED EARTH STRUCTURES
THIS DRAWING CONTAINS INFORMATION PROPRIETARY TO SSL AND IS FURNISHED FOR THE PROJECT SHOWN ONLY. THIS INFORMATION SHALL NOT BE TRANSMITTED TO ANY OTHER PERSON OR AGENCY WITHOUT WRITTEN CONSENT OF SSL.
THE DESIGN CONTAINED ON THESE DRAWINGS IS BASED ON INFORMATION PROVIDED BY THE OWNER. ON THE BASIS OF THIS INFORMATION, SSL HAS DESIGNED THE STRUCTURE(S) SHOWN AND IS RESPONSIBLE FOR INTERNAL STABILITY ONLY. THE OWNER REMAINS RESPONSIBLE FOR EXTERNAL STABILITY INCLUDING FOUNDATION (BEARING CAPACITY AND SETTLEMENT) AND SLOPE STABILITY (SLIDING AND ROTATION).
STANDARD DETAILS: 2 OF 3
BRIGHAM YOUNG UNIVERSITY
MSE TEST WALL
LATERAL PILE RESISTANCE
RW-06
Scale: NTS
Sheet 06 of 12
REVISION DESCRIPTION

MATERIAL PROPERTIES NOTES:

1. PANEL REINFORCEMENT BARS SHALL BE DEFORMED BILLET STEEL BARS FOR CONCRETE REINFORCEMENT CONFORMING TO THE SPECIFICATION OF ASTM DESIGNATION A615, GRADE 60, INCLUDING SUPPLEMENTARY REQUIREMENT S1 OR LOW ALLOY STEEL DEFORMED BARS CONFORMING TO THE SPECIFICATIONS OF ASTM DESIGNATION A706. STRUCTURAL WELDED WIRE REINFORCEMENT THAT CONFORMS TO ASTM A496 AND A497 SPECIFICATIONS MAY BE SUBSTITUTED FOR ASTM DESIGNATION A615.
2. W4.5, W11, W15, W20, W24 & W30 STEEL WIRE SHALL CONFORM TO THE ASTM DESIGNATION A82. THE WELDED WIRE SOIL REINFORCEMENT AND LOOP EMBED SHALL BE WELDED IN ACCORDANCE WITH ASTM DESIGNATION A185. ALL SOIL REINFORCEMENT MESH SHALL BE COMPOSED OF SMOOTH WIRE. DEFORMED WIRE SHALL NOT BE USED FOR SOIL REINFORCEMENT, LOOP EMBEDS AND CONNECTION PIN.
3. THE LOOP EMBEDS, SOIL REINFORCEMENT AND CONNECTION PINS SHALL BE GALVANIZED IN ACCORDANCE WITH ASTM DESIGNATION A123 AFTER BENDING.
4. CONCRETE PANELS TO HAVE A 28-DAY COMPRESSIVE STRENGTH OF 4000 PSI.
5. ALL PANEL REINFORCEMENT MUST HAVE A MINIMUM OF 1 1/4" COVERAGE WITH CONCRETE ON ALL SIDES.
6. FOR PANELS WITH W11 MESH USE "A" PANEL REINFORCEMENT. PANELS WITH W20 MESH USE "X" PANEL REINFORCEMENT. PANELS WITH W24 MESH USE "Y" OR "Z" PANEL REINFORCEMENT.
7. FILTER FABRIC IS A NON-WOVEN GEOTEXTILE COMPOSED OF POLYPROPYLENE FIBERS, WHICH ARE FORMED INTO A STABLE NETWORK SUCH THAT THE FIBERS RETAIN THEIR RELATIVE POSITION. FILTER FABRIC IS INERT TO BIOLOGICAL DEGRADATION AND RESISTS NATURALLY ENCOUNTERED CHEMICALS, ALKALIS AND ACIDS.
8. THE MINIMUM INSIDE BEND DIAMETER SHALL BE NO LESS THAN TWICE THE NOMINAL DIAMETER OF THE WIRE SIZE AND IN NO INSTANCE BE LESS THAN 1 INCH.
9. CROSS WIRES, BEARING BARS WIRE AND LONGITUDINAL WIRES ON SOIL REINFORCEMENT SHALL BE THE SAME SIZE.
10. UNIVERSAL MESH SHALL BE SUPPLIED FOR THE USE OF REPLACING ANY STYLE OF MESH FOR THE PROJECT. THE UNIVERSAL MESH SHALL HAVE THE GREATEST NUMBER OF LONGITUDINAL WIRES, THE LARGEST CROSS SECTIONAL AREA OF LONGITUDINAL WIRES, THE SMALLEST CROSS BAR SPACING, THE GREATEST CROSS SECTIONAL AREA OF CROSS BARS, AND THE LONGEST LENGTH OF ANY STYLE OF SOIL REINFORCEMENT ON THE PROJECT. THE CONTRACTOR IS RESPONSIBLE FOR NOTING WHERE THE UNIVERSAL SOIL REINFORCING IS PLACED DURING CONSTRUCTION.

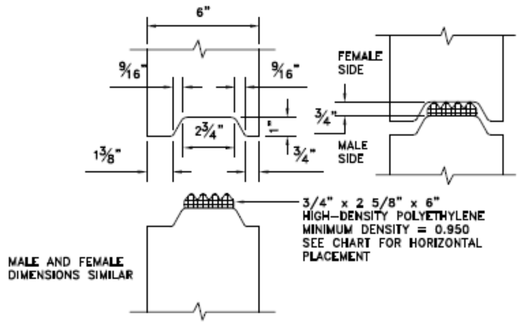

HORIZONTAL PANEL JOINT DETAIL

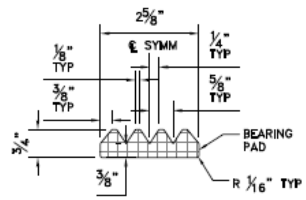

BEARING PAD DETAIL

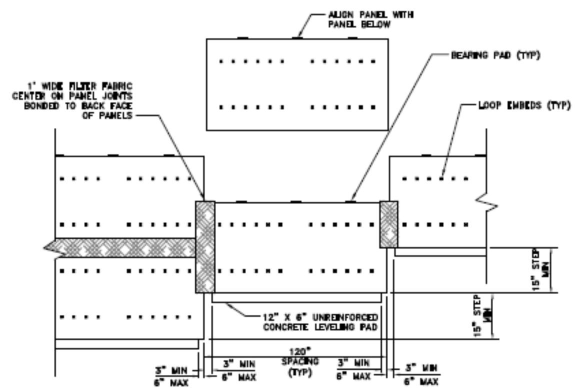

FILTER FABRIC DETAIL AND PANEL PLACEMENT

BACK FACE VIEW

ISSUED FOR REVIEW 5/12/14

CERTIFIED ONLY WITH RESPECT TO INTERNAL STABILITY OF REINFORCED EARTH STRUCTURES

SSL™ INNOVATIVE CONSTRUCTION PRODUCTS
4740 SCOTTS VALLEY DRIVE, SUITE E
SCOTTS VALLEY, CA 95066
PHONE: (831) 430-6000 FAX: (831) 430-6040

THIS DRAWING CONTAINS INFORMATION PROPRIETARY TO SSL AND IS FURNISHED FOR THE PROJECT SHOWN ONLY. THIS INFORMATION SHALL NOT BE TRANSMITTED TO ANY OTHER PERSON OR AGENCY WITHOUT WRITTEN CONSENT OF SSL.

THE DESIGN CONTAINED ON THESE DRAWINGS IS BASED ON INFORMATION PROVIDED BY THE OWNER. ON THE BASIS OF THIS INFORMATION, SSL HAS DESIGNED THE STRUCTURE(S) SHOWN AND IS RESPONSIBLE FOR INTERNAL STABILITY ONLY. THE OWNER REMAINS RESPONSIBLE FOR EXTERNAL STABILITY INCLUDING FOUNDATION (BEARING CAPACITY AND SETTLEMENT) AND SLOPE STABILITY (SLIDING AND ROTATION).

DRAWN BY: AJM	5/12/14	
CHECK BY: GTF	5/12/14	
DESIGN BY: AJM	5/12/14	
CHECK BY: SVR	5/12/14	
PROJ. ENGR: AJM		

NO.	DATE	REVISION DESCRIPTION	BY

STANDARD DETAILS: 3 OF 3

BRIGHAM YOUNG UNIVERSITY
MSE TEST WALL
LATERAL PILE RESISTANCE

Scale: NTS
Job:
Sheet: RW-07
Sheet 07 of 12

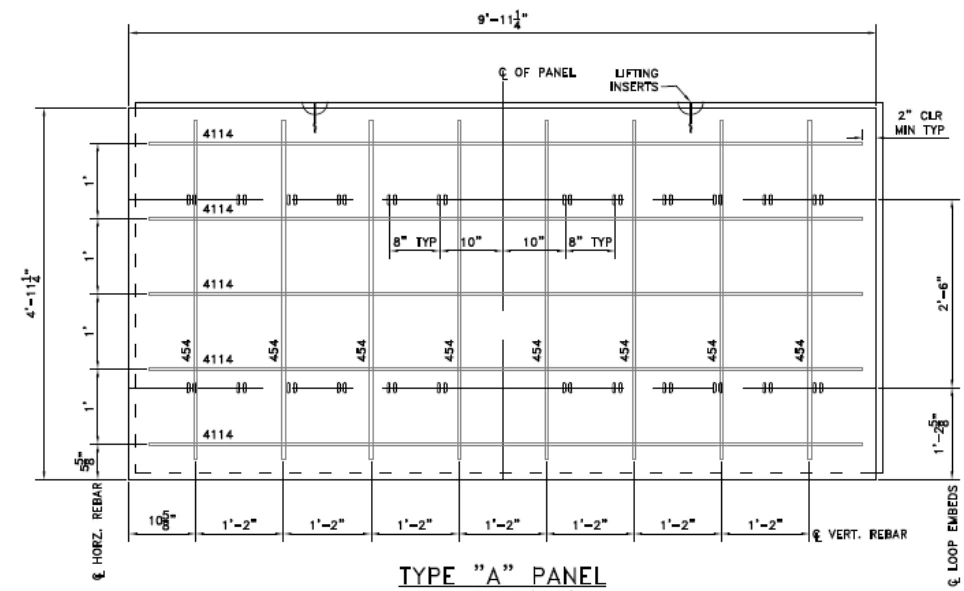

TYPE "A" PANEL

SHOWN FROM BACK FACE

Qt.	ITEM	DESCRIPTION
8	VERTICAL BAR	#4 BAR – GRADE 60
5	HORIZONTAL BAR	#4 BAR – GRADE 60
2	LIFTING INSERTS	2 TON BURKE
4	LOOP EMBEDS	6 CONNECTION EMBED

ISSUED FOR REVIEW 5/12/14

CERTIFIED ONLY WITH RESPECT TO INTERNAL STABILITY OF REINFORCED EARTH STRUCTURES

SSL™
INNOVATIVE CONSTRUCTION PRODUCTS
4740 SCOTTS VALLEY DRIVE, SUITE E
SCOTTS VALLEY, CA 95066
PHONE: (831) 430-9300 FAX: (831) 430-9340

THIS DRAWING CONTAINS INFORMATION PROPRIETARY TO SSL AND IS FURNISHED FOR THE PROJECT SHOWN ONLY. THIS INFORMATION SHALL NOT BE TRANSMITTED TO ANY OTHER PERSON OR AGENCY WITHOUT WRITTEN CONSENT OF SSL.

THE DESIGN CONTAINED ON THESE DRAWINGS IS BASED ON INFORMATION PROVIDED BY THE OWNER. ON THE BASIS OF THIS INFORMATION, SSL HAS DESIGNED THE STRUCTURE(S) SHOWN AND IS RESPONSIBLE FOR INTERNAL STABILITY ONLY. THE OWNER REMAINS RESPONSIBLE FOR EXTERNAL STABILITY INCLUDING FOUNDATION (BEARING CAPACITY AND SETTLEMENT) AND SLOPE STABILITY (SLIDING AND ROTATION).

DRAWN BY: AJM	5/12/14				
CHECK BY: GTP	5/12/14				
DESIGN BY: AJM	5/12/14				
CHECK BY: SVR	5/12/14				
PROJ. ENGR: AJM		NO.	DATE	REVISION DESCRIPTION	BY

PANEL REBAR DETAILS: 1 OF 5

BRIGHAM YOUNG UNIVERSITY
MSE TEST WALL
LATERAL PILE RESISTANCE

Scale: NTS
Job:
Sheet: RW-08
Sheet 08 of 12

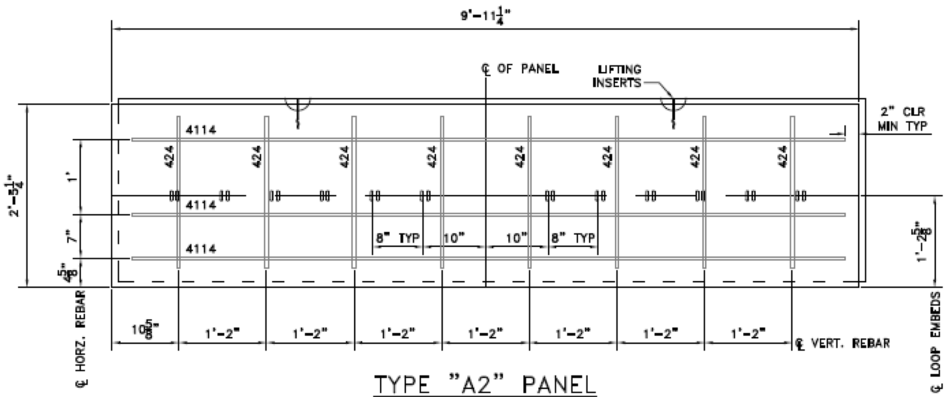

TYPE "A2" PANEL

SHOWN FROM BACK FACE

Qt.	ITEM	DESCRIPTION
8	VERTICAL BAR	#4 BAR – 24" LONG
3	HORIZONTAL BAR	#4 BAR – 114" LONG
2	LIFTING INSERTS	2 TON BURKE
2	LOOP EMBEDS	6 CONNECTION EMBED

ISSUED FOR REVIEW 5/12/14

CERTIFIED ONLY WITH RESPECT TO INTERNAL STABILITY OF REINFORCED EARTH STRUCTURES

SSL™
INNOVATIVE CONSTRUCTION PRODUCTS
4740 SCOTTS VALLEY DRIVE, SUITE E
SCOTTS VALLEY, CA 95066
PHONE: (831) 430-9300 FAX: (831) 430-9340

THE DESIGN CONTAINED ON THESE DRAWINGS IS BASED ON INFORMATION PROVIDED BY THE OWNER. ON THE BASIS OF THIS INFORMATION, SSL HAS DESIGNED THE STRUCTURE(S) SHOWN AND IS RESPONSIBLE FOR INTERNAL STABILITY ONLY. THE OWNER REMAINS RESPONSIBLE FOR EXTERNAL STABILITY INCLUDING FOUNDATION (BEARING CAPACITY AND SETTLEMENT) AND SLOPE STABILITY (SLIDING AND ROTATION).

DRAWN BY: AJM 5/12/14
CHECK BY: GTP 5/12/14
DESIGN BY: AJM 5/12/14
CHECK BY: SVR 5/12/14
PROJ. ENGR: AJM

NO.	DATE	REVISION DESCRIPTION	BY

PANEL REBAR DETAILS: 2 OF 5

BRIGHAM YOUNG UNIVERSITY
MSE TEST WALL
LATERAL PILE RESISTANCE

Scale: NTS
Job:
Sheet: RW-09
Sheet 09 of 12

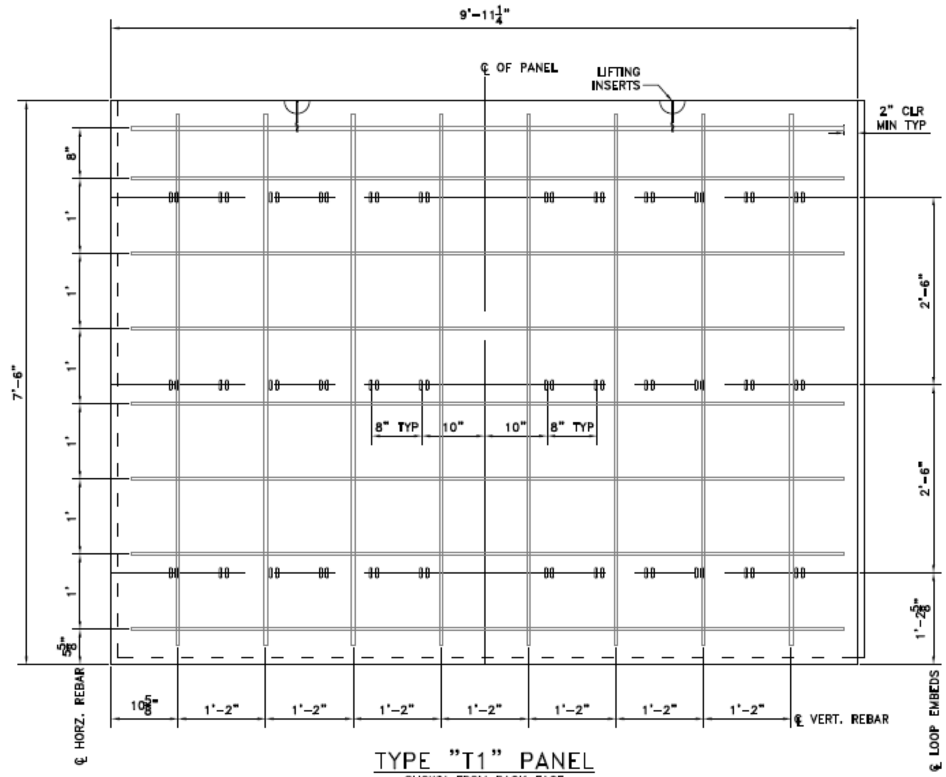

TYPE "T1" PANEL
SHOWN FROM BACK FACE

Qt.	ITEM	DESCRIPTION
8	VERTICAL BAR	#4 BAR – GRADE 60
8	HORIZONTAL BAR	#4 BAR – GRADE 60
2	LIFTING INSERTS	2 TON BURKE
6	LOOP EMBEDS	6 CONNECTION EMBED

ISSUED FOR REVIEW 5/12/14

CERTIFIED ONLY WITH RESPECT TO INTERNAL STABILITY OF REINFORCED EARTH STRUCTURES

SSL™
INNOVATIVE CONSTRUCTION PRODUCTS
4740 SCOTTS VALLEY DRIVE, SUITE E
SCOTTS VALLEY, CA 95066
PHONE: (831) 430-6000 FAX: (831) 430-6040

THIS DRAWING CONTAINS INFORMATION PROPRIETARY TO SSL AND IS FURNISHED FOR THE PROJECT SHOWN ONLY. THIS INFORMATION SHALL NOT BE TRANSMITTED TO ANY OTHER PERSON OR AGENCY WITHOUT WRITTEN CONSENT OF SSL.

THE DESIGN CONTAINED ON THESE DRAWINGS IS BASED ON INFORMATION PROVIDED BY THE OWNER. ON THE BASIS OF THIS INFORMATION, SSL HAS DESIGNED THE STRUCTURE(S) SHOWN AND IS RESPONSIBLE FOR INTERNAL STABILITY ONLY. THE OWNER REMAINS RESPONSIBLE FOR EXTERNAL STABILITY INCLUDING FOUNDATION (BEARING CAPACITY AND SETTLEMENT) AND SLOPE STABILITY (SLIDING AND ROTATION).

DRAWN BY: AJM 5/12/14
CHECK BY: GTP 5/12/14
DESIGN BY: AJM 5/12/14
CHECK BY: SVR 5/12/14
PROJ. ENGR: AJM

NO. | DATE | REVISION DESCRIPTION | BY

PANEL REBAR DETAILS: 3 OF 5

BRIGHAM YOUNG UNIVERSITY
MSE TEST WALL
LATERAL PILE RESISTANCE

Scale: NTS
Job:
Sheet: RW-10
Sheet 10 of 12

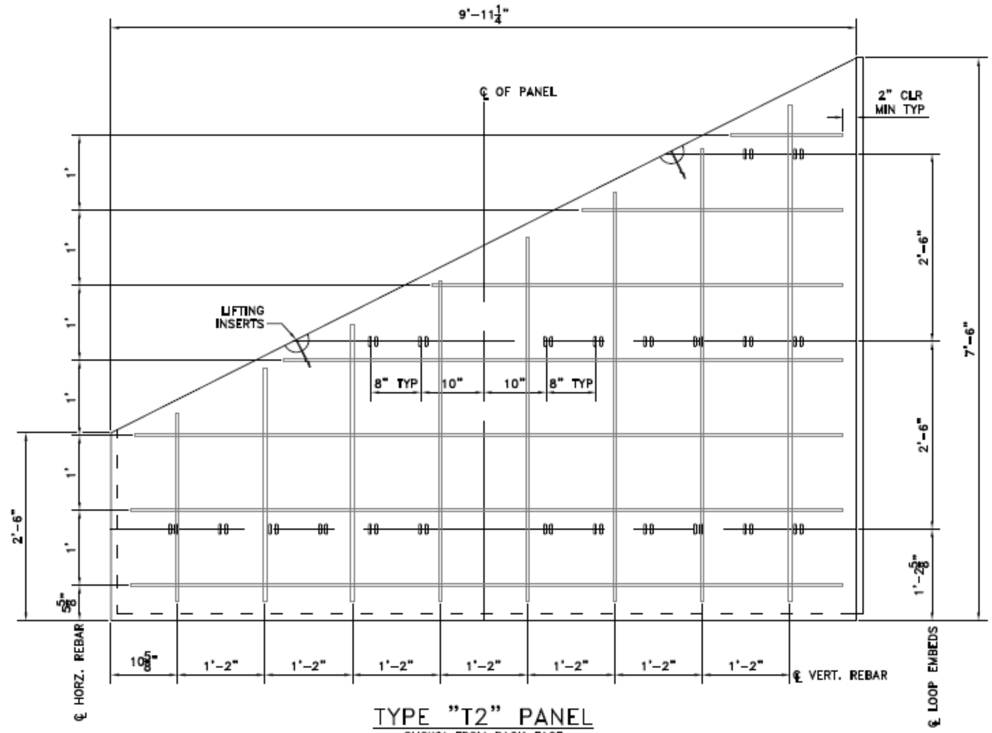

TYPE "T2" PANEL

SHOWN FROM BACK FACE

Qt.	ITEM	DESCRIPTION
8	VERTICAL BAR	#4 BAR – GRADE 60
7	HORIZONTAL BAR	#4 BAR – GRADE 60
2	LIFTING INSERTS	2 TON BURKE
5	LOOP EMBEDS	CONNECTION VARIES

ISSUED FOR REVIEW 5/12/14

CERTIFIED ONLY WITH RESPECT TO INTERNAL STABILITY OF REINFORCED EARTH STRUCTURES

SSL

INNOVATIVE CONSTRUCTION PRODUCTS
4740 SCOTTS VALLEY DRIVE, SUITE E
SCOTTS VALLEY, CA 95066
PHONE: (831) 430-6000 FAX: (831) 430-6040

THIS DRAWING CONTAINS INFORMATION PROPRIETARY TO SSL AND IS FURNISHED FOR THE PROJECT SHOWN ONLY. THIS INFORMATION SHALL NOT BE TRANSMITTED TO ANY OTHER PERSON OR AGENCY WITHOUT WRITTEN CONSENT OF SSL.

THE DESIGN CONTAINED ON THESE DRAWINGS IS BASED ON INFORMATION PROVIDED BY THE OWNER. ON THE BASIS OF THIS INFORMATION, SSL HAS DESIGNED THE STRUCTURE(S) SHOWN AND IS RESPONSIBLE FOR INTERNAL STABILITY ONLY. THE OWNER REMAINS RESPONSIBLE FOR EXTERNAL STABILITY INCLUDING FOUNDATION (BEARING CAPACITY AND SETTLEMENT) AND SLOPE STABILITY (SLIDING AND ROTATION).

DRAWN BY: AJM	5/12/14				
CHECK BY: GTF	5/12/14				
DESIGN BY: AJM	5/12/14				
CHECK BY: SVR	5/12/14				
PROJ. ENGR:	AJM	NO.	DATE	REVISION DESCRIPTION	BY

PANEL REBAR DETAILS: 4 OF 5

BRIGHAM YOUNG UNIVERSITY
MSE TEST WALL
LATERAL PILE RESISTANCE

Scale: NTS
Job:
Sheet: RW-11
Sheet 11 of 12

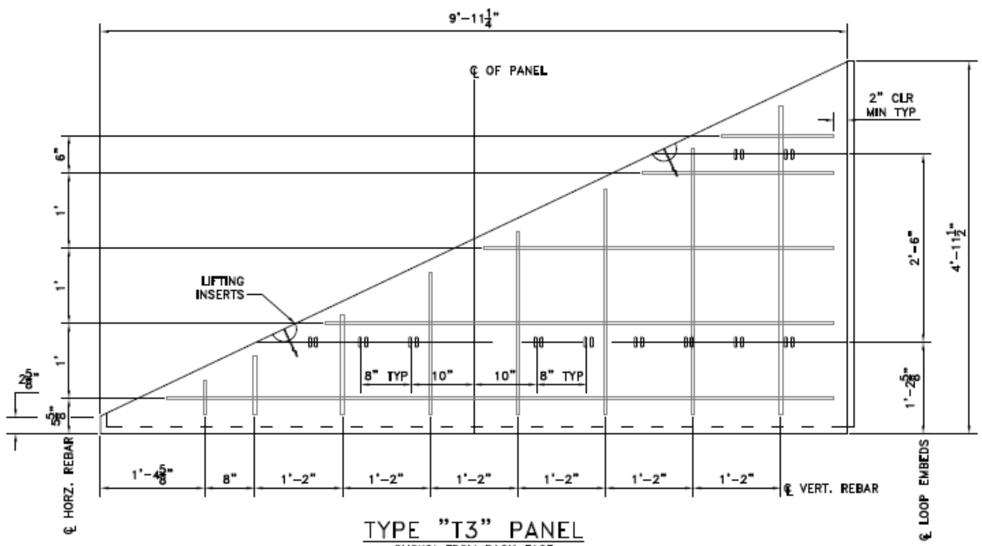

TYPE "T3" PANEL
SHOWN FROM BACK FACE

Qt.	ITEM	DESCRIPTION
8	VERTICAL BAR	#4 BAR – GRADE 60
5	HORIZONTAL BAR	#4 BAR – GRADE 60
2	LIFTING INSERTS	2 TON BURKE
3	LOOP EMBEDS	CONNECTION VARIES

ISSUED FOR REVIEW 5/12/14

CERTIFIED ONLY WITH RESPECT TO INTERNAL STABILITY OF REINFORCED EARTH STRUCTURES

SSL™
INNOVATIVE CONSTRUCTION PRODUCTS
4740 SCOTTS VALLEY DRIVE, SUITE E
SCOTTS VALLEY, CA 95066
PHONE: (831) 430-9300 FAX: (831) 430-9340

THIS DRAWING CONTAINS INFORMATION PROPRIETARY TO SSL AND IS FURNISHED FOR THE PROJECT SHOWN ONLY. THIS INFORMATION SHALL NOT BE TRANSMITTED TO ANY OTHER PERSON OR AGENCY WITHOUT WRITTEN CONSENT OF SSL.

THE DESIGN CONTAINED ON THESE DRAWINGS IS BASED ON INFORMATION PROVIDED BY THE OWNER. ON THE BASIS OF THIS INFORMATION, SSL HAS DESIGNED THE STRUCTURE(S) SHOWN AND IS RESPONSIBLE FOR INTERNAL STABILITY ONLY. THE OWNER REMAINS RESPONSIBLE FOR EXTERNAL STABILITY INCLUDING FOUNDATION (BEARING CAPACITY AND SETTLEMENT) AND SLOPE STABILITY (SLIDING AND ROTATION).

DRAWN BY: AJM	5/12/14				
CHECK BY: GTP	5/12/14				
DESIGN BY: AJM	5/12/14				
CHECK BY: SVR	5/12/14				
PROJ. ENGR: AJM		NO.	DATE	REVISION DESCRIPTION	BY

PANEL REBAR DETAILS: 5 OF 5

BRIGHAM YOUNG UNIVERSITY
MSE TEST WALL
LATERAL PILE RESISTANCE

Scale: NTS
Job:
Sheet: RW-12
Sheet 12 of 12

APPENDIX C – LABORATORY RESULTS FOR BACKFILL PROPERTIES

GENEVA ROCK

GENEVA ROCK PRODUCTS, INC. PHASE I

1565 West 400 North • P.O. Box 538 • Orem, UT 84059 • (801) 765-7800 • Fax (801) 765-7830 • www.genevarock.com

AGGREGATE SUBMITTAL

Report of Physical Properties

GRP Material Description: Fill - 3/8" HARDPAC **Report Date:** April 15, 2014

GRP Material Code: FINE **Reviewed by:** Victor Johnson

Source Location/Code: North Hansen / 527 **Report No.** 527FINE00114

TEST RESULTS

Standard	PHYSICAL PROPERTIES		Result	Test Source
ASTM C 29	Unit	Unit Weight, lbs./cu.ft. =	112.0	
AASHTO T19	Weight	Voids, % =	30	
		☐ Jigged ☐ Loose ☑ Rodded		
ASTM D1557	Modified	Max. density, lbs./cu.ft. =	133.0	
AASHTO T180	Proctor	Optimum Moisture, % =	7	
ASTM D698	Standard	Max. density, lbs./cu.ft. =	128.0	
AASHTO T99	Proctor	Optimum Moisture, % =	7.8	
ASTM D4318	Liquid Limit	Liquid Limit=	0	
AASHTO T89/90	Plastic Limit	Plastic Limit=	0	
	Plasticity Index	Plasticity Index=	NP	
ASTM C131	L.A.	Small Coarse Loss, % =		
AASHTO T96	Abrasion	Grading/Revolutions, =		
ASTM C535	L.A.	Large Coarse Loss, % =		
	Abrasion	Grading/Revolutions, =		
	Fine	Bulk Specific Gravity (dry) =	2.581	
ASTM C 128	Specific	Bulk Specific Gravity, SSD =	2.599	
AASHTO T84	Gravity &	Apparent Specific Gravity =	2.628	
	Absorption	Absorption, % =	0.7	
	Coarse	Bulk Specific Gravity (dry) =		
ASTM C 127	Specific	Bulk Specific Gravity, SSD =		
AASHTO T85	Gravity &	Apparent Specific Gravity =		
	Absorption	Absorption, % =		
ASTM D2419	Sand	Sand Equivalent, % =	34	
AASHTO T176	Equivalent			
	Soundness	Coarse Soundness Loss, % =		
ASTM C 88		Magnesium No. of Cycles =		
AASHTO T104	Soundness	Fine Soundness Loss, % =	1.0	
		Sodium Sulfate No. of Cycles =		
ASTM C 1252	Fine Aggregate	Uncompacted Voids, % =	48.3	
AASHTO T304	Angularity	Method C (as received material)		
ASTM C40	Organic	Coarse Aggregate, % =	Lighter Plate # 1	
AASHTO T21	Impurities	Fine Aggregate, % =		
ASTM C142	Clay / Friable	Coarse Aggregate, % =		
AASHTO T112	Particles	Fine Aggregate, % =	0.0	
ASTM C123	Lightweight	Coarse Aggregate, % =		
AASHTO T113	Pieces	Fine Aggregate, % =		
ASTM D1883	CBR	Surcharge = 10 lbs CBR @ 0.1"=	50	
AASHTO T193		Swell% = 0.0% CBR @ 0.2"=	99	
ASTM D5821	Fractured Face	1 or 2 Faces =		
		Fractured Face, % =		
ASTM D2487	Soil Classification	Group Symbol =	GW-GM	
		Group Name =	Well-graded gravel with silt and sand	
ASTM D2488	Soil Description & Identification	Group Symbol =	Cu=66.7 Cc=1.8	
		Group Name =		

SIEVE ANALYSIS

ASTM C136 AASHTO T27

Sieve Size	% Passing	Spec.
450 mm (18")		
375 mm (15")		
300 mm (12")		
250 mm (10")		
225 mm (9")		
200 mm (8")		
150 mm (6")		
125 mm (5")		
100 mm (4")		
75.0 mm (3")		
63.0 mm (2-1/2")		
50.0 mm (2")		
37.5 mm (1-1/2")		
25.0 mm (1")		
19.0 mm (3/4")		
12.5 mm (1/2")	100	
9.5 mm (3/8")	100	
6.3 mm (1/4")		
4.75 mm (No.4)	77	
2.36 mm (No.8)	52	
2.00 mm (No.10)		
1.18 mm (No.16)	37	
0.600 mm (No.30)	30	
0.425 mm (No.40)		
0.300 mm (No.50)	25	
0.180 mm (No.80)		
0.150 mm (No.100)	20	
0.075 mm (No.200)	14	
ASTM D422 Hydrometer =		
ASTM C566 AASHTO T255 Moisture Content, % =		
ASTM C136 AASHTO T27 Fineness Modulus (FM) =		
AASHTO M145 Classification of Soils =	A1B	
ASTM D4791 Ratio = Flat & Elongated =		

GENEVA ROCK PRODUCTS, INC.
1565 West 400 North • P.O. Box 538 • Orem, UT 84059 • (801) 765-7800 • Fax (801) 765-7830 • www.genevarock.com

AGGREGATE SUBMITTAL

Report of Physical Properties

GRP Material Description: Fill - 3/8" HARDPAC
Report Date: July 17, 2014
GRP Material Code: FINE
Reviewed by: Victor Johnson
Source Location/Code: North Hansen / 527
Report No. 527FINE00114

TEST RESULTS

Standard	PHYSICAL PROPERTIES		Result	Test Source
ASTM C 29	Unit	Unit Weight, lbs./cu.ft. =	112.0	
AASHTO T19	Weight	Voids, % =	30	
		☐ Jigged ☐ Loose ☑ Rodded		
ASTM D1557	Modified	Max. density, lbs./cu.ft. =	131.7	
AASHTO T180	Proctor	Optimum Moisture, % =	8.7	
ASTM D698	Standard	Max. density, lbs./cu.ft. =		
AASHTO T99	Proctor	Optimum Moisture, % =		
ASTM D4318	Liquid Limit	Liquid Limit=	0	
AASHTO T89/90	Plastic Limit	Plastic Limit=	0	
	Plasticity Index	Plasticity Index=	NP	
ASTM C131	L.A.	Small Coarse Loss, % =		
AASHTO T96	Abrasion	Grading/Revolutions, =		
ASTM C535	L.A.	Large Coarse Loss, % =		
	Abrasion	Grading/Revolutions, =		
	Fine	Bulk Specific Gravity (dry) =	2.581	
ASTM C 128	Specific	Bulk Specific Gravity, SSD =	2.599	
AASHTO T84	Gravity &	Apparent Specific Gravity =	2.628	
	Absorption	Absorption, % =	0.7	
	Coarse	Bulk Specific Gravity (dry) =		
ASTM C 127	Specific	Bulk Specific Gravity, SSD =		
AASHTO T85	Gravity &	Apparent Specific Gravity =		
	Absorption	Absorption, % =		
ASTM D2419	Sand	Sand Equivalent, % =	34	
AASHTO T176	Equivalent			
	Soundness	Coarse Soundness Loss, % =		
ASTM C 88		Magnesium No. of Cycles =		
AASHTO T104	Soundness	Fine Soundness Loss, % =	1.0	
		Sodium Sulfate No. of Cycles =		
ASTM C 1252	Fine Aggregate	Uncompacted Voids, % =	48.3	
AASHTO T304	Angularity	Method C (as received material)		
ASTM C40	Organic	Coarse Aggregate, % =	Lighter Plate # 1	
AASHTO T21	Impurities	Fine Aggregate, % =		
ASTM C142	Clay / Friable	Coarse Aggregate, % =		
AASHTO T112	Particles	Fine Aggregate, % =	0.0	
ASTM C123	Lightweight	Coarse Aggregate, % =		
AASHTO T113	Pieces	Fine Aggregate, % =		
ASTM D1883	CBR	Surcharge = 10 lbs CBR @ 0.1"=	50	
AASHTO T193		Swell% = 0.0% CBR @ 0.2"=	99	
ASTM D5821	Fractured Face	1 or 2 Faces =		
		Fractured Face, % =		
ASTM D2487	Soil Classification	Group Symbol =	GW-GM	
		Group Name =	Well-graded gravel with silt and sand	
ASTM D2488	Soil Description & Identification	Group Symbol =	Cu=66.7 Cc=1.8	
		Group Name =		

SIEVE ANALYSIS

ASTM C136 AASHTO T27

Sieve Size	% Passing	Spec.
450 mm (18")		
375 mm (15")		
300 mm (12")		
250 mm (10")		
225 mm (9")		
200 mm (8")		
150 mm (6")		
125 mm (5")		
100 mm (4")		
75.0 mm (3")		
63.0 mm (2-1/2")		
50.0 mm (2")		
37.5 mm (1-1/2")		
25.0 mm (1")		
19.0 mm (3/4")		
12.5 mm (1/2")	100	
9.5 mm (3/8")	100	
6.3 mm (1/4")		
4.75 mm (No.4)	79	
2.36 mm (No.8)	51	
2.00 mm (No.10)		
1.18 mm (No.16)	33	
0.600 mm (No.30)	25	
0.425 mm (No.40)		
0.300 mm (No.50)	20	
0.180 mm (No.80)		
0.150 mm (No.100)	16	
0.075 mm (No.200)	11.5	
ASTM D422 Hydrometer =		
ASTM C566 AASHTO T255 Moisture Content, % =		
ASTM C136 AASHTO T27 Fineness Modulus (FM) =		
AASHTO M145 Classification of Soils =	A1B	
ASTM D4791 Ratio = Flat & Elongated =		

GRP Materials Aggregate Physical Properties Report Version 02.11.08

APPENDIX D.1 – LOAD-DEFLECTION CURVES FOR PIPES WITH WELDED WIRE

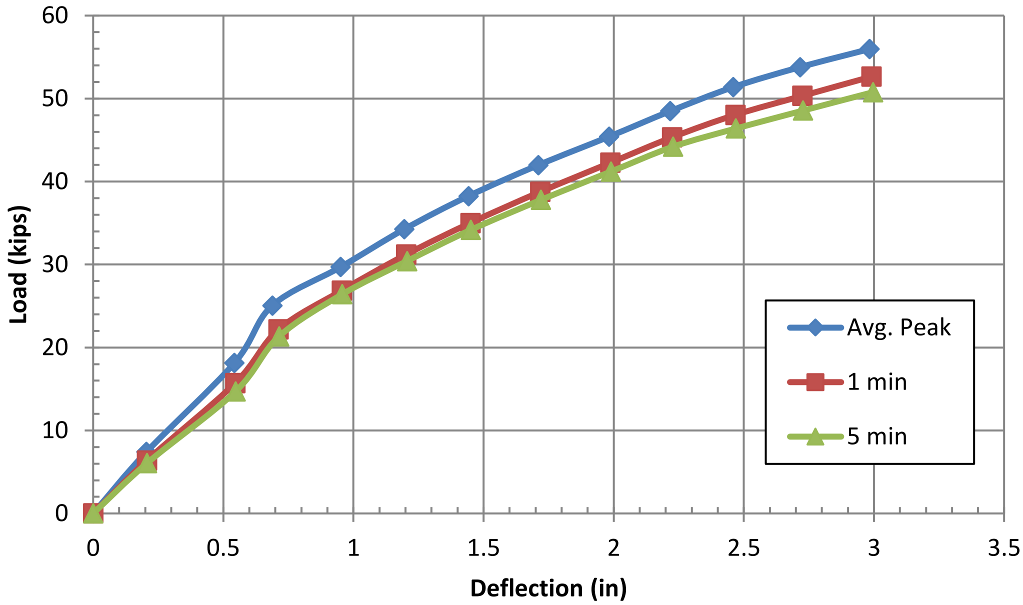

Figure D.1-1: Load-deflection curves for the 5.2D test.

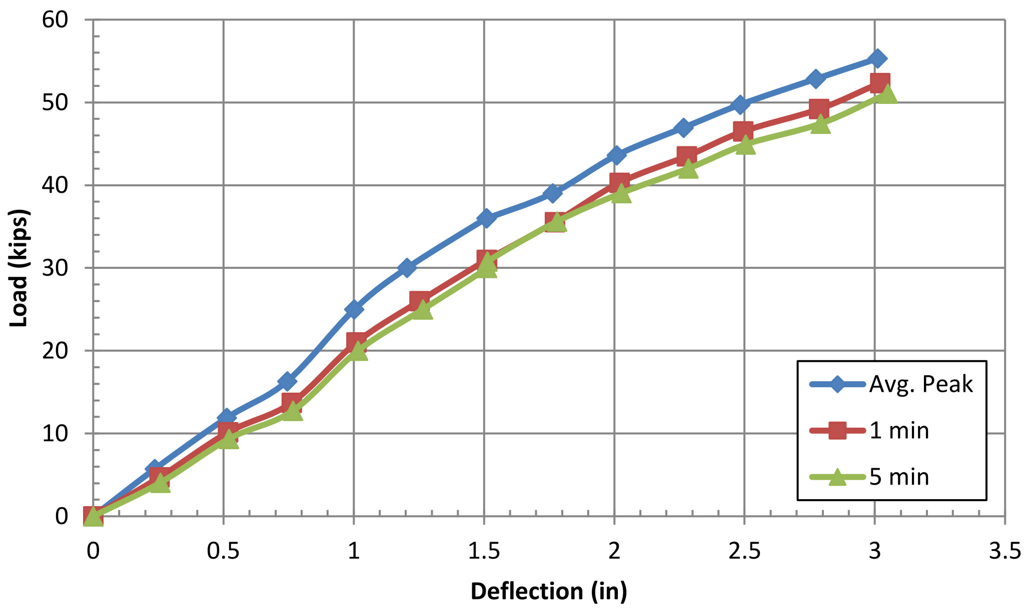

Figure D.1-2: Load-deflection curves for the 4.3D test.

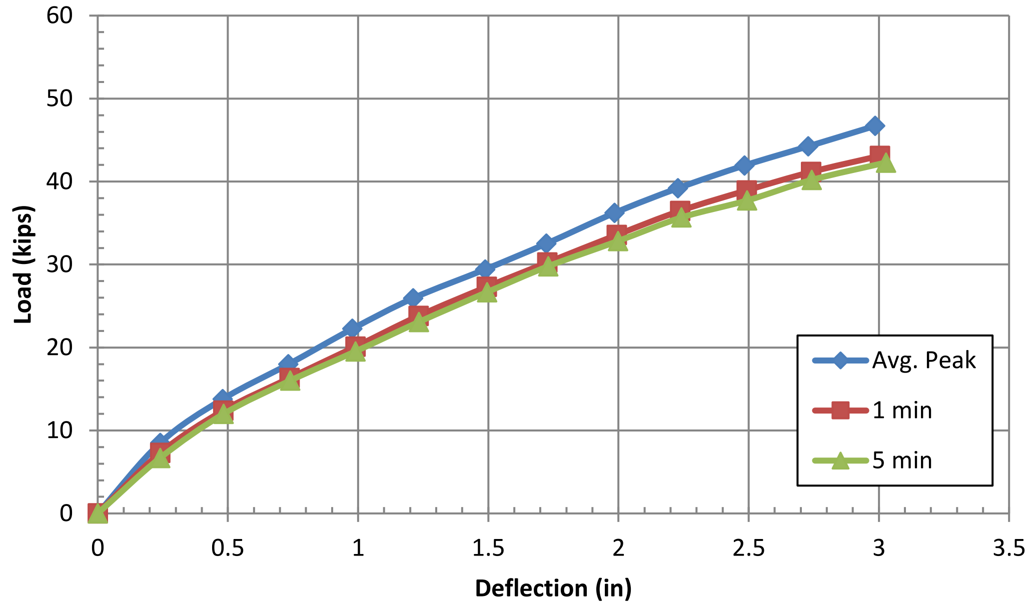

Figure D.1-3: Load-deflection curves for the 3.4D test.

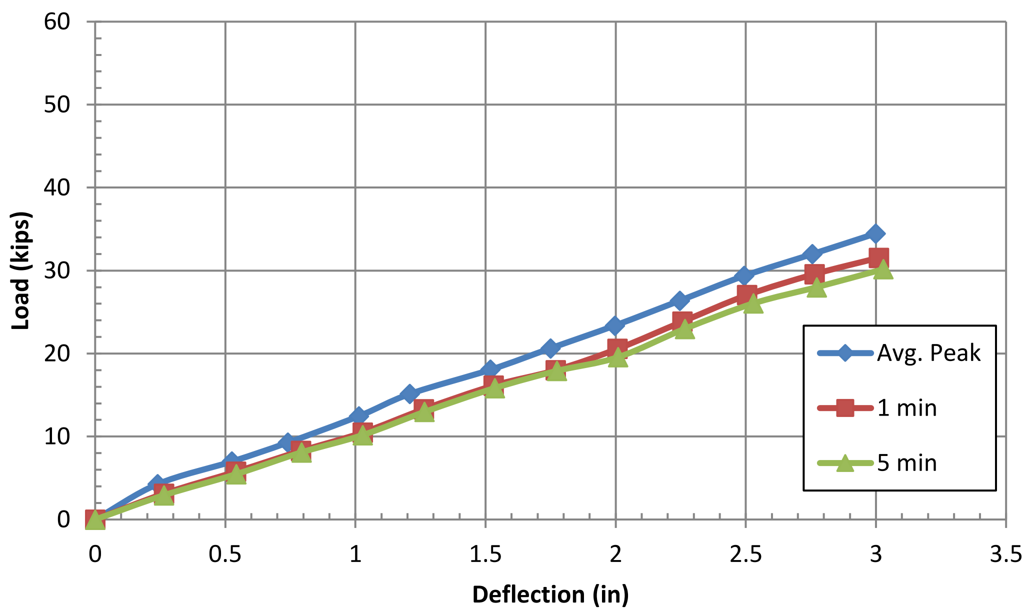

Figure D.1-4: Load-deflection curves for the 1.8D test.

APPENDIX D.2 – LOAD-DEFLECTION CURVES FOR PIPES WITH RIBBED STRIP

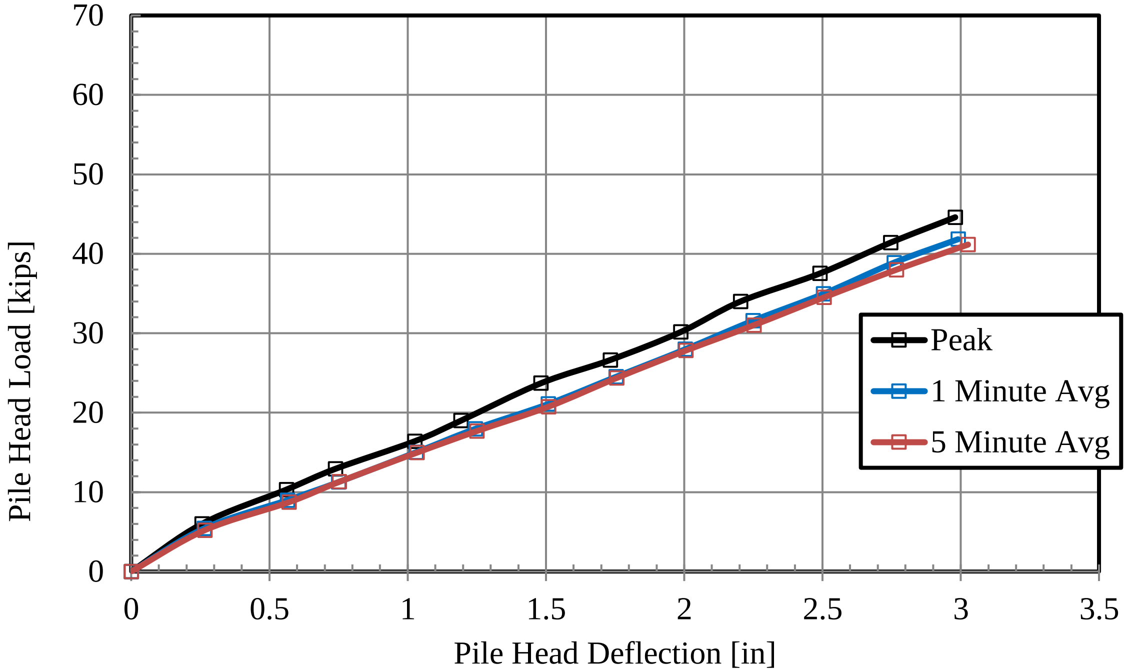

Figure D.2-1. Load-deflection curves for 1.7D test.

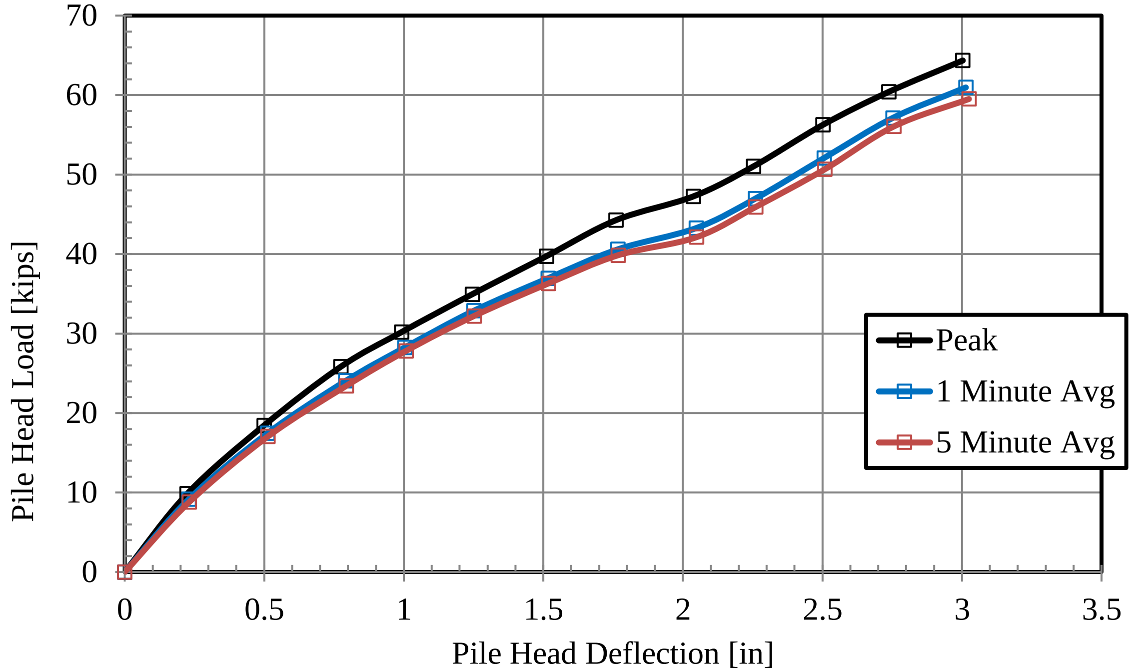

Figure D.2-2. Load-deflection curves for 2.8D test.

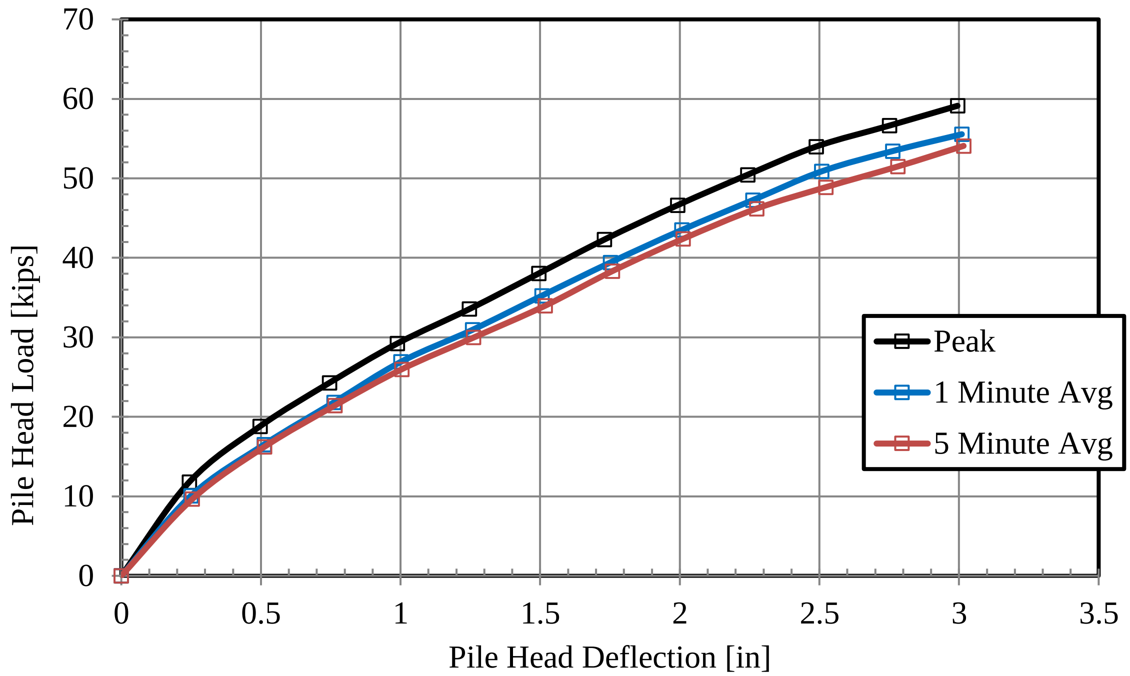

Figure D.2-3. Load-deflection curves for 2.9D test.

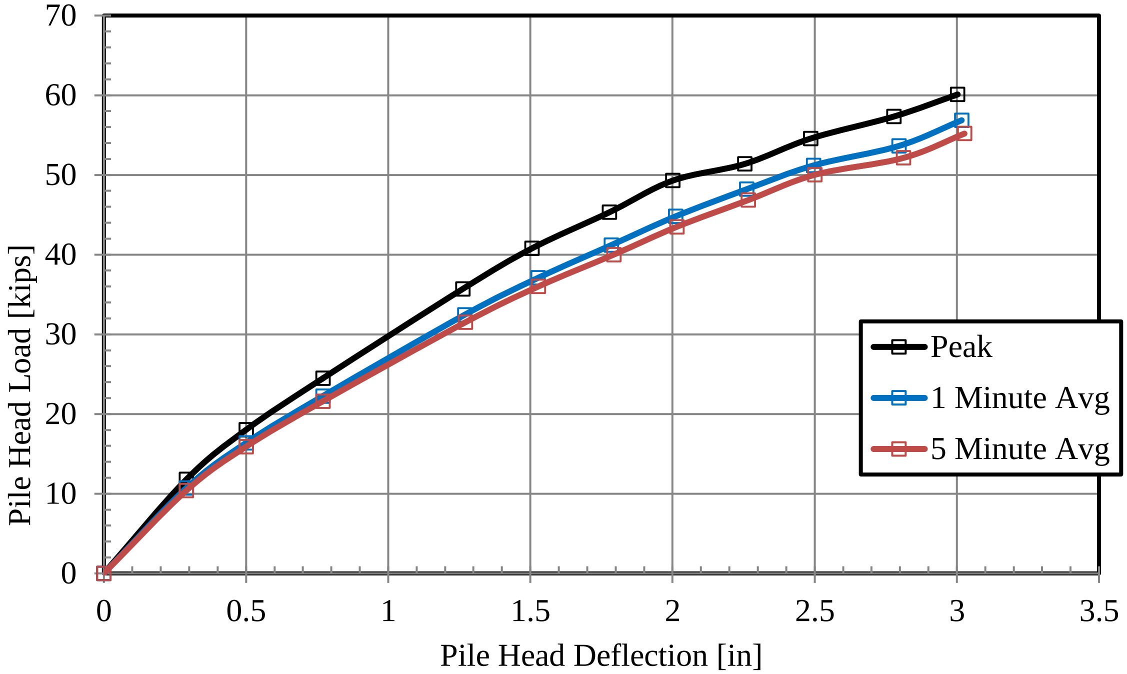

Figure D.2-4. Load-deflection curves for 3.9D test.

APPENDIX E.1 – GROUND DISPLACEMENT CURVES FOR PIPES WITH WELDED WIRE

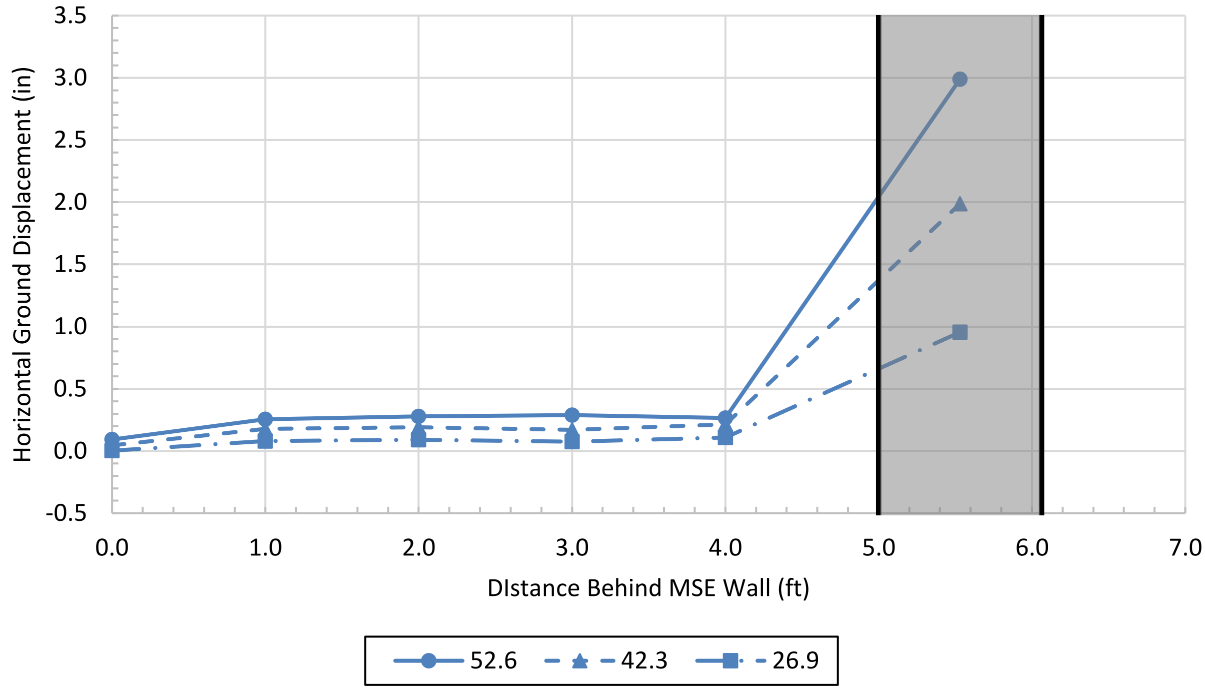

Figure E.1-1: Horizontal ground displacement for the 5.2D test.

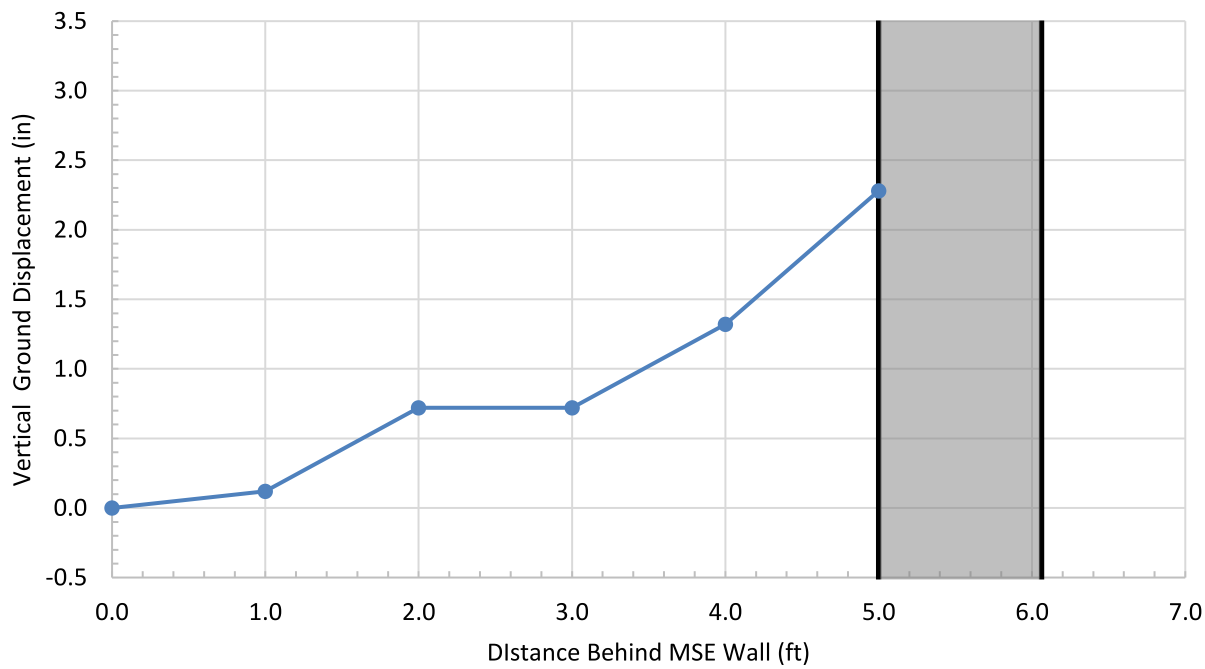

Figure E.1-2: Vertical ground displacement for the 5.2D test.

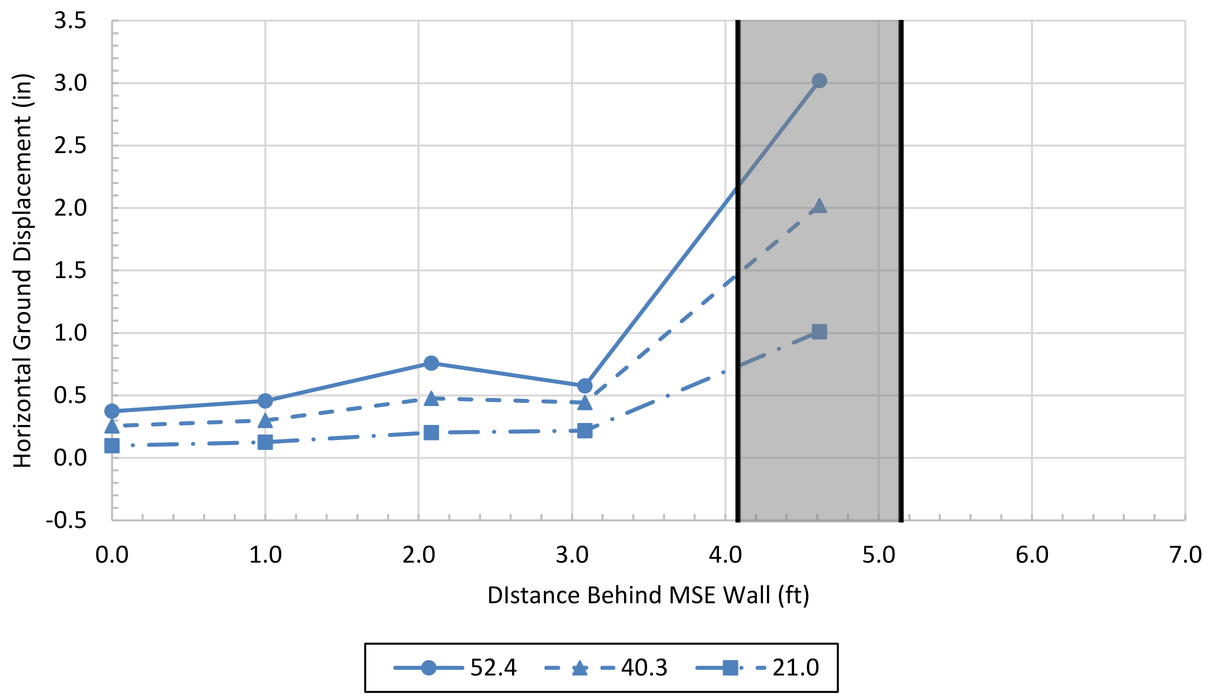

Figure E.1-3: Horizontal ground displacement for the 4.3D test.

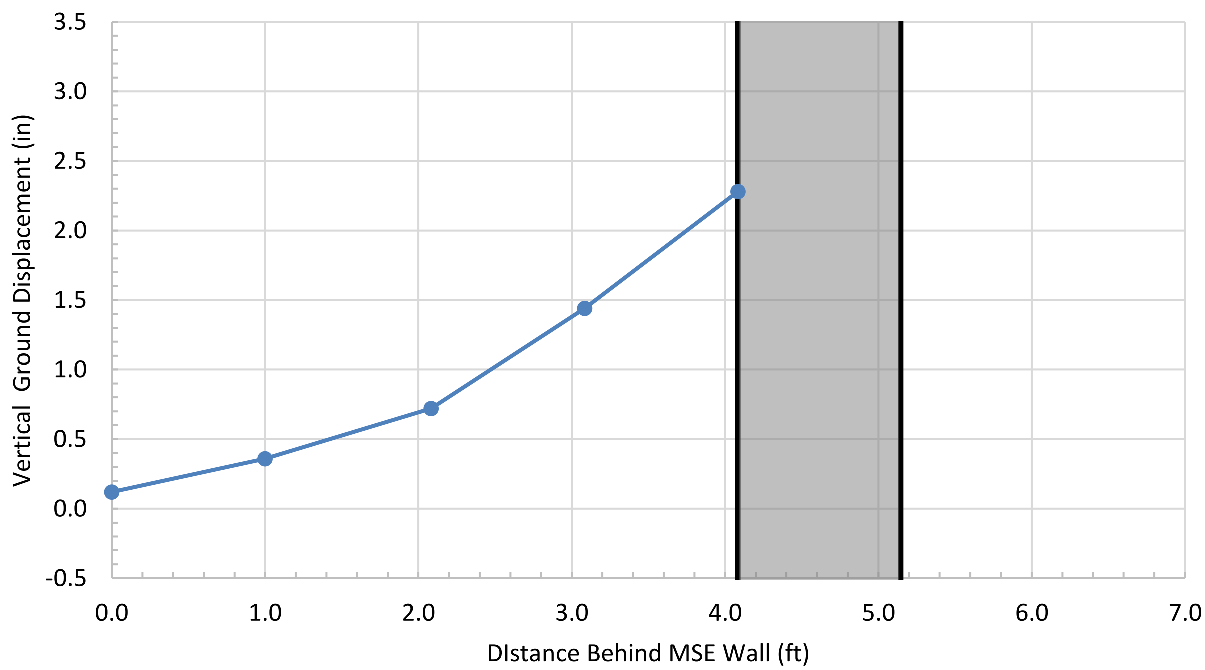

Figure E.1-4: Vertical ground displacement for the 4.3D test.

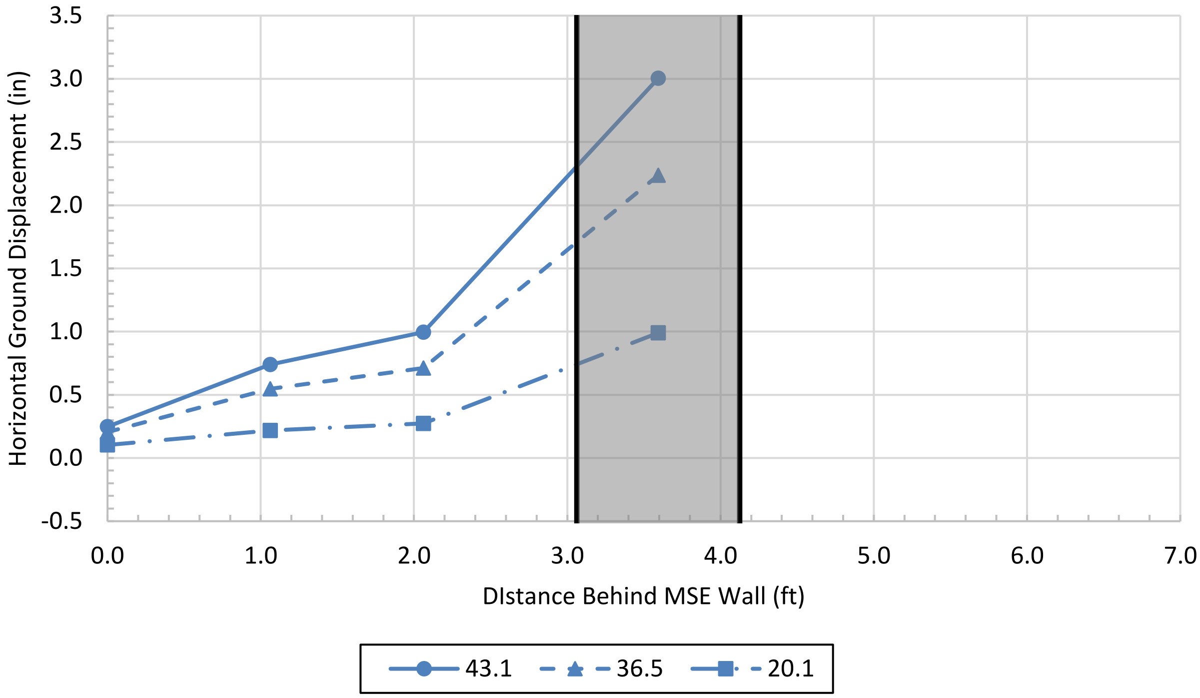

Figure E.1-5: Horizontal ground displacement for the 3.4D test.

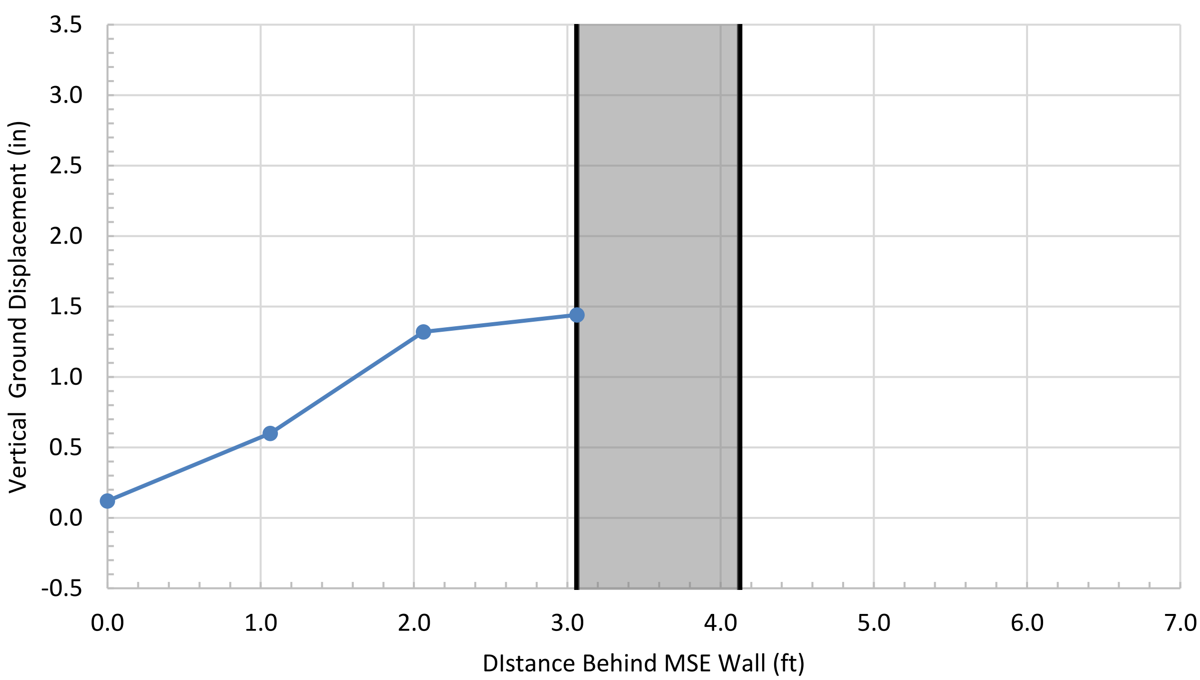

Figure E.1-6: Vertical ground displacement for the 3.4D test.

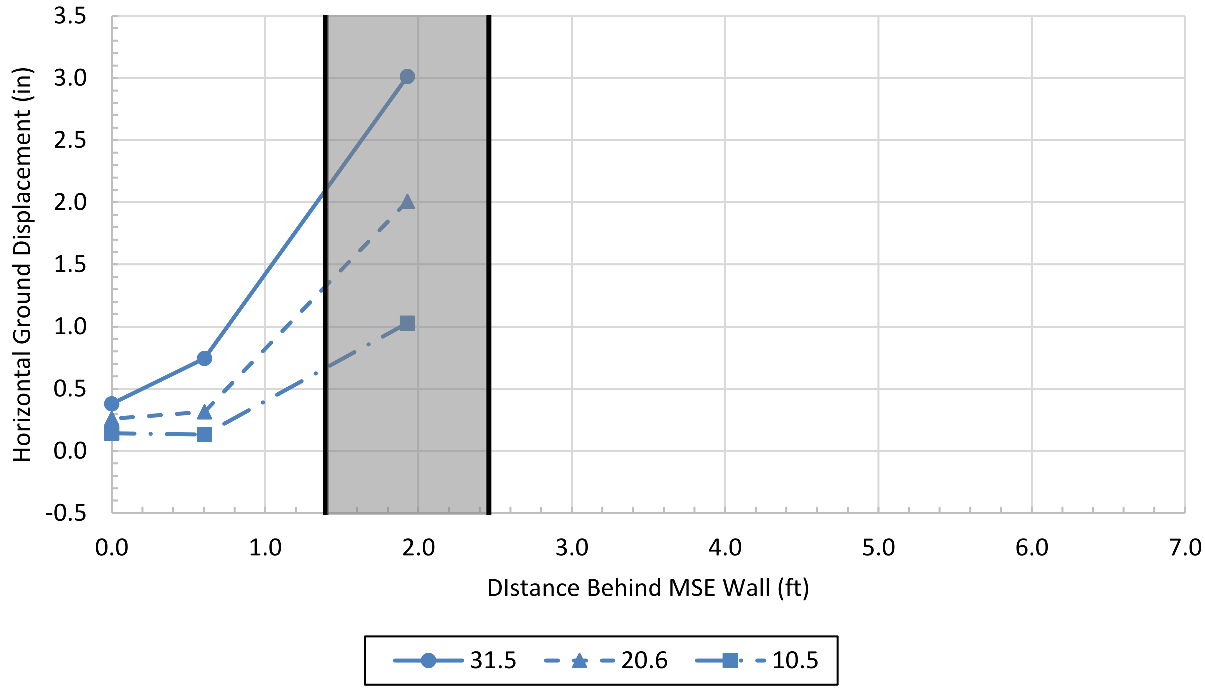

Figure E.1-7: Horizontal ground displacement for the 1.8D test.

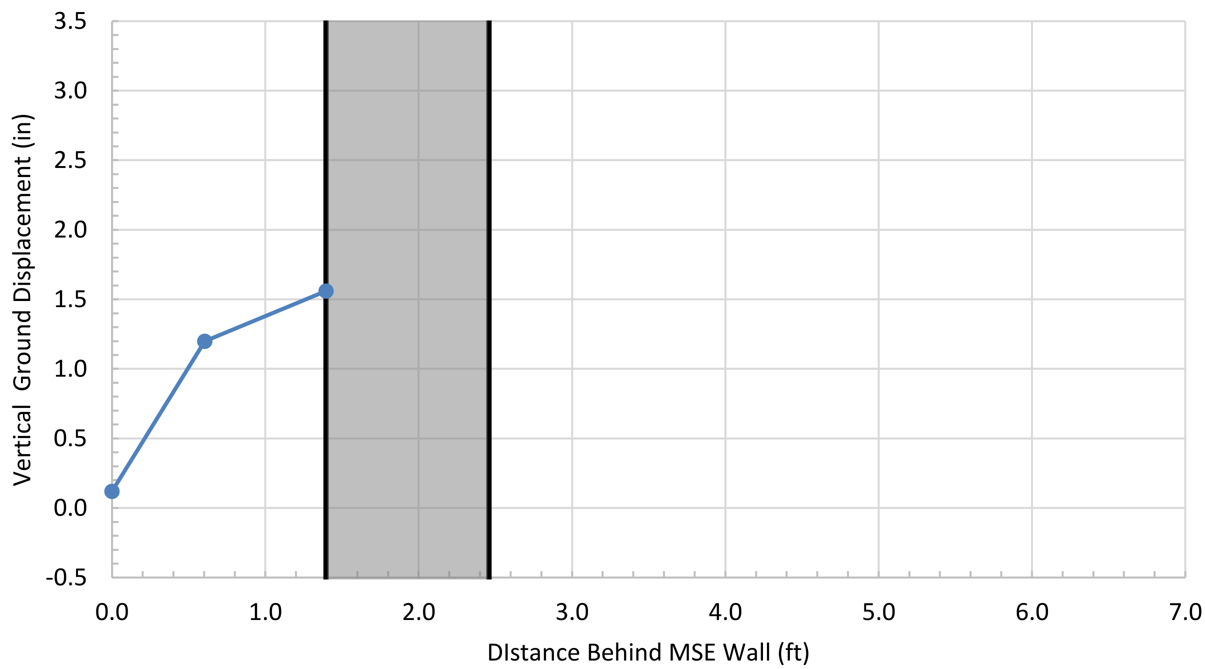

Figure E.1-8: Vertical ground displacement for the 1.8D test.

APPENDIX E.2 – GROUND DISPLACEMENT CURVES FOR PIPES WITH RIBBED STRIP

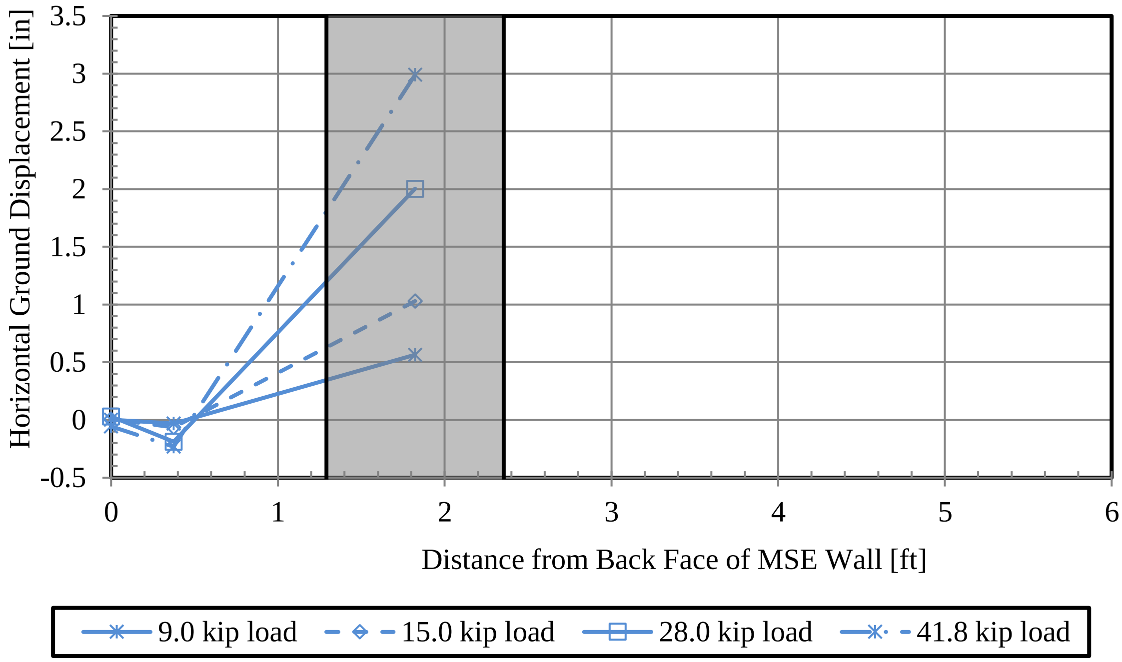

Figure E.2-1: Horizontal ground displacement at several load levels for 1.7D test.

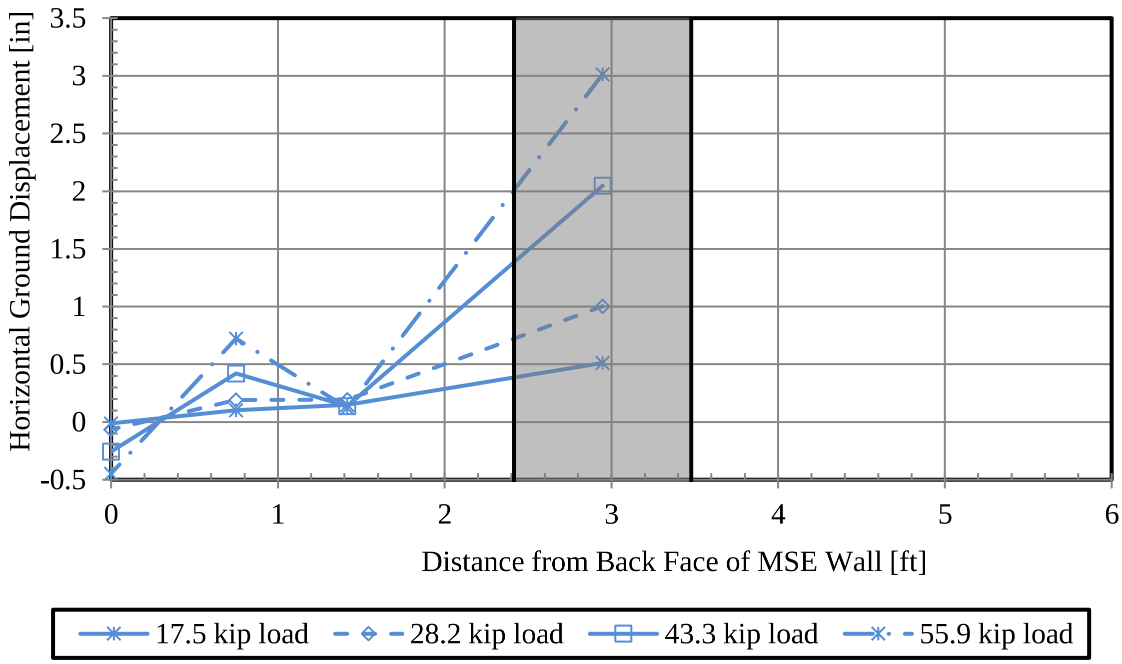

Figure E.2-2: Horizontal ground displacement at several load levels for 2.8D test.

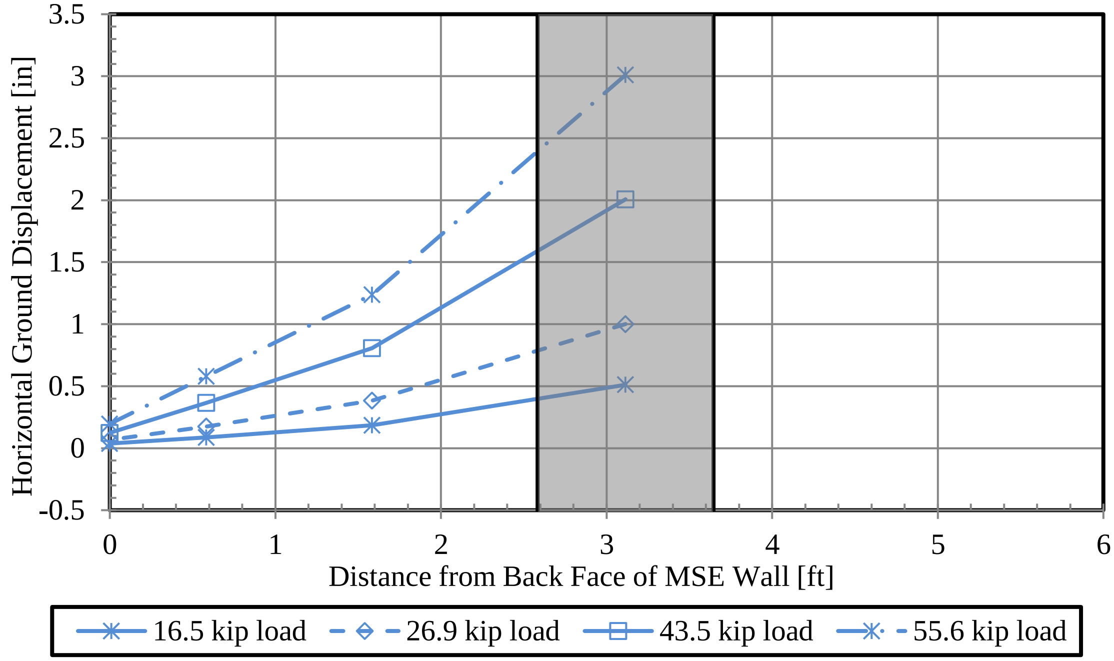

Figure E.2-3: Horizontal ground displacement at several load levels for 2.9D test.

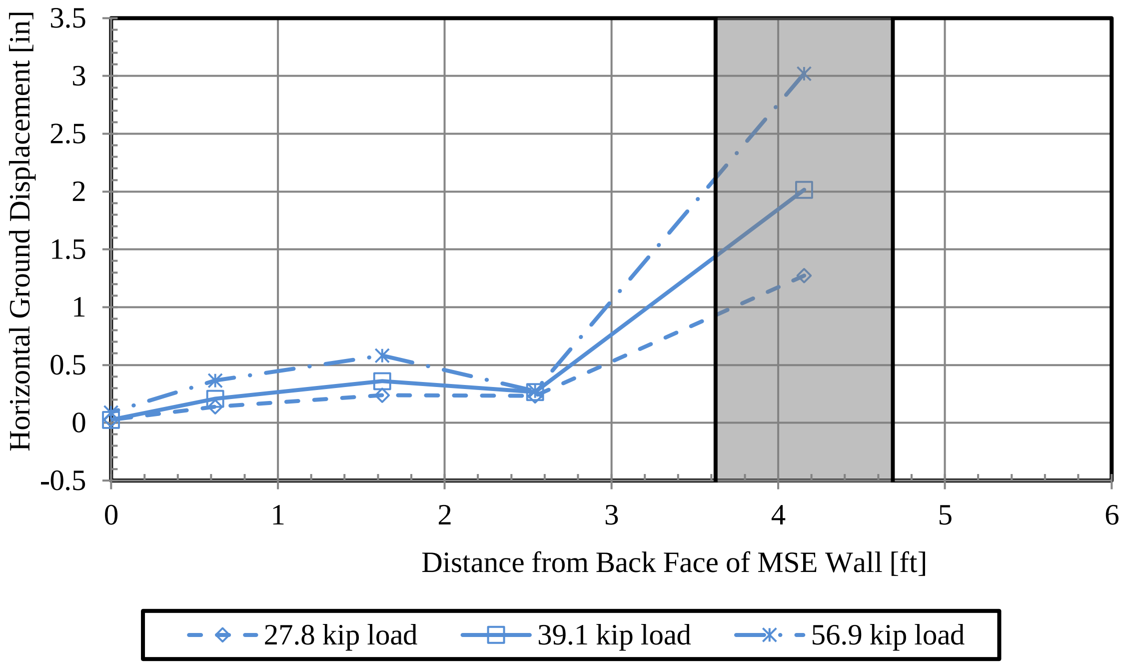

Figure E.2-4: Horizontal ground displacement at several load levels for 3.9D test.

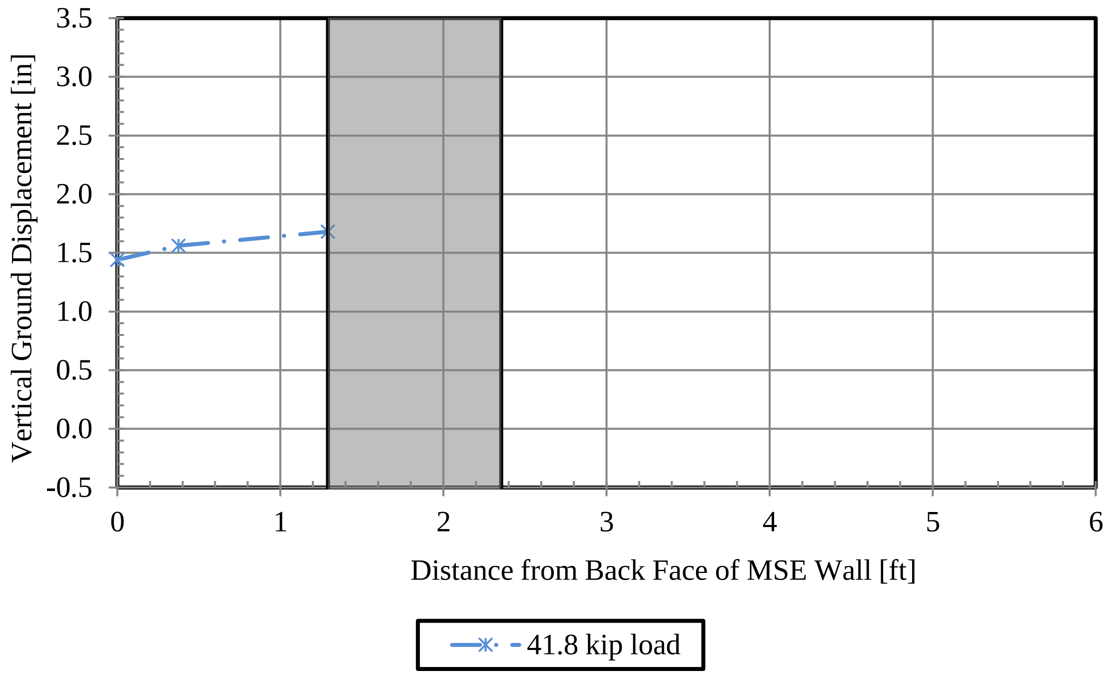

Figure E.2-5: Vertical ground displacement at peak pile load for 1.7D test.

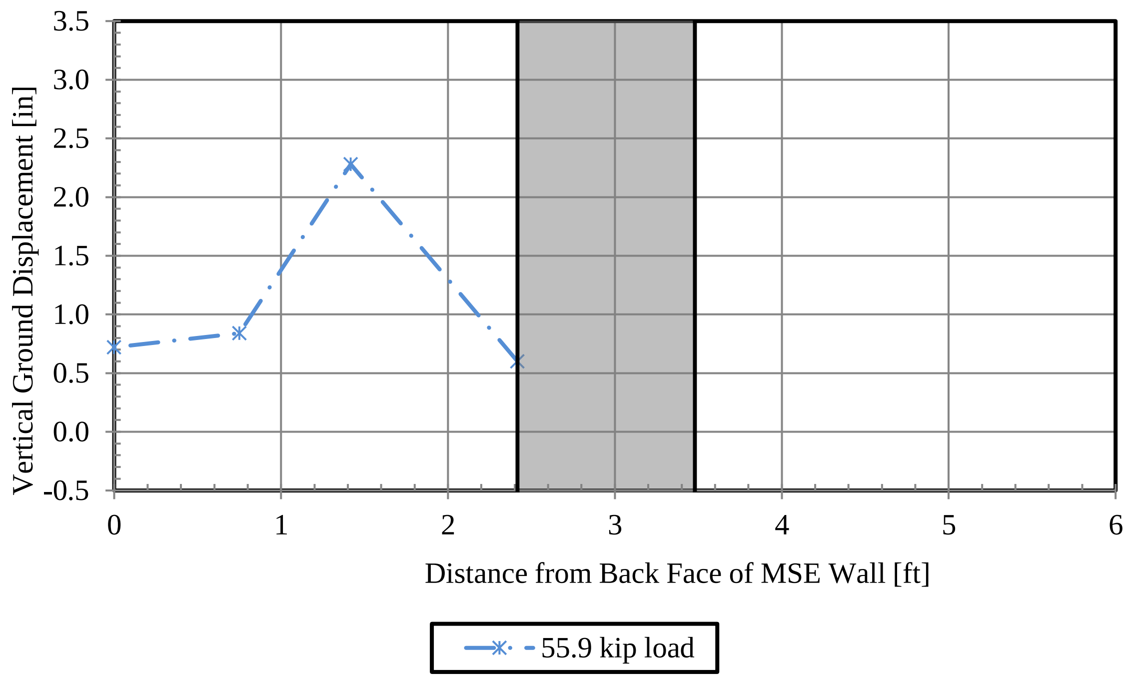

Figure E.2-6: Vertical ground displacement at peak pile load for 2.8D test.

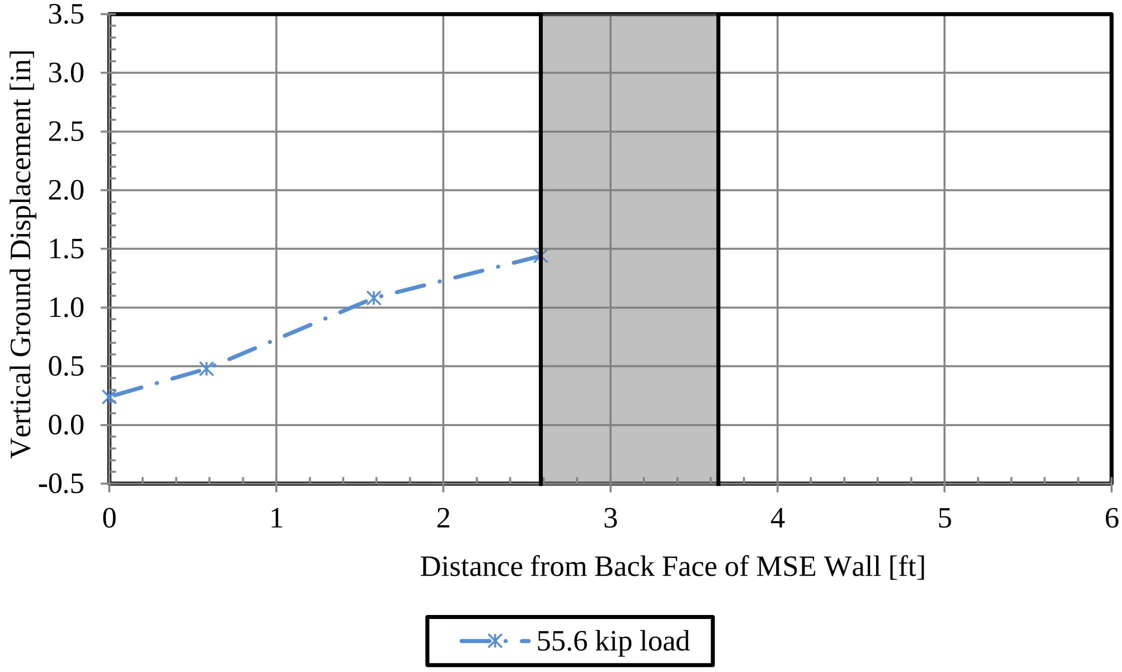

Figure E.2-7: Vertical ground displacement at peak pile load for 2.9D test.

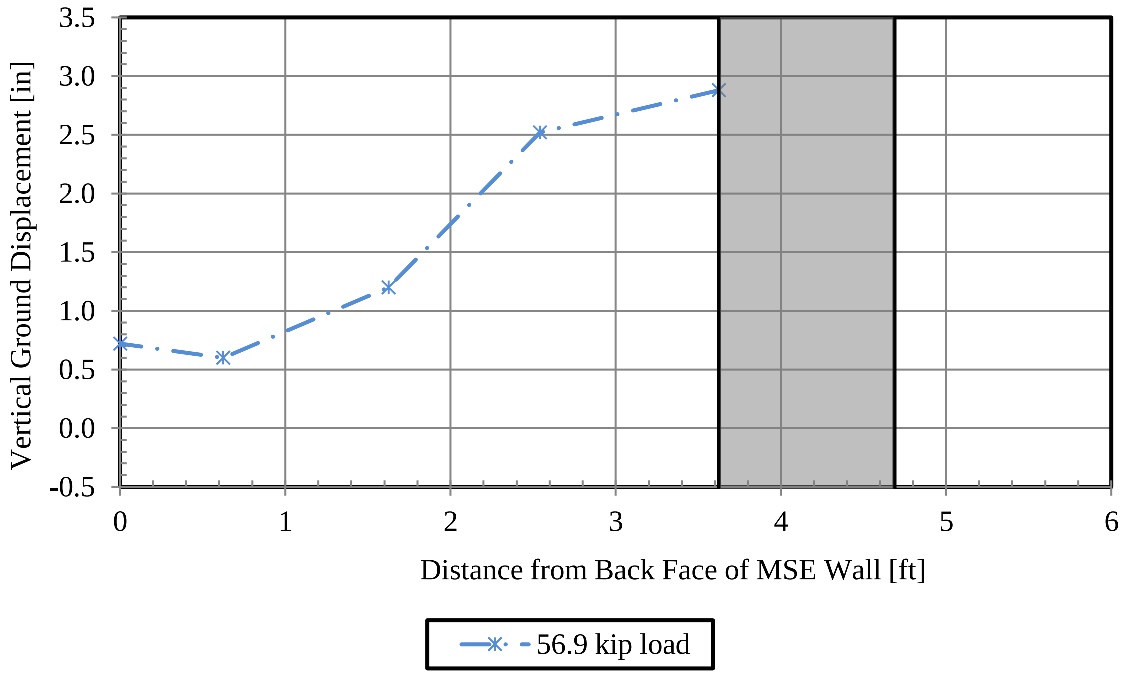

Figure E.2-8: Vertical ground displacement at peak pile load for 3.9D test.

APPENDIX F.1 – SOIL REINFORCEMENT INDUCED LOAD CURVES FOR PIPES WITH WELDED WIRE

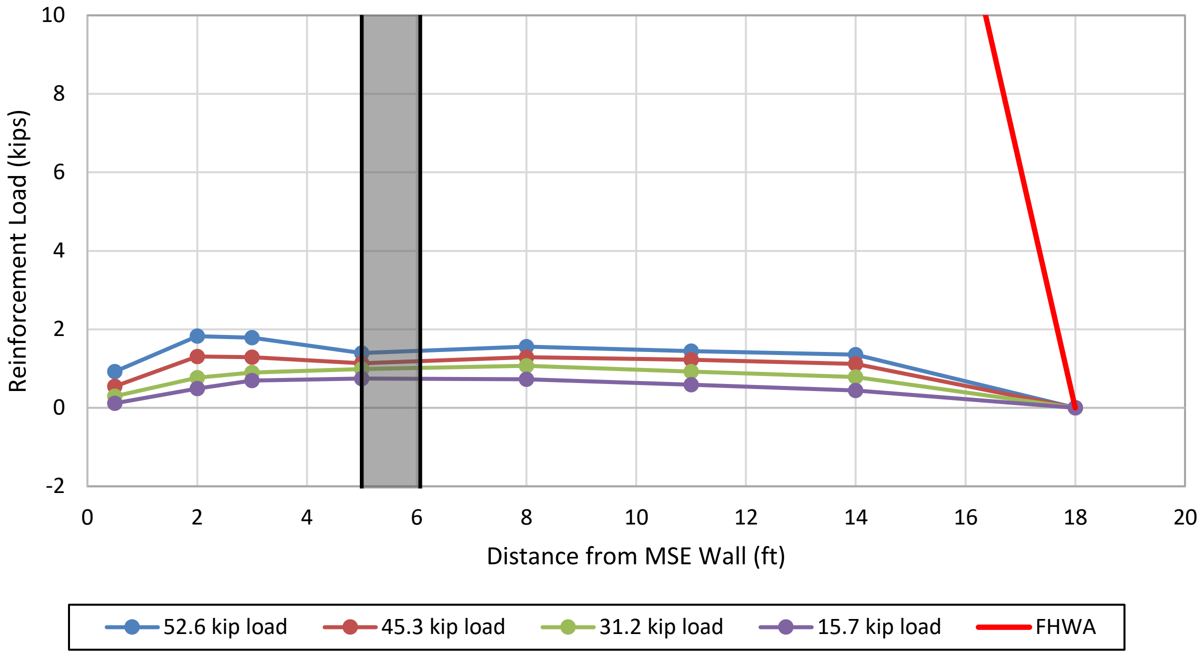

Figure F.1-1: Induced loads in the soil reinforcement at different pile head loads relative to distance from the back of the MSE wall (5.2D pile, layer L1, 46.5 in. transverse spacing).

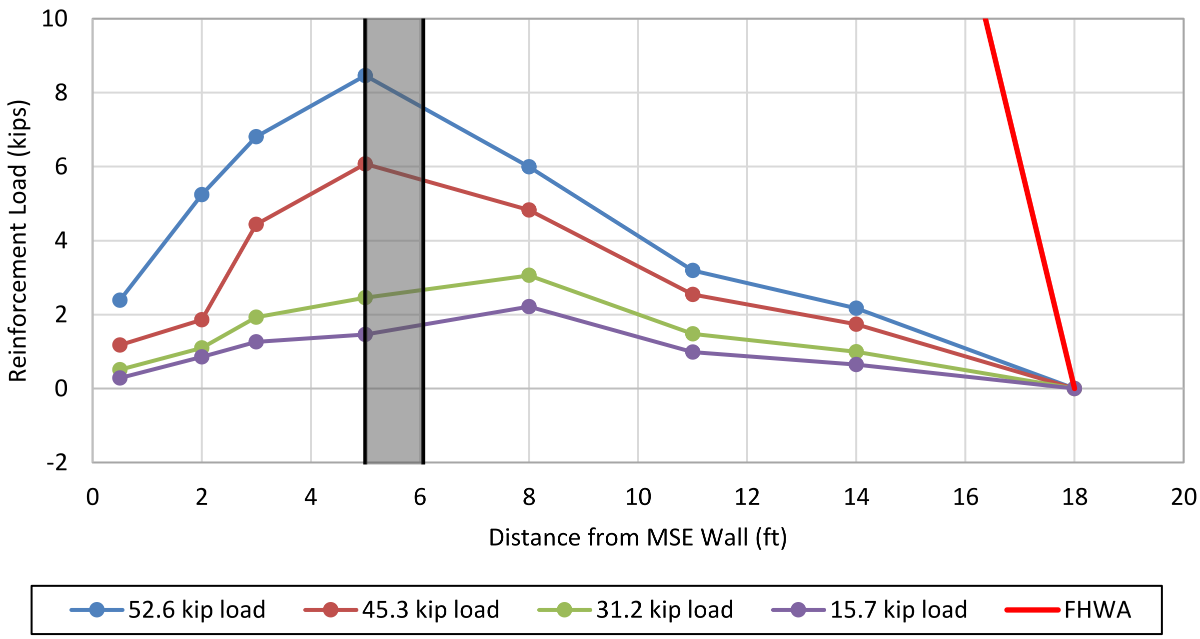

Figure F.1-2: Induced loads in the soil reinforcement at different pile head loads relative to distance from the back of the MSE wall (5.2D pile, layer L1, 15 in. transverse spacing).

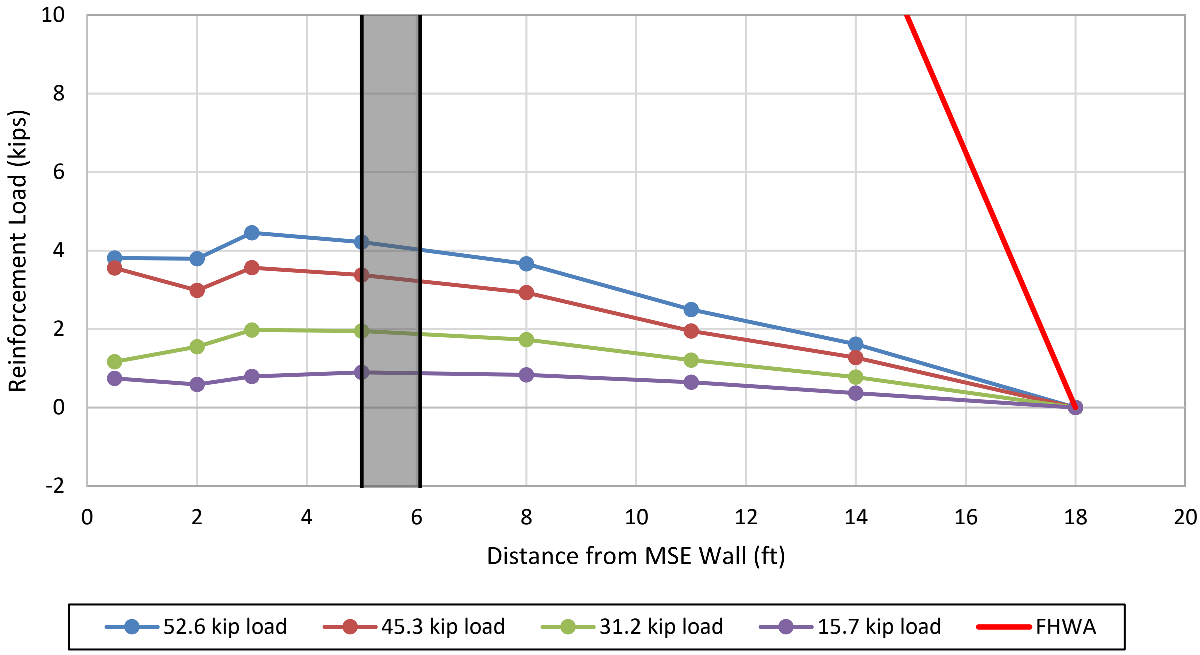

Figure F.1-3: Induced loads in the soil reinforcement at different pile head loads relative to distance from the back of the MSE wall (5.2D pile, layer L2, 38.5 in. transverse spacing).

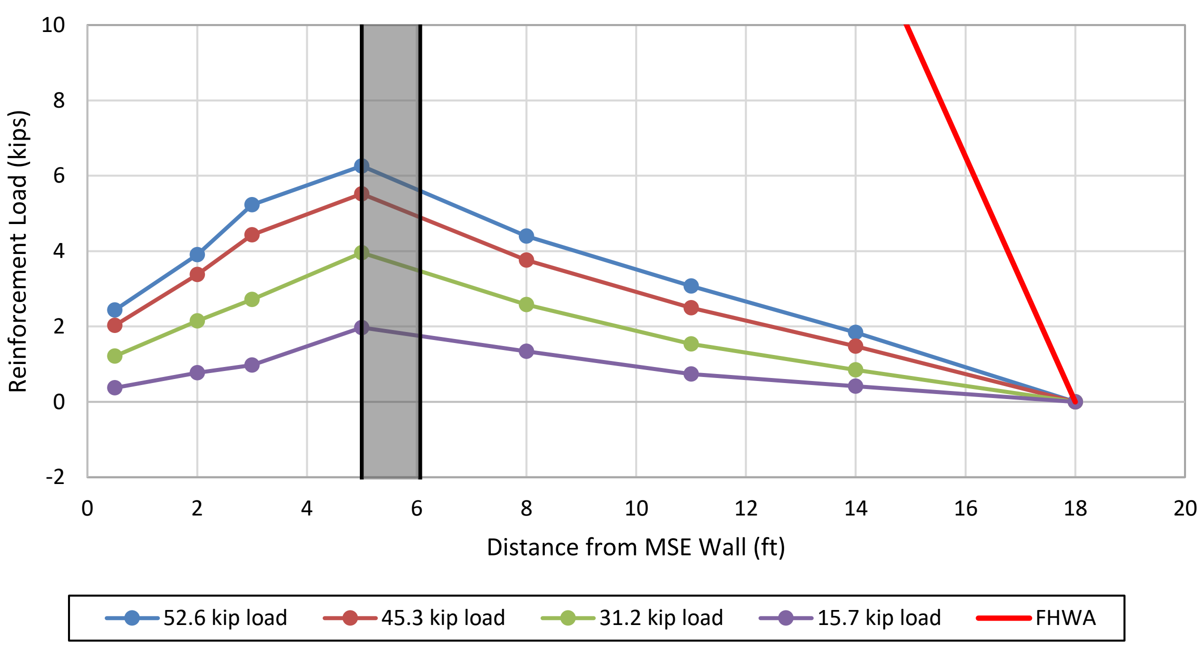

Figure F.1-4: Induced loads in the soil reinforcement at different pile head loads relative to distance from the back of the MSE wall (5.2D pile, layer L2, 22.5 in. transverse spacing).

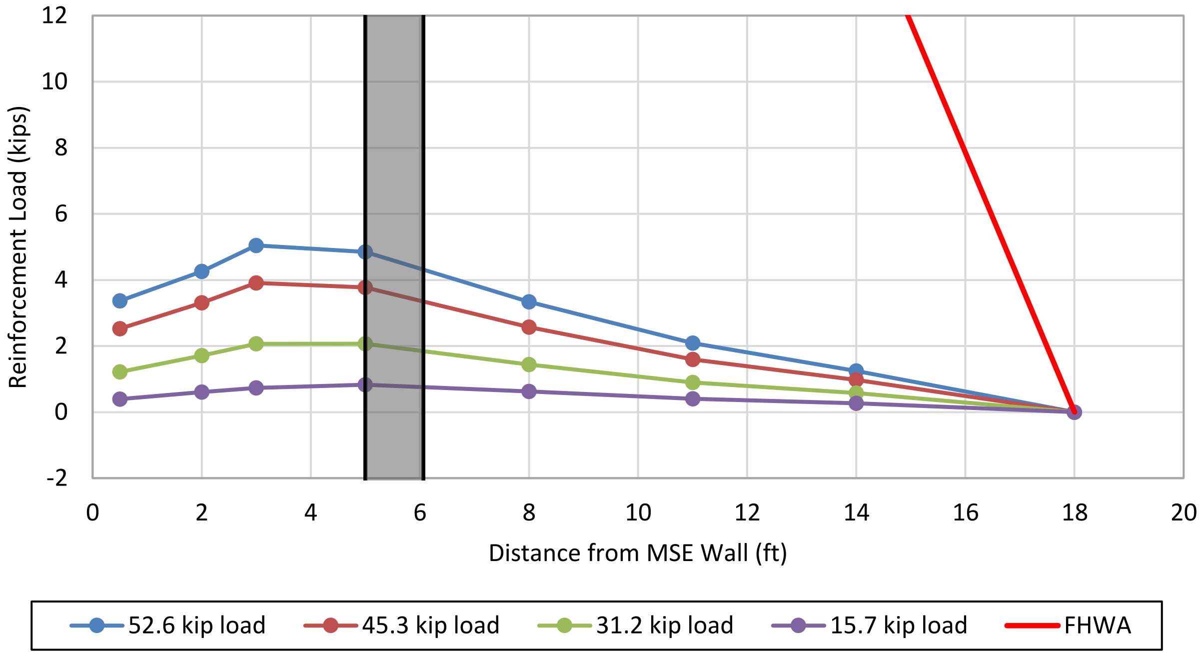

Figure F.1-5: Induced loads in the soil reinforcement at different pile head loads relative to distance from the back of the MSE wall (5.2D pile, layer L3, 46 in. transverse spacing).

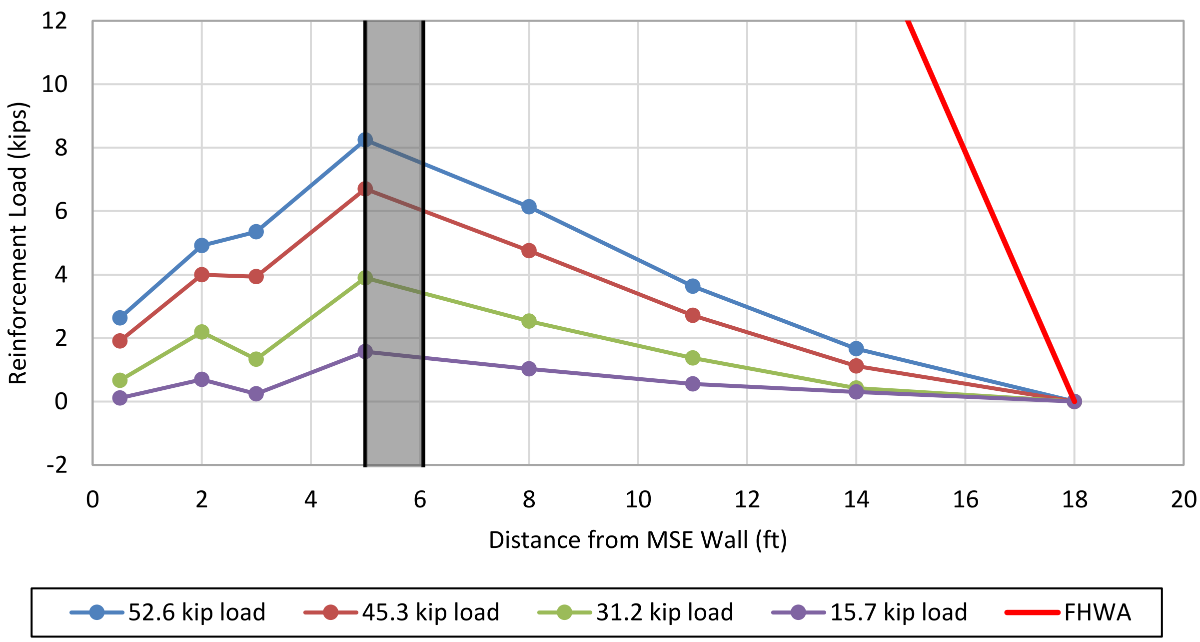

Figure F.1-6: Induced loads in the soil reinforcement at different pile head loads relative to distance from the back of the MSE wall (5.2D pile, layer L3, 21.5 in. transverse spacing).

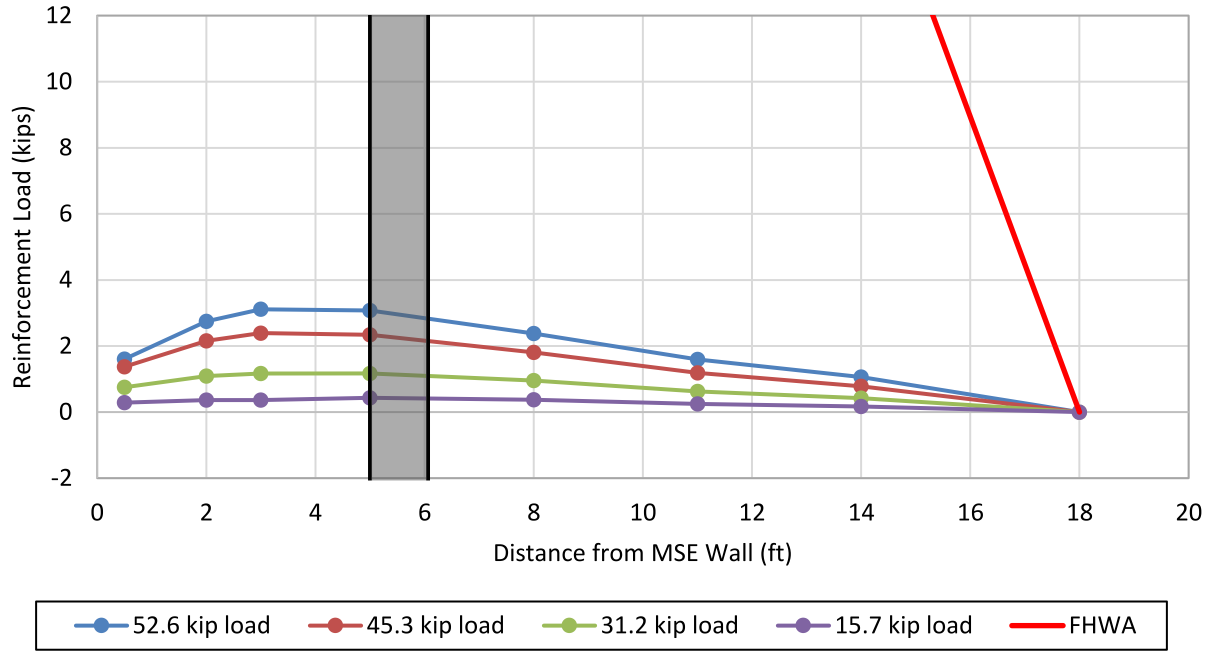

Figure F.1-7: Induced loads in the soil reinforcement at different pile head loads relative to distance from the back of the MSE wall (5.2D pile, layer L4, 39 in. transverse spacing).

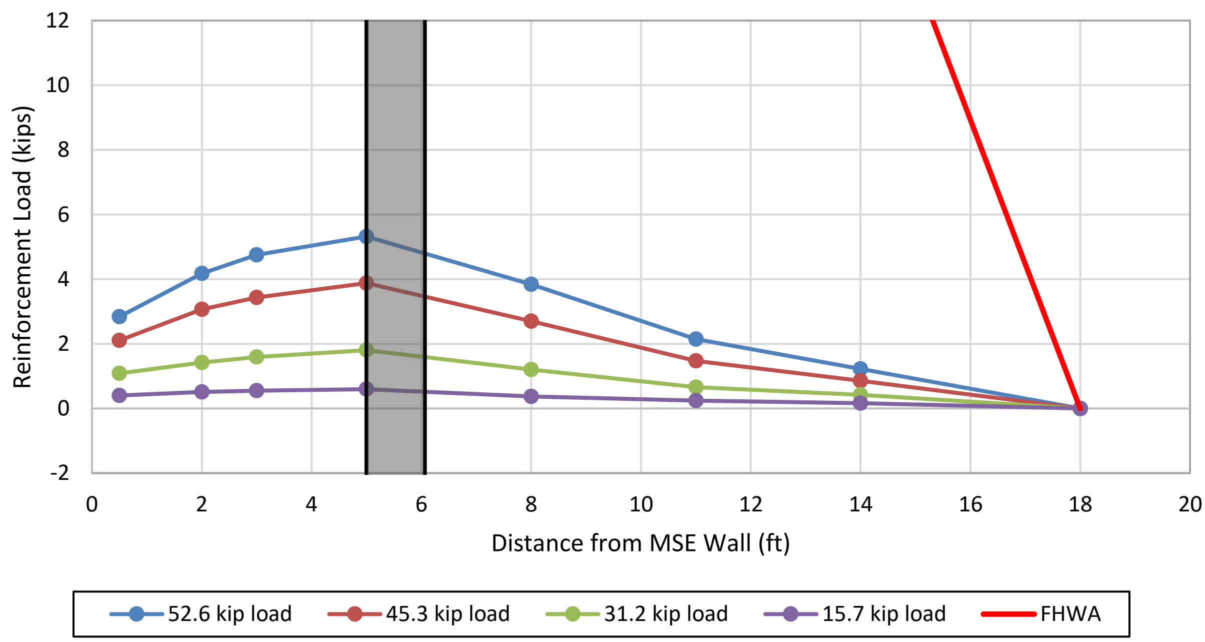

Figure F.1-8: Induced loads in the soil reinforcement at different pile head loads relative to distance from the back of the MSE wall (5.2D pile, layer L4, 23 in. transverse spacing).

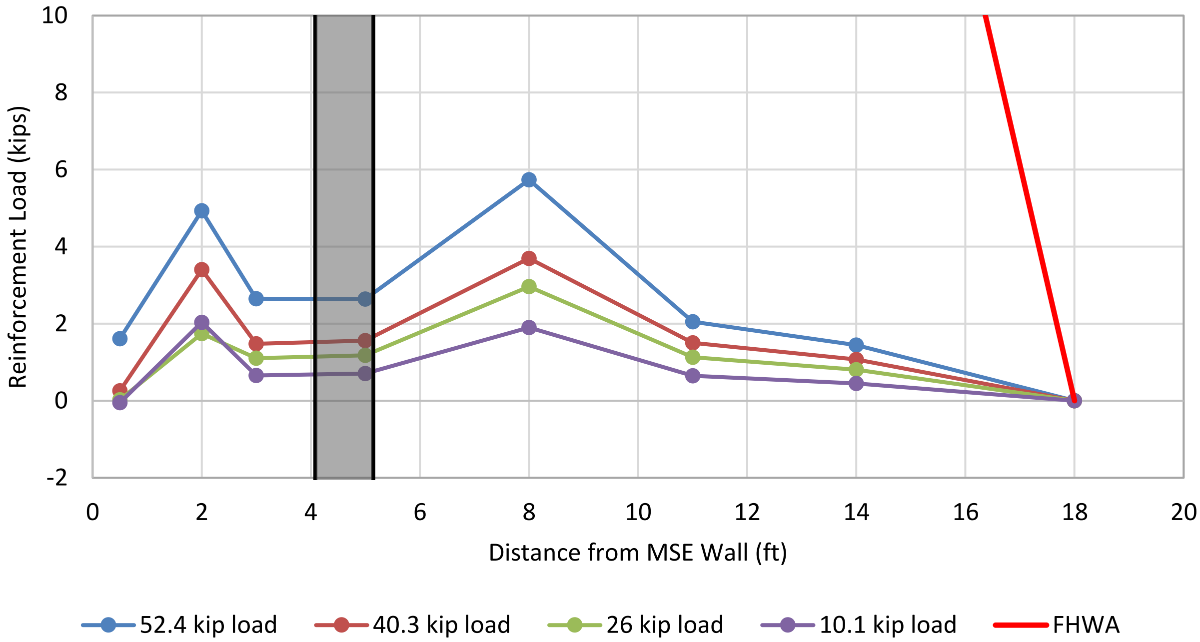

Figure F.1-9: Induced loads in the soil reinforcement at different pile head loads relative to distance from the back of the MSE wall (4.3D pile, layer L1, 40.5 in. transverse spacing).

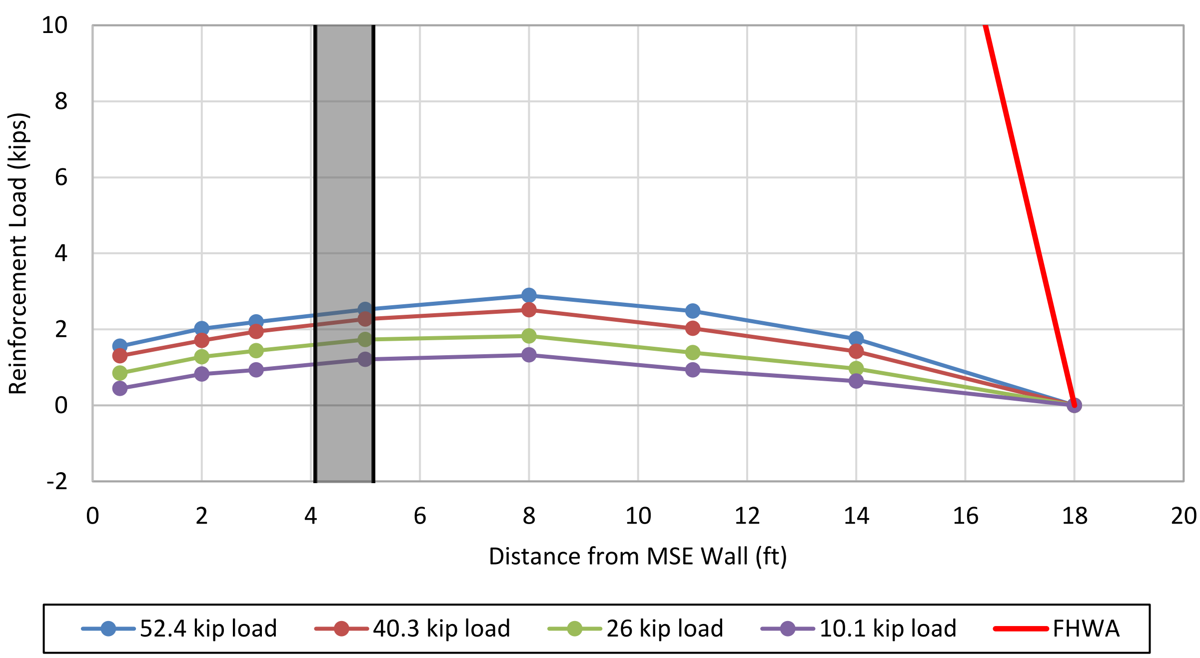

Figure F.1-10: Induced loads in the soil reinforcement at different pile head loads relative to distance from the back of the MSE wall (4.3D pile, layer L1, 17.5 in. transverse spacing).

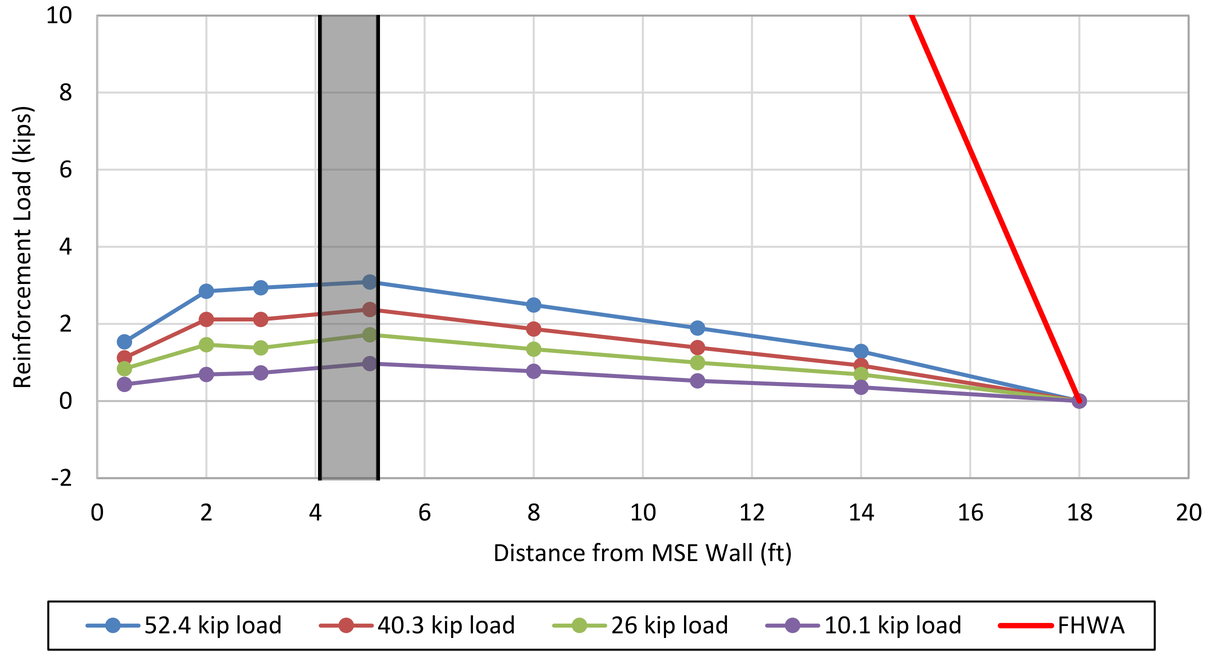

Figure F.1-11: Induced loads in the soil reinforcement at different pile head loads relative to distance from the back of the MSE wall (4.3D pile, layer L2, 33.5 in. transverse spacing).

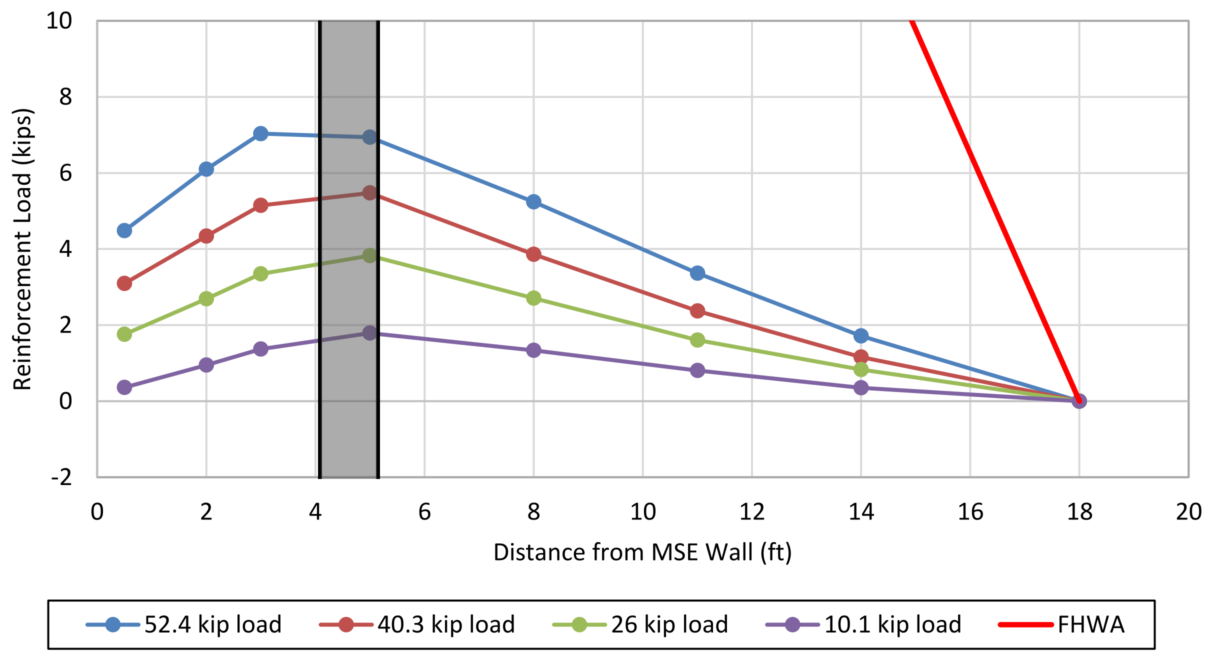

Figure F.1-12: Induced loads in the soil reinforcement at different pile head loads relative to distance from the back of the MSE wall (4.3D pile, layer L2, 18.5 in. transverse spacing).

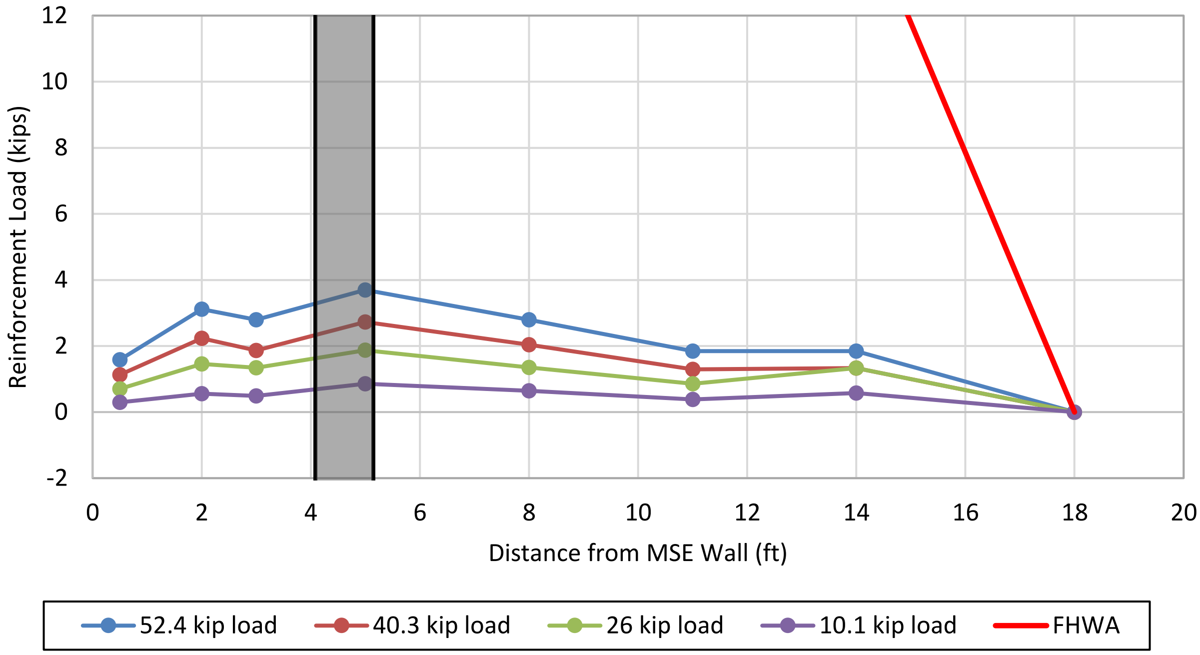

Figure F.1-13: Induced loads in the soil reinforcement at different pile head loads relative to distance from the back of the MSE wall (4.3D pile, layer L3, 34.5 in. transverse spacing).

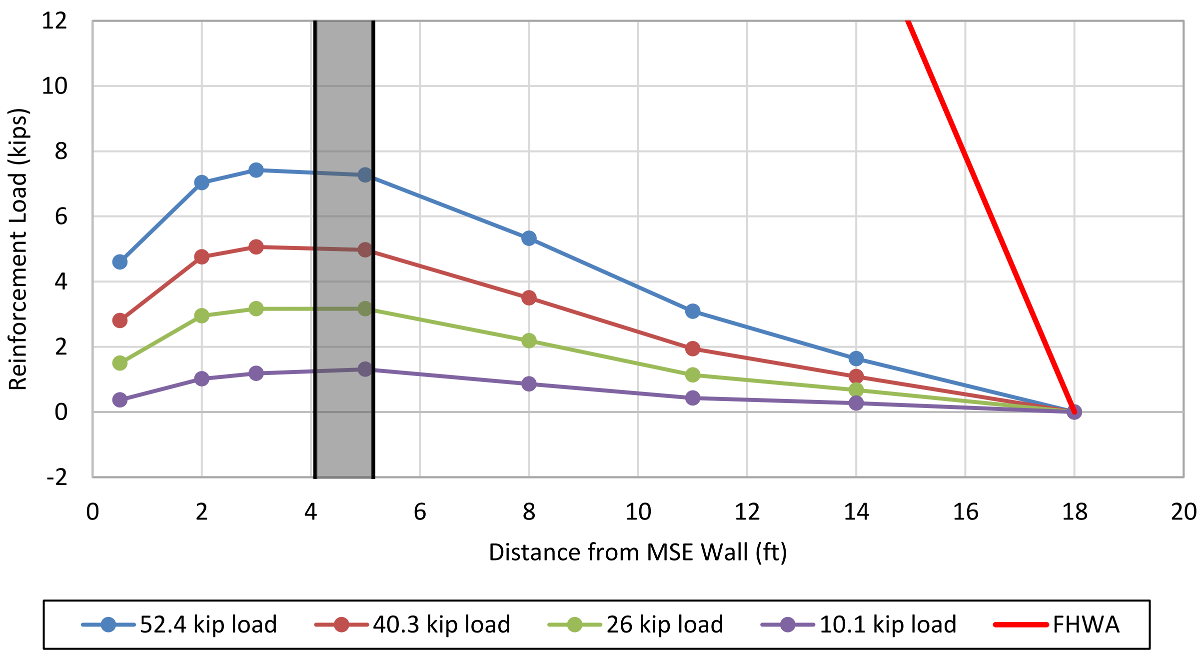

Figure F.1-14: Induced loads in the soil reinforcement at different pile head loads relative to distance from the back of the MSE wall (4.3D pile, layer L3, 17.5 in. transverse spacing).

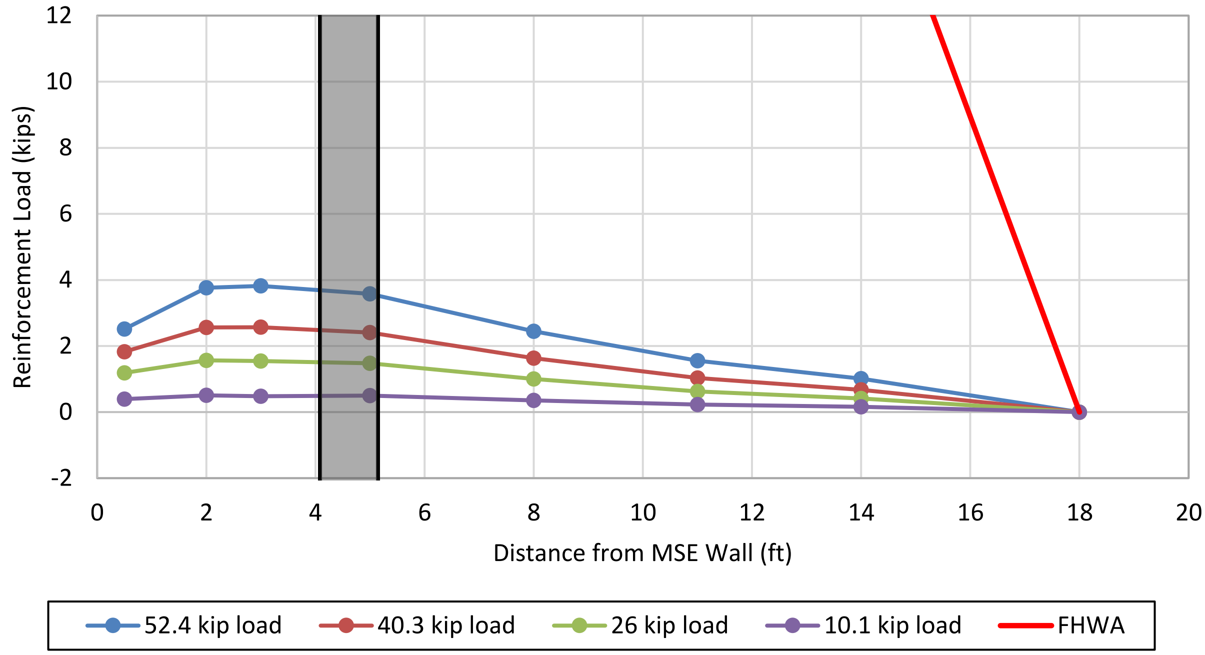

Figure F.1-15: Induced loads in the soil reinforcement at different pile head loads relative to distance from the back of the MSE wall (4.3D pile, layer L4, 34 in. transverse spacing).

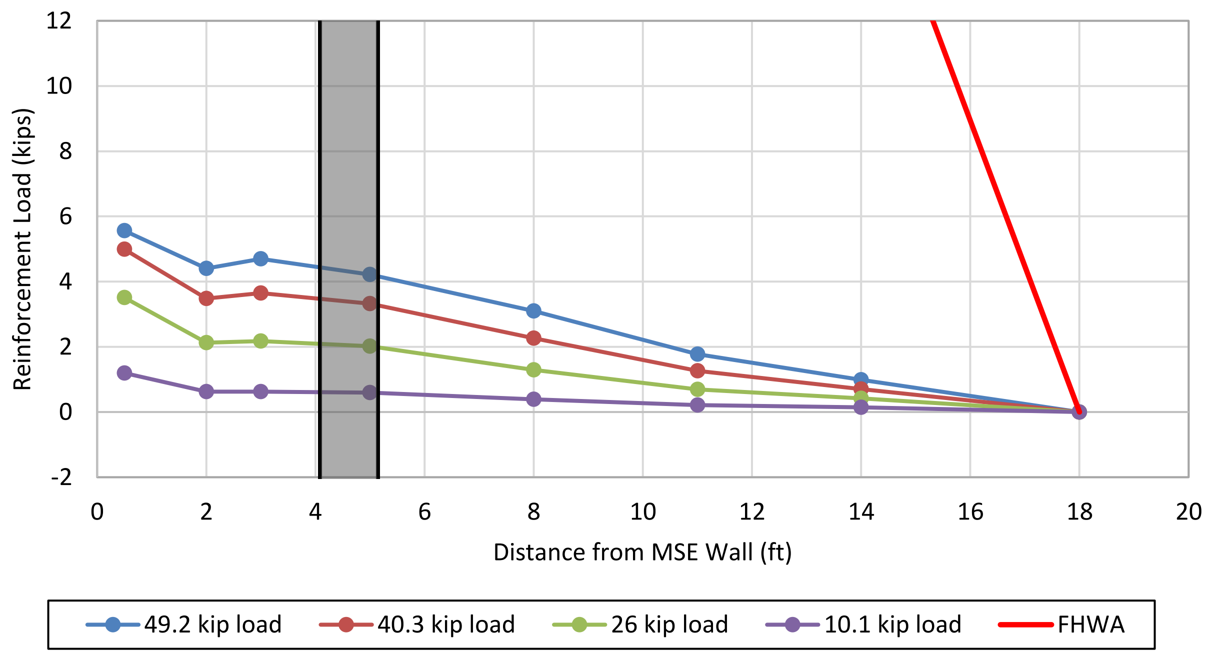

Figure F.1-16: Induced loads in the soil reinforcement at different pile head loads relative to distance from the back of the MSE wall (4.3D pile, layer L4, 19 in. transverse spacing).

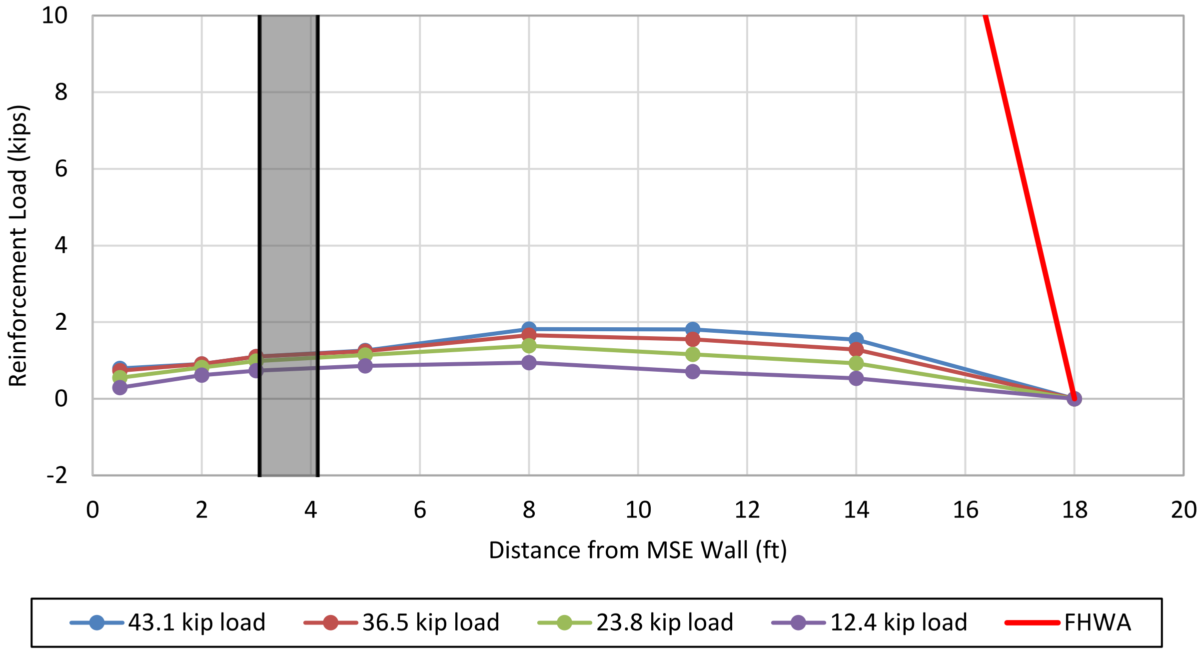

Figure F.1-17: Induced loads in the soil reinforcement at different pile head loads relative to distance from the back of the MSE wall (3.4D pile, layer L1, 38 in. transverse spacing).

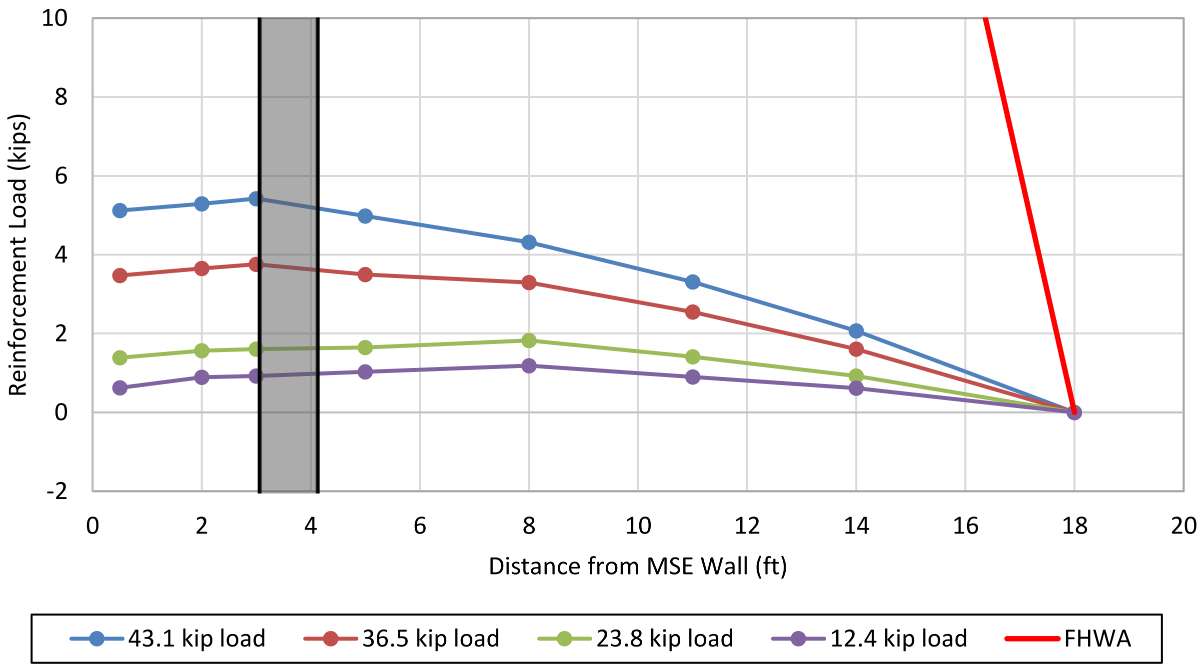

Figure F.1-18: Induced loads in the soil reinforcement at different pile head loads relative to distance from the back of the MSE wall (3.4D pile, layer L1, 24.5 in. transverse spacing).

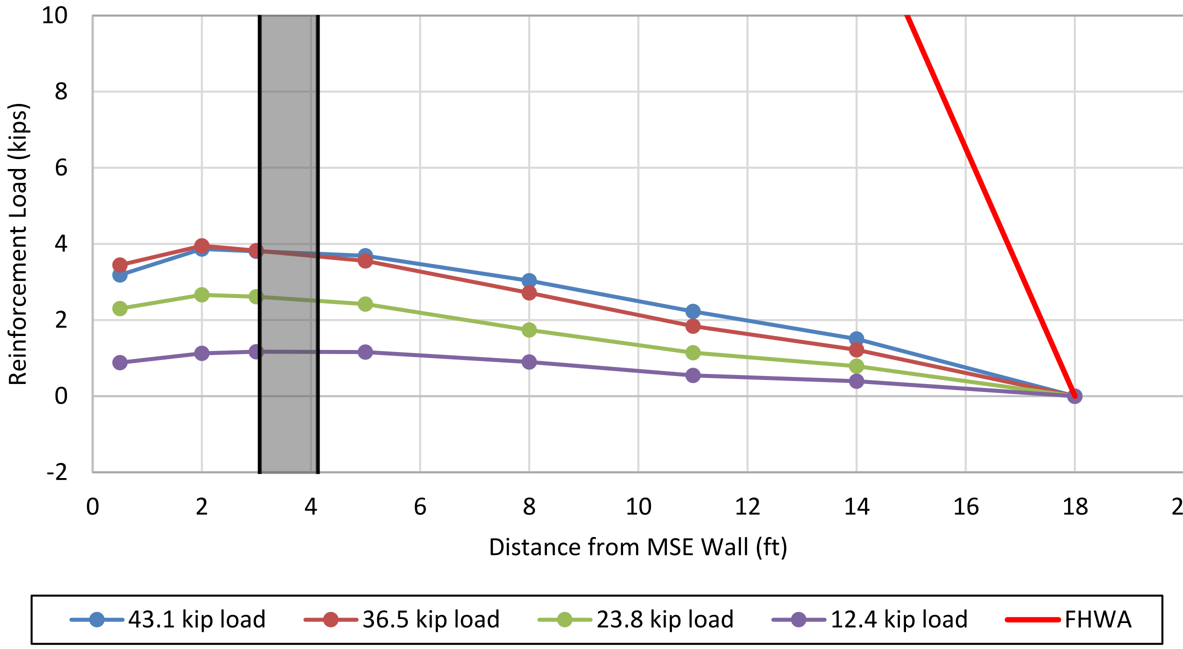

Figure F.1-19: Induced loads in the soil reinforcement at different pile head loads relative to distance from the back of the MSE wall (3.4D pile, layer L2, 37.5 in. transverse spacing).

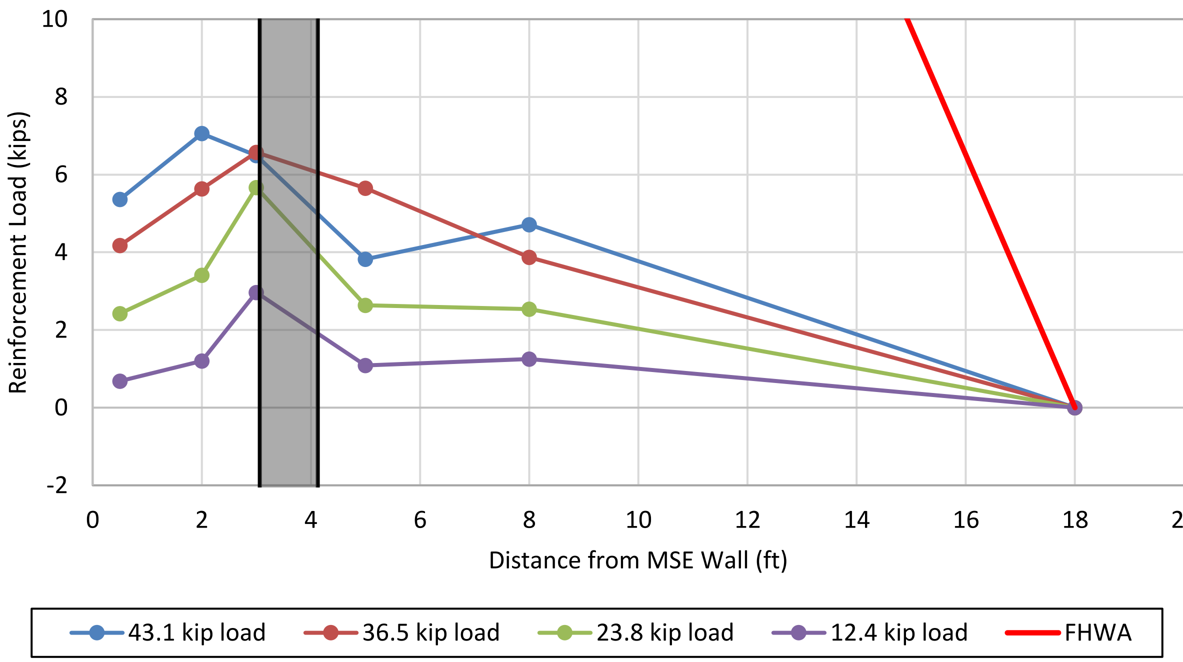

Figure F.1-20: Induced loads in the soil reinforcement at different pile head loads relative to distance from the back of the MSE wall (3.4D pile, layer L2, 23 in. transverse spacing).

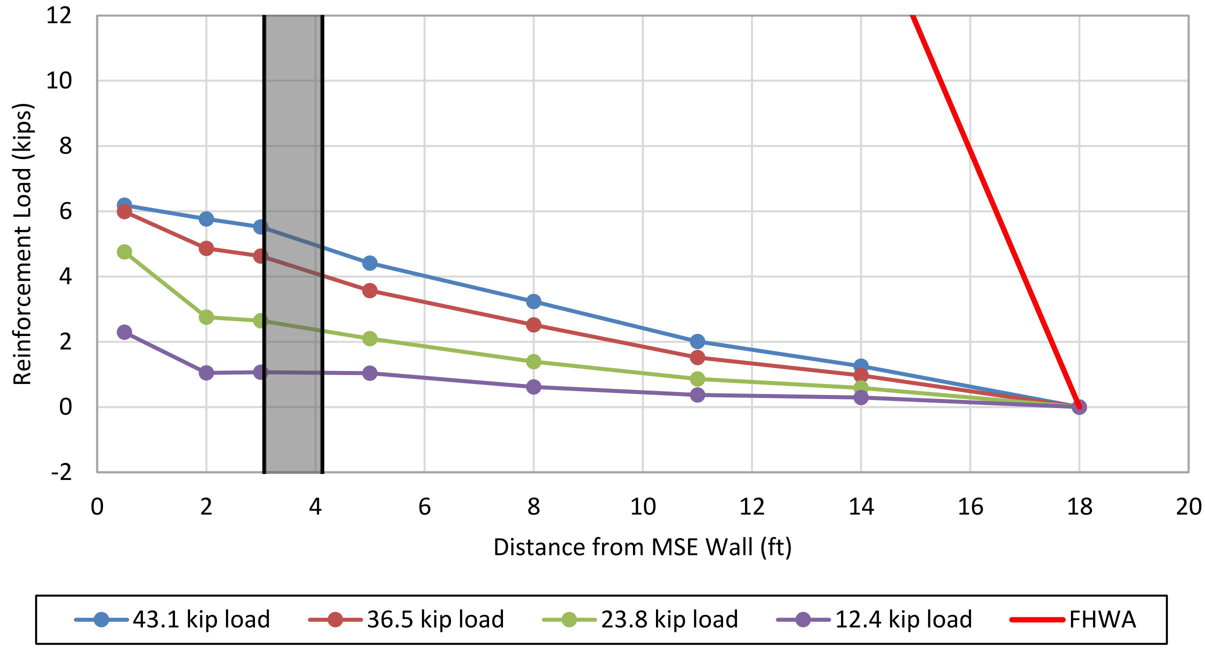

Figure F.1-21: Induced loads in the soil reinforcement at different pile head loads relative to distance from the back of the MSE wall (3.4D pile, layer L3, 38 in. transverse spacing).

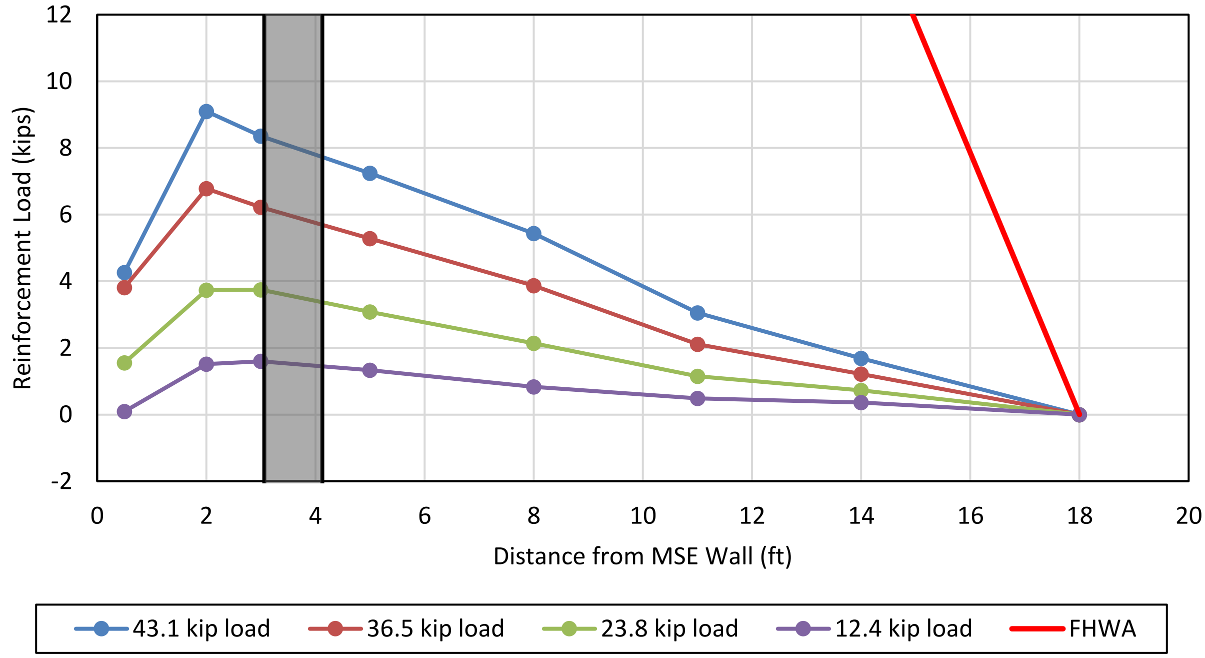

Figure F.1-22: Induced loads in the soil reinforcement at different pile head loads relative to distance from the back of the MSE wall (3.4D pile, layer L3, 23 in. transverse spacing).

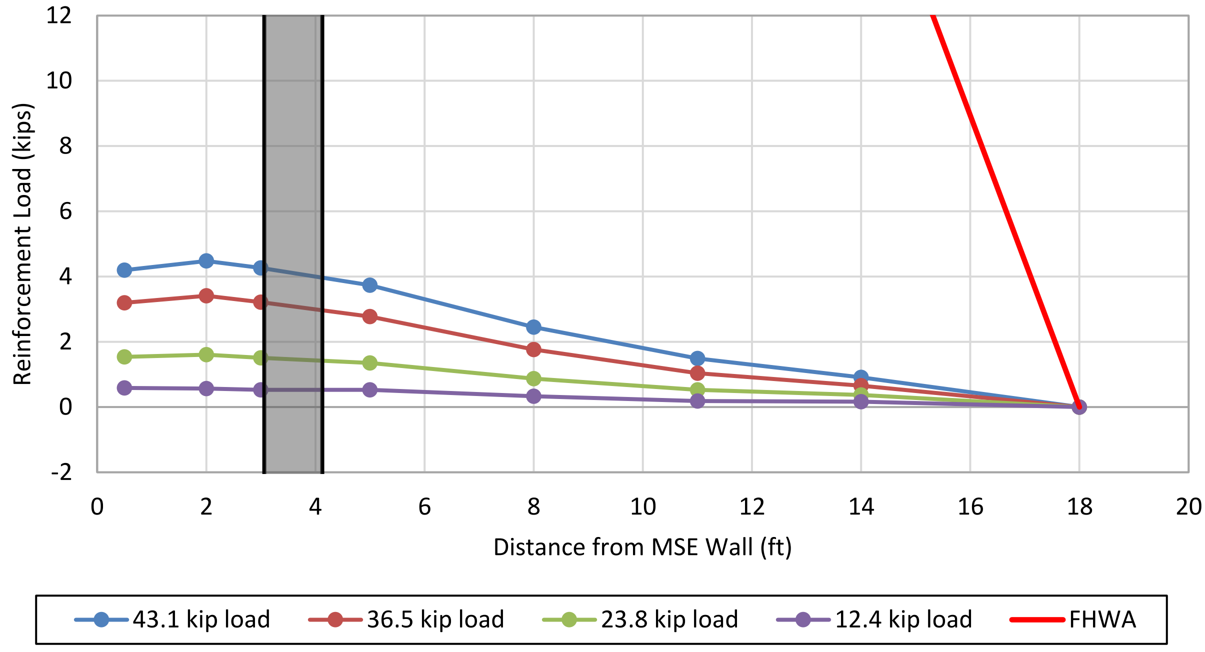

Figure F.1-23: Induced loads in the soil reinforcement at different pile head loads relative to distance from the back of the MSE wall (3.4D pile, layer L4, 38 in. transverse spacing).

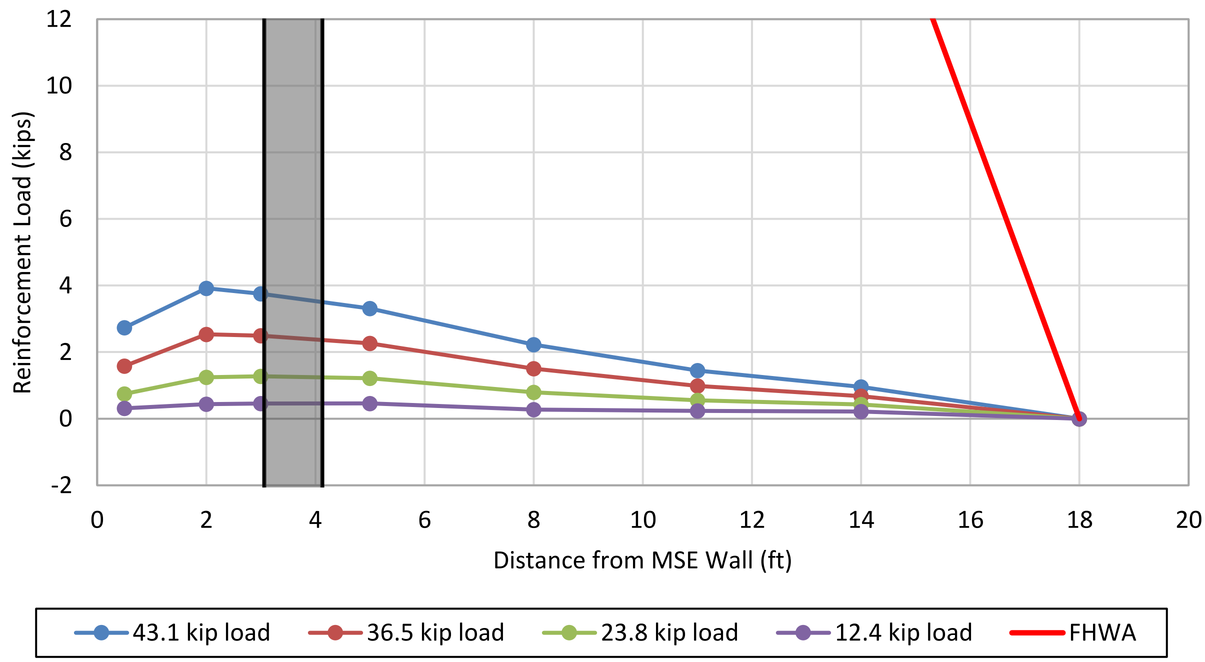

Figure F.1-24: Induced loads in the soil reinforcement at different pile head loads relative to distance from the back of the MSE wall (3.4D pile, layer L4, 31 in. transverse spacing).

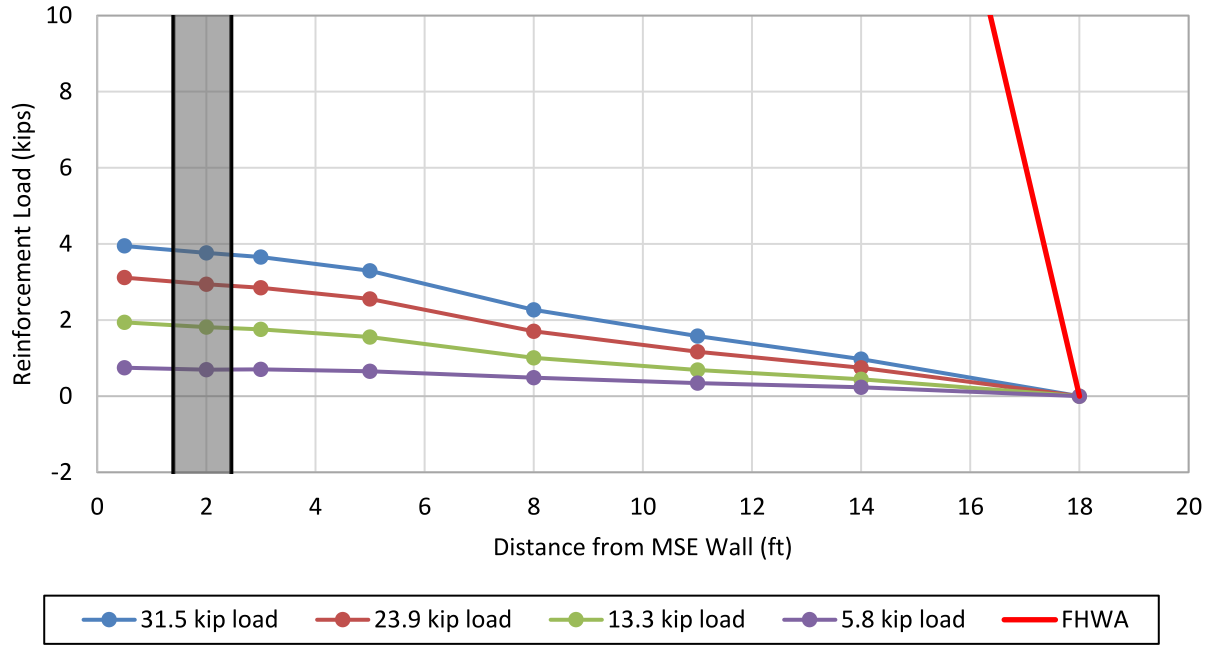

Figure F.1-25: Induced loads in the soil reinforcement at different pile head loads relative to distance from the back of the MSE wall (1.8D pile, layer L1, 42 in. transverse spacing).

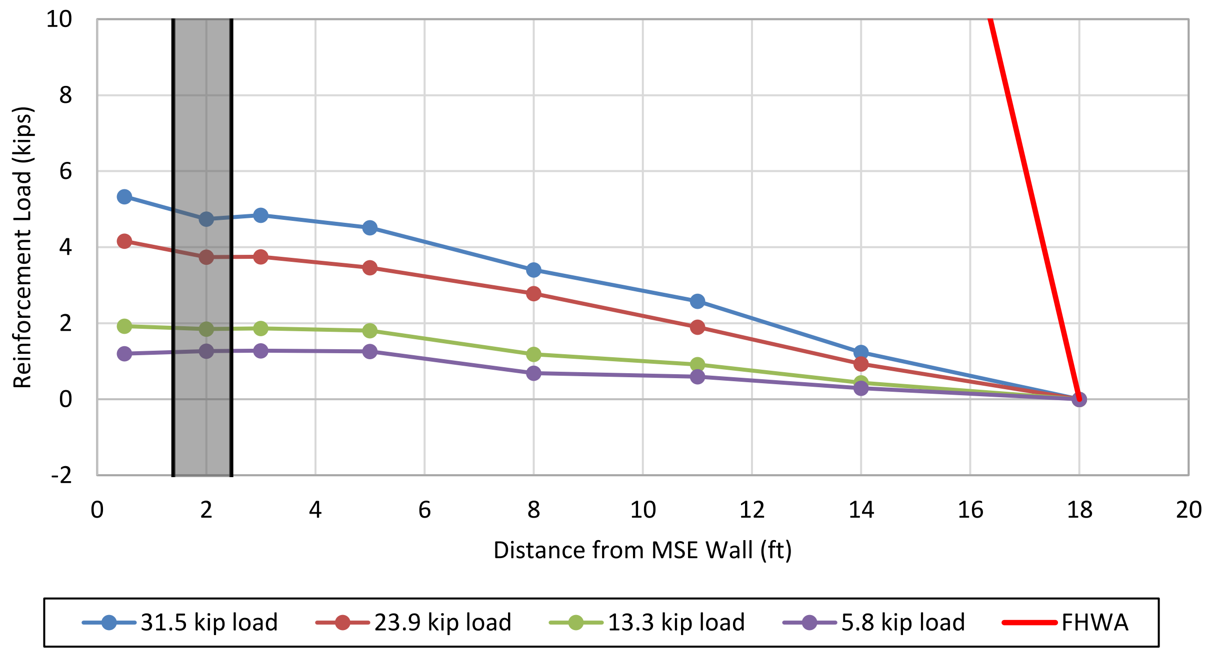

Figure F.1-26: Induced loads in the soil reinforcement at different pile head loads relative to distance from the back of the MSE wall (1.8D pile, layer L1, 17.5 in. transverse spacing).

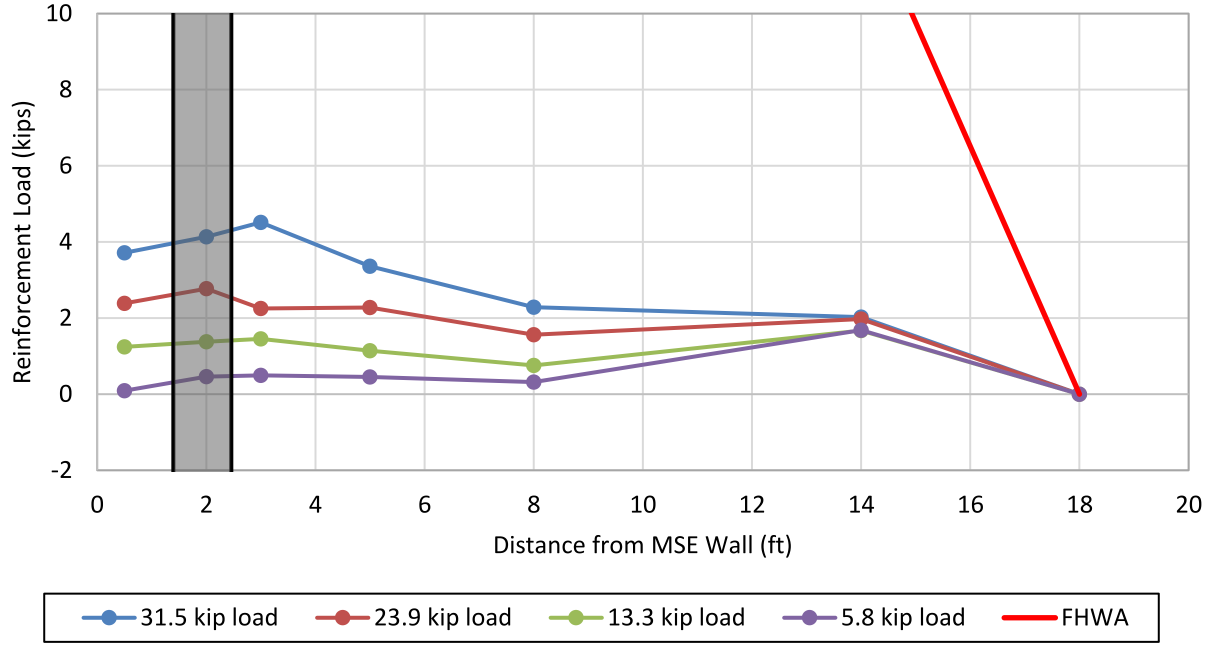

Figure F.1-27: Induced loads in the soil reinforcement at different pile head loads relative to distance from the back of the MSE wall (1.8D pile, layer L2, 43 in. transverse spacing).

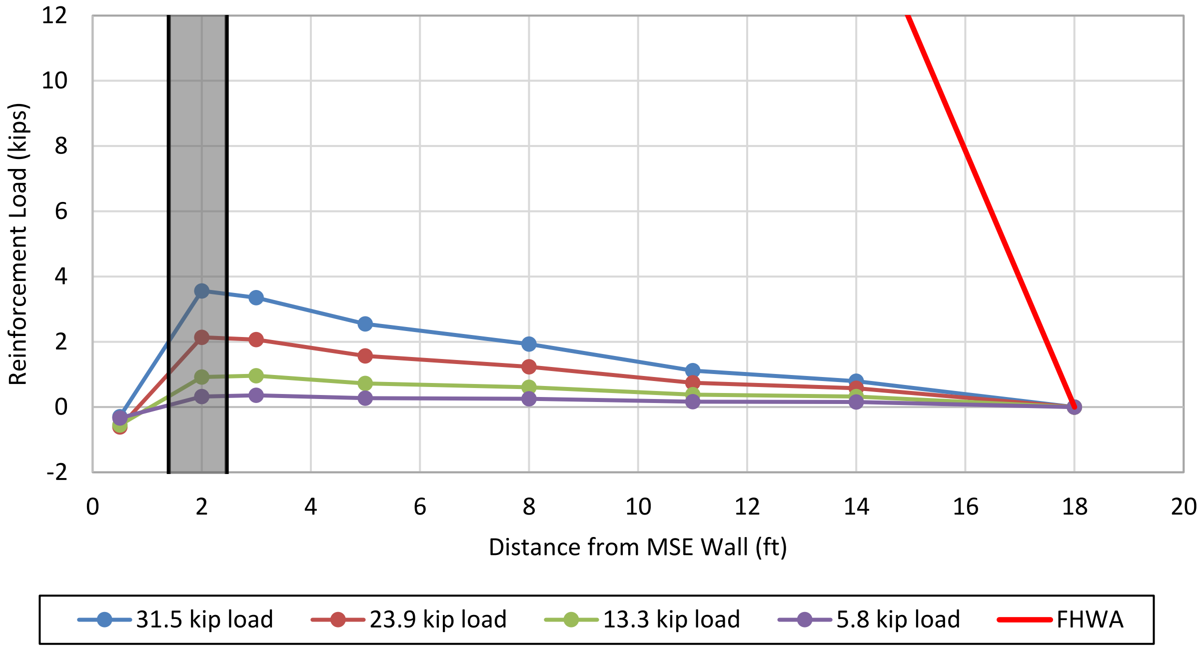

Figure F.1-28: Induced loads in the soil reinforcement at different pile head loads relative to distance from the back of the MSE wall (1.8D pile, layer L3, 43 in. transverse spacing).

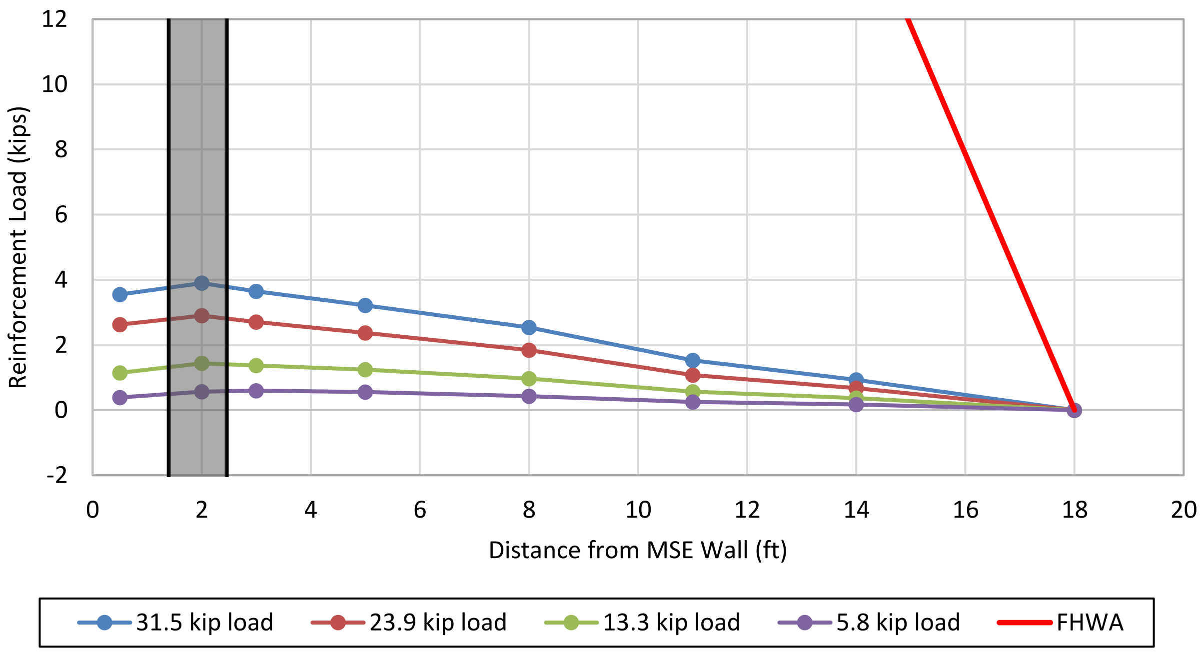

Figure F.1-29: Induced loads in the soil reinforcement at different pile head loads relative to distance from the back of the MSE wall (1.8D pile, layer L3, 22 in. transverse spacing).

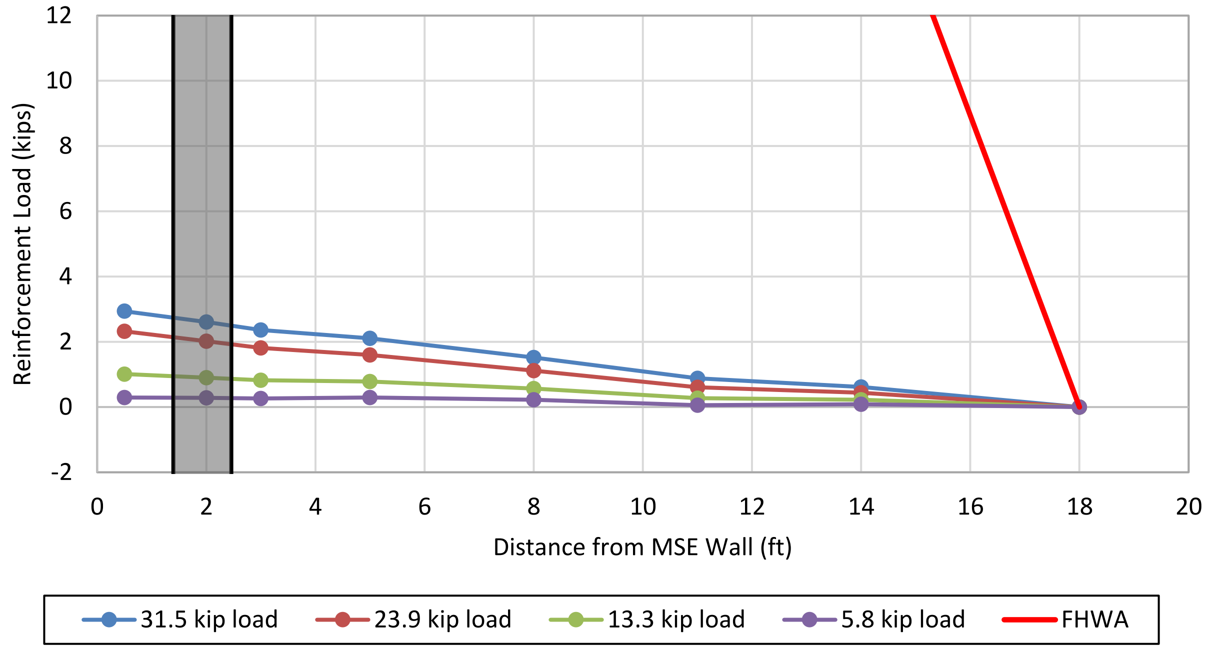

Figure F.1-30: Induced loads in the soil reinforcement at different pile head loads relative to distance from the back of the MSE wall (1.8D pile, layer L4, 35 in. transverse spacing).

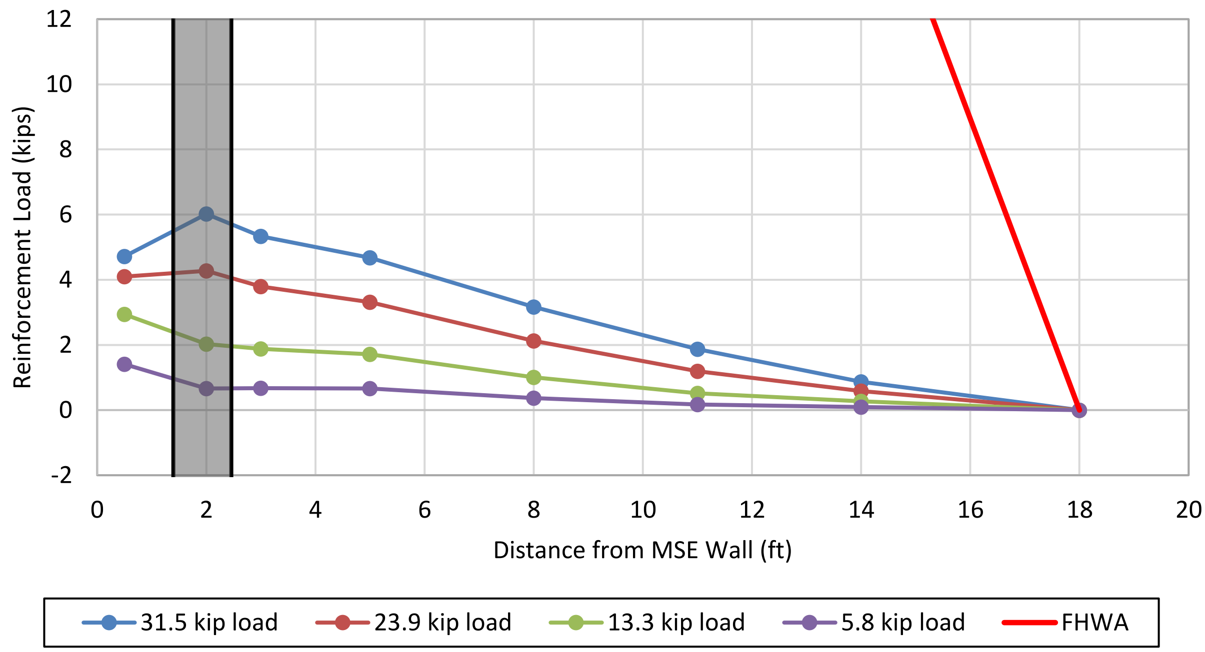

Figure F.1-31: Induced loads in the soil reinforcement at different pile head loads relative to distance from the back of the MSE wall (1.8D pile, layer L4, 17 in. transverse spacing).

APPENDIX F.2 – INDUCED FORCE IN THE REINFORCEMENT CURVES FOR PIPES WITH RIBBED STRIP

1.7D Soil Reinforcement Curves

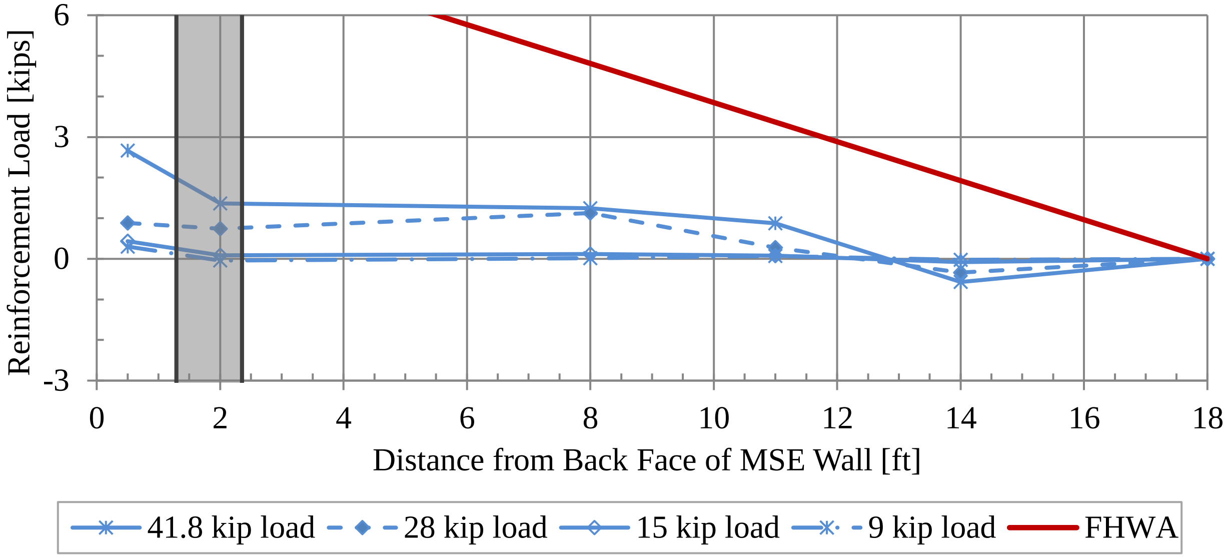

Figure F.2-1: Induced force in soil reinforcement at varying pile head loads and distances from the back face of the MSE wall for the 1.7D test; 15 in. depth and 9.5 in. transverse spacing from center of pile.

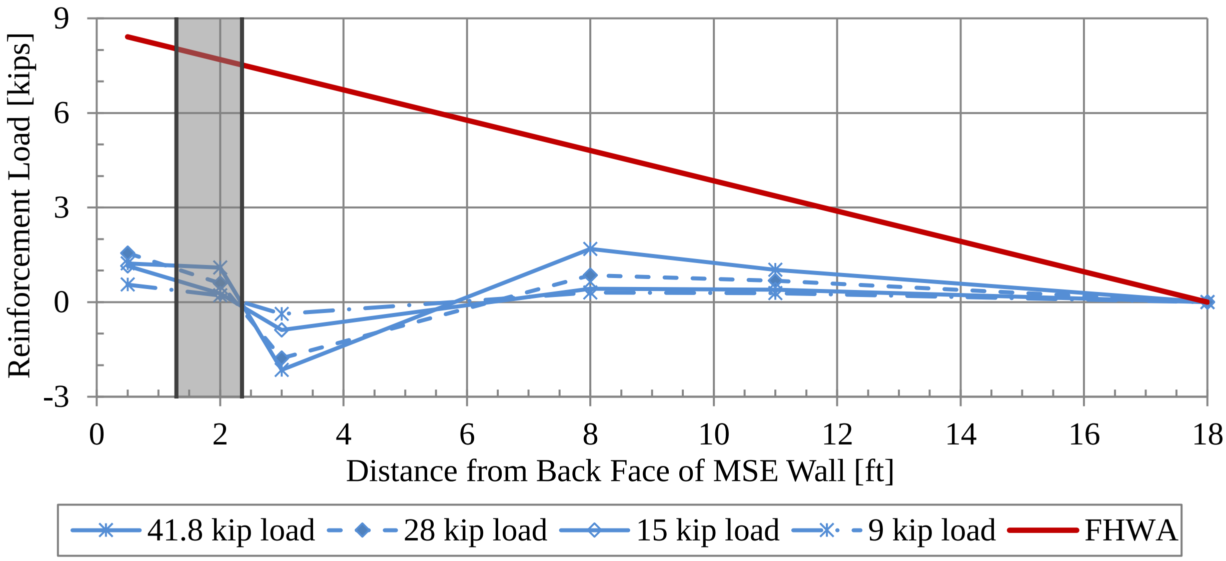

Figure F.2-2: Induced force in soil reinforcement at varying pile head loads and distances from the back face of the MSE wall for the 1.7D test; 15 in. depth and 35 in. transverse spacing from center of pile.

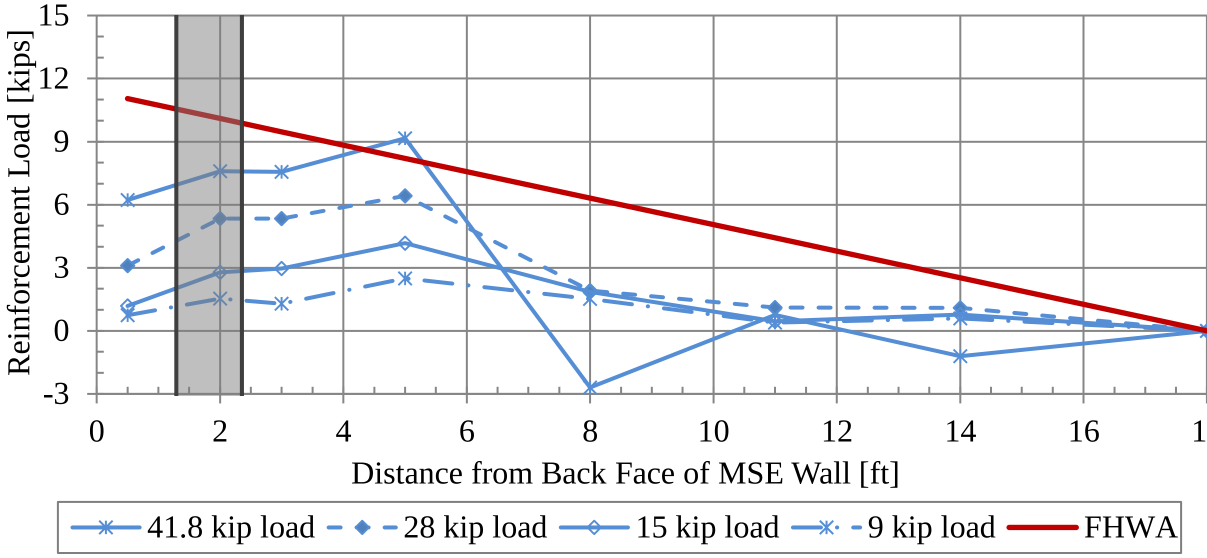

Figure F.2-3: Induced force in soil reinforcement at varying pile head loads and distances from the back face of the MSE wall for the 1.7D test; 45 in. depth and 11 in. transverse spacing from center of pile.

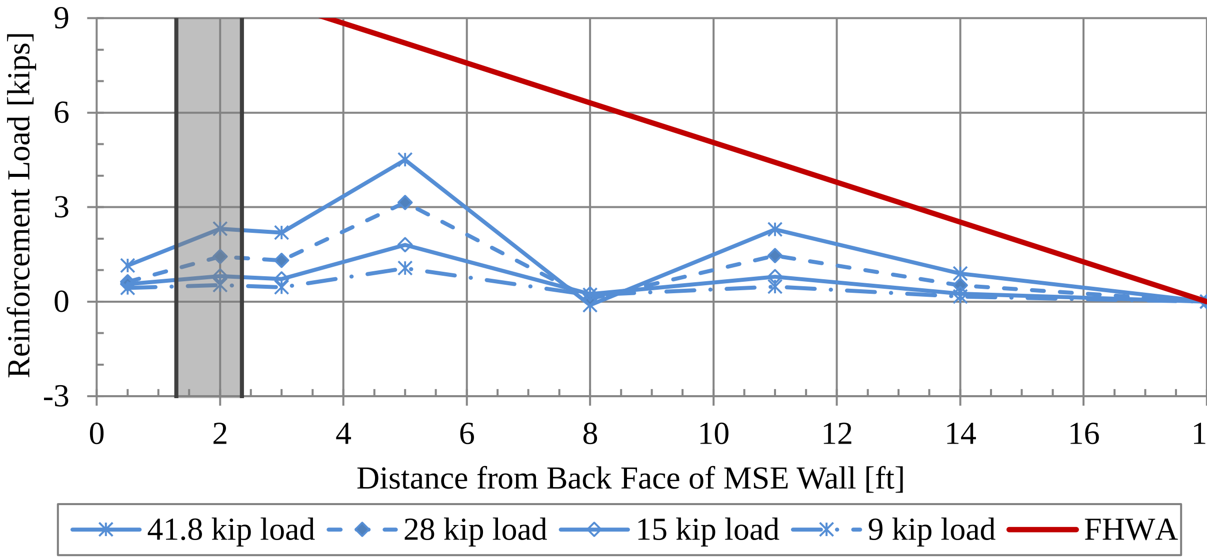

Figure F.2-4: Induced force in soil reinforcement at varying pile head loads and distances from the back face of the MSE wall for the 1.7D test; 45 in. depth and 37.5 in. transverse spacing from center of pile.

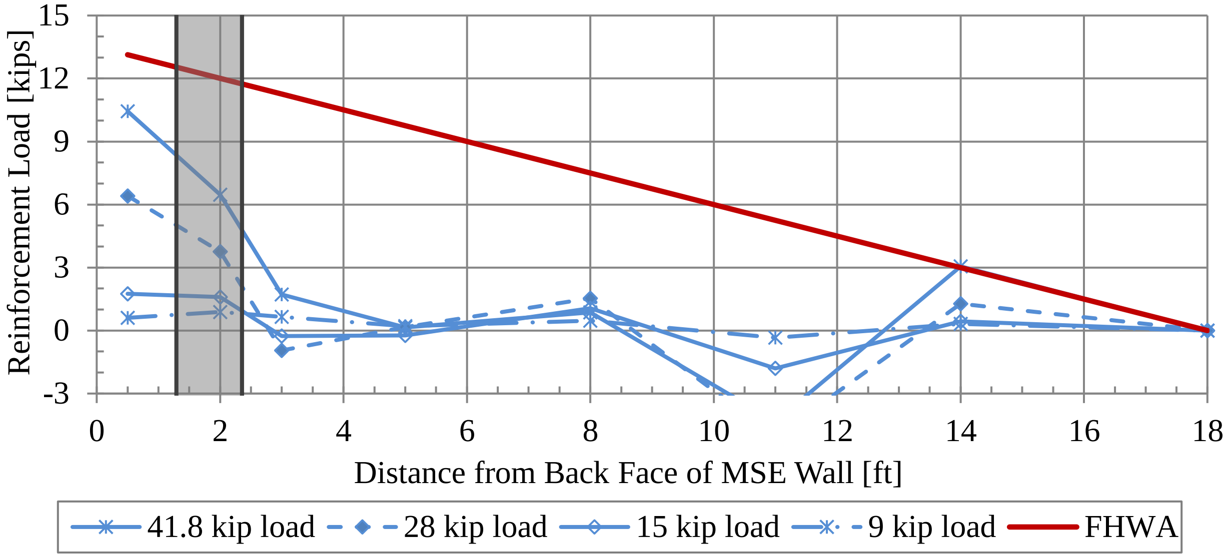

Figure F.2-5: Induced force in soil reinforcement at varying pile head loads and distances from the back face of the MSE wall for the 1.7D test; 75 in. depth and 9 in. transverse spacing from center of pile.

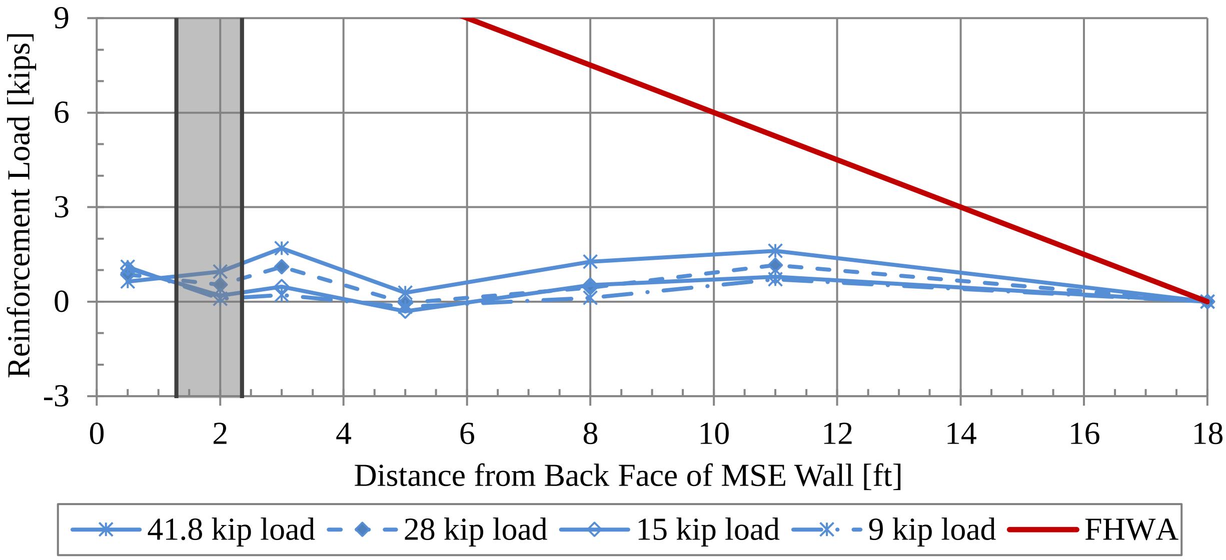

Figure F.2-6: Induced force in soil reinforcement at varying pile head loads and distances from the back face of the MSE wall for the 1.7D test; 75 in. depth and 36 in. transverse spacing from center of pile.

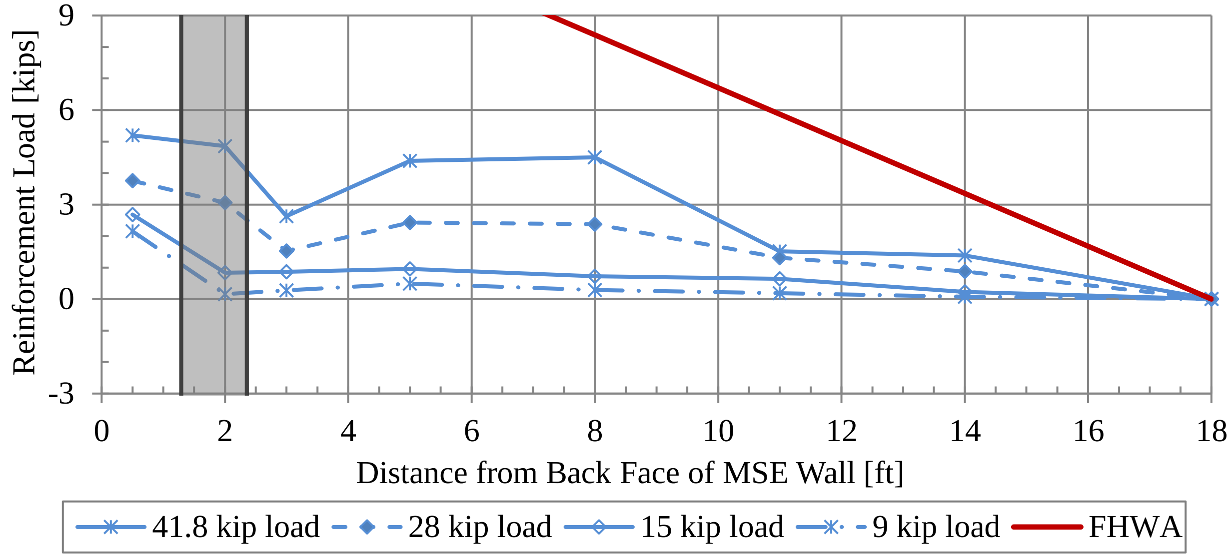

Figure F.2-7: Induced force in soil reinforcement at varying pile head loads and distances from the back face of the MSE wall for the 1.7D test; 105 in. depth and 9 in. transverse spacing from center of pile.

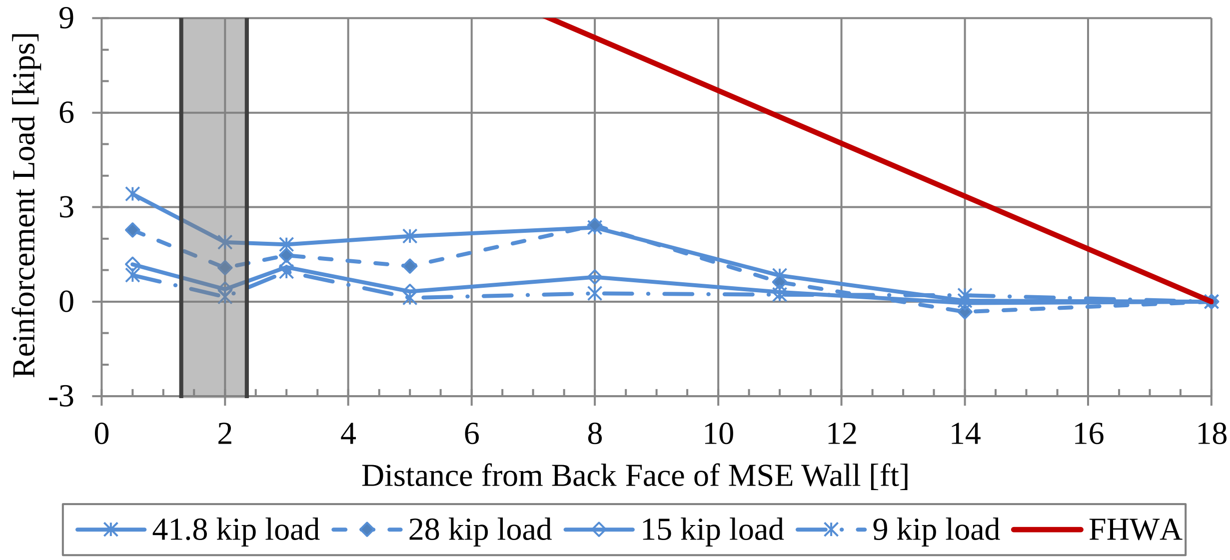

Figure F.2-8: Induced force in soil reinforcement at varying pile head loads and distances from the back face of the MSE wall for the 1.7D test; 105 in. depth and 35 in. transverse spacing from center of pile.

2.8D Soil Reinforcement Curves

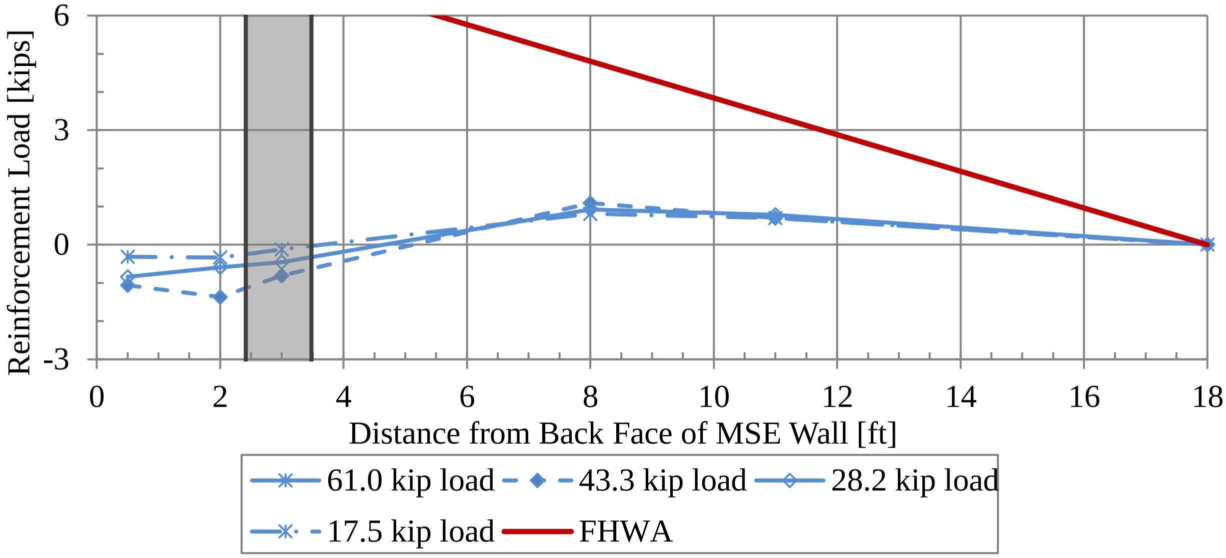

Figure F-9: Induced force in soil reinforcement at varying pile head loads and distances from the back face of the MSE wall for the 2.8D test; 15 in. depth and 24.5 in. transverse spacing from center of pile.

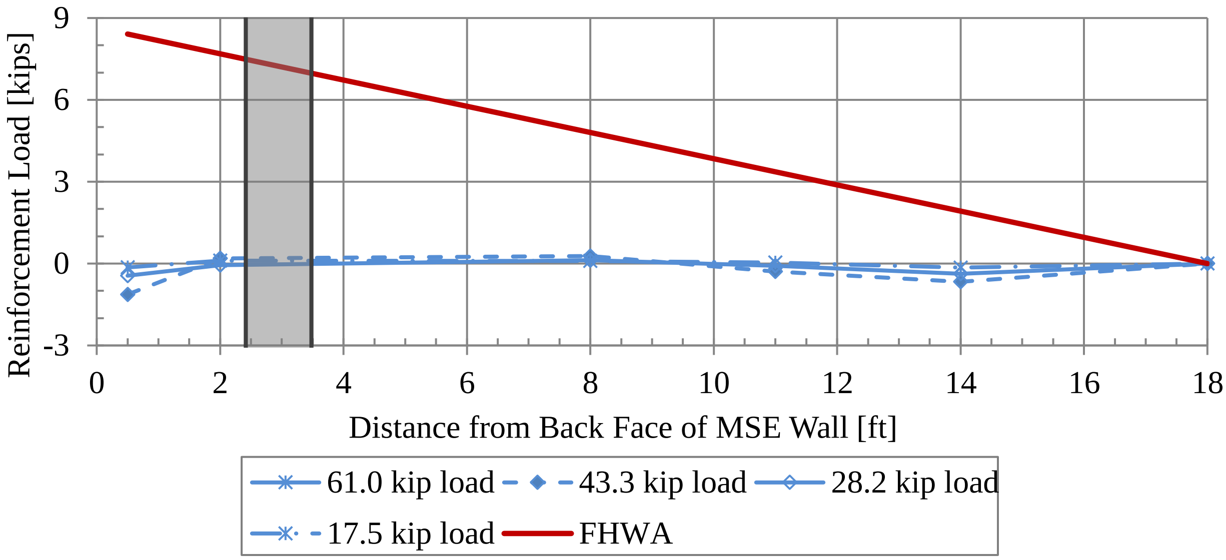

Figure F.2-10: Induced force in soil reinforcement at varying pile head loads and distances from the back face of the MSE wall for the 2.8D test; 15 in. depth and 50 in. transverse spacing from center of pile.

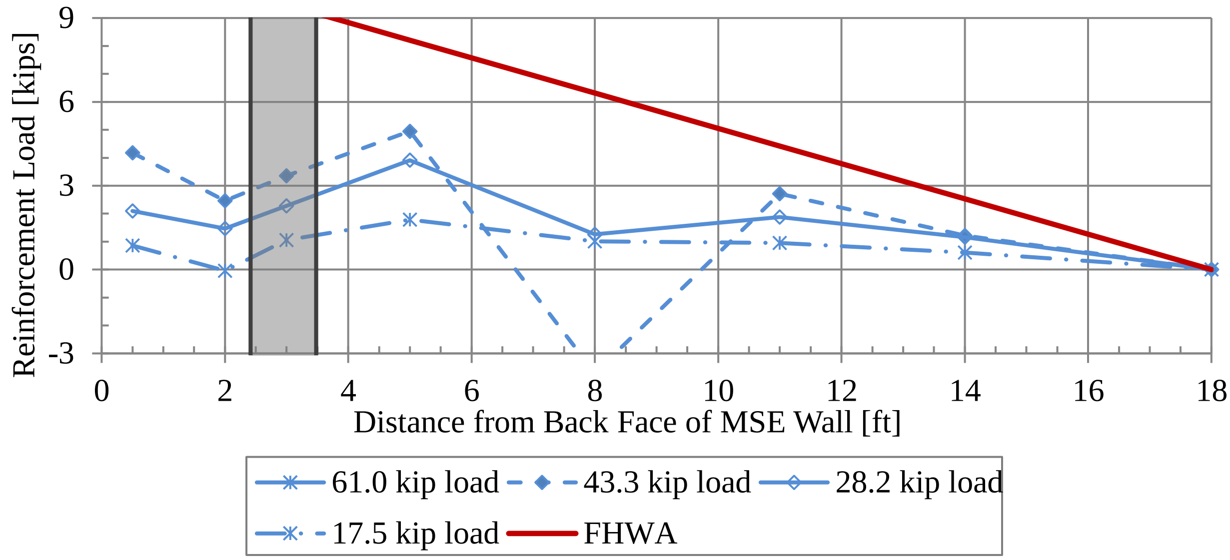

Figure F.2-11: Induced force in soil reinforcement at varying pile head loads and distances from the back face of the MSE wall for the 2.8D test; 45 in. depth and 20.5 in. transverse spacing from center of pile.

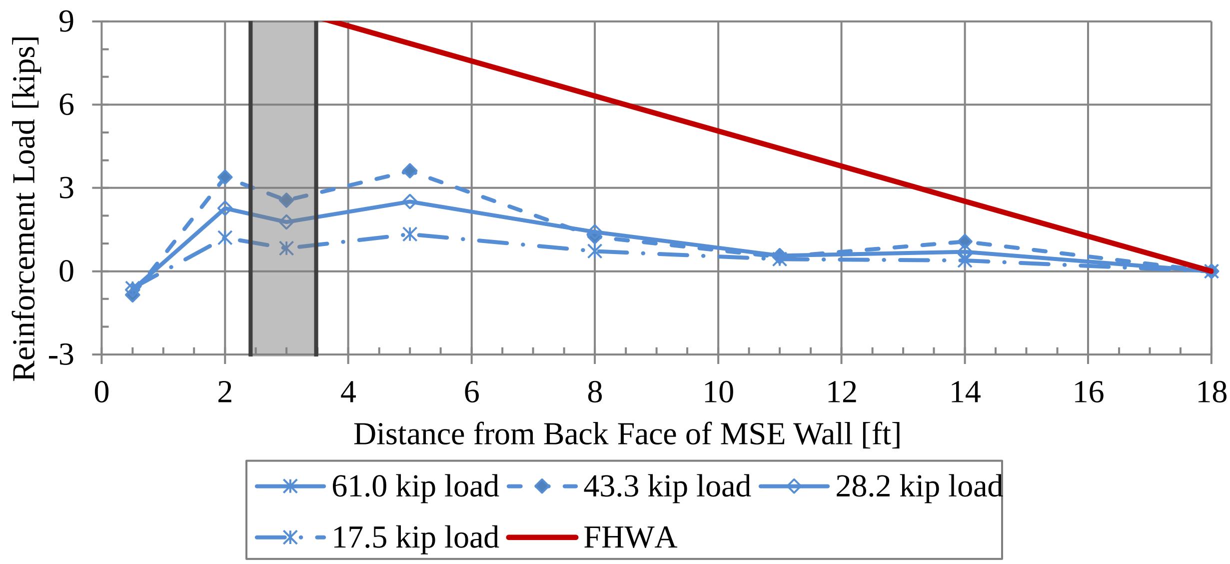

Figure F.2-12: Induced force in soil reinforcement at varying pile head loads and distances from the back face of the MSE wall for the 2.8D test; 45 in. depth and 47 in. transverse spacing from center of pile.

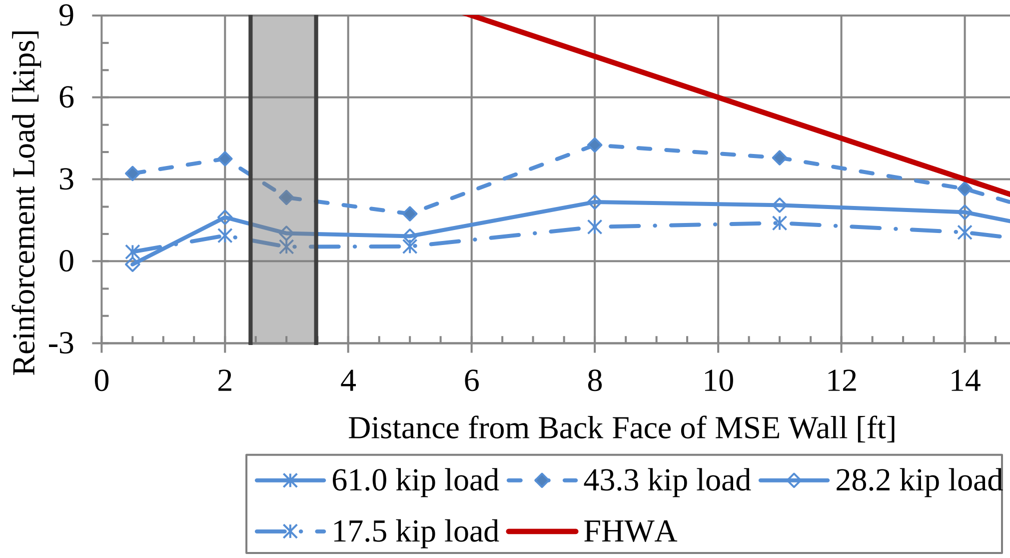

Figure F.2-13: Induced force in soil reinforcement at varying pile head loads and distances from the back face of the MSE wall for the 2.8D test; 75 in. depth and 22.5 in. transverse spacing from center of pile.

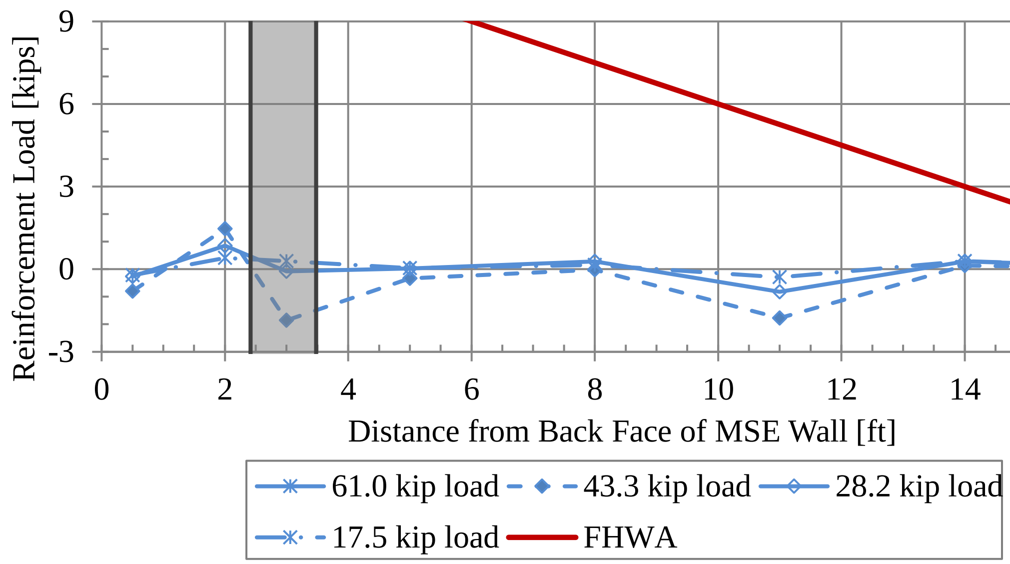

Figure F.2-14: Induced force in soil reinforcement at varying pile head loads and distances from the back face of the MSE wall for the 2.8D test; 75 in. depth and 49.5 in. transverse spacing from center of pile.

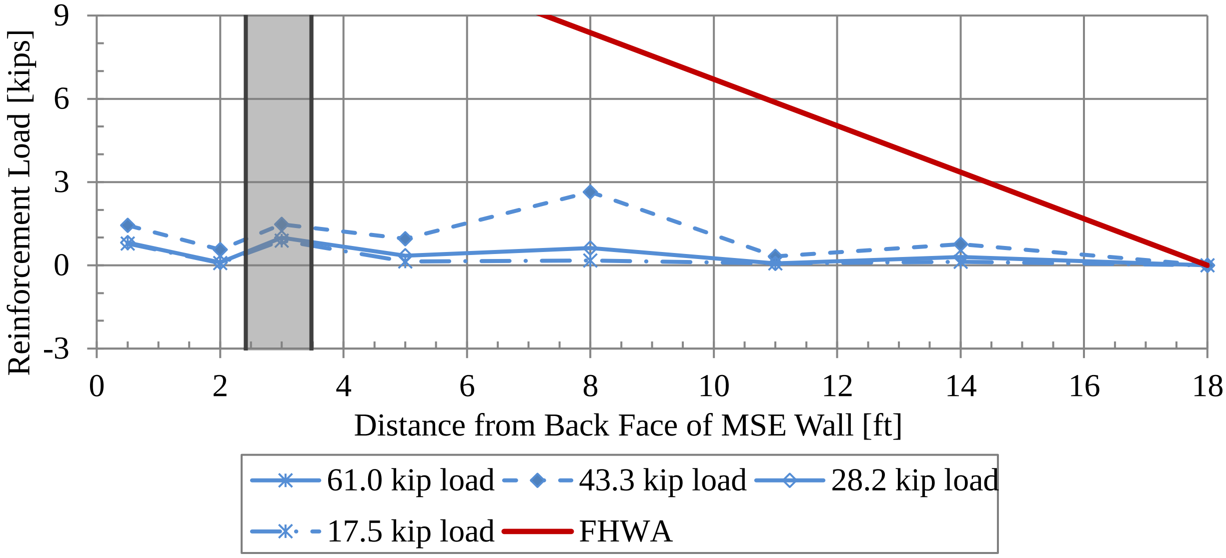

Figure F.2-15: Induced force in soil reinforcement at varying pile head loads and distances from the back face of the MSE wall for the 2.8D test; 105 in. depth and 23.5 in. transverse spacing from center of pile.

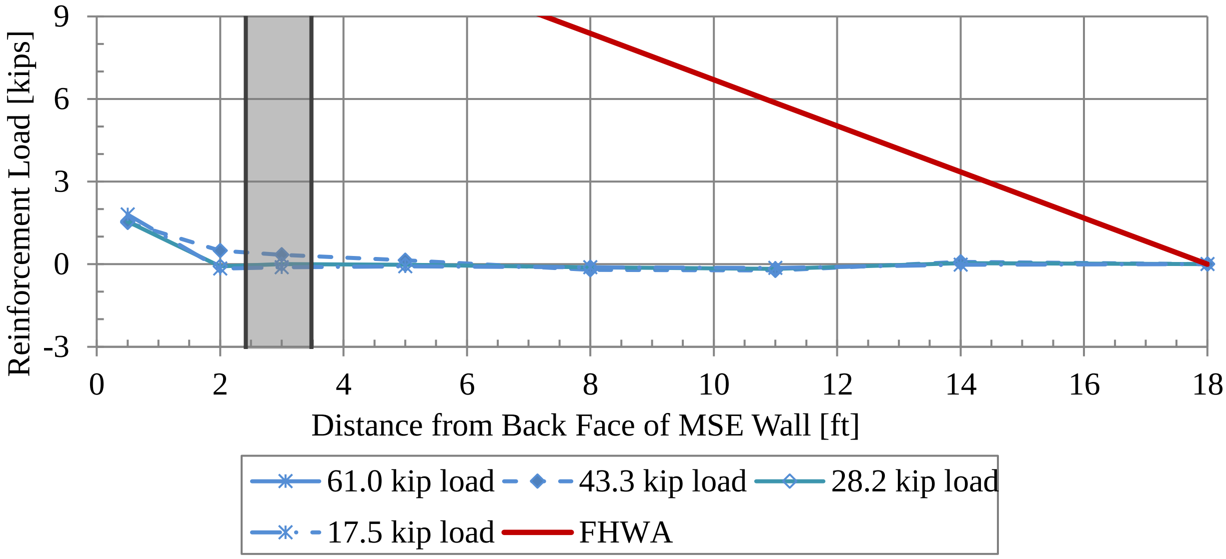

Figure F.2-16: Induced force in soil reinforcement at varying pile head loads and distances from the back face of the MSE wall for the 2.8D test; 105 in. depth and 50 in. transverse spacing from center of pile.

2.9D Soil Reinforcement Curves

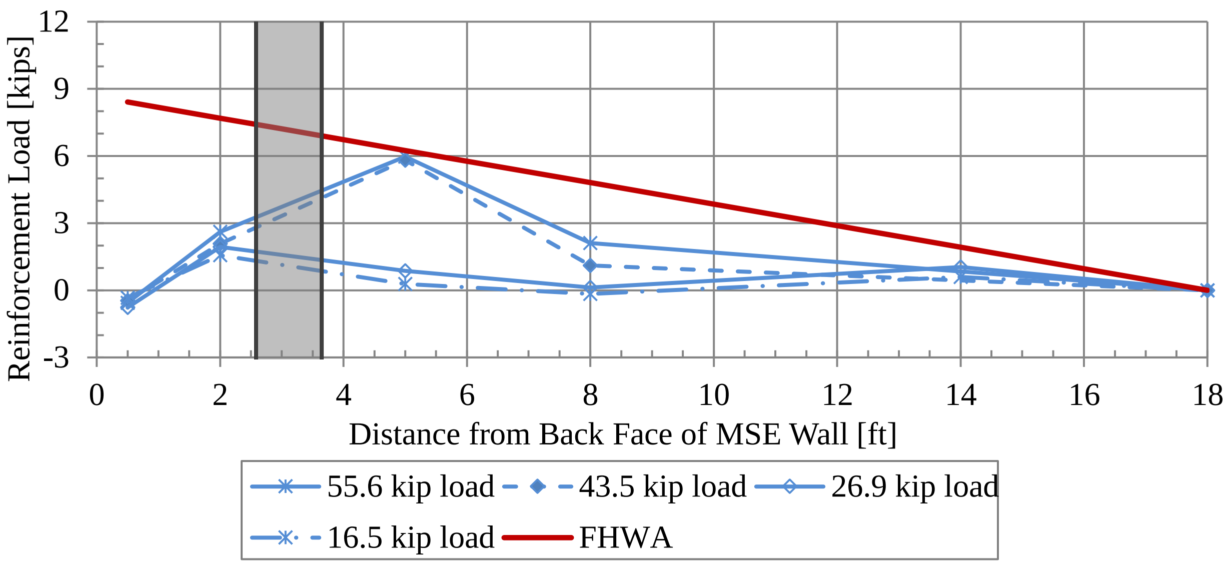

Figure F.2-17: Induced force in soil reinforcement at varying pile head loads and distances from the back face of the MSE wall for the 2.9D test; 15 in. depth and 10 in. transverse spacing from center of pile.

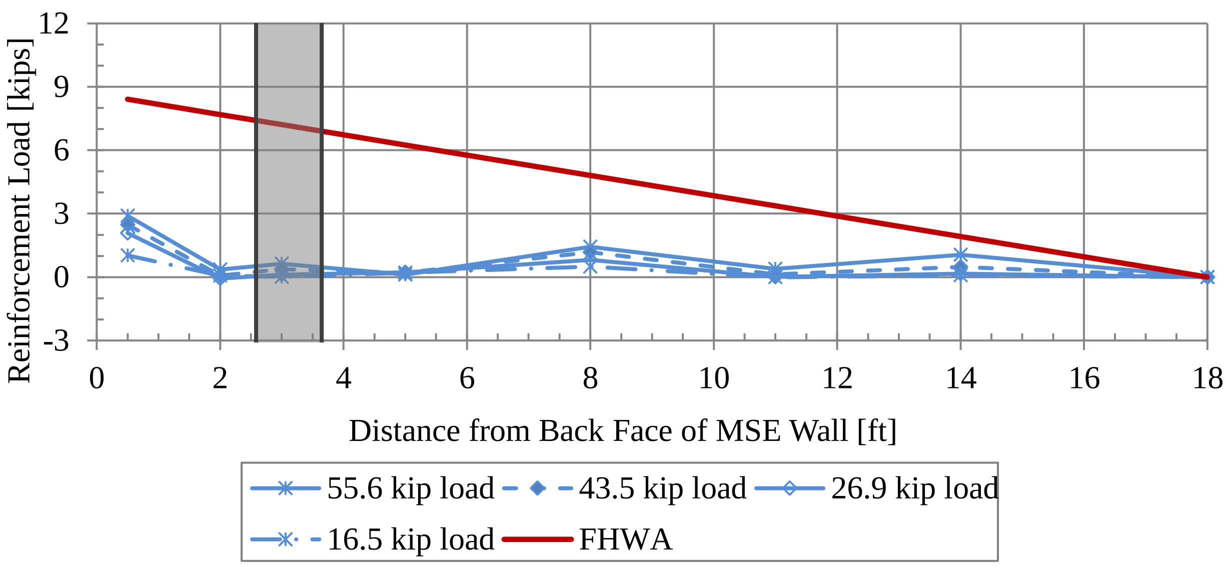

Figure F.2-18: Induced force in soil reinforcement at varying pile head loads and distances from the back face of the MSE wall for the 2.9D test; 15 in. depth and 35.5 in. transverse spacing from center of pile.

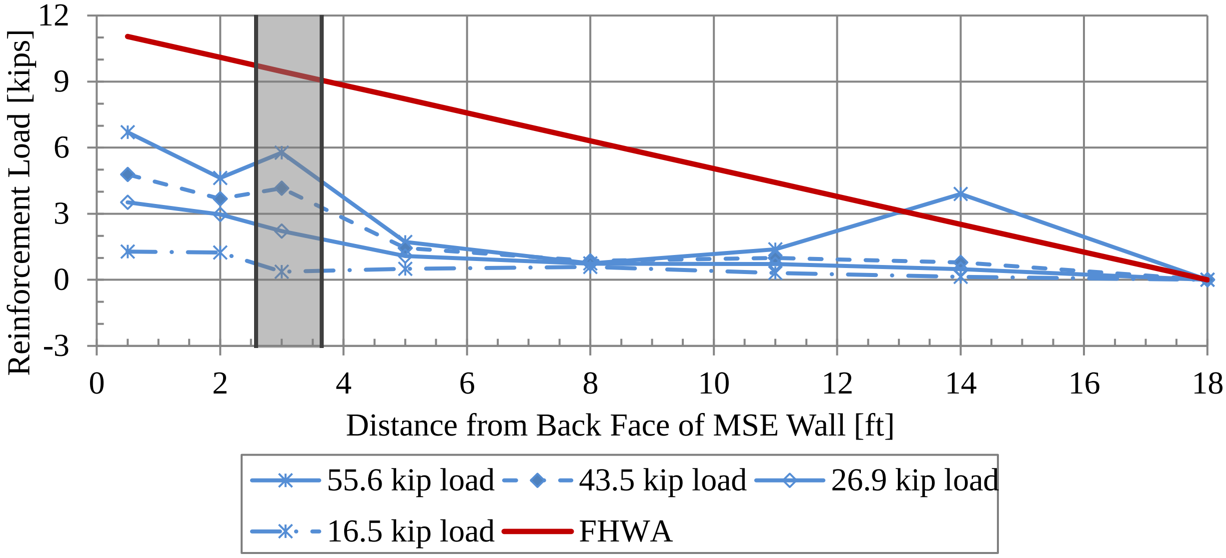

Figure F.2-19: Induced force in soil reinforcement at varying pile head loads and distances from the back face of the MSE wall for the 2.9D test; 45 in. depth and 12 in. transverse spacing from center of pile.

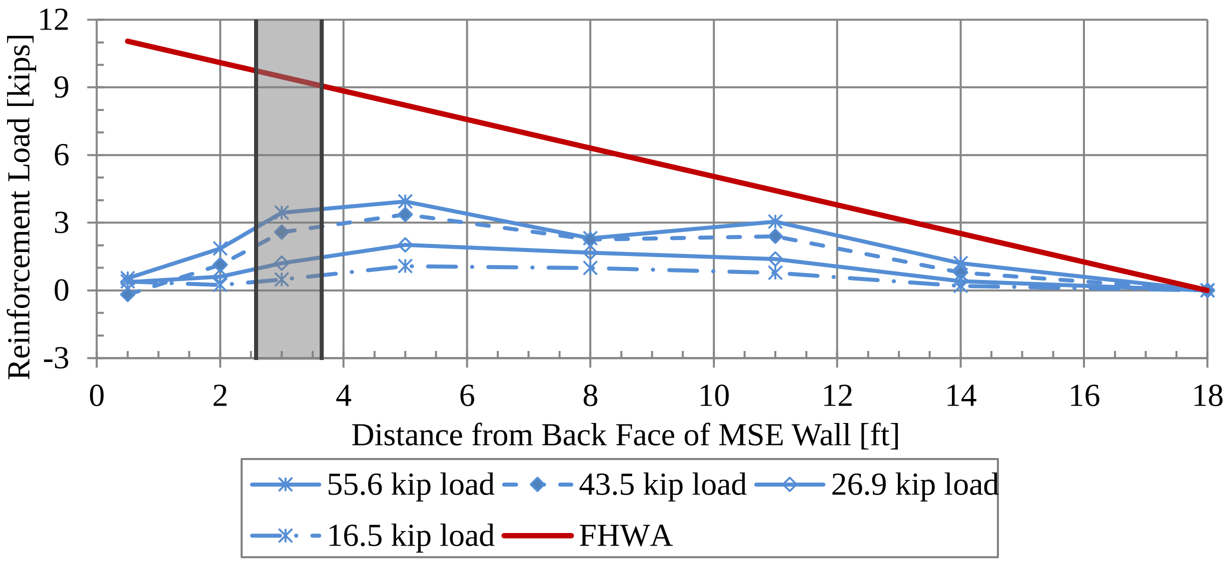

Figure F.2-20: Induced force in soil reinforcement at varying pile head loads and distances from the back face of the MSE wall for the 2.9D test; 45 in. depth and 38 in. transverse spacing from center of pile.

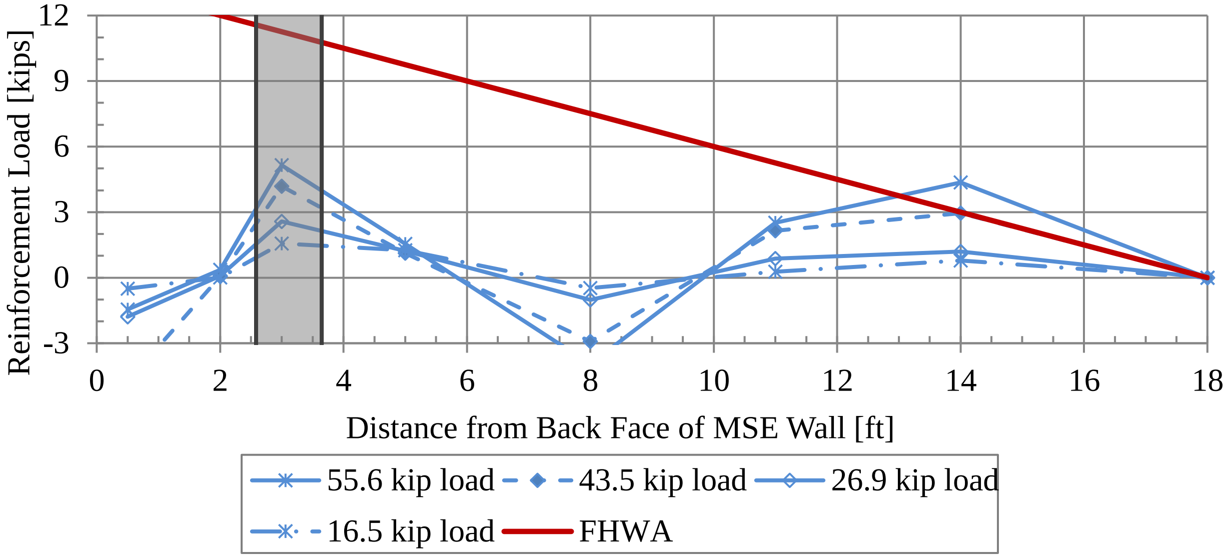

Figure F.2-21: Induced force in soil reinforcement at varying pile head loads and distances from the back face of the MSE wall for the 2.9D test; 75 in. depth and 11.5 in. transverse spacing from center of pile.

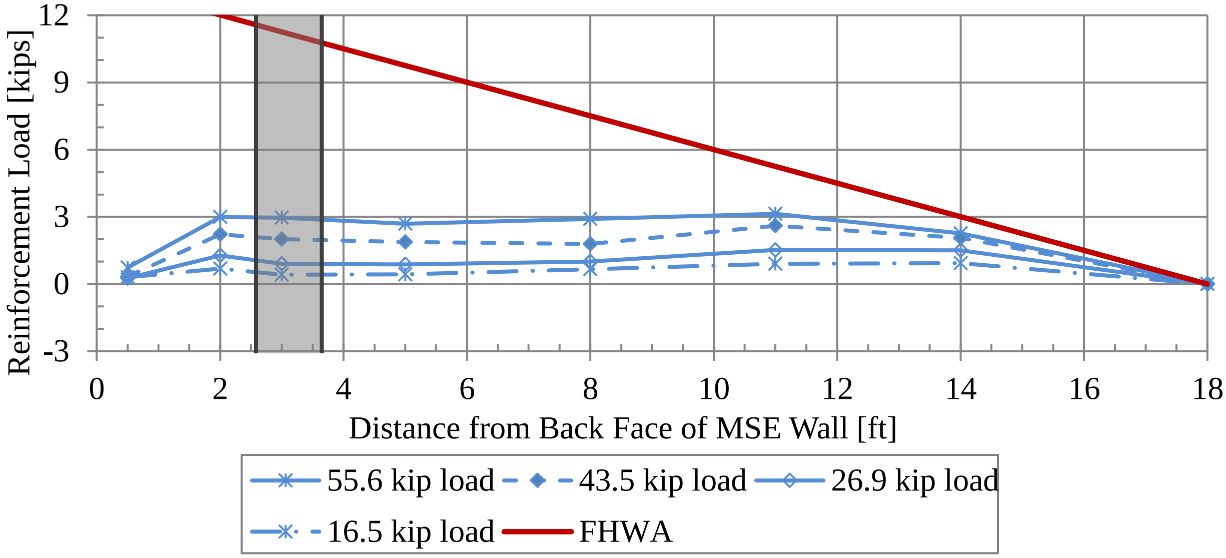

Figure F.2-22: Induced force in soil reinforcement at varying pile head loads and distances from the back face of the MSE wall for the 2.9D test; 75 in. depth and 37 in. transverse spacing from center of pile.

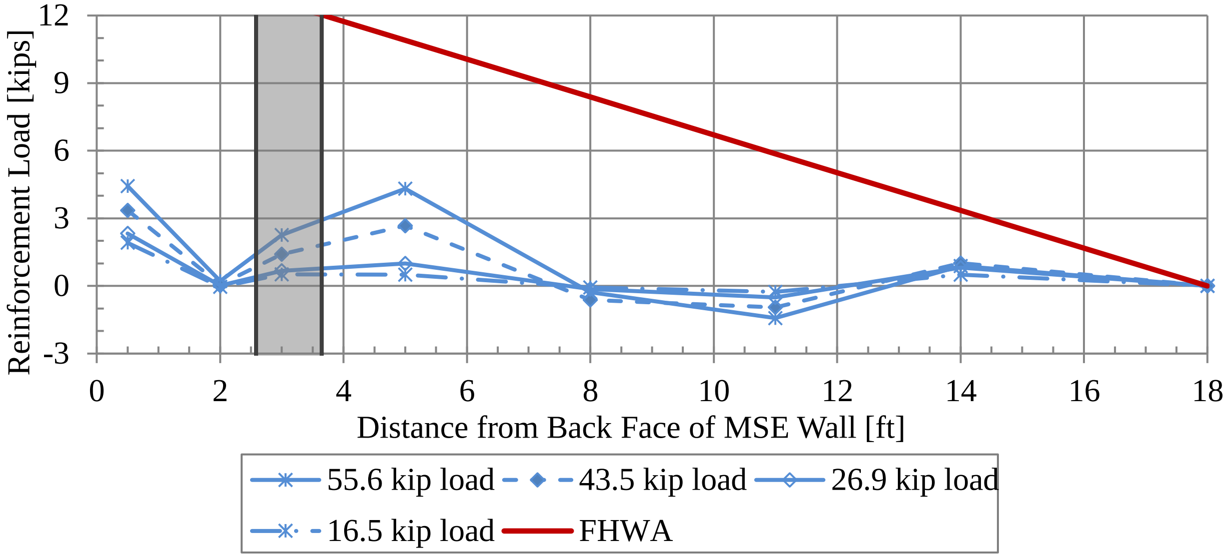

Figure F.2-23: Induced force in soil reinforcement at varying pile head loads and distances from the back face of the MSE wall for the 2.9D test; 105 in. depth and 10.5 in. transverse spacing from center of pile.

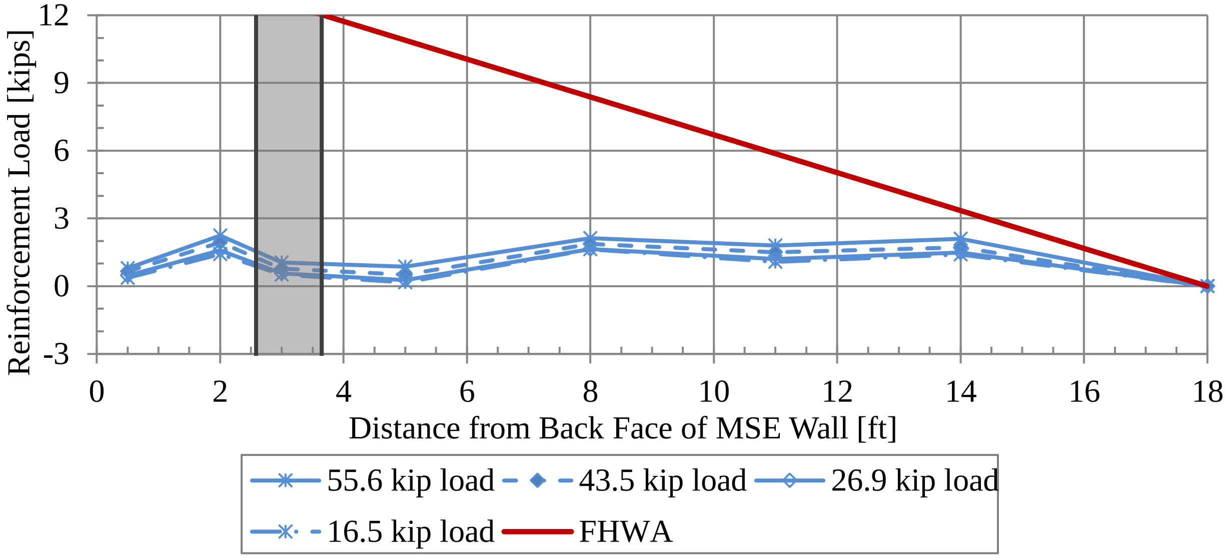

Figure F.2-24: Induced force in soil reinforcement at varying pile head loads and distances from the back face of the MSE wall for the 2.9D test; 105 in. depth and 38 in. transverse spacing from center of pile.

3.9D Soil Reinforcement Curves

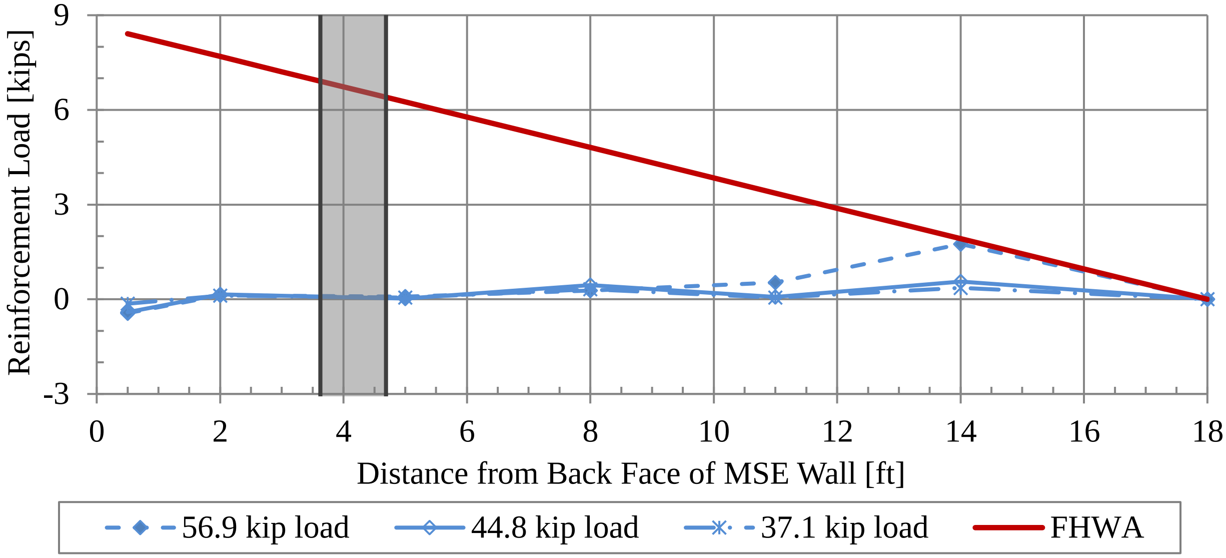

Figure F.2-25: Induced force in soil reinforcement at varying pile head loads and distances from the back face of the MSE wall for the 3.9D test; 15 in. depth and 26 in. transverse spacing from center of pile.

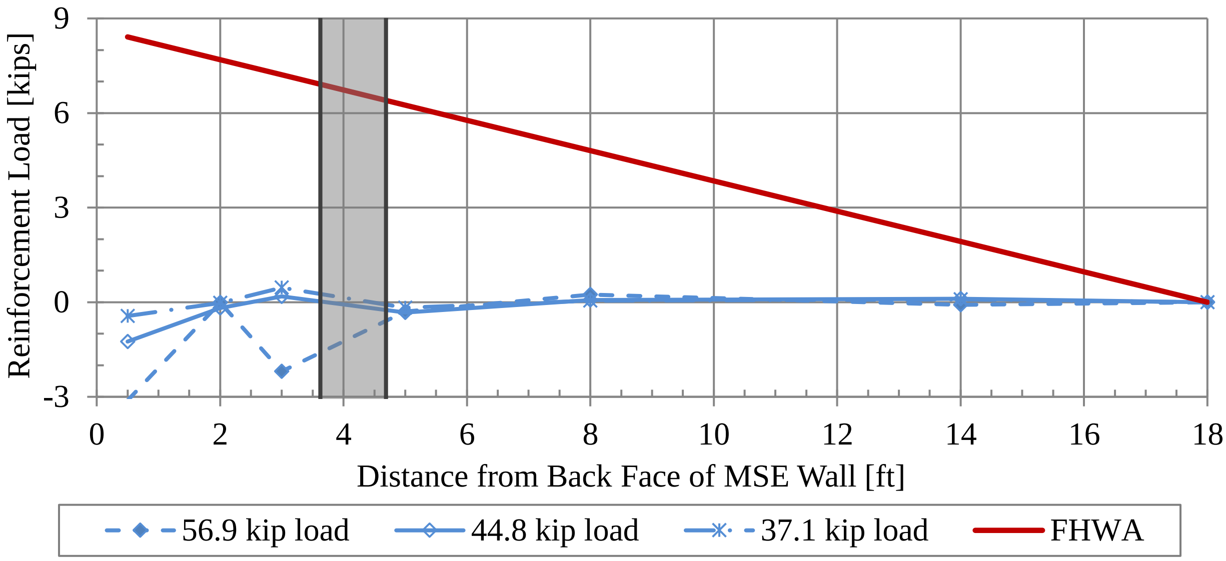

Figure F.2-26: Induced force in soil reinforcement at varying pile head loads and distances from the back face of the MSE wall for the 3.9D test; 15 in. depth and 51 in. transverse spacing from center of pile.

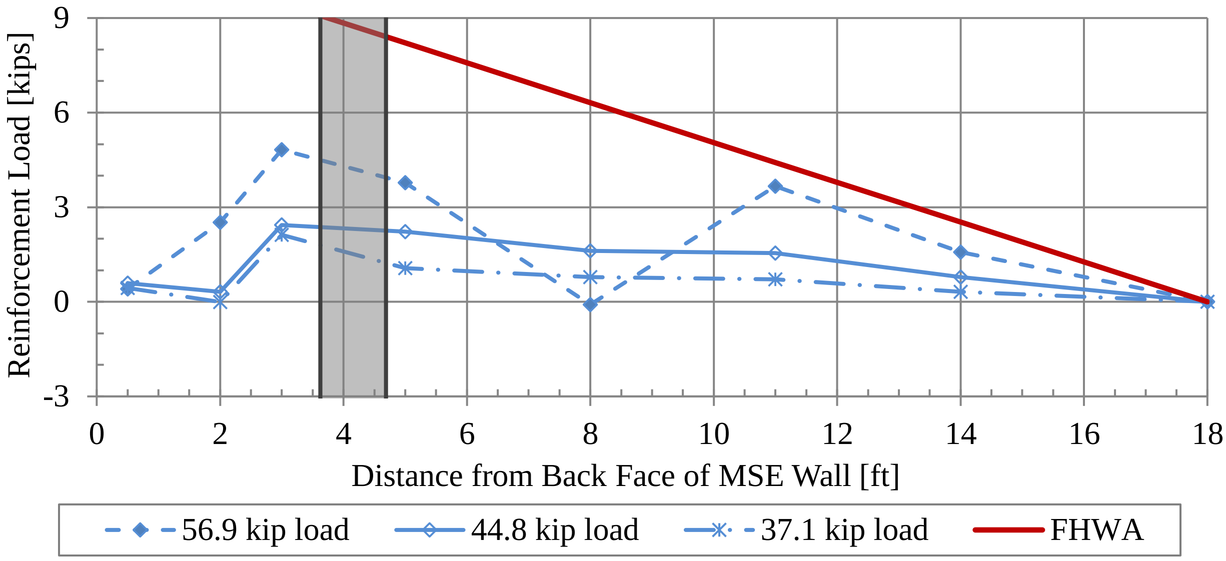

Figure F.2-27: Induced force in soil reinforcement at varying pile head loads and distances from the back face of the MSE wall for the 3.9D test; 45 in. depth and 22.5 in. transverse spacing from center of pile.

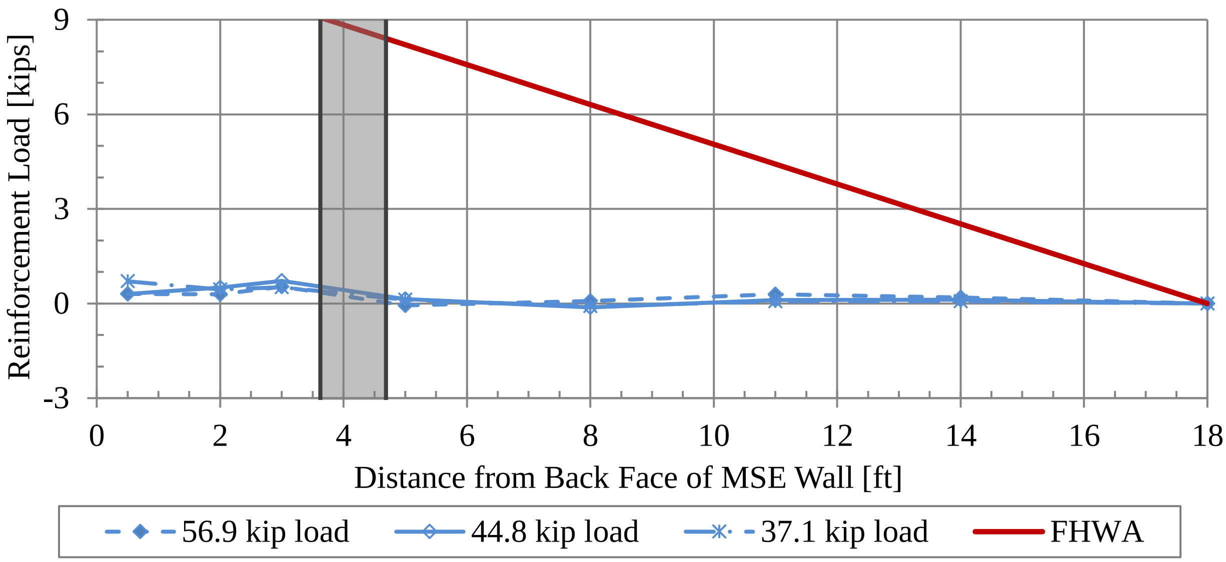

Figure F.2-28: Induced force in soil reinforcement at varying pile head loads and distances from the back face of the MSE wall for the 3.9D test; 45 in. depth and 49 in. transverse spacing from center of pile.

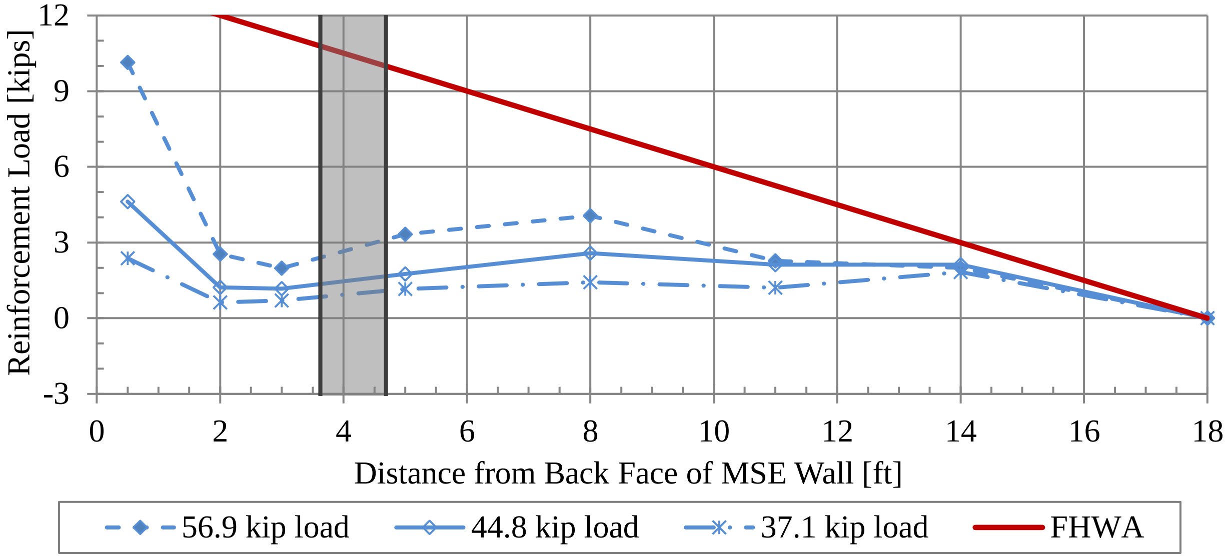

Figure F.2-29: Induced force in soil reinforcement at varying pile head loads and distances from the back face of the MSE wall for the 3.9D test; 75 in. depth and 24.5 in. transverse spacing from center of pile.

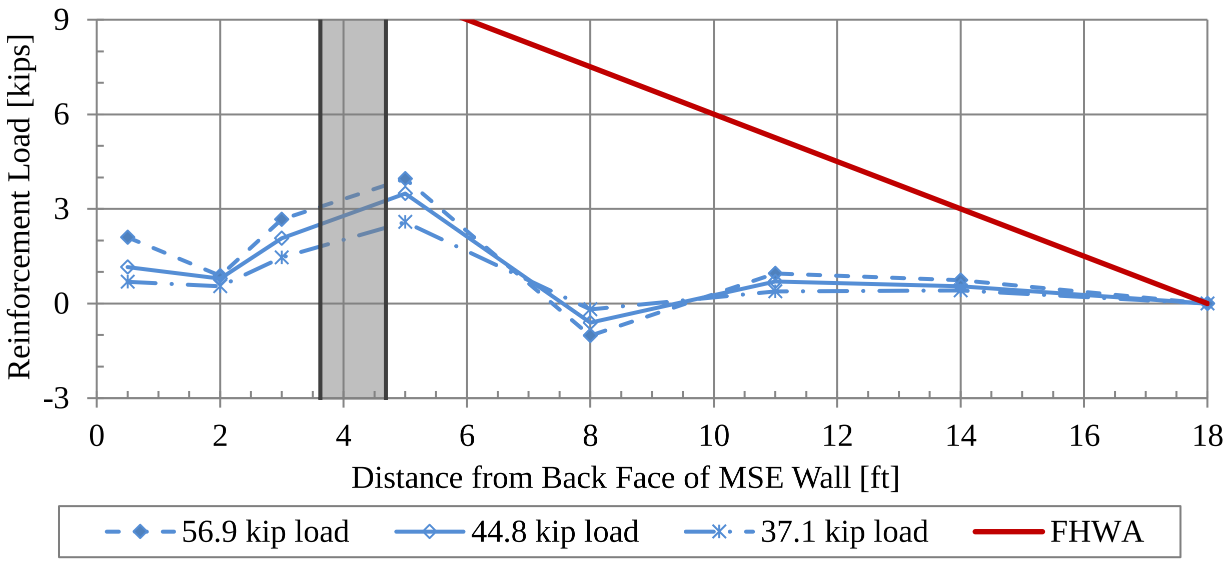

Figure F.2-30: Induced force in soil reinforcement at varying pile head loads and distances from the back face of the MSE wall for the 3.9D test; 75 in. depth and 50 in. transverse spacing from center of pile.

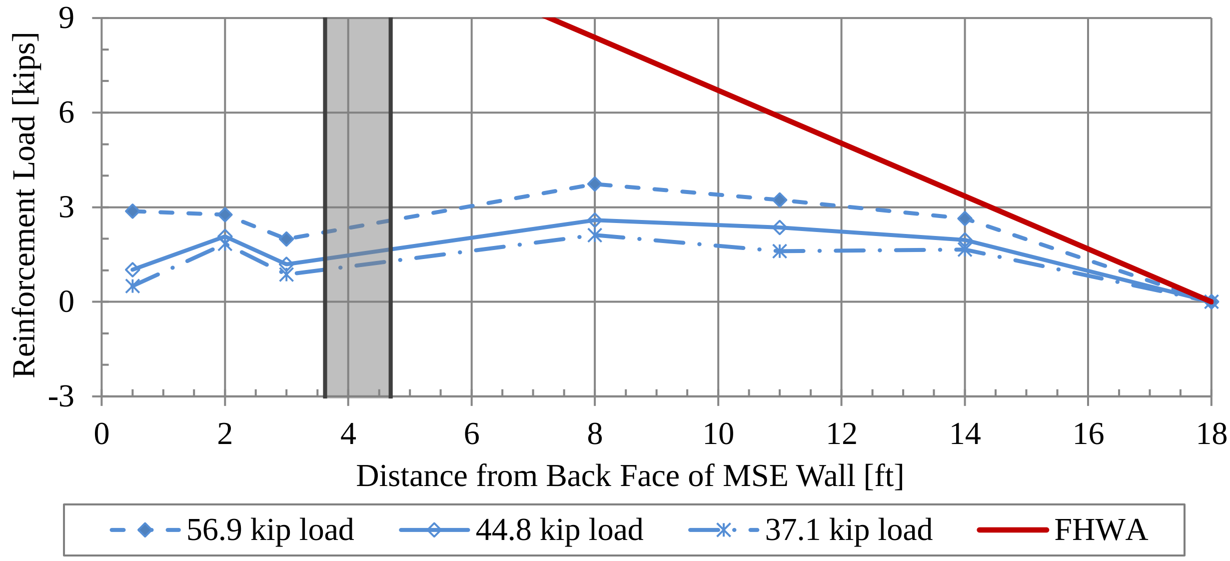

Figure F.2-31: Induced force in soil reinforcement at varying pile head loads and distances from the back face of the MSE wall for the 3.9D test; 105 in. depth and 24.5 in. transverse spacing from center of pile.

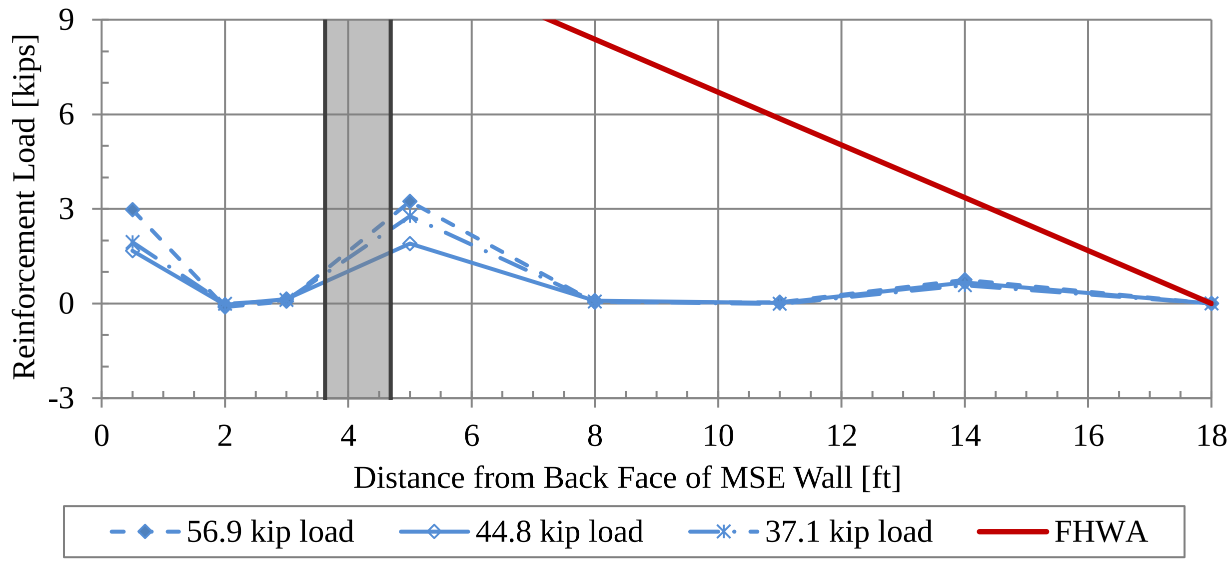

Figure F.2-32: Induced force in soil reinforcement at varying pile head loads and distances from the back face of the MSE wall for the 3.9D test; 105 in. depth and 51.5 in. transverse spacing from center of pile.

APPENDIX G – PILE DRIVING BLOWCOUNTS FOR PIPES WITH RIBBED STRIP

Table G-1: Pile driving blowcounts at various depths for each of the test piles

Depth (ft)	N (blowcount)			
	1.7D	2.8D	2.9D	3.9D
1				
2				
3			2	
4		1		
5	1			
6			1	2
7				
8		2	1	
9	2		1	2
10	1	2	1	1
11	1	1	2	3
12	1	2	5	3
13	3	6	5	5
14	5	5	5	5
15	6	4	5	4
16	4	4	4	2
17	4	1	1	2
18	2	2	3	3
Total	30	30	36	32